PNNL-26328

Pacific Northwest
NATIONAL LABORATORY

*Proudly Operated by* Battelle *Since 1965*

# NDE Technology Development Program for Non-Visual Volumetric Inspection Technology

## Technology Screening Report

**March 2017**

TL Moran
MR Larche
KM Denslow
SW Glass

U.S. DEPARTMENT OF ENERGY

Prepared for the U.S. Department of Energy
under Contract DE-AC05-76RL01830

**DISCLAIMER**

This report was prepared as an account of work sponsored by an agency of the United States Government. Neither the United States Government nor any agency thereof, nor Battelle Memorial Institute, nor any of their employees, makes **any warranty, express or implied, or assumes any legal liability or responsibility for the accuracy, completeness, or usefulness of any information, apparatus, product, or process disclosed, or represents that its use would not infringe privately owned rights**. Reference herein to any specific commercial product, process, or service by trade name, trademark, manufacturer, or otherwise does not necessarily constitute or imply its endorsement, recommendation, or favoring by the United States Government or any agency thereof, or Battelle Memorial Institute. The views and opinions of authors expressed herein do not necessarily state or reflect those of the United States Government or any agency thereof.

PACIFIC NORTHWEST NATIONAL LABORATORY
*operated by*
BATTELLE
*for the*
UNITED STATES DEPARTMENT OF ENERGY
*under Contract DE-AC05-76RL01830*

**Printed in the United States of America**

**Available to DOE and DOE contractors from the**
**Office of Scientific and Technical Information,**
**P.O. Box 62, Oak Ridge, TN 37831-0062;**
**ph: (865) 576-8401**
**fax: (865) 576-5728**
**email: reports@adonis.osti.gov**

**Available to the public from the National Technical Information Service**
**5301 Shawnee Rd., Alexandria, VA 22312**
**ph: (800) 553-NTIS (6847)**
**email: orders@ntis.gov <http://www.ntis.gov/about/form.aspx>**
**Online ordering: http://www.ntis.gov**

This document was printed on recycled paper.
(8/2010)

PNNL-26328

# NDE Technology Development Program for Non-Visual Volumetric Inspection Technology

Technology Screening Report

TL Moran
MR Larche
KM Denslow
SW Glass

March 2017

Prepared for
the U.S. Department of Energy
under Contract DE-AC05-76RL01830

Pacific Northwest National Laboratory
Richland, Washington 99352

# Summary

The U.S. Department of Energy (DOE) and the Hanford Site Tank Operations Contractor, Washington River Protection Solutions, LLC (WRPS), recognize the need to expand the scope of double-shell tank (DST) primary liner volumetric inspections to include the primary liner bottoms. This need was underscored by the recent leak discovered in one of the DSTs, 241-AY-102. Thus, WRPS initiated a non-destructive examination (NDE) Technology Development Program in FY2017 to begin a process of identifying and selecting candidate NDE technologies for under-tank inspection.

The NDE Technology Development Program for *non-visual volumetric inspection* is comprised of three phases that will ultimately culminate in inspection technology with sensors adapted to overcome riser and/or air slot access challenges and equipped with a robotic delivery system for unmanned inspections. The first and current phase of the program is focused on identifying NDE volumetric inspection technology that can satisfy the program's flaw detection requirements, which need to be satisfied in order to warrant future sensor adaptation and robotic delivery. Phase I is designed to determine the extent to which current or emerging non-visual volumetric NDE technology can satisfy the program's flaw detection requirements by baselining the flaw detection and characterization abilities of these technologies using a DST primary liner mockup. In support of Phase I, Pacific Northwest National Laboratory (PNNL) hosted and administered an initial *Technology Screening* test that allowed all interested NDE technology vendors or experts to demonstrate NDE volumetric inspection technologies for tank bottom inspection using a DST primary liner test mockup. The participating NDE technologies included a variety of ultrasonic techniques that were proposed in response to the WRPS Expression of Interest issued in September 2016. The *Technology Screening* test was designed to identify participating technologies capable of detecting larger flaw sizes of interest in order to qualify them for more rigorous Phase I *Effectiveness Testing. Effectiveness Testing* will ultimately be used to identify a system or set of non-visual volumetric NDE technologies at the conclusion of Phase I that should be further matured for Hanford DST primary liner bottom inspection under Phase II.

The primary liner test mockup used for *Technology Screening* contains nine surrogate flaws that represent cracks or corrosion-type pitting. The flaws are positioned in the 1/2-inch thick bottom plate of the mockup and the transition weld that joins the 7/8- to 1/2-inch thick bottom plates. Four NDE technology vendors participated in the *Technology Screening* test campaign by delivering overview presentations on their candidate technology and providing flaw detection demonstrations on the DST primary liner mockup. Each of the four participants (Guidedwave, Innerspec, Penn State, and Southwest Research Institute (SwRI)) brought different non-visual volumetric NDE technologies and approaches for flaw detection in the bottom plates of the DST primary liner mockup. *Technology Screening* was performed in a non-nuclear research laboratory test environment at PNNL in Richland, Washington.

The NDE technology presented and demonstrated by Guidedwave used an ultrasonic guided-wave phased-array technique where a single transducer containing several ultrasonic elements steered an ultrasonic beam (shear horizontal waves) to scan an area 360 degrees around the stationary transducer. The transducer was placed in a variety of locations along the bottom plate of the mockup and data from each location was combined to produce a composite image of flaws in the mockup.

Multiple electromagnetic acoustic transducer (EMAT) inspection approaches were demonstrated by Innerspec. The technique that was ultimately evaluated employed an adhesive-backed magnetostrictive strip temporarily attached to the mockup. Measurements performed with the magnetostrictive EMAT featured the strip placed on the top surface of the bottom plate along the long edge, perpendicular to the weld direction. The EMAT consisting of a meander coil circuit in a short flexible strip was then placed over the magnetostrictive strip to induce guided waves (shear horizontal waves) that traversed the bottom

plate. The magnetostrictive EMAT sensor was placed at several locations along the magnetostrictive strip and manually angled at each position to control sound beam direction and detect flaws in the mockup.

Penn State demonstrated a permanent-magnet EMAT approach where Lorentz force transduction was used to generate ultrasonic guided waves (shear horizontal waves) in the mockup. The technique employed a pair of transmit-receive EMATs separated by a distance that mimicked adjacent DST air slot separation distances. Measurements were performed at multiple locations along the mockup bottom plate. A synthetic aperture focusing technique (SAFT) was applied to the data during post-processing to create a composite image of flaws in the mockup.

SwRI demonstrated a guided-wave (shear horizontal waves) magnetostrictive EMAT approach for remotely detecting surrogate flaws in the bottom plates of the DST mockup. The magnetically coupled EMAT transducers were placed on the wall of the mockup to propagate guided waves around the knuckle and into the bottom plates. The EMATs were placed at multiple locations along the width of the mockup wall to scan the width of the mockup and detect flaws in the bottom plates. SAFT processing was applied to the data to create a composite image of flaws in the mockup.

Under *Technology Screening,* technologies are considered qualified for more rigorous *Effectiveness Testing* under Phase I if the following conditions are satisfied:

- a technology is capable of detecting a majority of flaws in its current state OR a technology can detect flaws that the others cannot (complementary technology); and
- a clear pathway to transducer adaptation is demonstrated or communicated and adaptation can be reasonably achieved within the time and cost constraints of the NDE Technology Development Program.

The evaluation of each non-visual volumetric NDE approach was performed using criteria and a scoring system that factored in the ability to detect the surrogate flaws in the mockup and accounted for multiple attributes that include sensor size, required proximity to flaws, and estimated sensor adaption time and cost. Guidedwave scored the highest number of points in the flaw detection category and overall with 35 total points. Innerspec and Penn State scored 32 and 31 total points, respectively, although Penn State had one more flaw detection point (16) than Innerspec (15). SwRI scored the fewest flaw detection points and the fewest total points with 24.

The *Technology Screening* scores earned by each technology indicate all three of the evaluated NDE technologies provided by Guidedwave, Penn State and Innerspec are capable of detecting a majority of the flaws and each participant has demonstrated or communicated the potential to overcome air-slot and riser access challenges. Therefore, all three air-slot inspection technologies are considered qualified to participate in final Phase I *Effectiveness Testing*. The score earned by the remote NDE inspection technology provided by SwRI detected the fewest number of flaws, but still detected more than half of them. Although it scored the lowest number of points, this technology satisfies the conditions listed above and is also considered qualified for Phase I *Effectiveness Testing.* A combination of these technologies have the potential to support a non-visual volumetric DST inspection approach that first utilizes remote inspection technology to provide coarse data on tank bottom conditions, and subsequently uses these data to identify the air-slots into which air-slot sensors should be deployed for higher-resolution examinations. This approach may be useful in the prioritization of air-slots for inspection and would support efficient and directed DST inspections. Therefore, a combination of remote and air-slot based inspections are recommended.

Based on the *Technology Screening* scores discussed above, and a recommendation to couple air-slot and remote inspection approaches, the following individual participants and teaming are recommended and ranked in the following order:

1. SwRI – the remote inspection technology will be well suited for rapidly screening around the primary liner tank wall to identify areas of concern in bottom plates that should be examined in greater detail with air-slot deployed sensors.

2. Guidedwave – the single-sensor technology is capable of scanning a large area and the image data quality supported easy data interpretation, which supported detection of all mockup flaws. The lack of need for coordinated dual air-slot sensor delivery and minimal need for sensor adaptation will support under-tank inspections and the program timeline.

3. Penn State with (Innerspec or Guidedwave) – Penn State's system was capable of detecting each flaw attempted (two were not attempted due to test time constraints). The lack of need for liquid couplant and minimal need for sensor adaptation will support under-tank inspections. The need for coordinated dual air-slot delivery presents a potential challenge. Improvement in signal-to-noise may be possible with better equipment from companies like Innerspec or Guidedwave. Penn State has worked with Guidedwave on sensor development and their prototype sensors are compatible with Innerspec instruments.

# Acronyms and Abbreviations

| | |
|---|---|
| DOE | U.S. Department of Energy |
| DST | double-shell tank |
| EMAT | electromagnetic acoustic transducer |
| EOI | expression of interest |
| GWPA | Guidedwave Phased-Array |
| ID | inner diameter or identification (context-specific) |
| NDE | non-destructive examination |
| OD | outer diameter |
| PNNL | Pacific Northwest National Laboratory |
| QAP | Quality Assurance Program |
| SAFT | synthetic aperture focusing technique |
| SH | shear horizontal |
| SNR | signal-to-noise ratio |
| SwRI | Southwest Research Institute |
| UT | ultrasonic testing |
| WRPS | Washington River Protection Solutions, LLC |

# Contents


Summary ..... iii
Acronyms and Abbreviations ..... vii
1.0 Introduction ..... 1.1
2.0 Background ..... 2.1
3.0 Purpose/Objective ..... 3.1
3.1 Purpose ..... 3.1
3.2 Test Objectives ..... 3.1
4.0 Scope ..... 4.1
4.1 Mockup ..... 4.1
4.2 Surrogate Flaws ..... 4.1
4.3 Test Conditions ..... 4.1
5.0 Quality Assurance ..... 5.1
6.0 Methods ..... 6.1
6.1 Guidedwave ..... 6.1
6.2 Innerspec ..... 6.2
6.3 Penn State ..... 6.3
6.4 Southwest Research Institute ..... 6.5
7.0 Results ..... 7.1
7.1 Flaw “a” (Priority Flaw) ..... 7.1
7.1.1 Guidedwave ..... 7.1
7.1.2 Innerspec ..... 7.3
7.1.3 Penn State ..... 7.4
7.1.4 SwRI ..... 7.5
7.2 Flaw “b” (Priority Flaw) ..... 7.6
7.2.1 Guidedwave ..... 7.7
7.2.2 Innerspec ..... 7.7
7.2.3 Penn State ..... 7.7
7.2.4 SwRI ..... 7.8
7.3 Flaw “c” (Priority Flaw) ..... 7.8
7.3.1 Guidedwave ..... 7.9
7.3.2 Innerspec ..... 7.10
7.3.3 Penn State ..... 7.10
7.3.4 SwRI ..... 7.11
7.4 Flaw “g” (Priority Flaw) ..... 7.11
7.4.1 Guidedwave ..... 7.11
7.4.2 Innerspec ..... 7.12
7.4.3 Penn State ..... 7.12

7.4.4 SwRI ..... 7.13
7.5 Flaw “h” ..... 7.13
7.5.1 Guidedwave ..... 7.13
7.5.2 Innerspec ..... 7.14
7.5.3 Penn State ..... 7.14
7.5.4 SwRI ..... 7.15
7.6 Flaw “I” ..... 7.16
7.6.1 Guidedwave ..... 7.16
7.6.2 Innerspec ..... 7.16
7.6.3 Penn State ..... 7.17
7.6.4 SwRI ..... 7.17
7.7 Flaw “k” (Priority Flaw) ..... 7.17
7.7.1 Guidedwave ..... 7.17
7.7.2 Innerspec ..... 7.18
7.7.3 Penn State ..... 7.18
7.7.4 SwRI ..... 7.18
7.8 Flaw “L” ..... 7.19
7.8.1 Guidedwave ..... 7.19
7.8.2 Innerspec ..... 7.19
7.8.3 Penn State ..... 7.19
7.8.4 SwRI ..... 7.20
7.9 Flaw “m” ..... 7.20
7.9.1 Guidedwave ..... 7.21
7.9.2 Innerspec ..... 7.21
7.9.3 Penn State ..... 7.21
7.9.4 SwRI ..... 7.21
7.10 Other Notable Features from Mockup ..... 7.22
7.10.1 Guidedwave ..... 7.22
7.10.2 Innerspec ..... 7.22
7.10.3 Penn State ..... 7.22
7.10.4 SwRI ..... 7.22
8.0 Analysis ..... 8.1
9.0 Conclusions/Recommendations ..... 9.1
10.0 References ..... 10.1
Appendix A – Guidedwave ..... A.1
Appendix B – Innerspec ..... B.1
Appendix C – Penn State ..... C.1
Appendix D – SwRI ..... D.1

# Figures


2.1 Hanford Double-Shell Tank Basic Design Detail ..... 2.2
2.2 Double-Shell Tank Annulus Riser Access ..... 2.2
2.3 Example of a Refractory Pad beneath a Primary Liner ..... 2.3
2.4 AY Farm Refractory Pad Air Slot Pattern and Cross Sections ..... 2.3
2.5 AZ, SY, AW, AN, and AP Farm Refractory Pad Air Slot Pattern and Cross Sections ..... 2.4
3.1 Summary of NDE Technology Development Program ..... 3.1
4.1 Top and Side View Drawings of the Primary Liner Mockup for Technology Screening ..... 4.2
4.2 Top and Side View Drawings of the 4-foot by 8-foot Extension Plate to Contain Surrogate Flaws for Technology Screening ..... 4.3
4.3 Illustration of a Top-down View of the Primary Liner Mockup ..... 4.4
6.1 Guided-Wave Sensor ..... 6.1
6.2 Inspection Locations on the 0.5-inch Bottom Plate ..... 6.2
6.3 EMAT Technique Using Magnetostrictive Strip ..... 6.3
6.4 EMAT Pitch-Catch and Pulse-Echo Technique ..... 6.3
6.5 Through-Transmission Configuration ..... 6.4
6.6 Pitch Catch Configuration ..... 6.4
6.7 Pulse-Echo Configuration ..... 6.5
6.8. Side View of the Sensor in Place above the Knuckle for Examining the Surrogate Flaws Remotely ..... 6.6
6.9 Sensor at the Starting Position of an Examination ..... 6.6
6.10 Meander Coil Being Replaced Between Examinations ..... 6.7
7.1 Photograph of Pit “a” (*left*) and Notch “k” (*right*) Located in the Transition Weld ..... 7.1
7.2 Guidedwave Phased-Array (GWPA) Scan on Plate 1 at Location 7 Pulsed at 200 kHz ..... 7.2
7.3 Composite Image Generated with Data Collected at 165 kHz from Five Locations ..... 7.3
7.4 Manual B-scan from Plate Edge with Magnetostrictive Technique ..... 7.4
7.5 SAFT-Reconstructed Image Combining the Results Obtained from Three Transmit-Receive Configurations ..... 7.5
7.6 SAFT Image Produced Using 57 kHz Data Set ..... 7.6
7.7 Photograph of Hole “b” ..... 7.7
7.8 Test Schematic (*left*), B-scan (*middle*), and Summary Graph (*right*) for Hole “b” ..... 7.8
7.9 Photograph of Pit “c” (*right*) and Notch “h” (*left*) ..... 7.9
7.10 GWPA Scan on Plate 1 at Location 1 Pulsed at 150 kHz ..... 7.10
7.11 Test Schematic (*left*), B-scan (*middle*), and Summary Graph (*right*) for Pit “c” ..... 7.10
7.12 Photograph of Notch “g” Located in the Transition Weld ..... 7.11
7.13 GWPA Scan on Plate 2 at Location 1 Pulsed with 150 kHz ..... 7.12
7.14 SAFT-Reconstructed Image Combining the Results Obtained from Three Transmit-Receive Configurations ..... 7.13

7.15 GWPA Scan on Plate 1 at Location 3 Pulsed at 200 kHz ..... 7.14
7.16 Test Schematic (*left*), B-scan (*middle*), and Summary Graph (*right*) for Notch "h" ..... 7.15
7.17 Photograph of Notch "i" (*left*) and Notch "m" (*right*) Located Near the Beveled Edge of the Plate ..... 7.16
7.18 Manual A-scan from Plate Edge (54 inch) with Magnetostrictive Technique ..... 7.17
7.19 GWPA Scan on Plate 1 at Location 4 Pulsed at 150 kHz ..... 7.18
7.20 Photograph of Notch "L" ..... 7.19
7.21 Test Schematic (*left*), B-scan (*middle*), and Summary Graph (*right*) for Notch "L" ..... 7.20
7.22 Manual A-scan from Plate Edge (59 inch) with Magnetostrictive Technique ..... 7.21

# Tables

4.1 Surrogate Flaw Matrix to Support *Technology Screening* ..... 4.5
8.1 *Technology Screening* Flaw Detection Scoring ..... 8.1
8.2 *Technology Screening* Attribute Scoring Criteria for Potential/Plan to Overcome Access Challenges ..... 8.2
8.3 Technology Screening Scores and Comparison ..... 8.3

# 1.0 Introduction

In September 2016, a Washington River Protection Solutions, LLC (WRPS) Request for Expression of Interest (EOI) was issued as a means of conducting market research to identify parties having an interest in and the resources to provide a non-destructive examination (NDE) system to meet the Hanford double-shell tank (DST) primary liner bottom inspection challenge. The EOI described the tank construction and physical layout, available access and access limitations, the history of tank inspections, relevant aspects of the apparent bottom leak of DST AY-102, and other information pertinent to primary liner bottom inspection.

The Pacific Northwest National Laboratory (PNNL) located in Richland, Washington, hosted and administered a *Technology Screening* test that allowed four different participants to demonstrate the NDE volumetric inspection technologies that were proposed in response to the WRPS EOI. This document provides a *Technology Screening* test report for the initial part of Phase I of a three-phase NDE Technology Development Program designed to identify and mature a system or set of non-visual volumetric NDE technologies for Hanford DST primary liner bottom inspection. Phase I of the program will baseline the performance of current or emerging non-visual volumetric NDE technologies for their ability to detect and characterize primary liner bottom flaws, and identify candidate technologies for adaptation and maturation for Phase II of the program.

This test report is organized with Section 2.0 containing the background on the DST Inspection Program, while Sections 3.0 and 4.0 outline the purpose and scope of the three-phase NDE Technology Development Program. Section 5.0 details the quality assurance program used at PNNL. The *Technology Screening* methods, test results, and analysis are presented in Sections 6.0, 7.0, and 8.0. Finally, Section 9.0 draws conclusion and recommendations from the results presented from each of the four teams that participated. Appendix A through Appendix D contain each of the participant's test reports and presentations.

# 2.0 Background

The first leak in a Hanford DST was discovered in 2012 in the first DST constructed at Hanford in 1968—Tank AY-102 (241-AY tank farm). The failure in AY-102 was determined to be in the bottom of its primary liner based on the presence of residual material in the secondary tank and the effects of sluicing during subsequent tank waste retrieval. The exact failure location(s) and degradation mechanism(s) are still undetermined because, up to this point, volumetric inspections of DST primary liners to assess their integrity have been limited to the side walls. The rationale behind this approach was that the condition of the side walls was expected to provide an indication of the condition of the primary liner bottoms and yield early warnings of potential primary liner bottom failures. This was based on expected low mechanical stresses in the tank bottom and the tank bottom waste sludge environment not being conducive to corrosion because of the lack of oxygen transport from the waste surface to the stagnant bottom layers. The failure of the AY-102 primary liner bottom in 2012 demonstrated that evaluating the integrity of the AY-102 primary liner bottom by proxy was not reliable and called the approach into question for the remaining 27 operating DSTs. The U.S. Department of Energy (DOE) and the Hanford Site Tank Operations Contractor, WRPS, recognize the need to expand the scope of DST primary liner volumetric inspections to include the primary liner bottoms. However, the expansion in coverage will require an expansion of volumetric inspection technology beyond that used for side-wall inspections in order to overcome access challenges associated with the primary liner bottom.

The DST primary liner side walls are currently inspected with ultrasonic NDE technology primarily based on conventional normal-beam ultrasonic testing (UT) transducers. The ultrasonic NDE transducers are deployed in the annular space between the secondary and primary liners on robotic crawler delivery systems that enter the annulus via the risers in the secondary liner. Figure 2.1 depicts the secondary and primary liners and Figure 2.2 depicts the risers.

The ultrasonic NDE technologies used for the primary liner side-wall inspections would be effective for the primary liner bottoms also, if access to the exterior surface of the primary liner bottoms was not obstructed by the refractory pad upon which the primary liners rest, as shown in Figure 2.3.

Direct access to the exterior surface of the primary liner bottoms is limited to channels (air slots) in the refractory pad that collectively expose approximately ~1% of the primary liner bottom surface area. The two primary air slot layouts used in the DST concrete refractory pads are provided in Figures 2.4 and 2.5. The two tanks in the 241-AY tank farm (Tanks AY-102 and AY-101) share a different refractory pattern from the remaining 26 operating DSTs. As depicted, the cross-sectional dimensions for these air slots vary within each pattern. The smallest and most limiting case is 1.5 inch × 1.5 inch on the outer most perimeter air slots of the AY Tank Farm.

Prior attempts have been made to utilize the air slots as access points to the primary bottom for volumetric inspection (Berman 2005). During this initial attempt, air slots in four of the six DSTs selected were found to be difficult to access due to obstructions presented by previously installed thermocouples and debris from deteriorating refractory pad material. Although these air slot obstructions do not completely preclude the use of the air slots for primary liner bottom inspection, it highlights the need for a well-rounded set of NDE technologies that are not completely dependent on air slot access for primary liner bottom inspection.

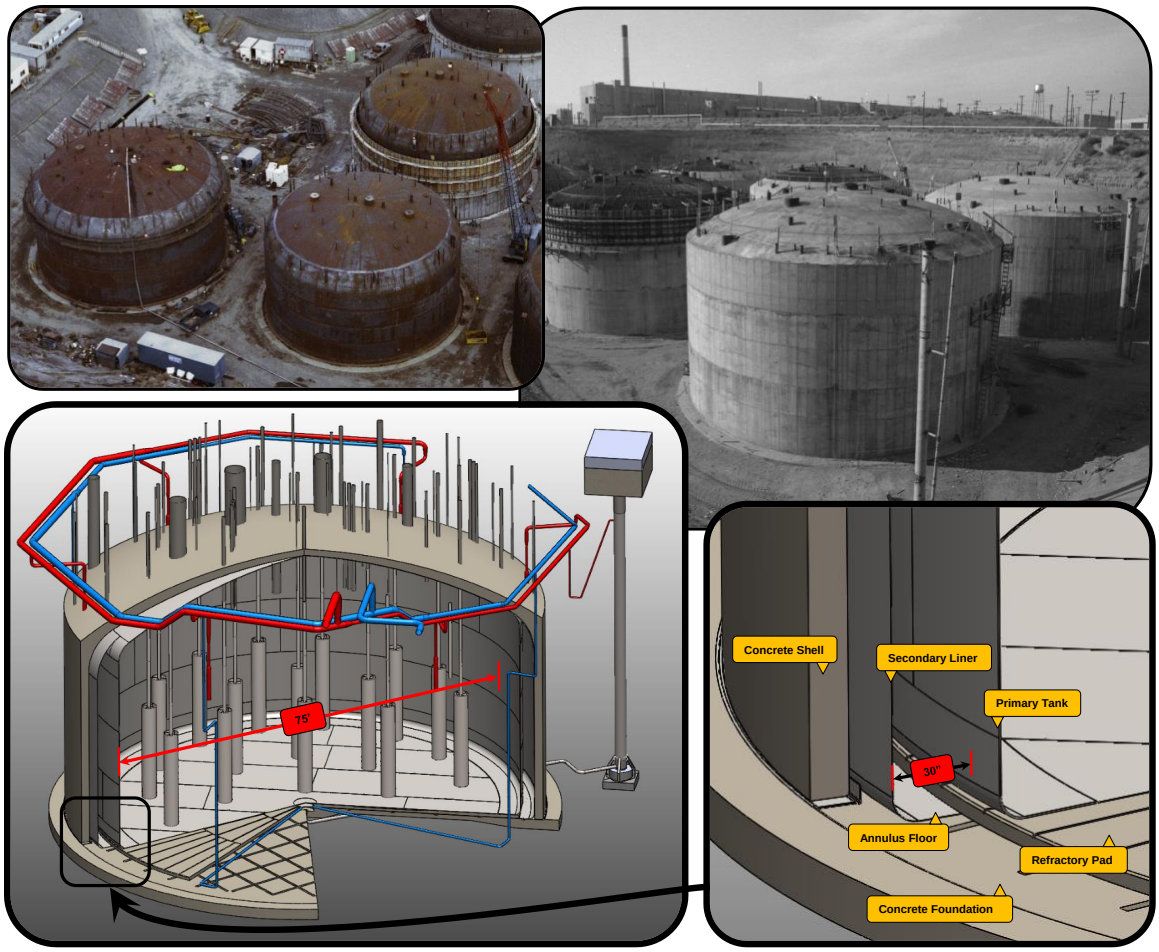


**Figure 2.1**. Hanford Double-Shell Tank Basic Design Detail

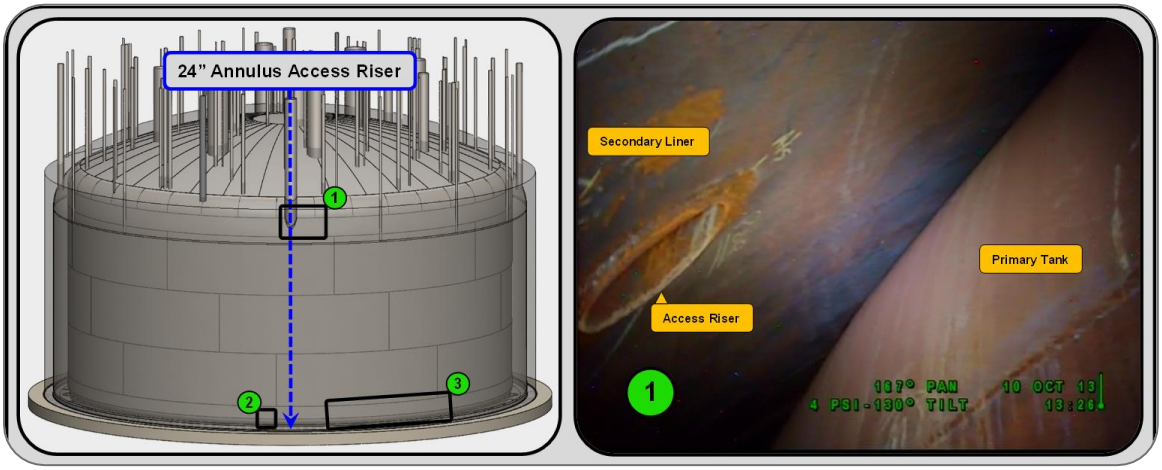


**Figure 2.2**. Double-Shell Tank Annulus Riser Access

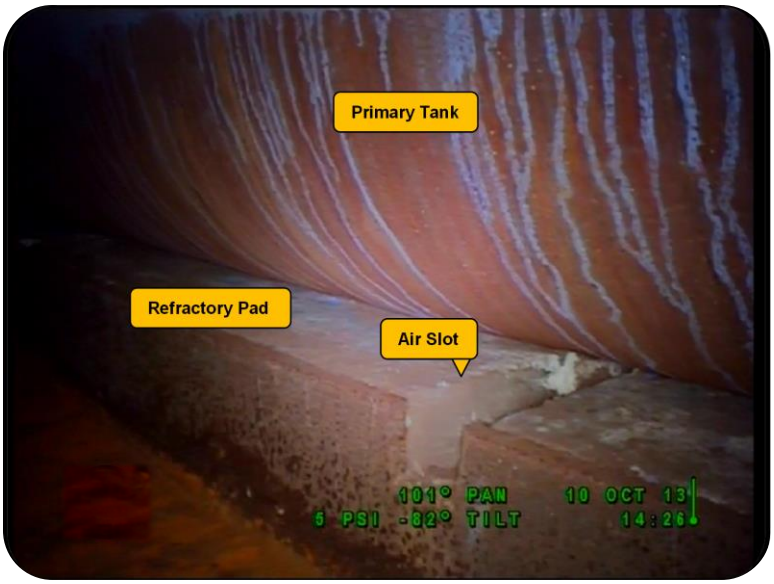


**Figure 2.3**. Example of a Refractory Pad beneath a Primary Liner

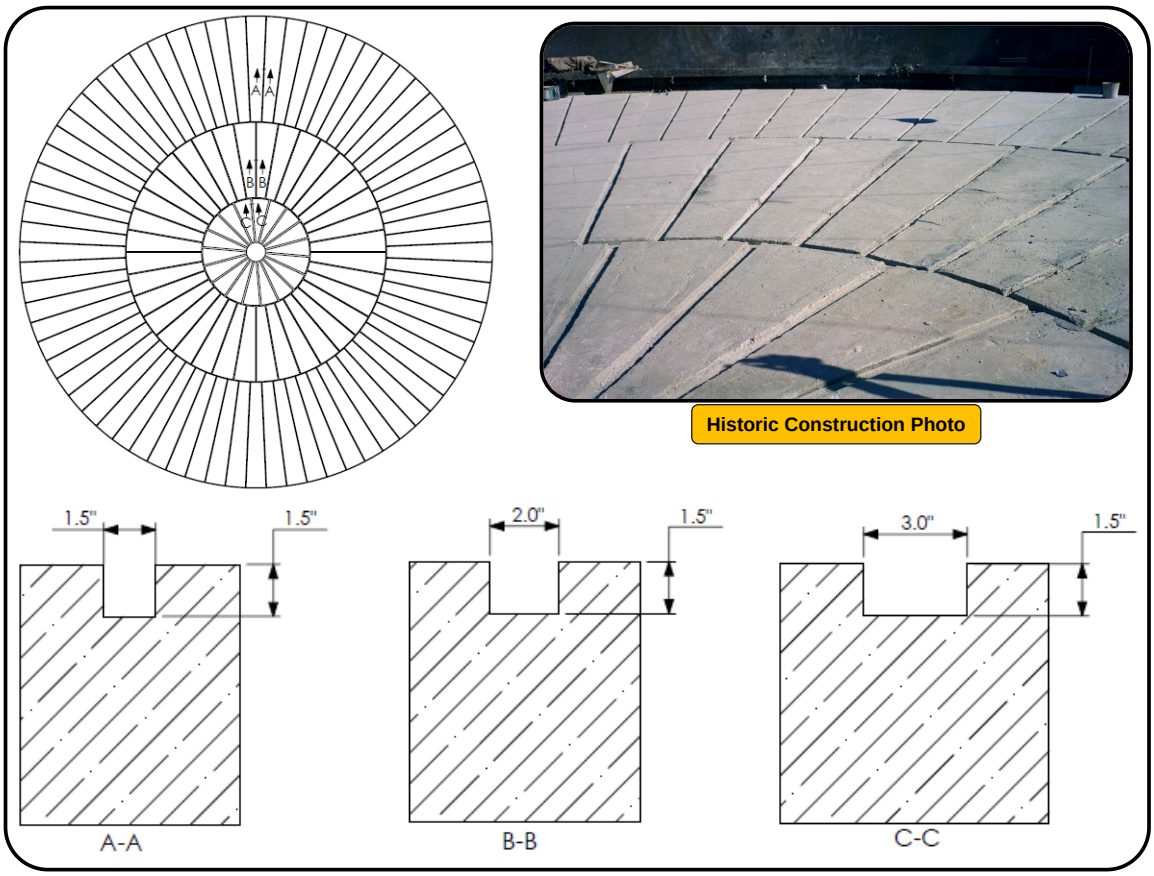


**Figure 2.4**. AY Farm Refractory Pad Air Slot Pattern and Cross Sections

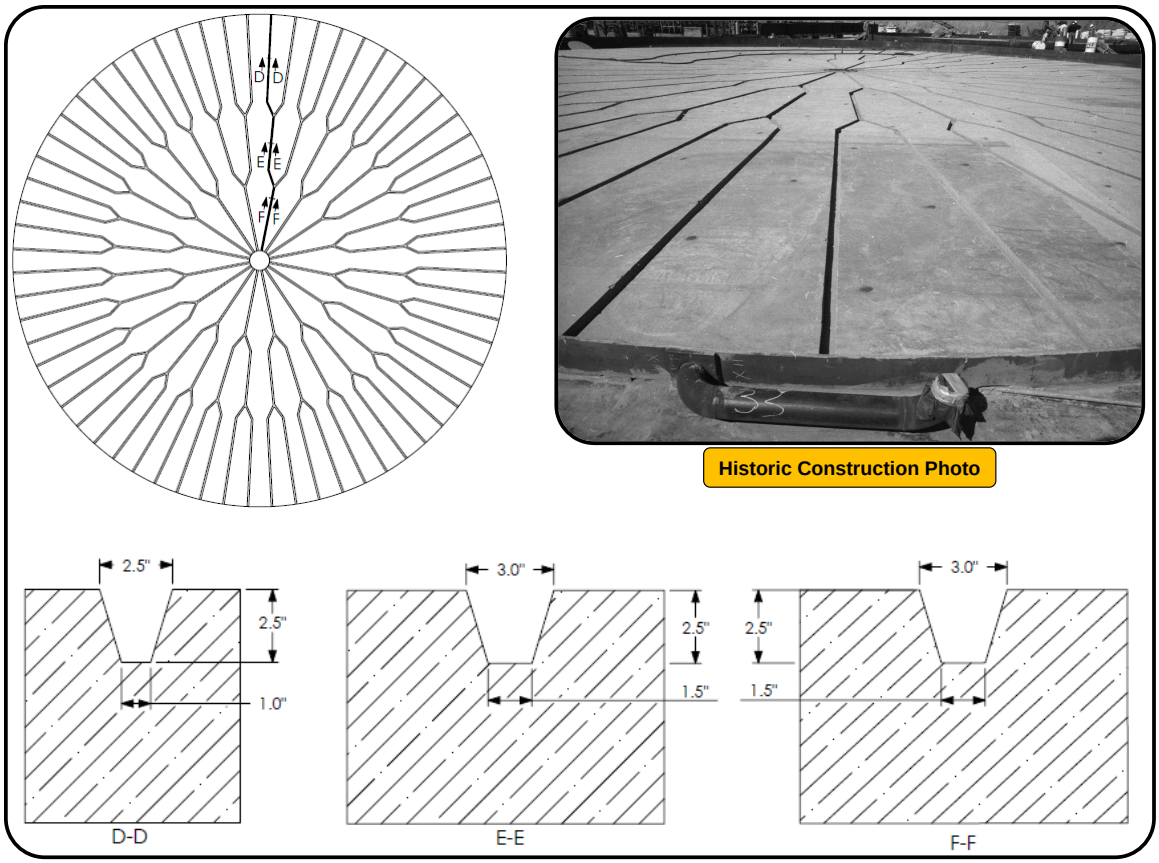


**Figure 2.5**. AZ, SY, AW, AN, and AP Farm Refractory Pad Air Slot Pattern and Cross Sections

# 3.0 Purpose/Objective

## 3.1 Purpose

In FY16, WRPS initiated an NDE Technology Development Program designed to address the need for non-visual volumetric NDE technologies for DST primary liner bottom inspection. The goal of the program is to identify and mature one or more volumetric NDE technologies that can be transitioned to the DST Integrity Program to enable that program to address non-visual volumetric inspection needs for primary liner bottoms identified in the 2015 DST Integrity Improvement Plan (Garfield et al. 2015).

The NDE Technology Development Program consists of three phases that will:

1. perform baseline evaluations of current or emerging NDE volumetric inspection technologies to identify the strongest candidates for flaw detection and flaw characterization in a mockup of a primary liner; then
2. mature the strongest candidate NDE volumetric inspection technologies by adapting transducer hardware and robotic delivery systems to overcome primary liner bottom access challenges; and finally
3. culminate in a system or set of integrated NDE volumetric inspection technologies for demonstration in a full-scale DST cold test platform, where both the ability to detect/characterize flaws and overcome primary liner access challenges will be attempted.

This planned three-phased approach is summarized in Figure 3.1.

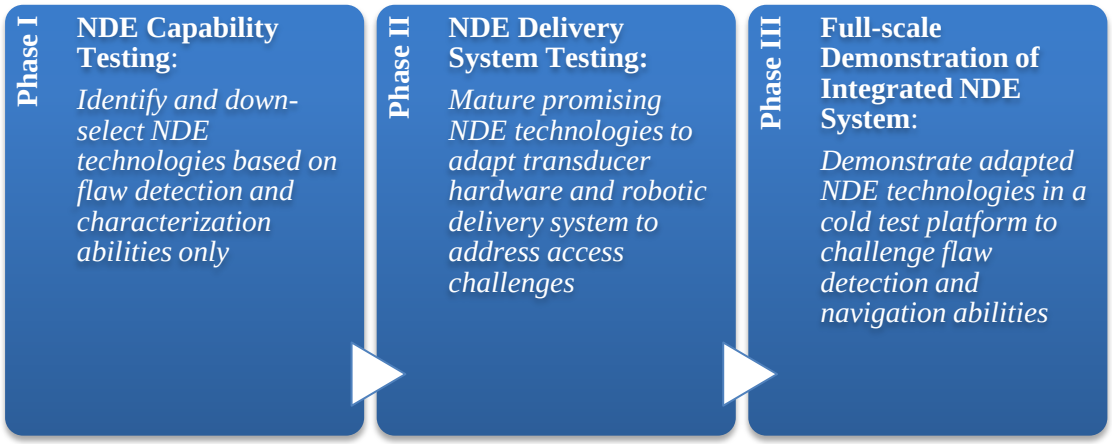


**Figure 3.1**. Summary of NDE Technology Development Program

The NDE Technology Development Program will start with Phase I and be carried out in series. The program is currently in Phase I. The purpose of Phase I is to evaluate and down-select NDE volumetric inspection technologies before advancing one or more to the prototype stage under Phase II and conducting the integrated NDE system demonstration under Phase III.

## 3.2 Test Objectives

To support the programmatic objective of Phase I, emerging or currently available NDE volumetric inspection technologies will be evaluated under two tests to baseline their abilities to detect flaws in a

primary liner mockup against a set of flaw detection and characterization criteria. The test results will be used to identify specific NDE volumetric inspection technologies that are strong candidates for adaptation and maturation under Phase II. Ideally, the technologies identified under Phase I would have the potential to be adapted in a 6-month time period or less under Phase II to overcome primary liner bottom access challenges so they could be adaptable to a robotic delivery system that would be deployable through DST access risers shown in Figure 2.2.

Specific Phase I test objectives are the following:

1. Conduct preliminary *Technology Screening* tests. This will entail providing an opportunity for interested NDE vendors to conduct a preliminary demonstration of their volumetric inspection technology on a mockup of a primary liner that contains surrogate flaws. This opportunity will be open to all interested vendors. *Technology Screening* criteria will be used to identify a qualified set of NDE volumetric inspection technologies based on the abilities of the technologies to detect relatively large flaws in the mockup as well as demonstration or communication of a realistic potential for timely transducer hardware adaptation. Qualified vendors will be invited to return for *Effectiveness Testing*, where the ability of their technology to detect and characterize more challenging surrogate flaws in the primary liner mockup will be evaluated more thoroughly.
2. Conduct Phase I *Effectiveness Testing*. This will entail conducting a more thorough evaluation of each NDE volumetric inspection technology that was qualified during *Technology Screening* tests using a similar primary liner mockup and an augmented set of surrogate flaws. NDE vendors will have approximately three months after *Technology Screening* to make any minor adjustments to their NDE volumetric inspection technologies before returning for *Effectiveness Testing*. More rigorous criteria will be used to determine the extent to which each down-selected technology can address the program's flaw detection and characterization requirements.
3. Use the outcomes of *Effectiveness Testing* to baseline the abilities of selected NDE volumetric inspection technologies against the flaw detection and characterization requirements established for the program to identify and recommend one or more candidate NDE volumetric inspection technologies that can both detect and characterize flaws of interest and have the potential to be adapted to overcome access challenges posed by the primary liner refractory pad and the DST risers.

The results and recommendations from the Phase I preliminary *Technology Screening* test are the subject of this report.

# 4.0 Scope

*Technology Screening* provided an opportunity for four NDE participants to communicate the adaptation potential of their NDE volumetric inspection technology and demonstrate its flaw detection abilities to WRPS and its subcontractor PNNL. Each participant was invited to deliver a presentation on their technology and bring their NDE volumetric inspection technology to demonstrate its flaw detection performance on a primary liner mockup that represents a vertical "swath" or strip of a DST primary liner wall, knuckle, and bottom. The *Technology Screening* tests were conducted January 31 through February 10, 2017.

## 4.1 Mockup

Drawings of the primary liner mockup are provided in Figures 4.1 through 4.3. The plate thicknesses are representative of those found in a majority of the DSTs. The bottom plate lengths and the curved plate (knuckle) length and radius are also representative of those found in DST primary liners. The 4-foot wide, 8-foot long plate represents the mid-floor plate dimensions used in the DSTs. The overall 12-foot length of the mockup is similar to distance from the outside knuckle of a DST to the first air slot transition in the refractory pads upon which primary liners rest. Reaching this first air slot transition is the first navigation goal for NDE volumetric inspection technologies that require direct contact with the exterior surface of the primary liner bottom and will deploy transducers under the primary liner.

## 4.2 Surrogate Flaws

To facilitate the flaw detection portion of *Technology Screening*, the primary liner mockup was fabricated with nine surrogate flaws that represent cracks or corrosion-type pitting. The basis for the *Technology Screening* flaw selection is provided in the test plan document *NDE Technology Development Program for Non-Visual Volumetric Inspection Technology: Phase I Test Plan*. The matrix of *Technology Screening* surrogate flaws is provided in Table 4.1, where the flaw identifications (IDs) correspond with those in the mockup drawings. The flaws are positioned in the 1/2-inch thick bottom plate and the transition weld that joins the 7/8- to 1/2-inch bottom plate such that the legacy flaws in and immediately adjacent to the knuckle of the mockup can be avoided during inspection. The surrogate knuckle flaws support other testing, but are not of interest for *Technology Screening*.

## 4.3 Test Conditions

*Technology Screening* was performed in a non-nuclear research laboratory test environment at PNNL in Richland, Washington. Presentations were delivered by each of the four participants and NDE volumetric inspection technology demonstrations were performed under an open format in a laboratory where all surrogate flaws in the primary liner test mockup were viewable during testing.

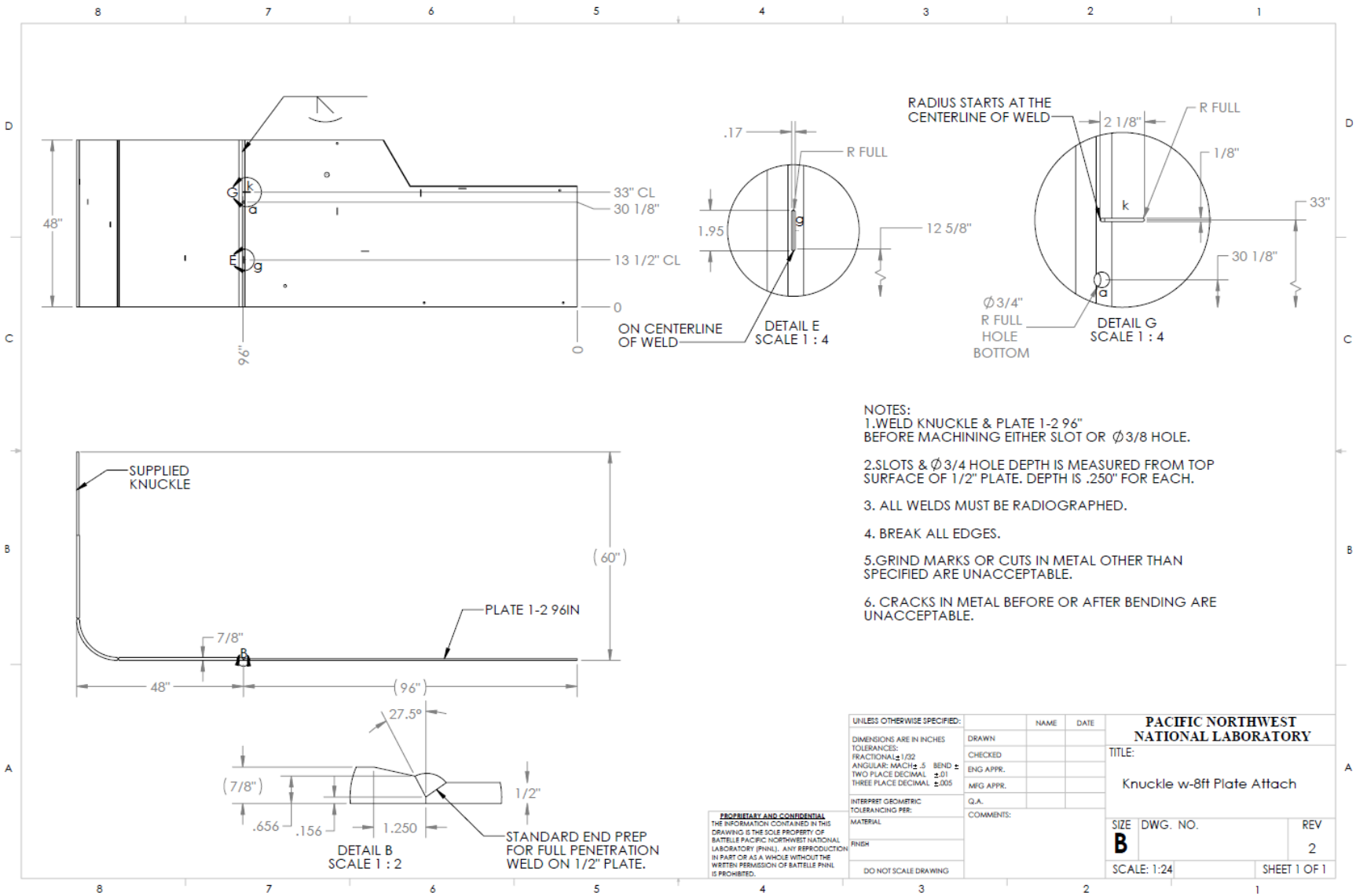


**Figure 4.1**. Top and Side View Drawings of the Primary Liner Mockup for Technology Screening

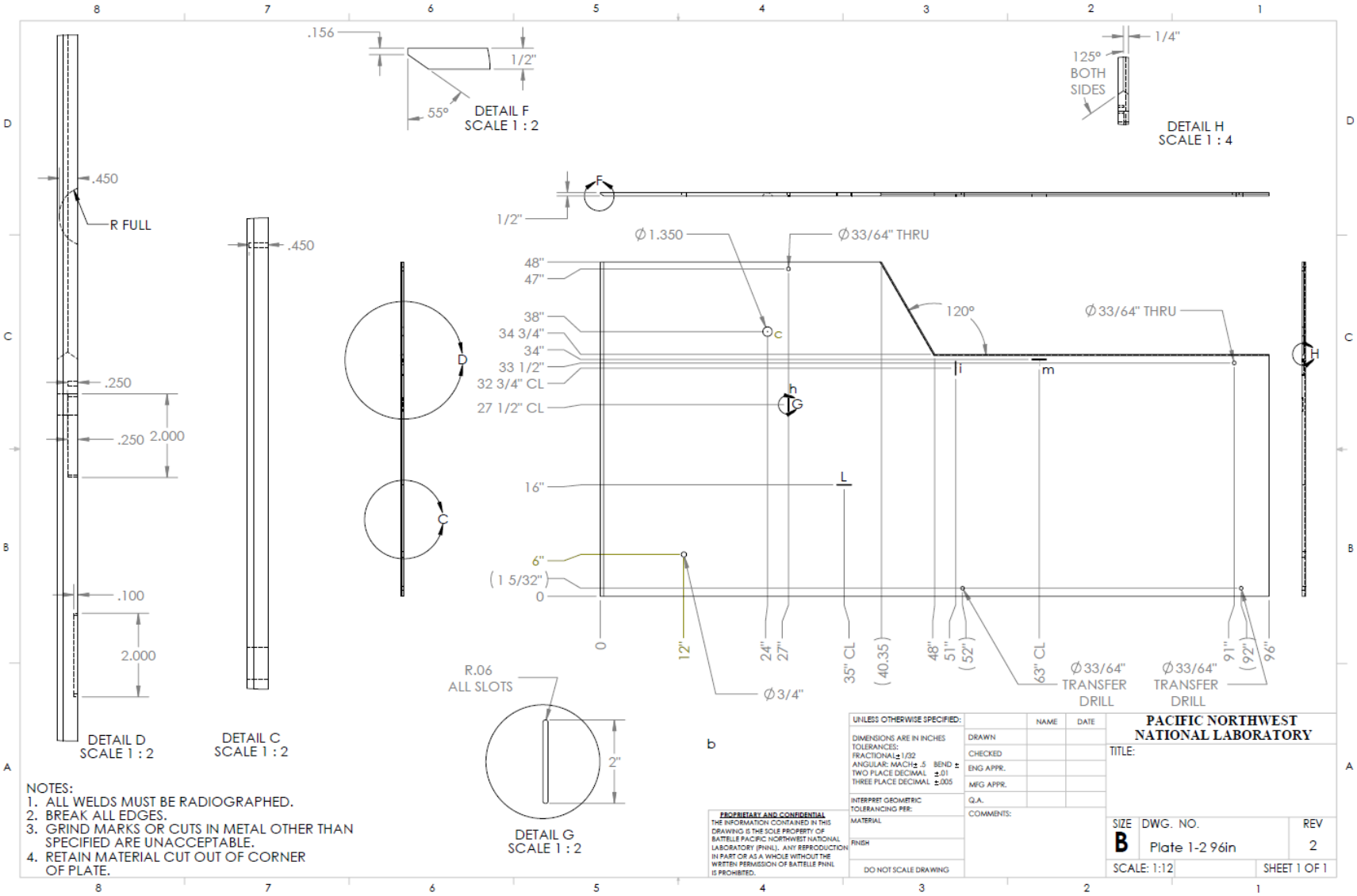


**Figure 4.2**. Top and Side View Drawings of the 4-foot by 8-foot Extension Plate to Contain Surrogate Flaws for Technology Screening

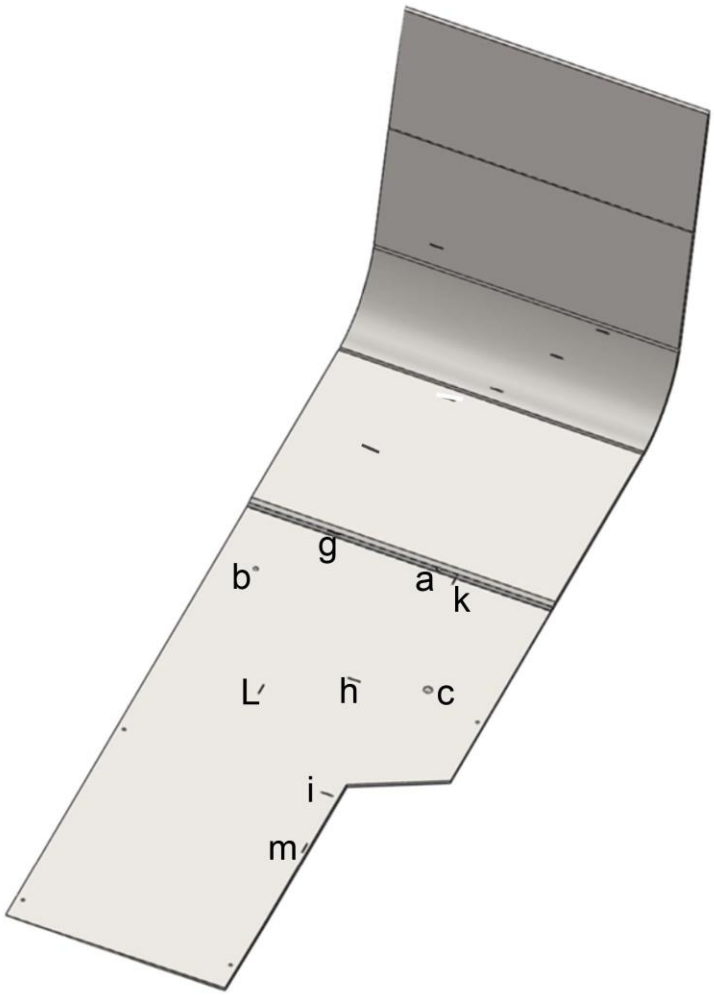


**Figure 4.3**. Illustration of a Top-down View of the Primary Liner Mockup

**Table 4.1**. Surrogate Flaw Matrix to Support *Technology Screening*

| Machined Surrogate Flaw* | Flaw Depth** | Length and Width | Flaw ID in Mockup | Flaw Location and Orientation in Mockup |
|---|---|---|---|---|
| Pit | 50% t, 0.25 in. | 0.75 in. diameter | **a** | 7/8 to ½ in. transition weld |
| Pit | 100% t, 0.50 in. | 0.75 in. diameter | **b** | Base plate |
| Pit | 90% t, 0.45 in. | 1.375 in. diameter | **c** | Base plate |
| Notch | 50% t, 0.25 in. | 2 in. long, 0.125 in. wide | **g** | 7/8 to ½ in. transition weld, circumferential orientation (i.e., parallel to weld) |
| Notch | 20% t, 0.10 in. | 2 in. long, 0.125 in. wide | h | Base plate, circumferential orientation (i.e., parallel to weld) |
| Notch | 50% t, 0.25 in. | 2 in. long, 0.125 in. wide | i | Base plate edge, circumferential orientation (i.e., parallel to weld) |
| Notch | 50% t, 0.25 in. | 2 in. long, 0.125 in. wide | **k** | 7/8 to ½ in. transition weld to base plate, axial orientation (i.e., perpendicular to weld) |
| Notch | 90% t, 0.45 in. | 2 in. long, 0.125 in. wide | L | Base plate, axial orientation (i.e., perpendicular to weld) |
| Notch | 50% t, 0.25 in. | 2 in. long, 0.125 in. wide | m | Base plate edge, axial orientation (i.e., perpendicular to weld) |

* Surrogate flaws will be machined full-radius pits with a diameter-to-depth ratio of 3:1 and machined notches.

** t = plate thickness

The primary liner mockup was oriented in the representative upright position as shown in Figure 4.3 to accommodate the four different NDE methods. The mockup was placed on a mobile platform with approximately four inches of gap between the base of the mockup and the base of the platform.

# 5.0 Quality Assurance

The Quality Management M&O Program Description document describes PNNL's DOE Pacific Northwest Site Office-approved Quality Assurance Program (QAP, also known as the QAPD). The source requirements for this QAP are: 10 CFR 830, *Nuclear Safety Management, Subpart A, Quality Assurance Requirements (QA Rule)*, and DOE O 414.1D, Attachment 1, *Contractor Requirements Documents (CRD), Quality Assurance (QA Order)*. The PNNL QAP uses the following voluntary consensus standards in deployment of the QAP:

ASME NQA-1-2000, *Quality Assurance Requirements for Nuclear Facility Applications, Part I: Requirements for Quality Assurance Programs for Nuclear Facilities (from Former NQA-1)*.

ASME NQA-1-2000, *Quality Assurance Requirements for Nuclear Facility Applications*, as graded using NQA-1-2000 Subpart 4.2, *Guidance on Graded Application for Quality Assurance (QA) for Nuclear-Related Research and Development* and as appropriate for the level of risk involved.

ASME NQA-1-2000, Part II, Subpart 2.7, *Quality Assurance Requirements for Computer Software for Nuclear Facility Applications*. These requirements, in addition to the requirements contained in Part I of NQA-1-2000, are the basis for PNNL's graded software QA controls including Safety Software.

Additional standards may be applied to address unique work activities or customer requirements on a project-by-project basis.

This work is designated by WRPS as Quality Level 3, which requires PNNL to operate under its Quality Assurance Program. The quality assurance requirements for this project are provided through PNNL's standards-based management approach entitled "How Do I?" (HDI). The HDI program allows for a graded QA approach to meet the requirements of individual projects.

# 6.0 Methods

Each of the four participants brought different non-visual volumetric NDE technologies and approaches for flaw detection in the bottom plates of the DST primary liner mockup. This section is organized into the following sub-sections: Sections 6.1 through 6.4 summarize the different technique, equipment, and inspection approach taken by each of the four participants—Guidedwave, Innerspec, Penn State, and Southwest Research Institute (SwRI).

## 6.1 Guidedwave

The demonstration conducted by Guidedwave consisted of a guided-wave phased-array technique where a single transducer containing several ultrasonic elements produced and steered an acoustic guided wave in the test material. This approach used specific time delays and excitation amplitudes for each element of the array to produce a guided wave in a specific direction. The data acquisition hardware controlled these delays and varied them in such a way to produce a 360° inspection around the single sensor. This approach required access to and direct contact with the bottom plate of the mockup and the use of a shear couplant to propagate the guided wave into the test material. The liquid couplant is easily removed with a minimal amount of water and wiping. The guided-wave sensor is shown in Figure 6.1, and their test report is included as Appendix A.

**Figure 6.1**. Guided-Wave Sensor

Guidedwave selected a 165 kHz, 30-element phased-array sensor for interrogation of the screening mockup. The active element portion of the transducer array would be small enough to fit into the air slots; however, modest re-design of the housing would be required to reduce height and to accommodate remote coupling delivery. Primarily, the sensor was used to make measurements on the 0.5-inch thick bottom plate of the mockup. Some measurements were also made on the 0.875-inch bottom plate and on the 0.5-inch wall plate above the knuckle weld. Data were acquired with the probe in a variety of locations on the mockup. Figure 6.2 shows the inspection locations for the 0.5-inch thick bottom plate not including the five locations along the simulated access channel along a diagonal on the plate used to generate composite images.

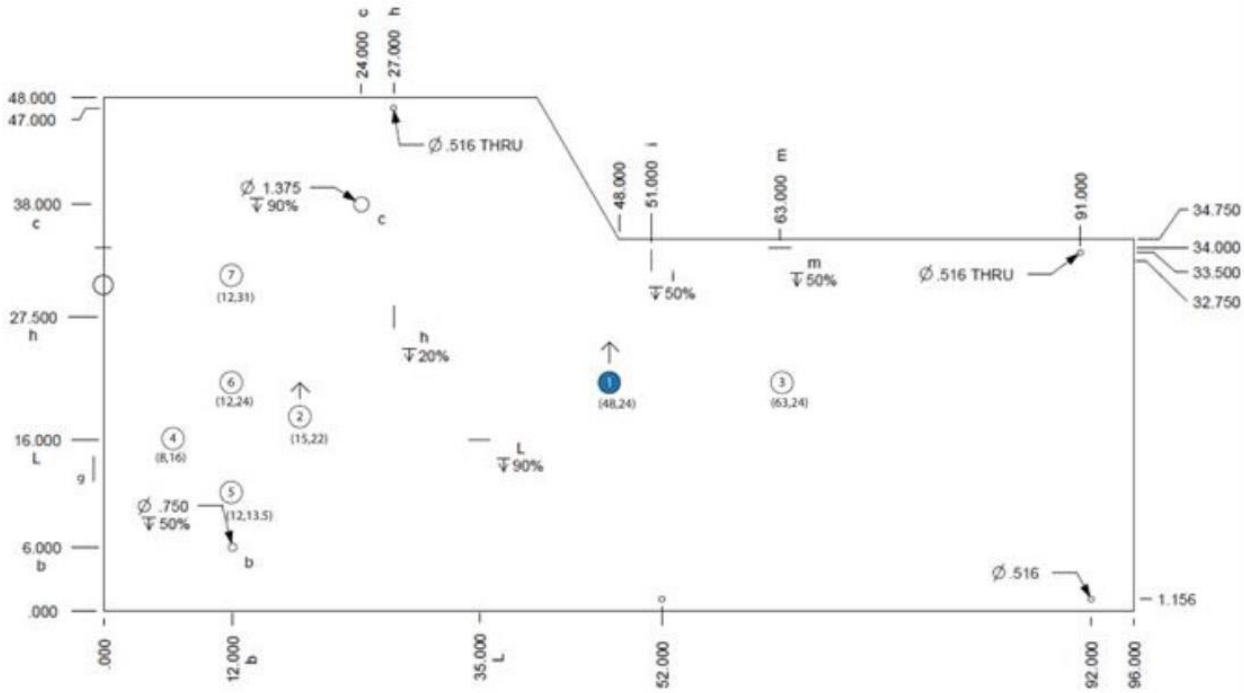


**Figure 6.2**. Inspection Locations on the 0.5-inch Bottom Plate

## 6.2 Innerspec

Multiple EMAT approaches were demonstrated by Innerspec for detecting the surrogate flaws in the DST mockup. All techniques required access to and direct contact with the bottom plate of the mockup. One EMAT technique used an adhesive-backed magnetostrictive strip that was temporarily attached to the mockup for generating shear horizontal guided waves (Figure 6.3). The other techniques demonstrated did not require the use of the magnetostrictive strip or couplant and used Lamb waves in both a pitch-catch-attenuation and pulse-echo mode, and shear vertical waves in pulse-echo mode. This combined technique consisted of two aligned EMAT sensors separated by a known distance. One sensor was operated as both the transmitter and receiver for the pulse-echo mode, and the other sensor was operated as the receiver for acquiring the pitch-catch-attenuation mode data (Figure 6.4). Unfortunately, the data from Innerspec's shear vertical approach was deleted by the vendor, so no results are documented in the report. Documentation by Innerspec (included as Appendix B) indicated the shear vertical approach was capable of flaw detection with good signal-to-noise ratios, but not as well as the magnetostrictive EMAT approach. For these two reasons, the evaluation of this vendor is focused on the magnetostrictive EMAT approach.

Measurements performed with the magnetostrictive EMAT featured the strip placed on the top surface of the bottom plate along the long edge, perpendicular to the weld direction. An EMAT sensor consisting of a meander coil circuit in a short flexible strip was then placed over the magnetostrictive strip as shown in Figure 6.3. This configuration induced guided waves that traversed across the bottom plate of the mockup. The magnetostrictive EMAT sensor was placed at several locations along the magnetostrictive strip and manually angled at each position to control sound beam direction and detect reflections from welds and the surrogate flaws. The magnetostrictive EMATs were used as Innerspec's main technology for the DST inspections; therefore, the analysis was conducted on this technique. The flexible strip magnetostrictive EMAT would currently fit within the air slots; however, an external housing would be

required to accommodate an air bladder that would be used to pressure couple the magnetostrictive layer and flexible strip to the tank bottom.

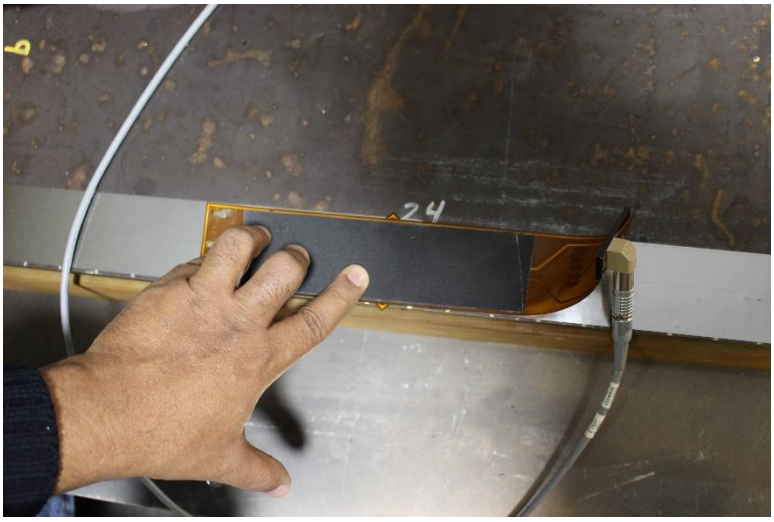


**Figure 6.3**. EMAT Technique Using Magnetostrictive Strip

**Figure 6.4**. EMAT Pitch-Catch and Pulse-Echo Technique

## 6.3 Penn State

The demonstration conducted by Penn State used a permanent magnet EMAT approach where Lorentz force transduction was used to generate acoustic guided waves (shear horizontal waves) in the mockup. Their test report is included as Appendix C. The technique required access to and direct contact with the bottom plate of the mockup. No couplant was required for this approach. Removing the magnetically attached EMAT from the tank bottom required a force of several pounds; however, it was demonstrated that similar sensitivities could be achieved with as much as one millimeter separation between the transducer and the steel bottom.

The system demonstrated used two EMAT sensors that were approximately 1-inch × 1-inch and used permanent magnets within the sensors for the necessary magnetic field. Data were acquired by generating

shear horizontal (SH) waves at 250 kHz in SH0, SH1, and SH2 modes. One sensor was used as the transmitter and the other as the receiver. The transmitter-receiver pair were used on the 0.5-inch thick plate in three configurations—through-transmission, pitch-catch, and pulse-echo.

The through-transmission configuration used a transmitter and receiver separated by 29 inches, which represents the spacing between adjacent air slots. The sensor pair was kept in alignment as shown below in Figure 6.5. Data were collected by moving the EMAT sensor pair in 1-inch increments over regions of the mockup containing four surrogate flaws.

**Figure 6.5**. Through-Transmission Configuration

The pitch-catch configuration consisted of placing the transmitter and receiver at a 45° orientation relative to the direction of the weld in the mockup as shown in Figure 6.6. In this configuration, measurements were made by placing the transmitter in a specific location and acquiring data with the receiver in 1-inch steps moving along a path perpendicular to the weld direction. The data from these positions were then combined to produce a composite image using synthetic aperture focusing technique (SAFT) processing algorithms.

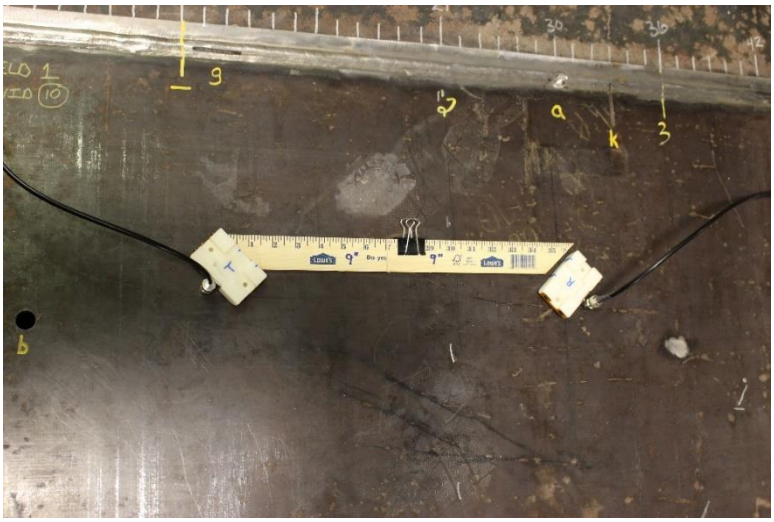

**Figure 6.6**. Pitch Catch Configuration

For the pulse-echo configuration, shown in Figure 6.7, the transmitter and receiver were used side-by-side with the active areas of the sensors in alignment. This setup required an electromagnetic shield to be placed between the transmitter and the receiver. SAFT processing was performed to reconstruct the raw data into an image. The data collected using this approach was intended to validate data collected using the other configurations.

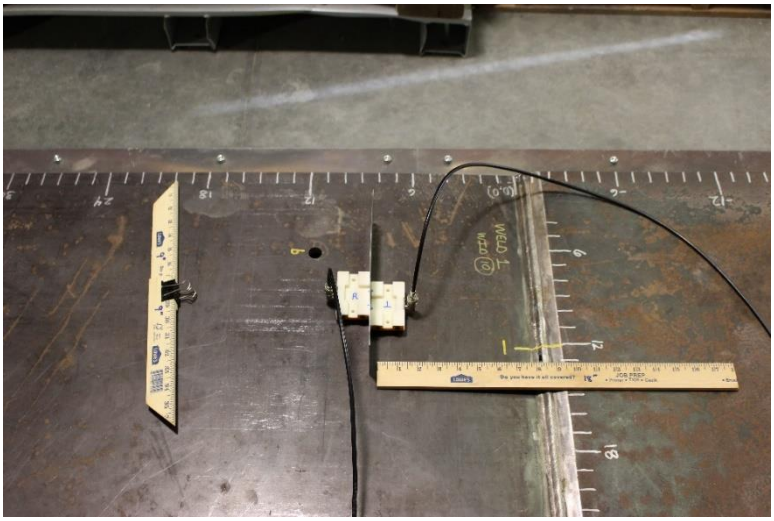

**Figure 6.7**. Pulse-Echo Configuration

The EMAT sensor size is nearly compatible with the range of air slot sizes, but will require modest modifications to the sensor housing to accommodate different air slot cross-section geometries. An Ultratek pulser was used to operate the sensors for *Technology Screening*, although the transducers can be operated by other higher-power commercially available pulsers.

## 6.4 Southwest Research Institute

Southwest Research Institute's (SwRI) test report is provided in Appendix D. They chose to demonstrate a guided wave approach for remotely detecting surrogate flaws in the DST mockup. This magnetostrictive approach employed the use of a magnetically coupled EMAT to generate guided acoustic waves in the test material. The system used a biasing electromagnet that is pulsed with transmit and receive meander coils. The coil spacing is used to determine the inspection frequency. This EMAT approach does not require the use of a couplant or direct access to the primary liner.

The sensor system demonstrated for the technology screening effort was specifically designed to inspect reactor containment vessels, although additional meander coil configurations, producing higher frequencies, were assembled specifically for this demonstration. The demonstrated system was rather large (~ 1 $ft^3$) and heavy (> 200 lbs.) but SwRI assured that the sensor could be reduced in size and weight to accommodate deployment through a 24-inch riser into the annulus space of a DST. The system was placed on the primary wall section of the mockup just above the upper knuckle weld. The meander coils, electromagnets, and some circuitry were positioned at the inspection site, and this equipment was connected to the power supply and data acquisition equipment through a long umbilical cable. A side view of the sensor equipment at the examination site is shown in Figure 6.8.

Data were collected by performing line scans across the wall portion of the mockup with the sensor located 5.5 inches above the upper knuckle weld. Figure 6.9 shows the sensor at the starting location of an examination. Data were acquired in 1-inch steps with the sensor being moved to the right as shown in this

figure. At each location, an A-scan display was visible but the data did not become meaningful until the entire set was collected and post-processed with a SAFT technique to produce a composite image of the inspection region. Multiple inspection frequencies—42, 49, 57, and 72 kHz—were used to acquire data on the surrogate flaws in the mockup. A higher inspection frequency is generally more sensitive to smaller discontinuities, but at the expense of propagation distance and signal amplitude. Because the meander coil determines the inspection frequency, multiple examinations were conducted with varying coils and filter settings for a total of nine data sets. Figure 6.10 shows the meander coil being replaced between examinations.

**Figure 6.8**. Side View of the Sensor in Place above the Knuckle for Examining the Surrogate Flaws Remotely

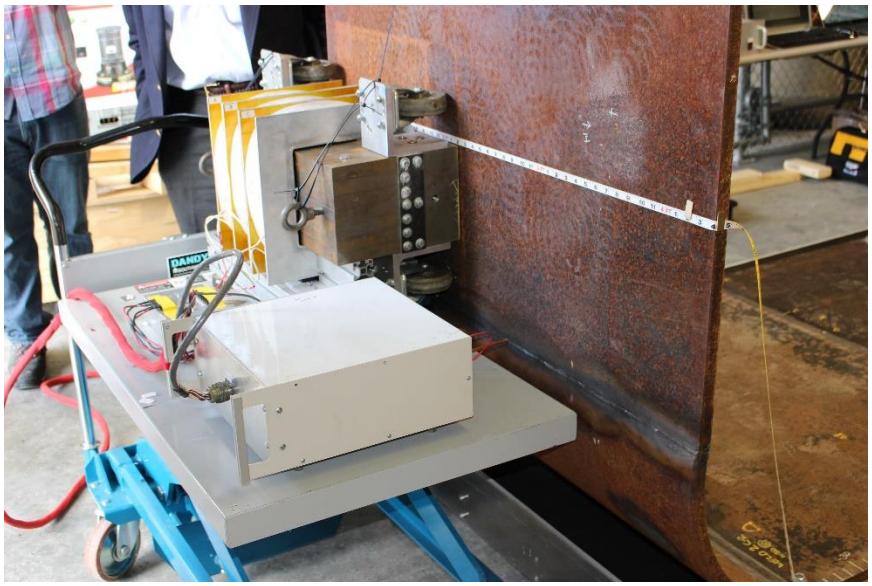

**Figure 6.9**. Sensor at the Starting Position of an Examination

**Figure 6.10**. Meander Coil Being Replaced Between Examinations

# 7.0 Results

The details for each of the nine surrogate flaws in this study and results for each of the four participants on the specific flaws are provided in Sections 7.1 through 7.9. Section 7.10 provides a small summary for the four participants on other features or flaws detected on the mockup but were not specifically part of the *Technology Screening* test. Appendices A through D provide the full detailed results and analysis for each of the participants.

## 7.1 Flaw "a" (Priority Flaw)

Flaw "a" is a 0.750-inch diameter pit with a height of 50% of the plate thickness (0.250 in.) located in the transition weld between the 7/8 inch and ½ inch plate. Pit "a" is in close proximity to Notch "k" as shown in Figure 7.1.

**Figure 7.1**. Photograph of Pit "a" (*left*) and Notch "k" (*right*) Located in the Transition Weld

### 7.1.1 Guidedwave

Pit "a" was detected by Guidedwave at two locations—12 and 16 inches from the transducer location, on the ½-inch bottom plate. When the transducer was 16 inches from the flaw, the data collected at 150 kHz showed a combined response from Pit "a" and Notch "k." When the transducer was 12 inches from Pit "a," the 200 kHz data clearly showed separate signals from Pit "a" and Notch "k" (Figure 7.2). The composite image generated from five different locations along a diagonal path (representing an access channel on the tank floor) at 165 kHz excitation frequency (Figure 7.3) also showed evidence of separation from Pit "a" and Notch "k." The signal-to-noise ratio (SNR) for Pit "a" ranged from 2.7 to 29 dB.

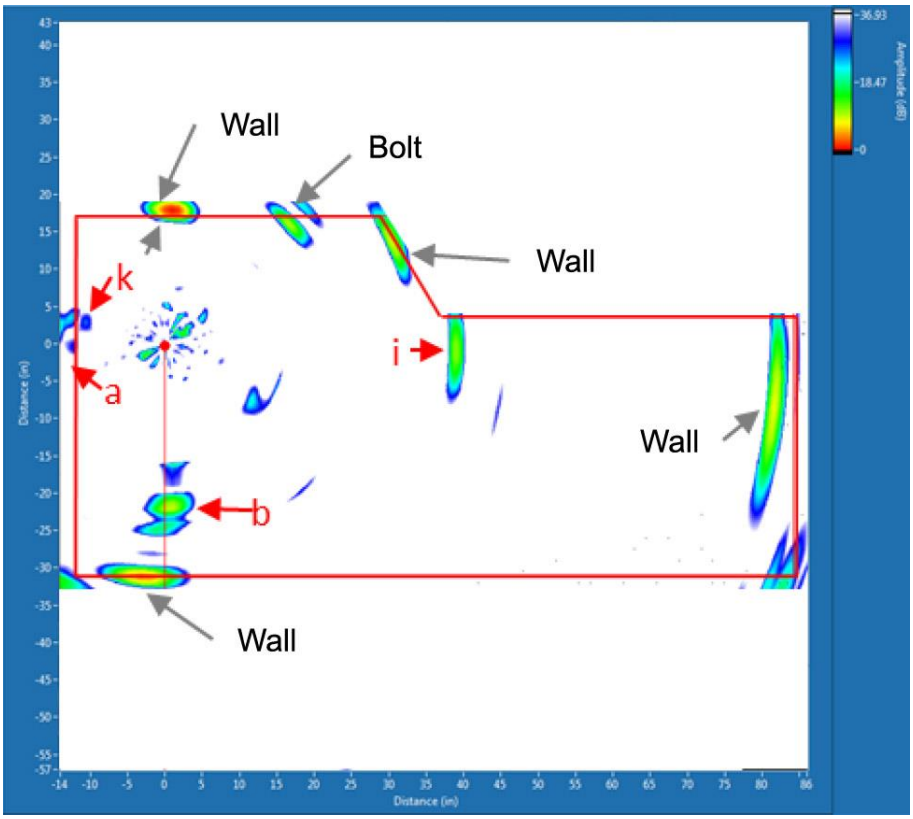


**Figure 7.2**. Guidedwave Phased-Array (GWPA) Scan on Plate 1 at Location 7 Pulsed at 200 kHz

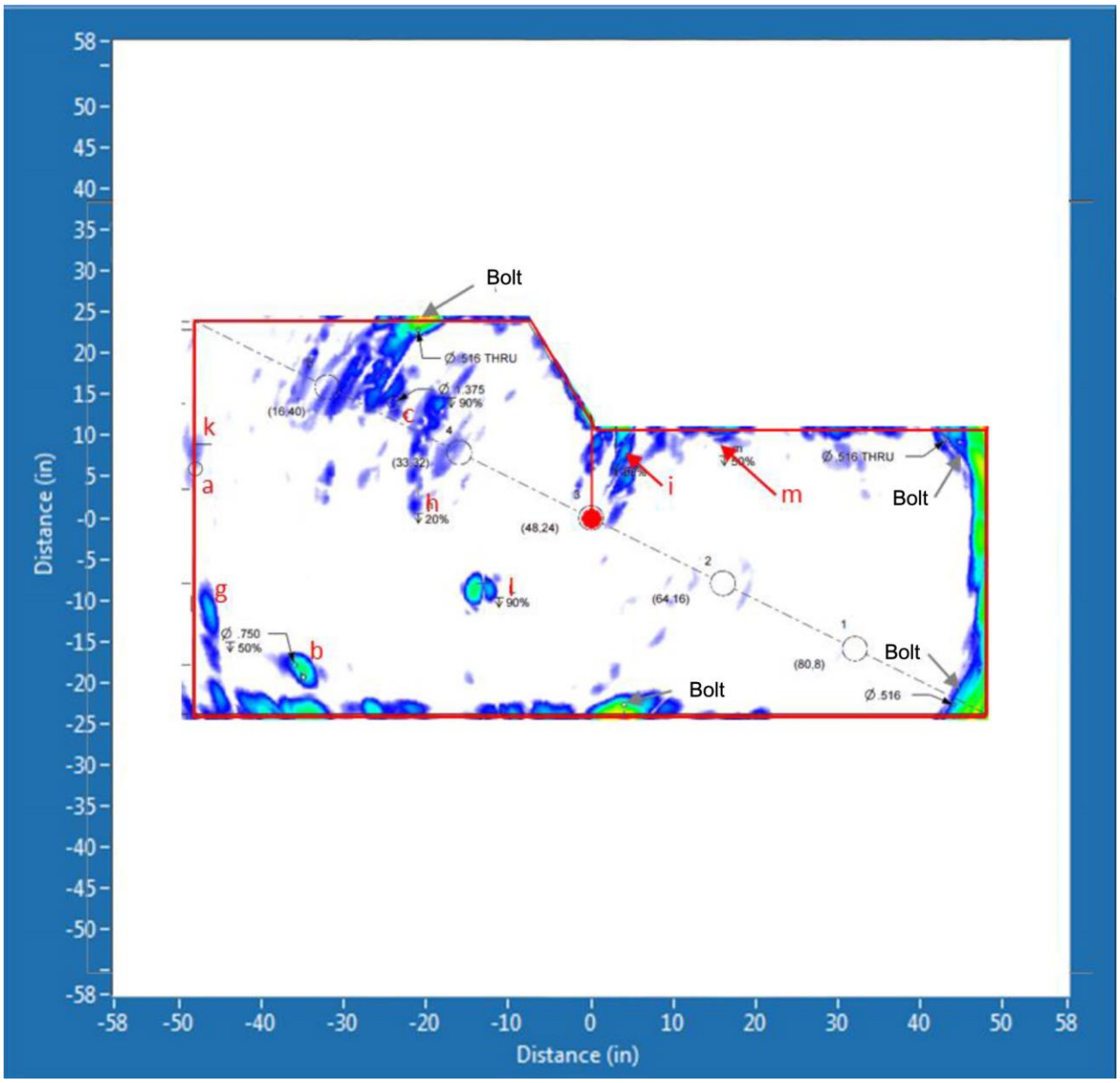


**Figure 7.3**. Composite Image Generated with Data Collected at 165 kHz from Five Locations

### 7.1.2 Innerspec

Pit "a" was masked by the response from Notch "k" when using Innerspec's magnetostrictive sensor from the edge of the plate, which was 28 inches away. The sensor angle was adjusted in an attempt to separate the two signals, but Pit "a" only provided a faint response, which was not enough to call it as a detection (Figure 7.4). **PNNL is not considering this as a detection in the analysis in the next section**. However, Pit "a" was detected using the lamb wave attenuation and reflection techniques with the sensors approximately five inches from the flaw. The SNR for the attenuation technique was −9 dB and 20 dB for the reflection technique (see Figures 22 and 23 in Appendix B).

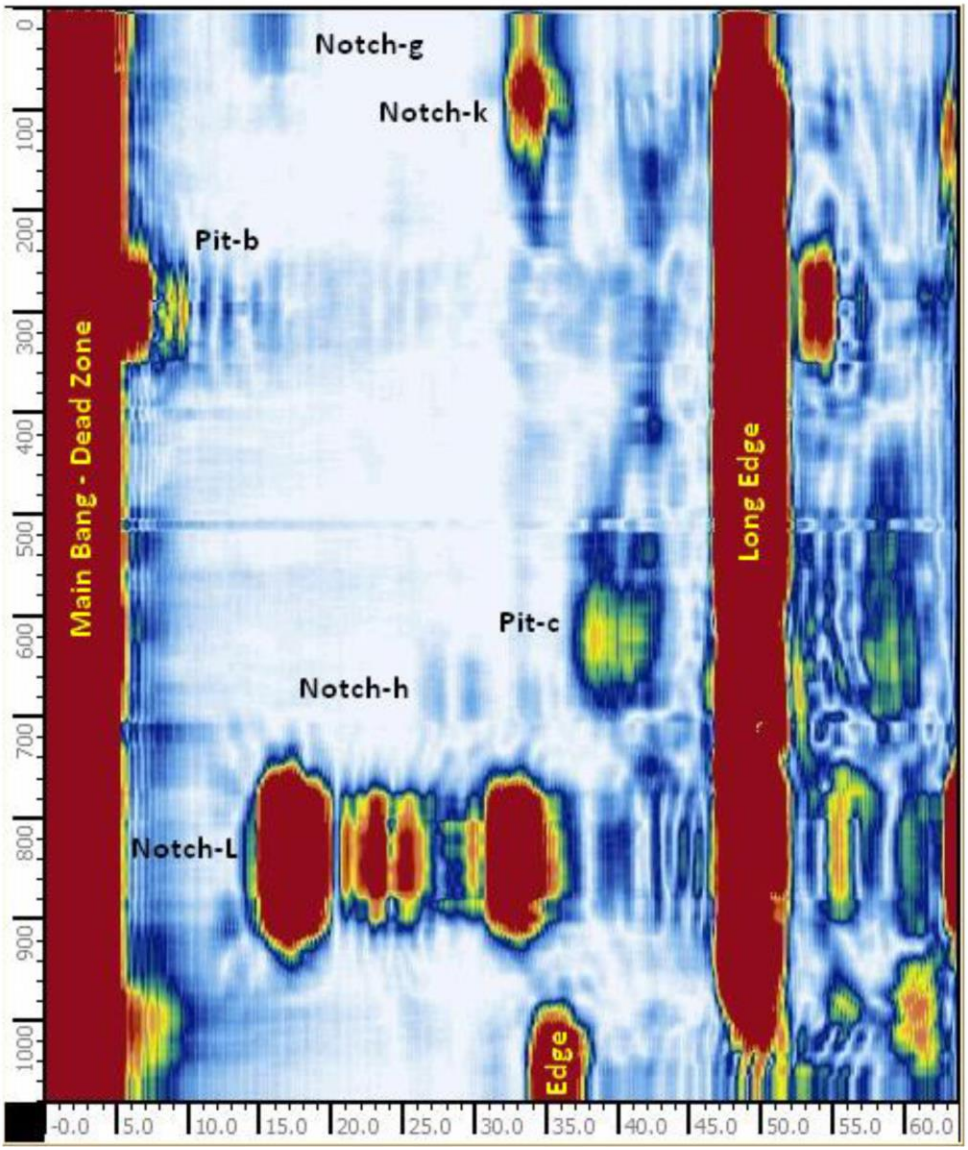


**Figure 7.4**. Manual B-scan from Plate Edge with Magnetostrictive Technique

### 7.1.3 Penn State

Penn State detected Pit "a" using the pitch-catch technique with the transmitter and receiver separated by 35 inches to simulate the distance between adjacent air slots in the DST. In the pitch-catch mode, Pit "a" was detected when the transmitter was closer to the defect. The transmitter ranged from 17 to 24 inches from the flaw during the three different scanning positions. The results compiled using SAFT showed a clear separation between Pit "a" and Notch "k." The SNR for Pit "a" ranged from 4 to 30 dB (Figure 7.5).

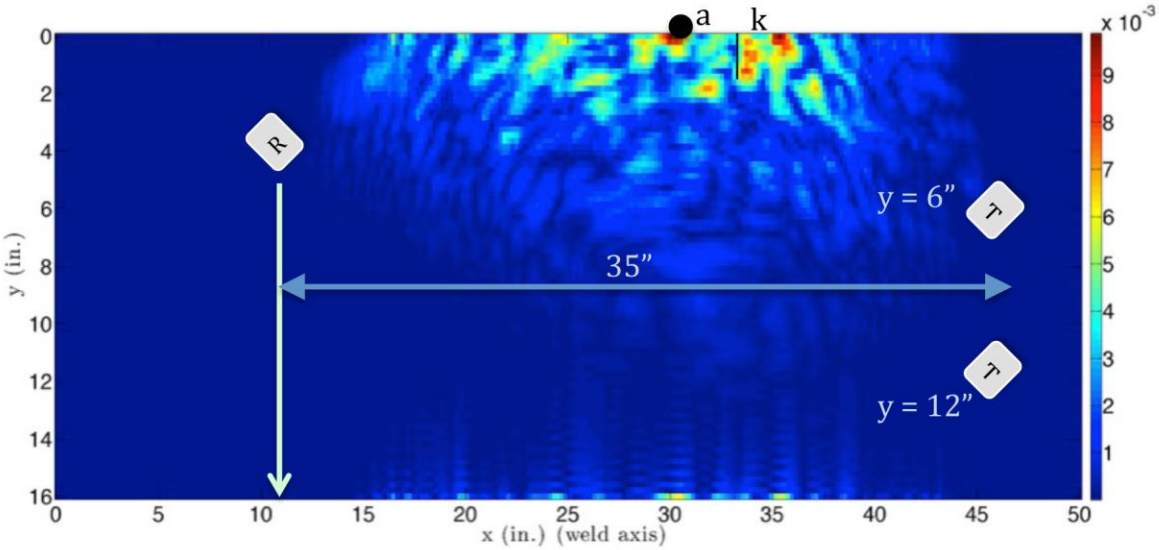


**Figure 7.5**. SAFT-Reconstructed Image Combining the Results Obtained from Three Transmit-Receive Configurations

### 7.1.4 SwRI

SwRI did not detect Pit “a” as this flaw was located in the transition weld. The weld produced a strong reflection from the transition from 7/8-inch to ½-inch plate and masked any response from the defects located in the weld (Figure 7.6).

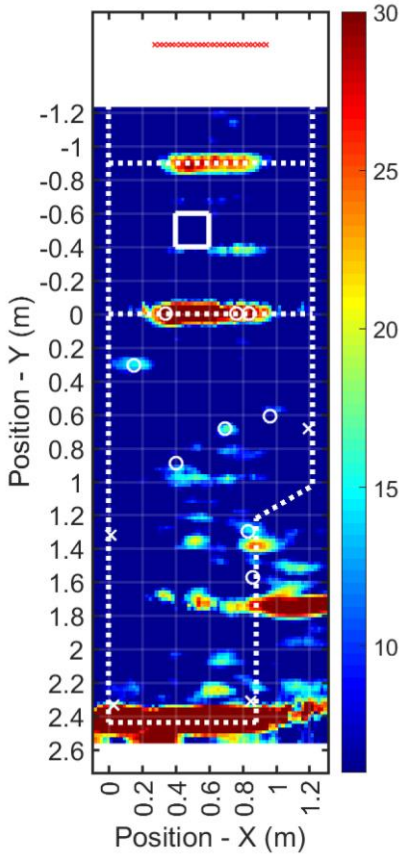


**Figure 7.6**. SAFT Image Produced Using 57 kHz Data Set

## 7.2 Flaw "b" (Priority Flaw)

Flaw "b" was intended to be a 0.750-inch diameter pit that was 50% of the plate thickness (0.250 in.) located in the ½-inch base plate. After receiving the mockup back from the manufacturer, Flaw "b" ended up as a 0.750-inch diameter 100% through-wall hole as displayed in Figure 7.7.

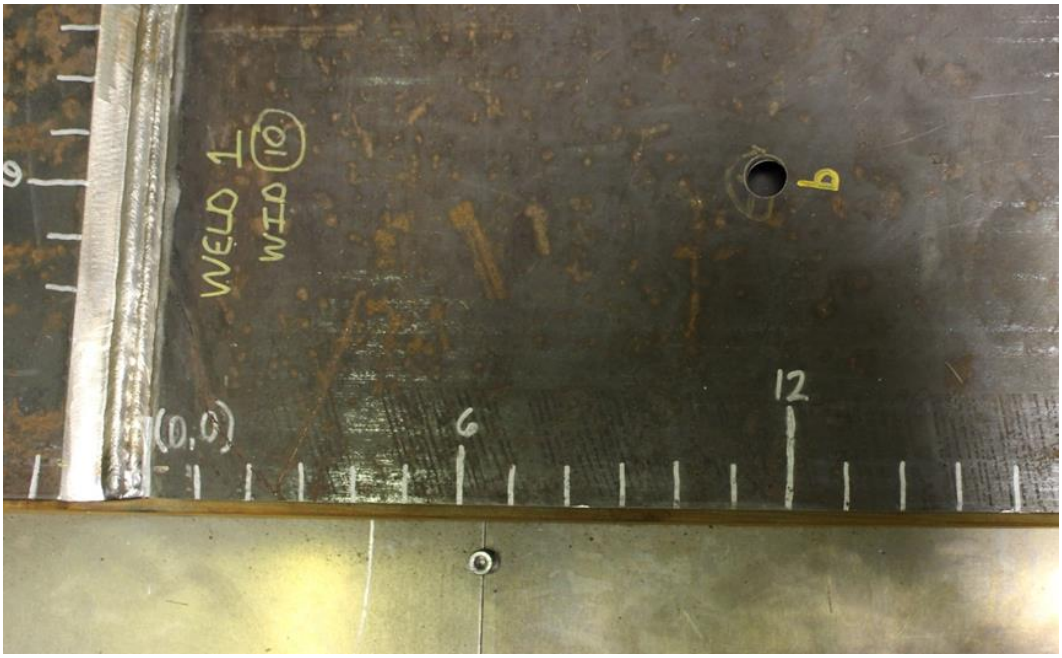


**Figure 7.7**. Photograph of Hole "b"

### 7.2.1 Guidedwave

Hole "b" was detected by Guidedwave from four different transducer locations and three different excitation frequencies (150, 165, and 200 kHz). Transducer Location 7 was the farthest from Hole "b" at 25 inches (Figure 7.2). Hole "b" was also clearly identified in the composite images derived from five different inspection locations at both the 165 and 150 kHz excitation frequency (Figure 7.3 and Figure 25 in Appendix A, respectively). The SNR for Hole "b" ranged from 9.3 to 37.2 dB.

### 7.2.2 Innerspec

Innerspec detected Hole "b" with the magnetostrictive sensor pulsed at 128 kHz frequency from the magnetic strips placed on the edge of the plate, 4 inches away from the flaw. As a result of the main-bang or dead zone from the sensor, this signal was partially masked; however, Hole "b" was a through-wall hole that resulted in a strong reflection with a SNR of approximately 22 dB (Figure 7.4).

### 7.2.3 Penn State

Penn State detected Hole "b" using through-transmission mode with the transmitter and receiver separated by a fixed distance of 29 inches to simulate the distance between adjacent air slots in the DST. In the through-transmission mode, Hole "b" was clearly detected when the transmitter and receiver were at distances of 6 and 23 inches from the flaw. The SNR for Hole "b" ranged from 22 to 37 dB (Figure 7.8).

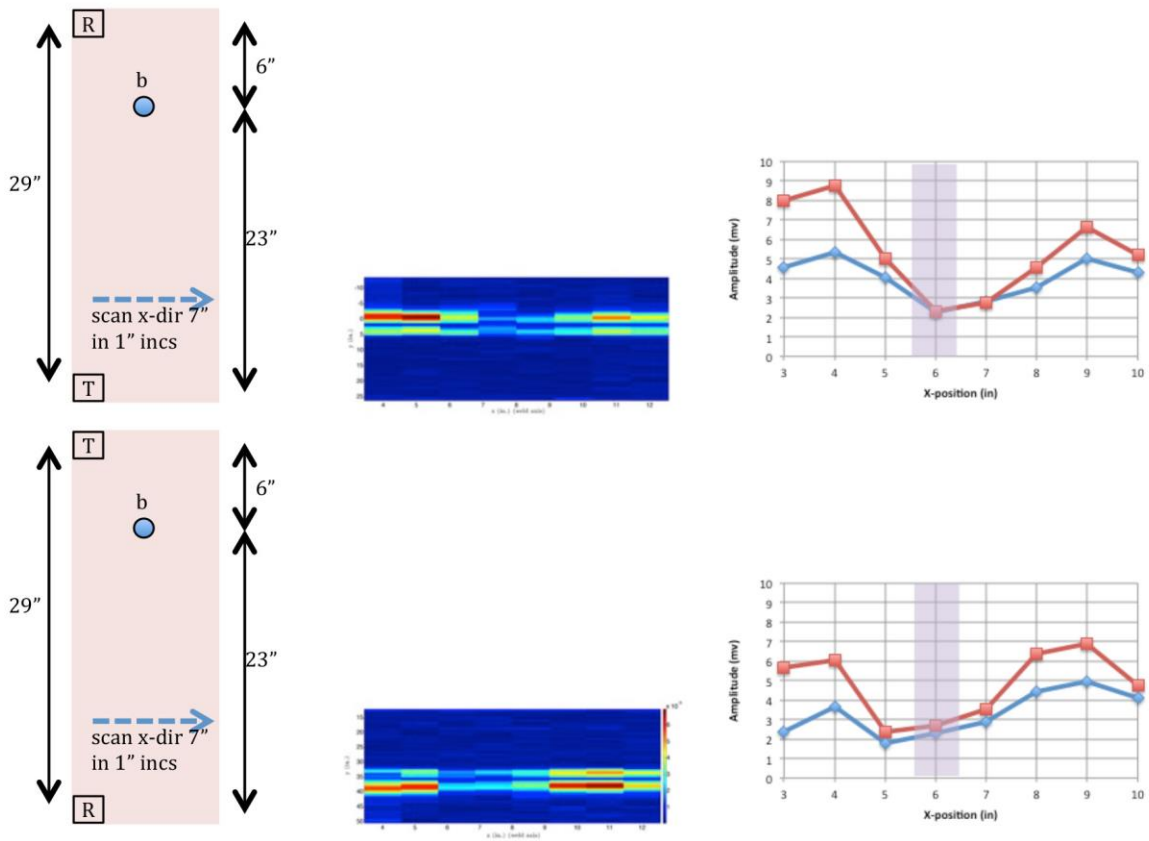


**Figure 7.8**. Test Schematic (*left*), B-scan (*middle*), and Summary Graph (*right*) for Hole "b"

### 7.2.4 SwRI

Hole "b" was clearly detected with a maximum SNR of over 15 dB. The location of the signal from the SAFT-processed image closely agreed with the actual flaw location. The EMAT instrument was positioned 59 inches from Hole "b" (Figure 7.6 and Figure 8 in Appendix D).

## 7.3 Flaw "c" (Priority Flaw)

Flaw "c" as viewed in Figure 7.9 was a 1.375-inch diameter pit with a height of 90% of the plate thickness (0.450 in.) located on the ½-inch base plate.

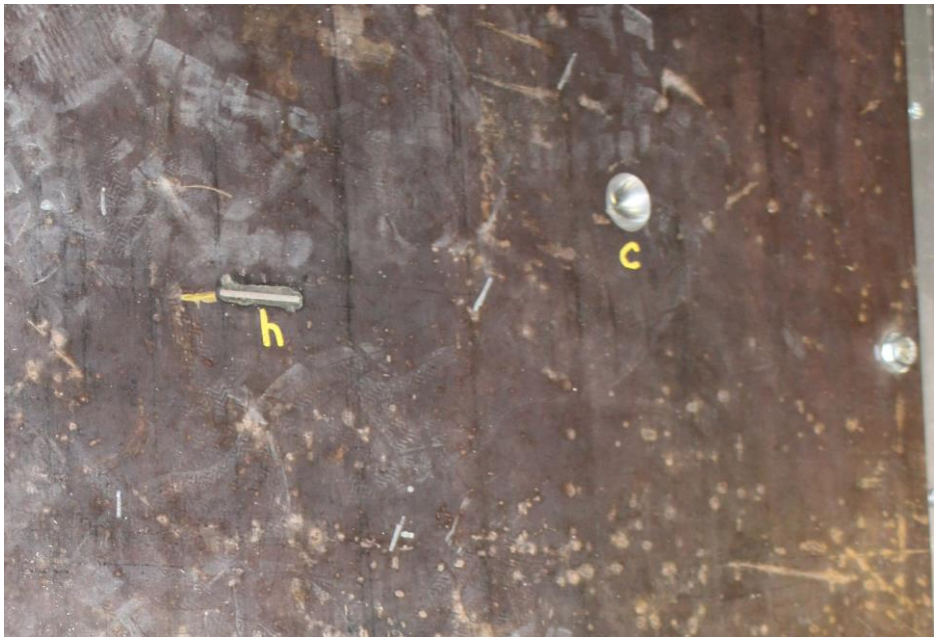


**Figure 7.9**. Photograph of Pit “c” (*right*) and Notch “h” (*left*)

### 7.3.1 Guidedwave

Pit “c” was detected by Guidedwave from four different transducer locations and two different excitation frequencies (150 and 165 kHz). The farthest position Pit “c” was detected from was 28 inches (Figure 7.10). Pit “c” was also detected in the composite images at both the 165 and 150 kHz excitation frequency (Figure 7.3 and Figure 25 in Appendix A, respectively). However, the composite images showed many other indications around this area that could be the result of sound bouncing between multiple defects, plate ends, and bolt holes. The SNR for Pit “c” ranged from 8.7 to 22 dB.

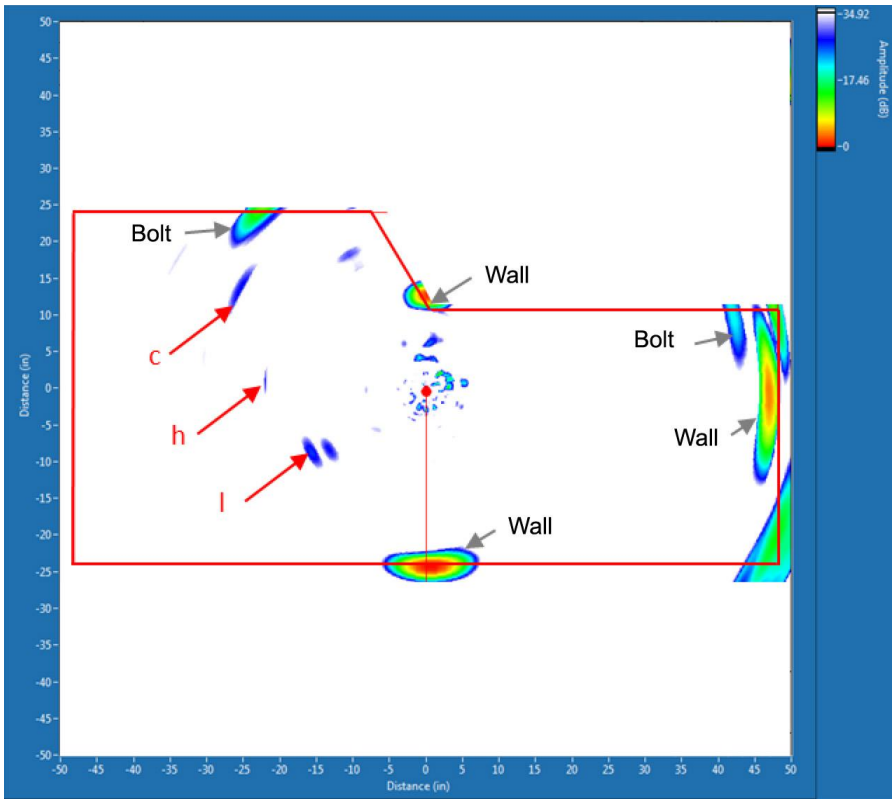


**Figure 7.10**. GWPA Scan on Plate 1 at Location 1 Pulsed at 150 kHz

### 7.3.2 Innerspec

Innerspec detected Pit "c" using the magnetostrictive sensor pulsed at 128 kHz frequency from the magnetic strips placed on the edge of the plate. The sensor was located 36 inches from Pit "c" and the SNR was 19 dB (Figure 7.4).

### 7.3.3 Penn State

Penn State detected Pit "c" using the through-transmission mode with the transmitter and receiver separated by a fixed distance of 29 inches. In the through-transmission mode, Pit "c" was clearly detected when the transmitter and receiver were at distances of 23 and 6 inches from the flaw, respectively. The SNR for Pit "c" ranged from 10 to 25 dB (Figure 7.11).

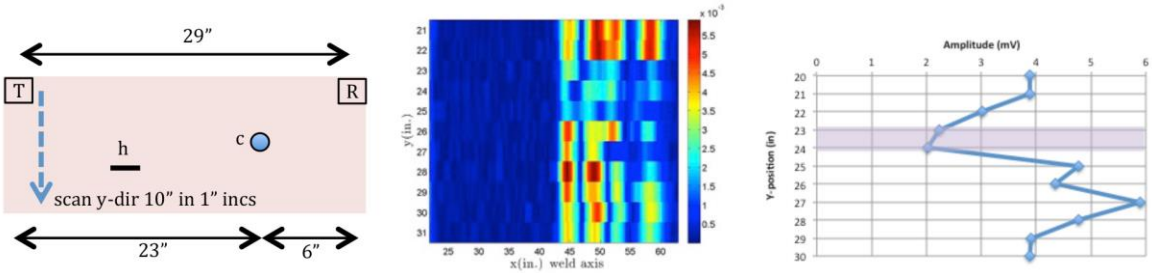


**Figure 7.11**. Test Schematic (*left*), B-scan (*middle*), and Summary Graph (*right*) for Pit "c"

### 7.3.4 SwRI

Pit “c” was detected by SwRI with a peak SNR of over 11 dB. The indication from the SAFT-processed image is approximately 1 inch closer than the actual flaw location. The EMAT instrument was positioned approximately 71 inches from Pit “c” (Figure 7.6 and Figure 9 in Appendix D).

## 7.4 Flaw “g” (Priority Flaw)

Flaw “g” was a 2-inch long, 0.125-inch wide machined notch that had a height of 50% of the plate thickness (0.250 in.). Notch “g” was located in the 7/8 to ½-inch transition weld and oriented parallel to the weld as shown in Figure 7.12.

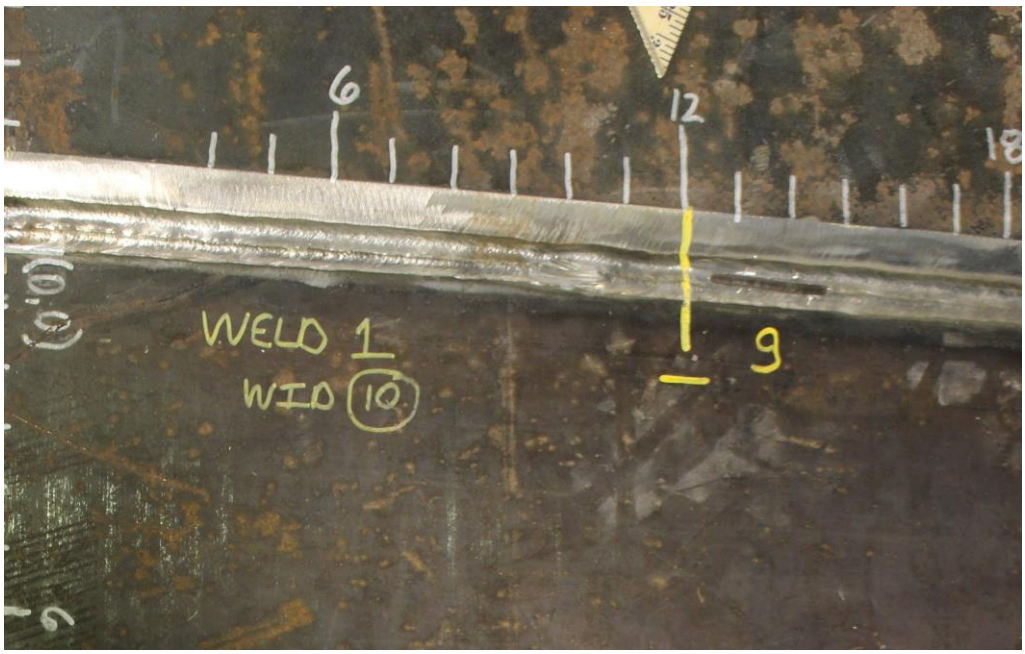


**Figure 7.12**. Photograph of Notch “g” Located in the Transition Weld

### 7.4.1 Guidedwave

Guidedwave detected Notch “g” from two different locations (Locations 4 and 5, Plate 1) on the ½-inch thick base plate and one location (Location 1, Plate 2) from the 7/8-inch thick base plate. Transducer Location 1 on Plate 2 was 28 inches from Notch “g” and was clearly detected as seen in Figure 7.13. The transducer frequencies were at 150 and 165 kHz. Because Notch “g” was located in the weld, the transducer placement needed to be perpendicular to the notch to detect it. Notch “g” was also detected in the composite images at both the 165 and 150 kHz excitation frequency (Figure 7.3 and Figure 25 in Appendix A, respectively). The SNR for Notch “g” ranged from approximately 8 to 32 dB.

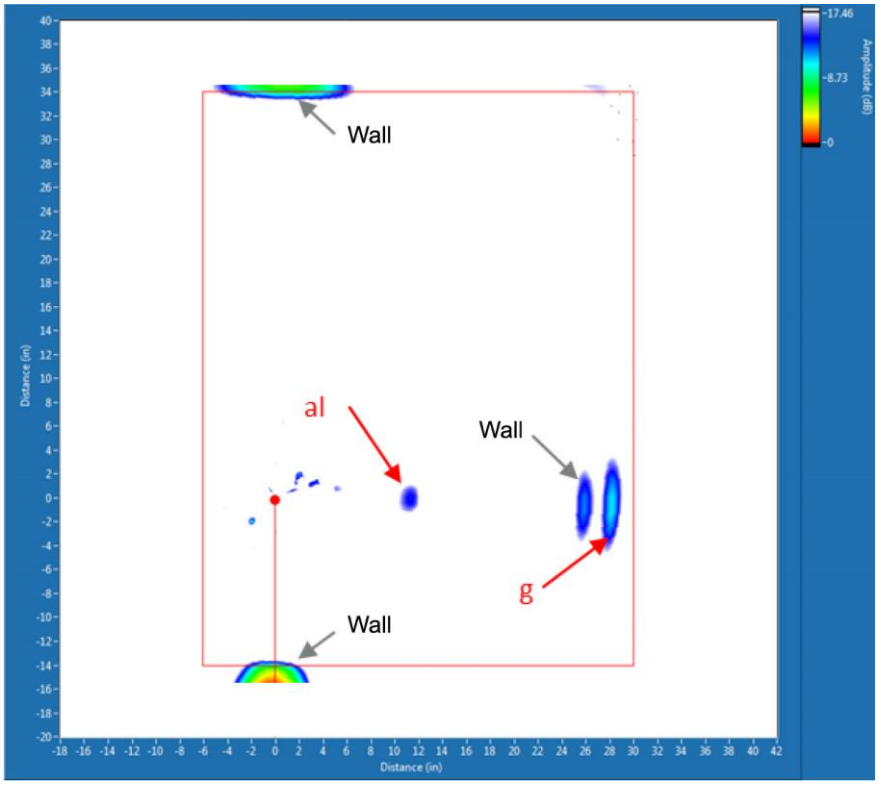


**Figure 7.13**. GWPA Scan on Plate 2 at Location 1 Pulsed with 150 kHz

### 7.4.2 Innerspec

Notch "g" was detected by Innerspec with a SNR of approximately 13 dB from the B-scan image formed by scanning with the magnetostrictive sensor from the edge of the plate. The sensor was located 12 inches from the notch. The sensor angle was adjusted by 15–20°, which increased the SNR by a factor of 3 (Figure 7.4).

### 7.4.3 Penn State

Penn State detected Notch "g" using the pitch-catch technique with the transmitter and receiver separated by 26 inches. In the pitch-catch mode, Notch "g" was detected when the transmitter was closer to the defect. The transmitter ranged from 8 to 19 inches from the flaw during the three different scanning positions. The results compiled using SAFT located Notch "g" within an inch of the true position. The SNR for Notch "g" ranged from 6 to 21 dB (Figure 7.14).

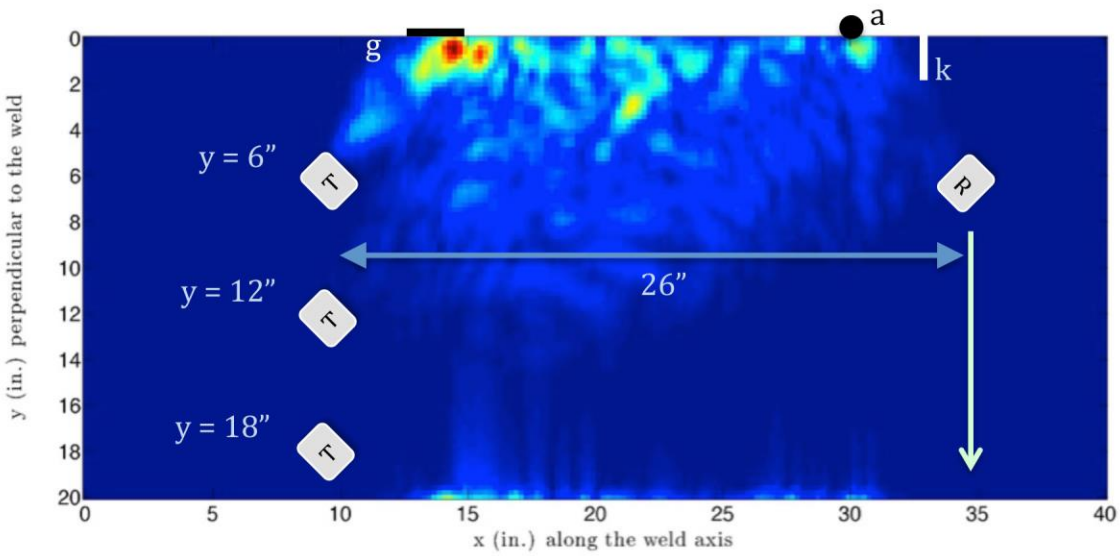


**Figure 7.14**. SAFT-Reconstructed Image Combining the Results Obtained from Three Transmit-Receive Configurations

### 7.4.4 SwRI

SwRI did not detect Notch “g” because this flaw was located in the transition weld. A strong reflection was produced from the 7/8-inch to ½-inch plate transition weld, which masked any response from the defects located in the weld (Figure 7.6).

## 7.5 Flaw “h”

Flaw “h,” shown in Figure 7.9, was a 2-inch long, 0.125-inch wide machined notch with a height of 20% of the plate thickness (0.100 in.). Notch “h” was located near the middle of the ½-inch base plate and oriented parallel to the weld.

### 7.5.1 Guidedwave

Notch “h” was detected from three different transducer locations using two different excitation frequencies (150 and 200 kHz). Transducer Location 3 was the farthest from Notch “h” at 36 inches (Figure 7.15). The SNR ranged from 6.8 to 11.7 dB. Notch “h” was also detected in the composite images at both the 165 and 150 kHz excitation frequencies (Figure 7.3 and Figure 25 in Appendix A, respectively). The composite images of this data show other indications around this area, which could be the result of sound reflecting between multiple defects, plate ends, and bolt holes.

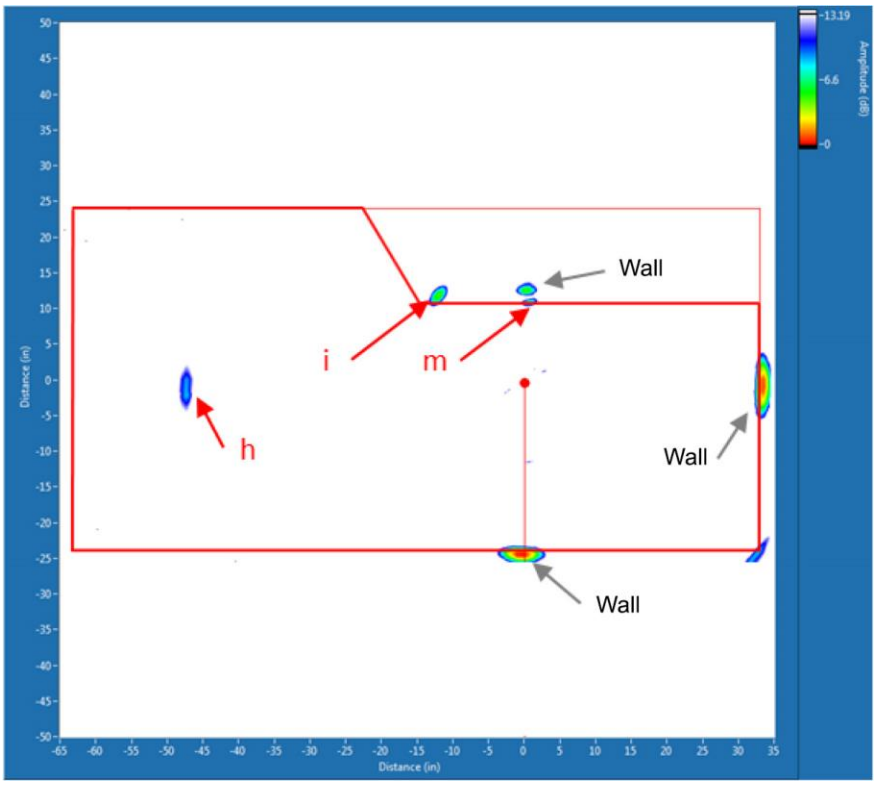


**Figure 7.15**. GWPA Scan on Plate 1 at Location 3 Pulsed at 200 kHz

### 7.5.2 Innerspec

Notch "h" was marginally detected by Innerspec with a SNR of approximately 3 dB from the B-scan image formed by scanning with the magnetostrictive sensor from the edge of the plate. The lower SNR was due to the orientation of the notch relative to the sound path. The sensor was located 26 inches from the center of the notch (Figure 7.4).

### 7.5.3 Penn State

Penn State detected Notch "h" using the through-transmission mode with the transmitter and receiver separated by a fixed distance of 29 inches. In the through-transmission mode, Notch "h" was marginally detected when the transmitter and receiver were at varying distances of 23 and 6 inches or 14 and 15 inches from the flaw. The SNR for Notch "h" ranged from 17 to 20 dB. PNNL would like to note that the data provided does not have a corresponding image (Figure 7.16) to support such a high SNR value.

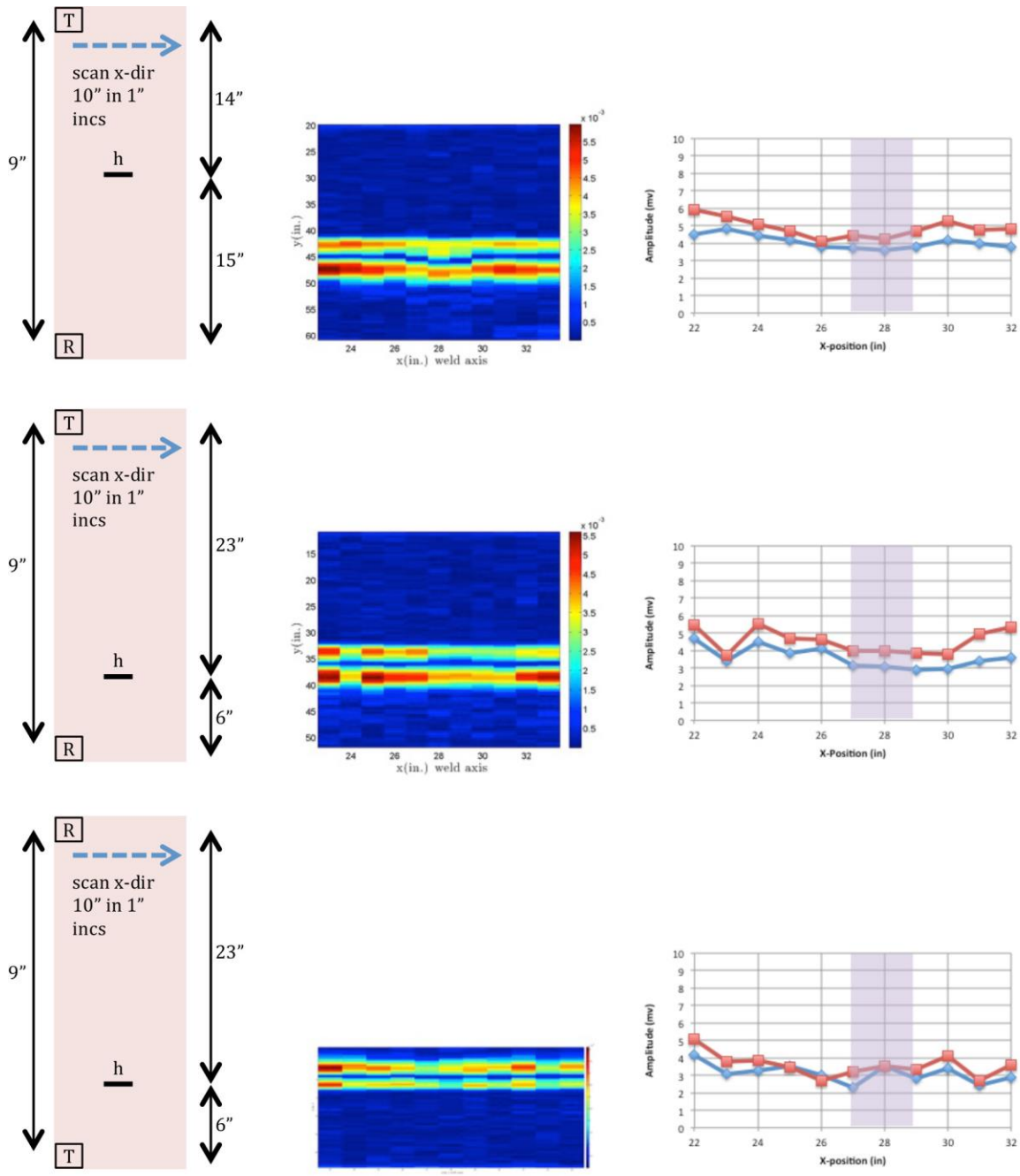


**Figure 7.16**. Test Schematic (*left*), B-scan (*middle*), and Summary Graph (*right*) for Notch "h"

### 7.5.4 SwRI

SwRI detected Notch "h" with a peak SNR of 16 dB. The location of the indication from the SAFT-processed image closely agreed with the actual flaw location. The EMAT sensor was positioned approximately 75 inches from Notch "h" (Figure 7.6 and Figure 9 in Appendix D).

## 7.6 Flaw "l"

Flaw "i" was a 2-inch long, 0.125-inch wide machined notch with a height of 50% of the plate thickness (0.100 in.). Notch "i" was located near the edge of the ½-inch base plate and oriented parallel to the weld direction as seen in Figure 7.17.

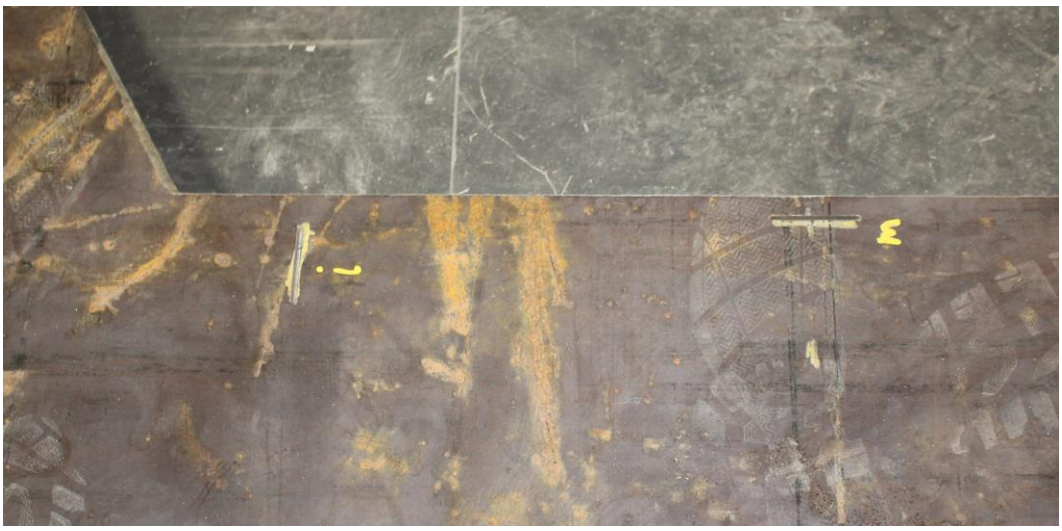

**Figure 7.17**. Photograph of Notch "i" (*left*) and Notch "m" (*right*) Located Near the Beveled Edge of the Plate

### 7.6.1 Guidedwave

Guidedwave detected Notch "i" from three different locations on the ½-inch thick base plate. Notch "i" was 39 inches from transducer at Location 7 and was clearly detected as seen in Figure 7.2. The SNR ranged from 7.4 to 26 dB. The transducer frequencies were at 150 and 200 kHz. Notch "i" was also detected in the composite images at both the 165 and 150 kHz excitation frequencies (Figure 7.3 and Figure 25 in Appendix A, respectively).

### 7.6.2 Innerspec

Notch "i" was detected by Innerspec using the magnetostrictive sensor pulsed at 128 kHz frequency from the magnetic strips placed on the edge of the plate. The sensor was located 31 inches from the notch. The relatively lower SNR (12 dB) was due to the orientation of the notch relative to the sound path (Figure 7.18).

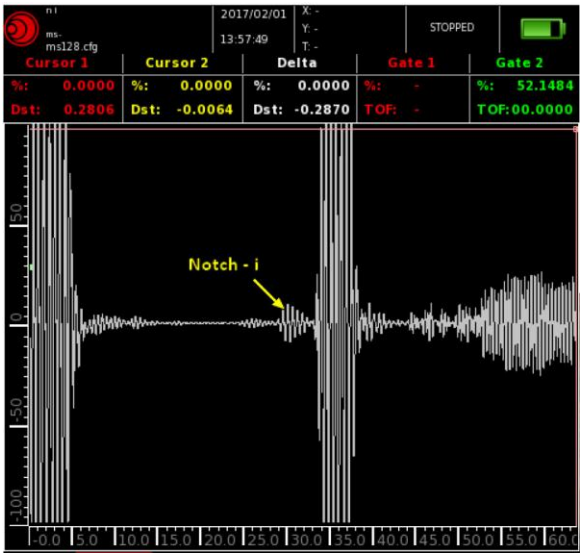


**Figure 7.18**. Manual A-scan from Plate Edge (54 inch) with Magnetostrictive Technique

### 7.6.3 Penn State

Penn State did not have time to examine Notch "I," but would have used the pitch-catch technique to detect and distinguish it from the plate edge reflection.

### 7.6.4 SwRI

Notch "i" was detected by SwRI with a peak SNR of over 25 dB. The indication from the SAFT-processed image was approximately 2.3 inches farther than the actual flaw location. The EMAT instrument location was positioned approximately 98.4 inches from Notch "i" (Figure 7.6 and Figure 10 in Appendix D).

## 7.7 Flaw "k" (Priority Flaw)

Flaw "k" was a 2-inch long, 0.125-inch wide machined notch with a height of 50% of the plate thickness (0.250 in.). Notch "k" was located in the 7/8 to ½-inch transition weld and oriented perpendicular to the weld. Notch "k" was in close proximity to Pit "a" as shown in Figure 7.1 above.

### 7.7.1 Guidedwave

Notch "k" was detected by Guidedwave at two locations, 11 and 18 inches from the transducer location (Figure 7.2 and Figure 7.19), on the ½-inch bottom plate. When the transducer was 18 inches from Notch "k," the 150 kHz data showed a combined response with Pit "a," but when the transducer was moved to a location 11 inches from Notch "k," the 200 kHz data showed clear separation between the flaws. The SNR for Notch "k" ranged from 6 to 29 dB. The composite image at a 165 kHz excitation frequency (Figure 7.3) also showed evidence of separation from Notch "k" and Pit "a."

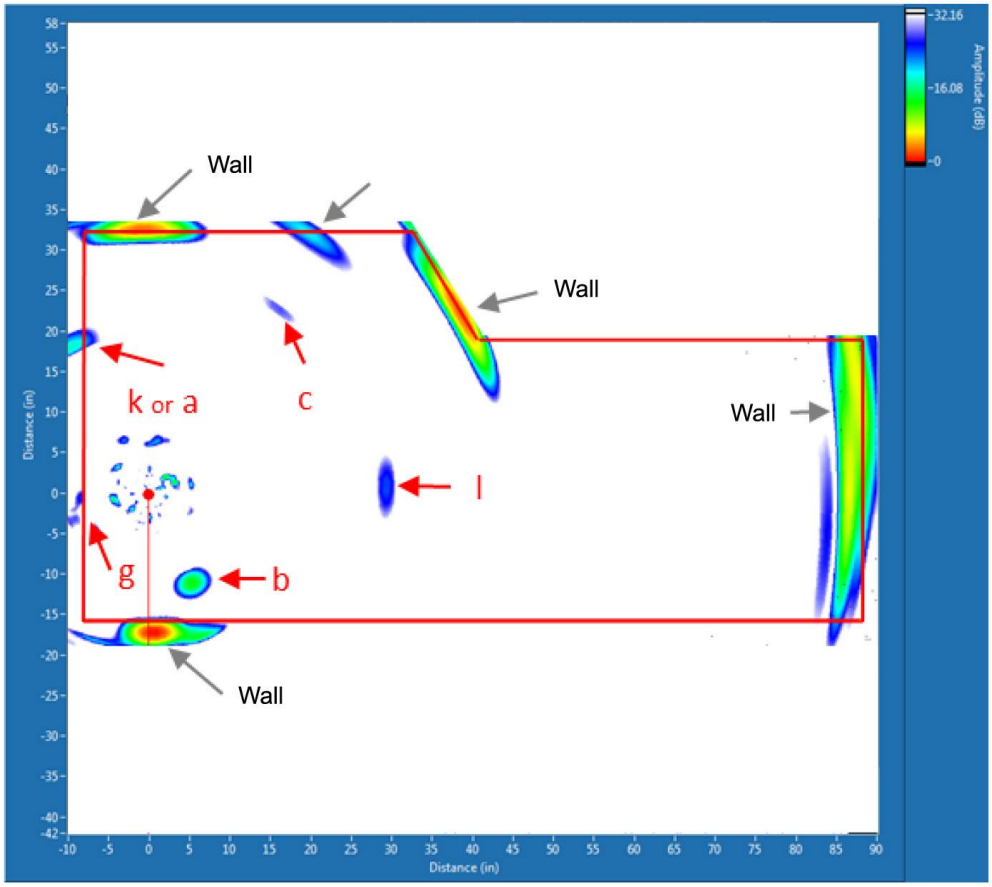


**Figure 7.19**. GWPA Scan on Plate 1 at Location 4 Pulsed at 150 kHz

### 7.7.2 Innerspec

Notch "k" was detected by Innerspec using the magnetostrictive sensor pulsed at 128 kHz frequency from approximately 31 inches away. The sensor angle was adjusted in an attempt to separate the signal from Pit "a," but Notch "k" was oriented perpendicular to the sound propagation direction such that is caused a very strong reflection with a SNR of 20.3 dB (Figure 7.4).

### 7.7.3 Penn State

Penn State detected Notch "k" using the pitch-catch technique with the transmitter and receiver separated by 35 inches. In the pitch-catch mode, Notch "k" was detected when the transmitter was closer to the defect. The transmitter ranged from 14 to 21 inches from the flaw at the three different scanning positions. The results compiled using SAFT show a clear separation between Notch "k" and Pit "a." The SNR for Notch "k" ranged from 2.5 to 31 dB (Figure 7.5).

### 7.7.4 SwRI

SwRI did not detect Notch "k" as this flaw was located in the transition weld. The 7/8 to ½-inch plate transition weld produced a large reflection and masked any response from the defects located in this region (Figure 7.6).

## 7.8 Flaw “L”

Flaw “L” was a 2-inch long, 0.125-inch wide machined notch with a height of 90% of the plate thickness (0.450 in.). Notch “L” was located near the middle of the ½-inch base plate and oriented perpendicular to the weld as shown in Figure 7.20.

**Figure 7.20**. Photograph of Notch “L”

### 7.8.1 Guidedwave

Guidedwave detected Notch “L” from four different locations (with two excitation frequencies—150 and 165 kHz). Transducer Location 4 was the farthest from Notch “L” at 27 inches (Figure 7.19). The SNR ranged from 8.5 to 25.8 dB. Notch “L” was also clearly identified in the composite images at both the 165 and 150 kHz excitation frequencies (Figure 7.3 and Figure 25 in Appendix A, respectively). At Locations 1 and 5 and on the composite images, there are two signals that are likely from the tips of each end of the flaw.

### 7.8.2 Innerspec

Notch “L” was detected by Innerspec using the magnetostrictive sensor pulsed at 128 kHz with the magnetic strips placed on the edge of the plate, 14 inches away from the flaw. Notch “L” was oriented perpendicular to the sound propagation direction causing a very large reflection with a SNR over 25 dB (Figure 7.4).

### 7.8.3 Penn State

Penn State detected Notch “L” using the through-transmission mode with the transmitter and receiver separated by a fixed distance of 29 inches. In the through-transmission mode, Notch “L” was clearly detected when the transmitter and receiver were at varied distances of 23 and 6 inches or 13 and 16 inches from the flaw. The SNR for Notch “L” ranged from 18 to 31 dB (Figure 7.21).

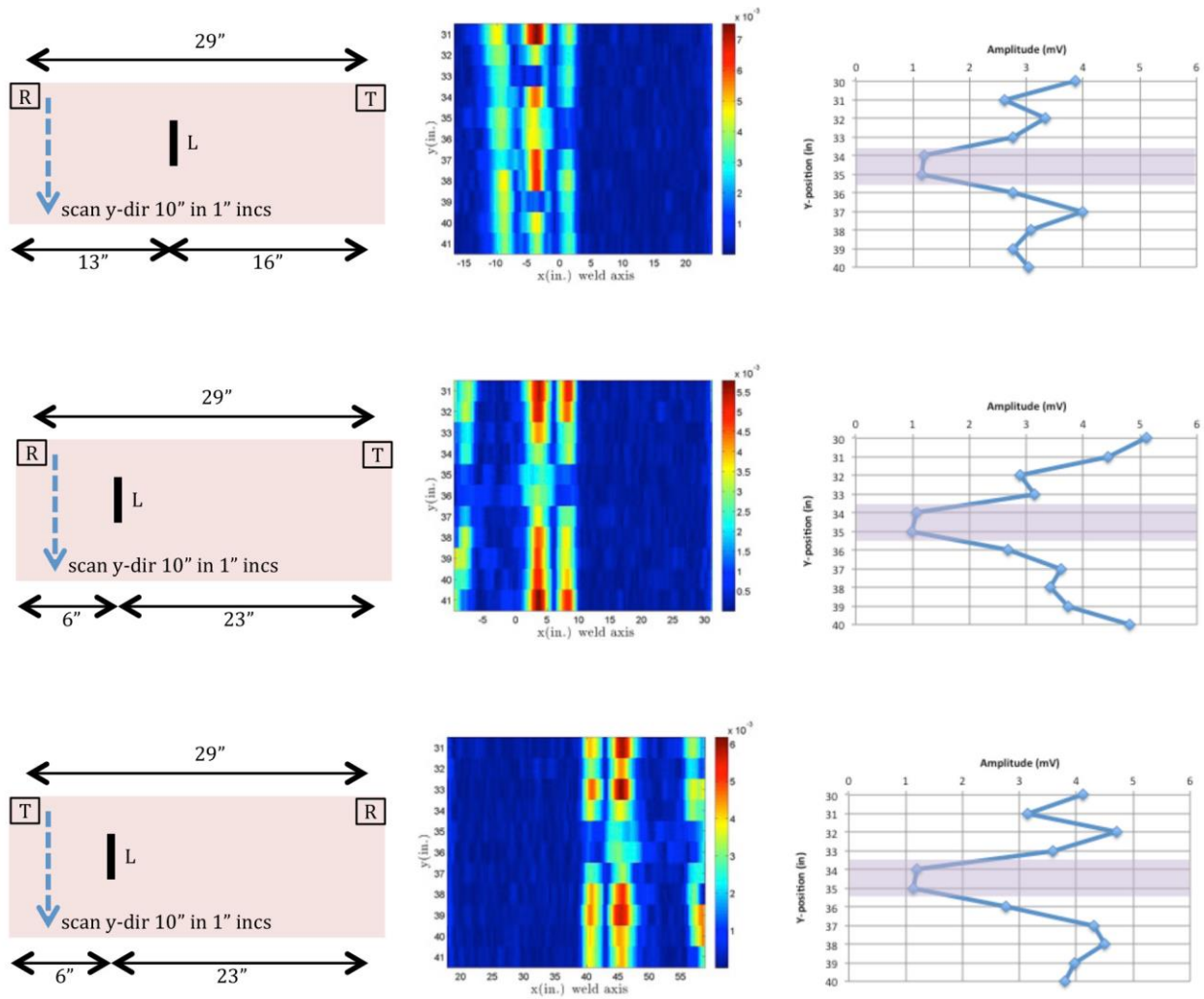


**Figure 7.21**. Test Schematic (*left*), B-scan (*middle*), and Summary Graph (*right*) for Notch “L”

### 7.8.4 SwRI

SwRI detected Notch “L” with a peak SNR of 14 dB. The indication location as determined by the SAFT-processed image was approximately 2 inches farther than the actual flaw location. Typically, a notch that is parallel to the sound propagation direction is challenging to detect, but the 90% through-wall depth of the Notch “L” increased the reflected energy and made it easier to detect. The EMAT instrument location was positioned approximately 83 inches from Notch “L” (Figure 7.6 and Figure 9 in Appendix D).

## 7.9 Flaw “m”

Flaw “m” was a 2-inch long, 0.125-inch wide machined notch with a height of 50% of the plate thickness (0.100 in.). Notch “m” was located near the edge of the ½-inch base plate and oriented perpendicular to the weld as seen in Figure 7.17.

### 7.9.1 Guidedwave

Notch “m” was detected by Guidedwave at transducer Location 3. This location was 10 inches away from the flaw and perpendicular to the notch and the plate edge. To resolve this flaw from the plate edge, an excitation frequency of 200 kHz was used (Figure 7.15). The SNR for Notch “m” was 8 dB. Notch “m” was the only flaw that was not distinguished in the composite images as the plate edge caused higher amplitude reflections.

### 7.9.2 Innerspec

Innerspec claimed to have detected Notch “m” with a SNR over 25 dB using the magnetostrictive sensor pulsed at 128 kHz frequency from the magnetic strips placed on the edge of the plate. The sensor was located 32 inches away from the flaw. Looking at Figure 7.22 and the description provided by Innerspec, this flaw was imbedded in the plate edge reflection signal and therefore **PNNL is not including this as a detect in the analysis in the next section**.

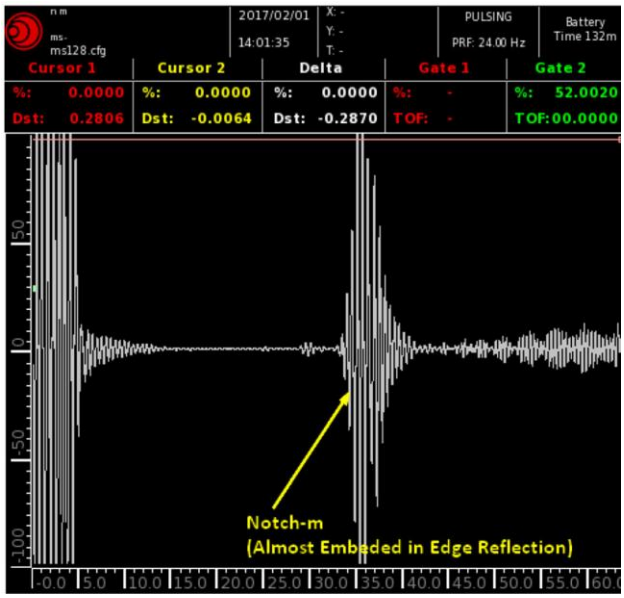


**Figure 7.22**. Manual A-scan from Plate Edge (59 inch) with Magnetostrictive Technique

### 7.9.3 Penn State

Penn State did not have time to examine Notch “m,” but would have used the pitch-catch technique to detect and distinguish from the plate edge reflection.

### 7.9.4 SwRI

SwRI did not detect Notch “m” as this flaw was located parallel to the direction of sound propagation. SwRI states that it may be possible to angle the guided-wave sensor on the sidewall so that the propagation direction is more favorable for radial notches relative to the tank geometry (Figure 7.6).

## 7.10 Other Notable Features from Mockup

Notch “wi” from the tank wall, Notches “N1,” “N2,” and “N3” from the knuckle region, and Notch “al” from the 7/8-inch base bottom plate were legacy flaws from previous examinations of this mockup. Each of these flaws were not included in the *Technology Screening* test but some of the participants were sensitive to these flaws during the demonstrations. A summary of the results for these “additional” features are presented below for each of the four teams.

### 7.10.1 Guidedwave

Guidedwave was able to detect Notch “al” located on the 7/8-inch bottom plate (Figure 7.13) and Notch “wi” from the tank wall (Figure 27 in Appendix A). Notch “wi” is an example of Guidedwave’s technique that can detect defects on the ID when the sensor is placed on the OD. The GWPA approach was also sensitive to the bolts that were securing the bottom plate of the mockup.

### 7.10.2 Innerspec

Innerspec detected Notches “N1” and “N2” when inspecting from the outer wall of the knuckle plate region (Figure 20 in Appendix B). This highlights the magnetostrictive technique is sensitive to defects on the ID when the sensor is placed on the OD.

### 7.10.3 Penn State

Penn State did not have time to examine any other features outside the intended flaws for the *Technology Screening* test.

### 7.10.4 SwRI

There are SAFT responses from defects “N1,” “N2,” and “N3” in the knuckle region and Notch “al” in the 7/8-inch bottom plate past the knuckle region. They are all located roughly at the true location, but these defects were not fully analyzed as these were not the focus of the current *Technology Screening* test.

# 8.0 Analysis

Under *Technology Screening*, technologies are considered qualified for more rigorous *Effectiveness Testing* under Phase I if the following conditions are satisfied:

- a technology is capable of detecting a majority of flaws in its current state OR a technology can detect flaws that the others cannot (complementary technology); and
- a clear pathway to transducer adaptation is demonstrated or communicated and adaptation can be reasonably achieved within the time and cost constraints of the NDE Technology Development Program.

The evaluation of each non-visual volumetric NDE approach was performed using criteria and a scoring system that factored in the ability to detect the surrogate flaws in the mockup and accounted for multiple attributes that include sensor size, required proximity to flaws, and estimated sensor adaption time and cost. Scoring values were awarded for each flaw that was detected and partial points were not awarded. The available point values, shown in Table 8.1, were determined by size, flaw orientation, and relative position to an edge or weld in the mockup. Each sensor attribute scoring category had five available points and partial points were not awarded. Details on the attribute scoring criteria are shown below in Table 8.2. A total of 21 points were available for flaw detection, sensor size and proximity attributes were worth 10 points, and time and cost adaption attributes were worth another 10 points. A total of 41 points were available.

**Table 8.1**. *Technology Screening* Flaw Detection Scoring

| Machined Surrogate Flaw | Flaw Depth[(a)] | Length and Width | Flaw ID in Mockup | Flaw Location and Orientation in Mockup | Points |
|---|---|---|---|---|---|
| Pit | 50% t, 0.25 in. | 0.75 in. diameter | a | 7/8-to-1/2 inch transition weld | 3 |
| Pit | 100% t, 0.50 in. | 0.75 in. diameter | b | Base plate | 2 |
| Pit | 90% t, 0.45 in. | 1.375 in. diameter | c | Base plate | 1 |
| Notch | 50% t, 0.25 in. | 2 in. long, 0.125 in. wide | g | 7/8-to-1/2 inch transition weld, circumferential orientation (i.e., parallel to weld) | 4 |
| Notch | 20% t, 0.10 in. | 2 in. long, 0.125 in. wide | h | Base plate, circumferential orientation (i.e., parallel to weld) | 2 |
| Notch | 50% t, 0.25 in. | 2 in. long, 0.125 in. wide | i | Base plate edge, circumferential orientation (i.e., parallel to weld) | 2 |
| Notch | 50% t, 0.25 in. | 2 in. long, 0.125 in wide | k | 7/8-to-1/2 inch transition weld to base plate, axial orientation (i.e., perpendicular to weld) | 3 |
| Notch | 90% t, 0.45 in. | 2 in. long, 0.125 in wide | L | Base plate, axial orientation (i.e., perpendicular to weld) | 1 |
| Notch | 50% t, 0.25 in. | 2 in. long, 0.125 in wide | m | Base plate edge, axial orientation (i.e., perpendicular to weld) | 3 |

(a) t = plate thickness

**Table 8.2**. *Technology Screening* Attribute Scoring Criteria for Potential/Plan to Overcome Access Challenges

| Attribute | Categories and Point System | | | | |
|---|---|---|---|---|---|
| Size | Currently Capable of fitting in AZ, SY, AW, AN, AP farm Air Slot D-D for inspection, or will be mounted on tank sidewall or knuckle | Currently Capable of fitting in AY-farm Air Slot A-A for inspection | Adaptable to AZ, SY, AW, AN, AP farm Air Slot D-D for inspection with today's materials, electronics and fabrication practices | Adaptable to AY-farm Air Slot A-A for inspection with today's materials, electronics and fabrication practices | Not currently adaptable |
| | 5 | 4 | 3 | 2 | 1 |
| Required Proximity to Flaw | Remotely, with transducer(s) placed on the knuckle or sidewall, or placed on the bottom place with propagation across a weld seam | On the bottom plate, with transducer(s) >12 inches away from the flaw | On the bottom plate, with transducer(s) within 6–12 inches of the flaw | On the bottom plate, with transducer(s) within 6 inches of the flaw | On the bottom plate, with transducer placement required directly over the flaw |
| | 5 | 4 | 3 | 2 | 1 |
| Timeframe for transducer size adaptation | 0–3 months | 3–6 months | 6–9 months | 9–12 months | >12 months |
| | 5 | 4 | 3 | 2 | 1 |
| Cost to adapt | $0–$50K | $50K–$100K | $100K–$200K | $200K–$300K | >$300K |
| | 5 | 4 | 3 | 2 | 1 |

The timeframe and cost criteria in Table 8.2 are applicable only to the sensor attributes that affect access to the air slots. The time and cost for a robotic deployment system is not factored in for these two *Technology Screening* criteria because they will be addressed during Phase II of the NDE technology development program.

The scores for each technology approach are compared in Table 8.3. Guidedwave scored the highest number of points in the flaw detection category and overall with 35 total points. Innerspec and Penn State scored 32 and 31 total points, respectively, although Penn State had one more flaw detection point (16) than Innerspec (15). SwRI scored the fewest flaw detection points and the fewest total points with 24.

**Table 8.3**. Technology Screening Scores and Comparison

| Surrogate Flaw | Total Points Available | Guidedwave | Innerspec[(a)] | Penn State | SwRI |
|---|---|---|---|---|---|
| Pit “a” | 3 | 3 | 0 | 3 | 0 |
| Pit “b” | 2 | 2 | 2 | 2 | 2 |
| Pit “c” | 1 | 1 | 1 | 1 | 1 |
| Notch “g” | 4 | 4 | 4 | 4 | 0 |
| Notch “h” | 2 | 2 | 2 | 2 | 2 |
| Notch “i” | 2 | 2 | 2 | 0 | 2 |
| Notch “k” | 3 | 3 | 3 | 3 | 0 |
| Notch “L” | 1 | 1 | 1 | 1 | 1 |
| Notch “m” | 3 | 3 | 0 | 0 | 0 |
| **Flaw Detection Subtotal** | **21** | **21** | **15** | **16** | **8** |
| Sensor Size Attribute Score | 5 | 3 | 4 | 3 | 5 |
| Flaw Proximity Attribute Score | 5 | 4 | 4 | 4 | 5 |
| Adaption Time Attribute Score | 5 | 3 | 4 | 4 | 3 |
| Adaption Cost Attribute Score | 5 | 4 | 5 | 4 | 3 |
| **Attribute Subtotal** | **20** | **14** | **17** | **15** | **16** |
| **Total Score** | **41** | **35** | **32** | **31** | **24** |

(a) Based on magnetostrictive technology.

The *Technology Screening* scores earned by each technology indicate all three of the evaluated NDE technologies provided by Guidedwave, Penn State and Innerspec are capable of detecting a majority of the flaws and each participant has demonstrated or communicated the potential to overcome air-slot and riser access challenges. Therefore, all three air-slot inspection technologies are considered qualified to participate in final Phase I *Effectiveness Testing*. The score earned by the remote NDE inspection technology provided by SwRI detected the fewest number of flaws, but still detected more than half of them. Although it scored the lowest number of points, this technology satisfies the conditions listed above and is also considered qualified for Phase I *Effectiveness Testing.*

# 9.0 Conclusions/Recommendations

The U.S. DOE and the Hanford Site Tank Operations Contractor, WRPS, recognize the need to expand the scope of DST primary liner volumetric inspections to include the primary liner bottoms. This need was underscored by the recent leak discovered in one of the double-shell tanks, 241-AY-102. Thus, WRPS initiated a non-visual NDE Technology Development Program in FY2017 to begin a process of identifying and selecting candidate NDE volumetric inspection technologies for under-tank inspection. The ultrasonic NDE technologies currently used for the DST primary liner side-wall inspections would be effective for the primary liner bottoms also, if access to the exterior surface of the primary liner bottoms was not obstructed by the refractory pad upon which the primary liners rest. Direct access to the exterior surface of the primary liner bottoms is limited to channels (air slots) in the refractory pad that collectively expose approximately ~1% of the primary liner bottom surface area. The two tanks in the 241-AY tank farm (Tanks AY-102 and AY-101) share a different refractory pattern from the remaining 26 operating DSTs. The cross-sectional dimensions for these air slots vary within each pattern. The smallest and most limiting case is 1.5 inch × 1.5 inch on the outer most perimeter air slots of the AY Tank Farm.

The NDE Technology Development Program is comprised of three phases. The first and current phase of the program is designed to baseline the performance of current or emerging non-visual volumetric NDE technologies for their ability to detect and characterize flaws in DST primary liner bottoms, and to ultimately identify candidate technologies for further maturation. In support of Phase I, PNNL hosted and administered an initial *Technology Screening* test that allowed all interested NDE technology vendors or experts to demonstrate NDE volumetric inspection technologies for tank bottom inspection using a DST primary liner test mockup. The participating NDE technologies included a variety of ultrasonic techniques that were proposed in response to the WRPS EOI. The *Technology Screening* test was designed to identify those participating technologies capable of detecting larger flaw sizes of interest in order to qualify them for more rigorous Phase I *Effectiveness Testing. Effectiveness Testing* will ultimately be used to identify a system or set of non-visual volumetric NDE technologies at the conclusion of Phase I that should be further matured for Hanford DST primary liner bottom inspection.

The primary liner test mockup used for *Technology Screening* contained nine surrogate flaws that represent cracks or corrosion-type pitting. The flaws were positioned in the 1/2-inch thick plate and the transition weld that joins the 7/8- to 1/2-inch bottom plates. *Technology Screening* was performed in a non-nuclear research laboratory test environment at PNNL in Richland, Washington. Presentations were given by each of the four participants and NDE volumetric inspection technology demonstrations were performed under an open format in a laboratory where all surrogate flaws were viewable during testing. Each of the four participants (Guidedwave, Innerspec, Penn State, and Southwest Research Institute) brought different technologies and approaches to solve the problem of performing a non-visual volumetric examination of the DST bottom mockup.

The technology presented by Guidedwave consisted of a guided-wave technique where a single sensor containing many elements produced an acoustic guided wave in the test material. The sensor was placed in a variety of locations and data from each location was combined to produce a composite image of data across the entire mockup.

Advantages:

- Guidedwave detected all nine of the surrogate flaws and showed the highest SNR for most of the flaws.

- Guidedwave used only one probe and would not need access to multiple channels to coordinate a scan for data collection.
- Data interpretation seemed more straightforward than for others.

Challenges:

- The feasibility of remote deployment of the ultrasonic shear couplant was not demonstrated so there is an unknown level of difficulty on this challenge.
- One drawback for Guidedwave is that they chose ideally positioned sensor locations for their demonstration. The actual tank will not necessarily allow such ideal location selection.

Multiple EMAT approaches were demonstrated by Innerspec for detecting the surrogate flaws in the DST mockup, but the technique that was graded used an adhesive-backed magnetostrictive strip that was temporarily attached to the mockup for generating shear horizontal guided waves. Measurements made using the magnetostrictive EMAT featured the strip placed along the edge of the bottom plate of the mockup perpendicular to the weld direction. An EMAT sensor consisting of a meander coil circuit in a short flexible strip was then placed over the magnetostrictive strip, which induced guided waves that traversed across the screening mockup and measured reflections from welds and the surrogate flaws.

Advantages:

- Innerspec had the widest range of technologies to detect flaws and they did not present some of their cleanest data (the shear vertical scan) due to an accidental loss of some data files.
- Innerspec would require the largest transducer design modifications from demonstrated technology. Such size reduction may adversely affect system performance.

Challenges:

- The feasibility of remote deployment of the magnetostrictive strip (pressure) was not demonstrated so there is an unknown level of difficulty on this challenge.

Penn State demonstrated multiple permanent-magnet EMAT approaches where Lorentz force transduction was used to generate acoustic guided waves (shear horizontal waves) in the mockup. The graded technique used a transmit-receive pair where measurements were made at multiple well known locations and SAFT post processing was used to create a composite image of data across the entire mockup.

Advantages:

- Penn State had the most readily deployed air-slot system regarding size.
- Penn State’s system did not need any couplant.

Challenges:

- Among the air-slot deployed systems, the pre-processed SNR was poorest.

Southwest Research Institute demonstrated a guided-wave approach for remotely detecting surrogate flaws in the DST mockup from the lower portion of the primary tank wall. This magnetostrictive approach used a magnetically coupled EMAT to generate guided acoustic waves in the test material. Multiple coil configurations were used to vary inspection frequency.

Advantages:

- SwRI technology requires access only to the tank wall and not through an air slot, which allows for quick screening and deployment.
- SwRI detected the flaws from the greatest distance away.

Challenges:

- Did not detect any defects in the weld and the SNR was poorest of all approaches.
- Shrinking and optimizing their transducer could have unknown effects on their flaw sensitivity

The *Technology Screening* scores provided in Table 8.3 indicate all three of the air-slot–deployed NDE technologies are capable of detecting a majority of the flaws and have the demonstrated or communicated ability to overcome air-slot and riser access challenges. Therefore, all three air-slot inspection technologies are considered qualified to participate in final Phase I *Effectiveness Testing*. The score earned by the remote NDE inspection technology provided by SwRI detected the fewest number of flaws, but still detected more than half of them. Although it scored the lowest number of points, this technology satisfies the conditions listed above and is also considered qualified for Phase I *Effectiveness Testing*.

A combination of these technologies have the potential to support a non-visual volumetric DST inspection approach that first utilizes remote inspection technology to provide coarse data on tank bottom conditions, and subsequently uses these data to identify the air-slots into which air-slot sensors should be deployed for higher-resolution examinations. This approach may be useful in the prioritization of air-slots for inspection and would support efficient and directed DST inspections. Therefore, a combination of remote and air-slot based inspections are recommended.

Based on the *Technology Screening* scores discussed above, and a recommendation to couple air-slot and remote inspection approaches, the following individual participants and teaming are recommended and ranked in the following order:

1. SwRI – the remote inspection technology will be well suited for rapidly screening around the primary liner tank wall to identify areas of concern in bottom plates that should be examined in greater detail with air-slot deployed sensors.

2. Guidedwave – the single-sensor technology is capable of scanning a large area and the image data quality supported easy data interpretation, which supported detection of all mockup flaws. The lack of need for coordinated dual air-slot sensor delivery and minimal need for sensor adaptation will support under-tank inspections and the program timeline.

3. Penn State with (Innerspec or Guidedwave) – Penn State's system was capable of detecting each flaw attempted (two were not attempted due to test time constraints). The lack of need for liquid couplant and minimal need for sensor adaptation will support under-tank inspections. The need for coordinated dual air-slot delivery presents a potential challenge. Improvement in signal-to-noise may be possible with better equipment from companies like Innerspec or Guidedwave. Penn State has worked with Guidedwave on sensor development and their prototype sensors are compatible with Innerspec instruments.

# 10.0 References

Berman HS. 2005. *Rationale for Requesting Deletion of the Double-Shell Tank Bottom Plate Ultrasonic Inspection Requirement*. RPP-25844, Rev. 0, CH2M Hill Hanford Group, Inc., Richland, Washington.

Garfield JS, BJ Vazquez, JR Gunter, AJ Feero and KD Boomer. 2015. *Double-Shell Tank Integrity Improvement Plan*. RPP-PLAN-57352, Rev. 1, Washington River Protection Solutions, Richland, Washington.

# Appendix A

# Guidedwave

# Guided Wave Phased Array Tests on Primary Tank Bottom Mock-up

*A summary of findings from guided wave phased array testing on the storage tank mockup at PNNL in Richland, Washington on 31 January, 2017*

*Contract #: 337915*

*performed for:*

Battelle
Battelle Boulevard, K8-03
P.O. Box 999
Richland, WA 99352-0999 USA

*provided by:*

Russell Love and Steve Owens
Guidedwave
450 Rolling Ridge Drive
Bellefonte, PA, USA 16823
+1-814-234-3437
rlove@gwultrasonics.com; sowens@gwultrasonics.com

14 February, 2017

FBS, Inc. DBA Guidedwave
© 2017

# Executive Summary

Guided wave phased array (GWPA) testing was carried out on the primary liner mock-up at the Pacific Northwest National Laboratory in Richland, Washington on January 31, 2017. These tests were to evaluate the performance of the GWPA technology on the primary liner mock-up floor and to identify the strengths and weaknesses of the technology for adaptation for inspecting the actual primary liner floor.

The use of bulk wave phased array has revolutionized the way we inspect structures when looking through the thickness of a specimen, by rapidly providing sector scans that are more intuitive than a traditional ultrasonic A-scan. In this same way, Guidedwave has proven it possible to develop probes that could revolutionize guided wave inspection by rapidly scanning large plates from a single probe position. The GWPA system steers and focuses guided wave energy 360° around a plate from a single sensor position to generate a "radar-like" scan of anomalies in the plate. Guidedwave accomplishes this guided wave beam steering by utilizing a small array of guided wave sensor elements packed into a single probe and applying signals with predetermined time delays and amplitude factors using a phased array pulser/receiver system and advanced algorithms. The technology does not provide an exact thickness map of the structure, but it does allow the user to rapidly locate and categorize severity of defects.

All the defects were successfully detected on the ½" base plate (plate 1) with the GWPA technology. Some of the more difficult defects, like those in welds or next to cut ends were able to be identified by utilizing multiple acquisition frequencies and sensor locations, which is common practice when performing GWPA inspections. On the thicker 7/8" plate (plate 2), the notch defect was detected with the GWPA technology. Also, on the 7/8" wall plate (plate 3), the GWPA sensor was placed on the OD for inspection. At this location, the notch defect on the ID was successfully identified.

All of the inspections on the mock-up were performed with a single GWPA 30-element probe. This probe provided enough frequency bandwidth, resolution, and penetration power to appropriately identify the defects in the base plate. Therefore, it is possible to outfit a robotic crawler with a single probe to perform the necessary inspections.

The internal sensor array of the GWPA sensors can be made small enough to meet the space limitations of the primary liner access channels.

GWPA technology is mature enough for rapid deployment on robotic crawlers. Guidedwave would consult with an established company that specializes in robotic crawler applications, e.g. Adaptive Energy, to design and outfit a crawler with GWPA technology for inspection of the primary tank liner.

FBS, Inc. DBA Guidedwave
© 2017

## Table of Contents

Executive Summary ..... 1

1. Introduction ..... 3

Ultrasonic Guided Waves ..... 3

Guided Wave Phased Array ..... 6

Inspection System Overview ..... 8

2. Inspection Results ..... 11

Defect Detection ..... 12

Plate 1 (Base Plate) ..... 12

Plate 2 ..... 20

Plate 3 ..... 21

Composite Imaging ..... 22

Inspection Summary ..... 25

3. Conclusions ..... 27

Appendix A ..... 28

# 1. Introduction

Guided wave phased array (GWPA) testing was carried out on the primary liner mock-up at the Pacific Northwest National Laboratory in Richland, Washington on January 31, 2017. These tests were to evaluate the performance of the GWPA technology on the primary liner mock-up floor and to identify the strengths and weaknesses of the technology for adaptation for inspecting the actual primary liner floor.

**Ultrasonic Guided Waves**

The use of ultrasonic guided waves has been increasing tremendously over the past decade due to a variety of reasons, notably improved understanding and computational efficiency for complex problem solving. Guided waves provide the ability to inspect hidden and inaccessible regions of structures, structures under soil, water, coatings, insulations, and concrete because of the inspection capability from a single remote probe position. The best example of guided wave success is in long-range ultrasonic pipeline inspection, where the technology has been accepted commercially for years. This technology has matured to the point that ASNT (American Society for Nondestructive Testing) is now developing a certification process for guided wave inspectors. Guided wave ultrasound differs substantially from traditional bulk wave ultrasonic testing (UT) and can often succeed where traditional UT techniques have failed.

A comparison of ultrasonic bulk waves and guided waves is made in Figure 1. Traditional bulk wave ultrasonic sensors send sound energy into an area directly below the transducer. They are used for thickness measurements, defect detection, and material characterization. The main disadvantage of bulk wave techniques is that to cover a large region, the probe must mechanically scan the entire area. Furthermore, it is difficult to inspect hidden or inaccessible structures, such as those under coatings or soil, using UT techniques.

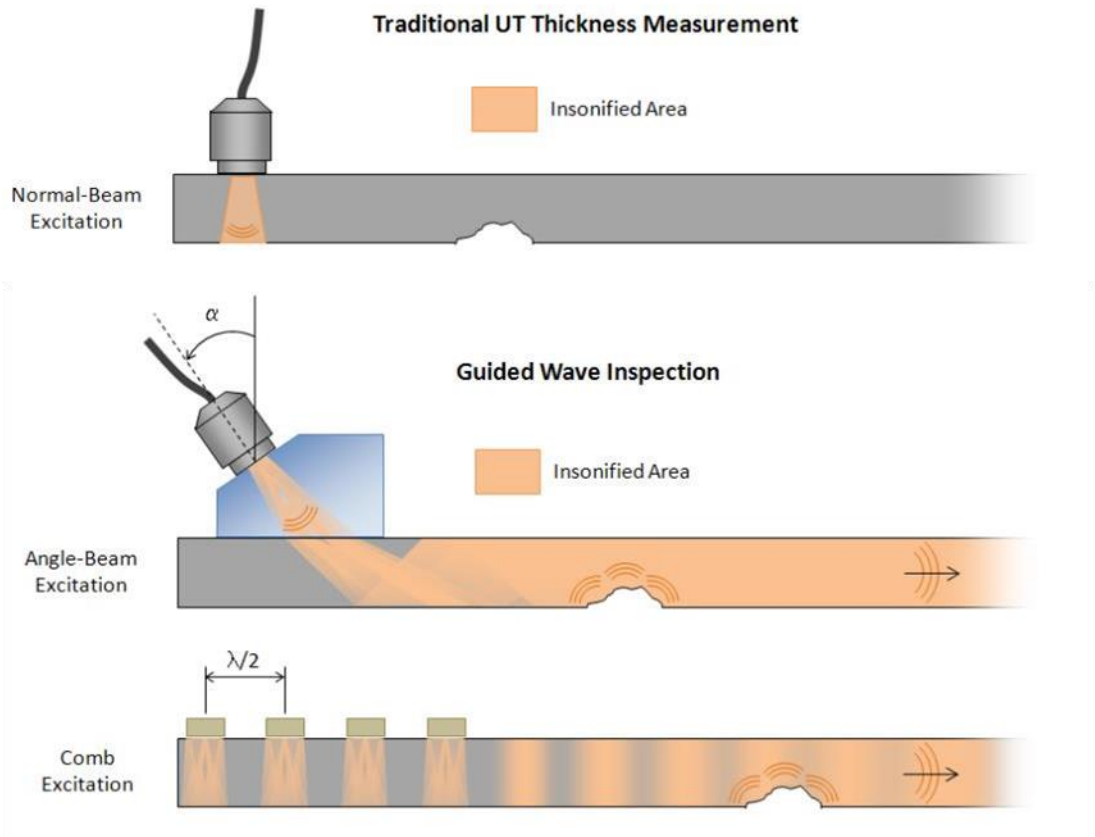


**Figure 1 Comparison of bulk wave excitation (top), and guided wave excitation (bottom) in a plate. The guided wave is capable of detecting reflections from the corrosion patch and the weld that are distant from the transducer location, which is not possible with traditional UT.**

Guided waves travel along or between two physical boundaries of a waveguide; two examples of such waveguides are a plate and a pipe. Other examples include rails, beams, composite materials, and any other structures that have physical boundaries. Guided waves take advantage of these boundaries to inspect over great distances by creating a resonance condition between the structural boundaries, which allows the waves to propagate much farther than bulk ultrasonic waves. A comparison between bulk wave and guided wave activation can be seen in Figure 1. It is possible to generate guided waves with different types of vibration and energy distributions through the cross-section of a structure. Exploiting these characteristics gives a skilled engineer the ability to create waves that are more or less sensitive to different types of defects and loading conditions. Different guided wave modes also have different velocity characteristics as a function of frequency. These are all considerations that can affect the performance of a guided wave system, and Guidedwave has the skills, knowledge, and tools to understand and exploit these nuances.

The generation of certain guided wave modes at particular frequencies to accomplish special tasks is scientifically-founded and physically-based. Advanced understanding and utilization is possible because of the tremendous advances in computational power and

analysis available today. For a given structure, a dispersion curve, such as the one presented for a ½ inch carbon steel plate in Figure 2, can be generated and wave structure profiles subsequently produced. A dispersion curve shows all of the possible guided wave modes that can be excited in a particular structure and the relationship between wave mode, frequency, and velocity. From the dispersion curves, wave structure profiles can be created. The wave structure profiles show how different types of energy are distributed throughout the thickness of that structure. For example, all of the energy can be concentrated at the surface or it can be evenly distributed throughout the thickness.

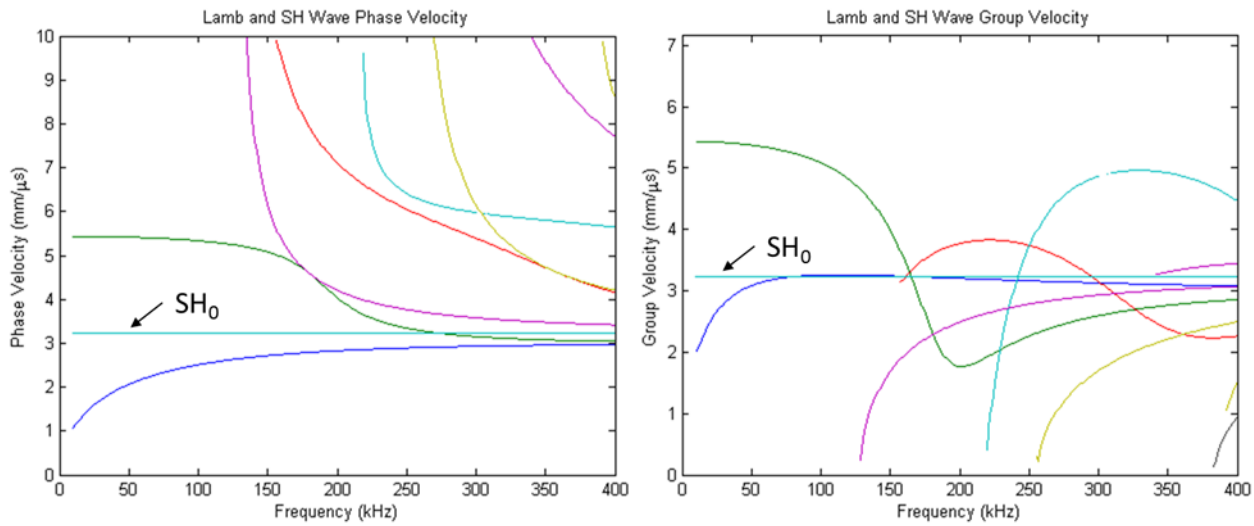


**Figure 2 A guided wave dispersion curve of a ½-inch carbon steel plate, which describes the relationship between wave velocity and frequency for all of the possible guided wave modes in the plate. The $SH_0$ mode that Guidedwave is utilizing for the GWPA inspection is highlighted.**

The wave vibration components can also be predominantly compressional, flexural, shear, or some combination of these. Guidedwave has a wealth of experience using this type of analysis to solve a variety of problems. In the case of the current application, it was determined that the shear horizontal, $SH_0$ mode, indicated on the dispersion curve in Figure 2, is the best candidate due to its non-dispersive nature, insensitivity to liquids on the surface of the structure, and even energy distribution throughout the cross-section of the pipe wall. The $SH_0$ mode propagates as a pure in plane vibration distributed uniformly through the plate thickness. This characteristic means it is unaffected by inviscid fluids on the surface or the interior due to the lack of shear coupling to liquids. The uniformity of the wave energy through the thickness of the structure also ensures a linear relationship between guided wave reflection amplitude and reflector cross-section.

Principal benefits of the shear horizontal guided wave mode include:

1. Zero out-of-plane displacement through the thickness of the plate

   - No sensitivity to fluids on either side of plate, which can be a serious problem with other guided wave modes.
2. Fundamental mode phase and group velocity are constant
   - Technology is readily adaptable to wide range of structures, less complex calculations and less knowledge required by user
3. Wave always travels at bulk shear wave speed
   - User only needs traditional UT wave velocity table
   - No need to calculate complex dispersion curves
4. Purely non-dispersive
   - No spreading of wave packet as with many other guided wave modes
   - Probe frequency can be changed without negative effects on focusing
5. Fundamental mode is independent of plate thickness
   - Technology is readily adaptable to wide range of structures, less complex calculations and less knowledge required by user

**Guided Wave Phased Array**

The use of bulk wave phased array has revolutionized the way we inspect structures when looking through the thickness of a specimen, by rapidly providing sector scans that are more intuitive than a traditional ultrasonic A-scan. In this same way, Guidedwave has proven it possible to develop probes that could revolutionize guided wave inspection by rapidly scanning large plates from a single probe position. Over the past several years, Guidedwave has been developing guided wave phased array technology for the rapid inspection of large areas of steel and aluminum ship hulls for the Navy, as illustrated in Figure 3. Guidedwave has two patents pending on GWPA technologies.

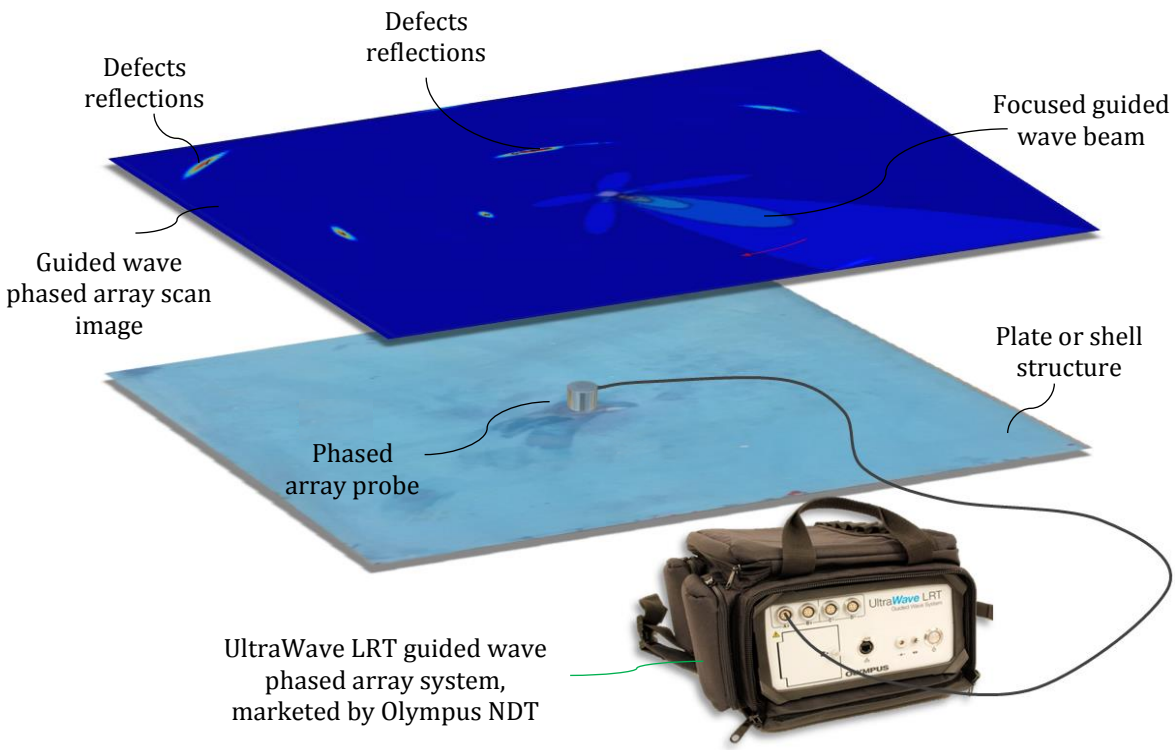


**Figure 3 Guided wave phased array technology uses a compact phased array probe to electronically steer and focus a guided wave beam around a plate-like structure; corrosion, cracks, and other anomalies can be detected. This technique resembles a radar or sonar scan and is the guided wave analogue of traditional ultrasonic bulk wave phased array, which revolutionized the UT field.**

The guided wave phased array technology performs in a manner akin to sonar, in which sound is electronically focused and swept in different directions to detect the location and distance of other ships, or radar, in which radio waves are steered to detect aircraft. Similarly, the guided wave phased array system steers and focuses guided wave energy 360° around a plate from a single sensor position to generate a "radar-like" scan of anomalies in the plate. Guidedwave accomplishes this guided wave beam steering by utilizing a small array of guided wave sensor elements packed into a single probe and applying signals with predetermined time delays and amplitude factors using a phased array pulser/receiver system and advanced algorithms. This beam steering allows the sensor to detect the presence of defects at distances of up to 10 feet in all directions around the probe. Guidedwave has performed guided wave phased array scans of ship hull mockups with an area of 50 $ft^2$ in less than 15 seconds. The damage image can be obtained either directly from the scan signals as a non-destructive evaluation (NDE) approach or by comparison with baseline signals as a structural health monitoring (SHM) method. The SHM approach can be useful in structures with complex geometry by taking advantage of baseline signal comparison. The technology does not provide an exact thickness map of the structure, but it does allow the user to rapidly locate and categorize severity of defects.

**Inspection System Overview**

The GWPA inspection system is comprised of an UltraWave LRT multi-channel pulser-receiver unit, a handheld GWPA sensor, a laptop loaded with purpose-built data collection and analysis software, and the associated cabling and accessories.

The UltraWave LRT unit, shown in Figure 4, is a multi-channel guided wave pulser-receiver platform sold and serviced through Olympus Scientific Solutions Americas (OSSA) that is currently used with the UltraWave long-range guided wave pipe inspection system, also offered by OSSA. This unit is a powerful, flexible platform for a variety of guided wave technologies, and can be utilized for GWPA applications.

**Figure 4 The UltraWave LRT guided wave pulser-receiver system sold and serviced by Olympus.**

Currently, Guidedwave has designed and manufactured multiple GWPA sensors for a multitude of applications. For the primary wall mock-up, Guidedwave has selected the 165 kHz 30-element GWPA sensor PA100466 (Figure 5). This sensor offers the optimal frequency bandwidth for the given plate thickness and defect sizes expected. However, with this sensor, the resolution is slightly reduced to minimize the side lobes produced. This is necessary when there are many features in the plates or cut ends, like in a mock-up, which will produce artifacts in the final GWPA image.

**Figure 5 Photograph of a GWPA sensor that was used during the primary liner mockup inspection feasibility study**

The current GWPA sensor has been designed to be handheld and ergonomic. The height and diameter of the 165 kHz 30-element GWPA sensor are 1.7 and 2.7 inches, respectively. However, the actual sensor array diameter is only 2 inches and the active element height is 3/8 inches. Guidedwave has fabricated sensors with diameters as small as 1.5 inches. Therefore, a smaller diameter GWPA probe is absolutely possible for this application. We have the tools and resources to redesign the probe for the limited-access channel geometry.

The sensor is applied to the structure with ultrasonic shear couplant. This couplant has a high viscosity to support the shear vibration. There are some limitations and complexities that would need to be addressed for the robotic application, but we are confident this can be addressed. Guidedwave has dispensed this couplant with a plunger system, and automating that process is very feasible.

Guidedwave has created specifically-designed software for GWPA applications. Several screen captures of the GWPA software are provided in Figure 6. The software and electronics record any reflected ultrasonic energy from the incident waves and display the waveforms on a radar type graph on the laptop screen. The user can then analyze the image to identify the known features and any anomalies that may be present. The software contains all necessary algorithms for completing a scan including: focusing calculations, data acquisition, data display, data analysis tools, and data saving and loading. This software has been created for use on a handheld device for rapid screening of plates, and can be adapted for robotic deployment. All of our software development is done in house and we have produced specialty versions for unique applications such as this in the past.

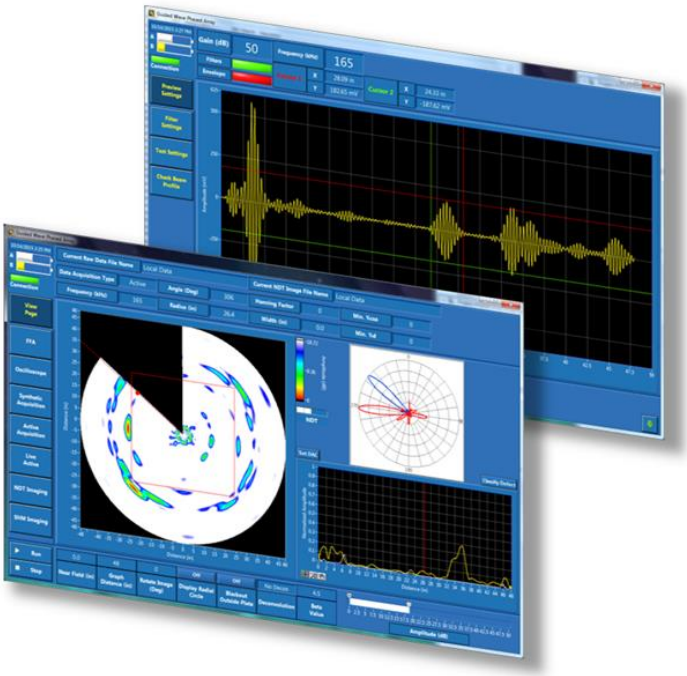

**Figure 6 Screen captures of the specially-designed software for collecting and analyzing GWPA data.**

## 2. Inspection Results

Guided wave phased array (GWPA) inspections were carried out on three different plates on the primary liner mockup including plate 1 (base plate), plate 2, and plate 3 (wall), with emphasis on plate 1. An illustration showing the numbering schemed used to identify the plates on the mock-up is provided in Figure 7. Most all the defects, which included the high-priority defects, were located in plate 1; therefore, the majority of the inspection tests were performed in this plate. These tests included defect detection from anywhere on the plate and defect detection from a simulated access channel along the plate. Data was also acquired on plate 2 and plate 3 to show the technology could identify defects in a thicker 7/8 inch plate. Also, data was collected on plate 3 from the OD to show the technology can correctly detect defects regardless of the defect location, i.e. ID or OD.

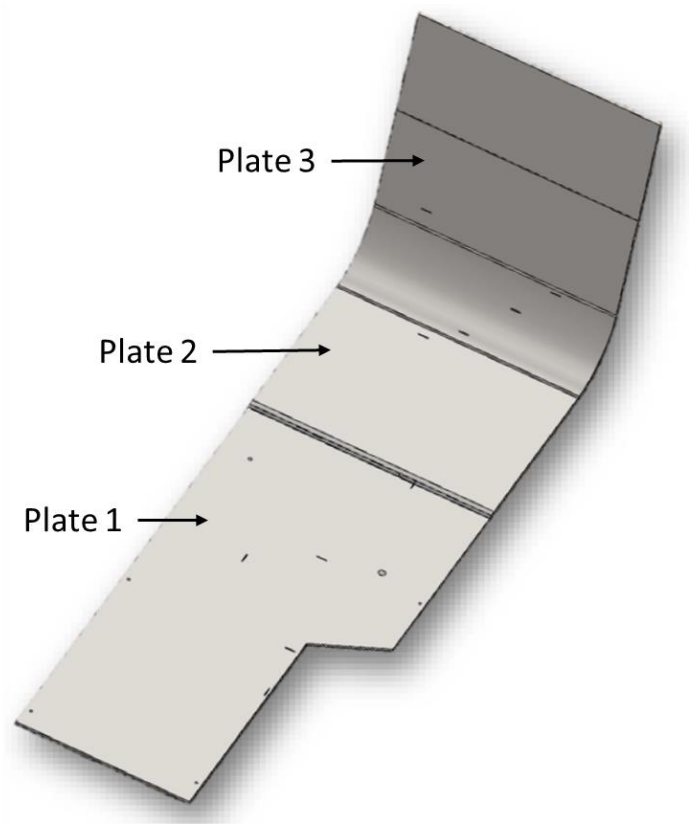


**Figure 7 Illustration showing the numbering scheme used to identify the plates on the mock-up.**

## Defect Detection

### *Plate 1 (Base Plate)*

*Plate 1 Location 1*

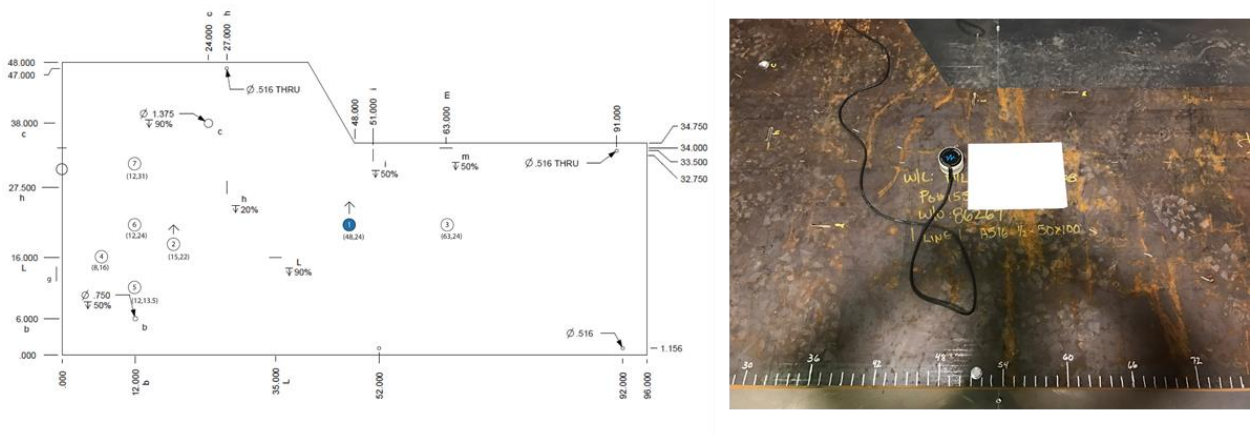

**Figure 8(Left) sketch and (right) photograph of the GWPA sensor on plate 1 at location 1.**

The center of the plate is commonly used as a starting point for GWPA inspections. At this location, location 1 (Figure 8), defects 'c', 'h', and 'l' were detectable as shown in Figure 9.

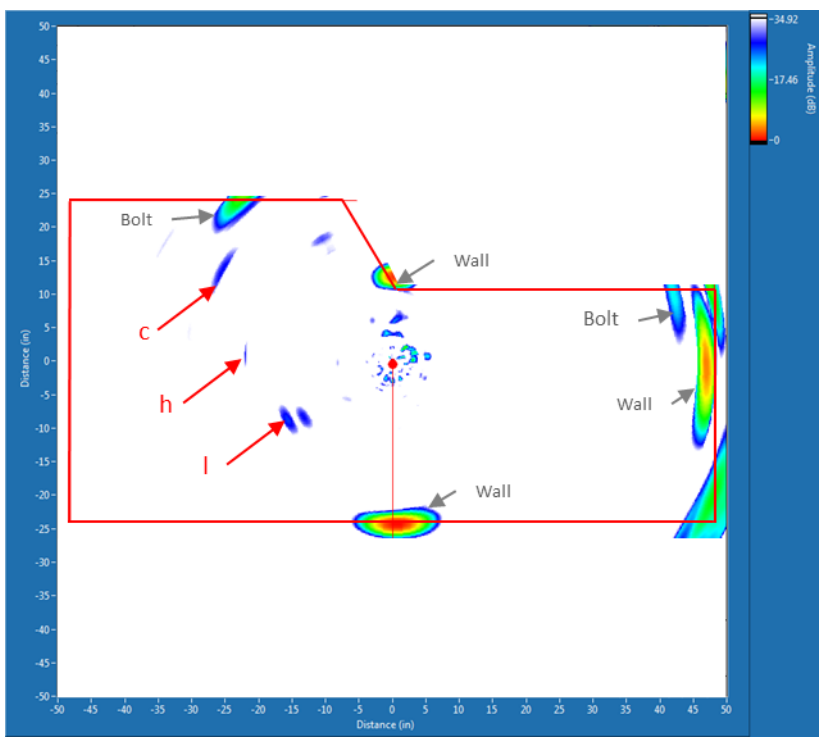


**Figure 9 GWPA scan on plate 1 at location 1. GWPA scan performed at 150 kHz.**

*Plate 1 Location 2*

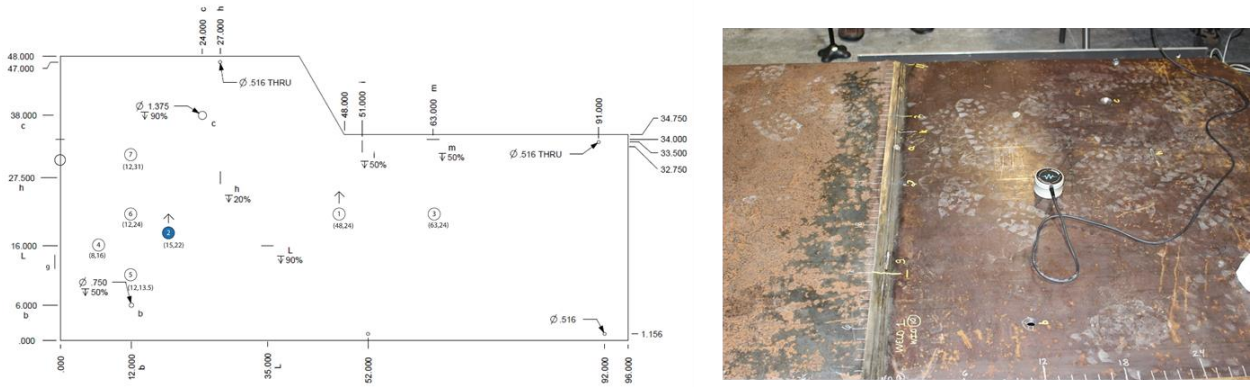

**Figure 10(Left) sketch and (right) photograph of the GWPA sensor on plate 1 at location 2.**

At the second location, location 2 (Figure 10), defects 'c', 'h', 'l', 'b', and 'I' were detectable as shown in Figure 11.

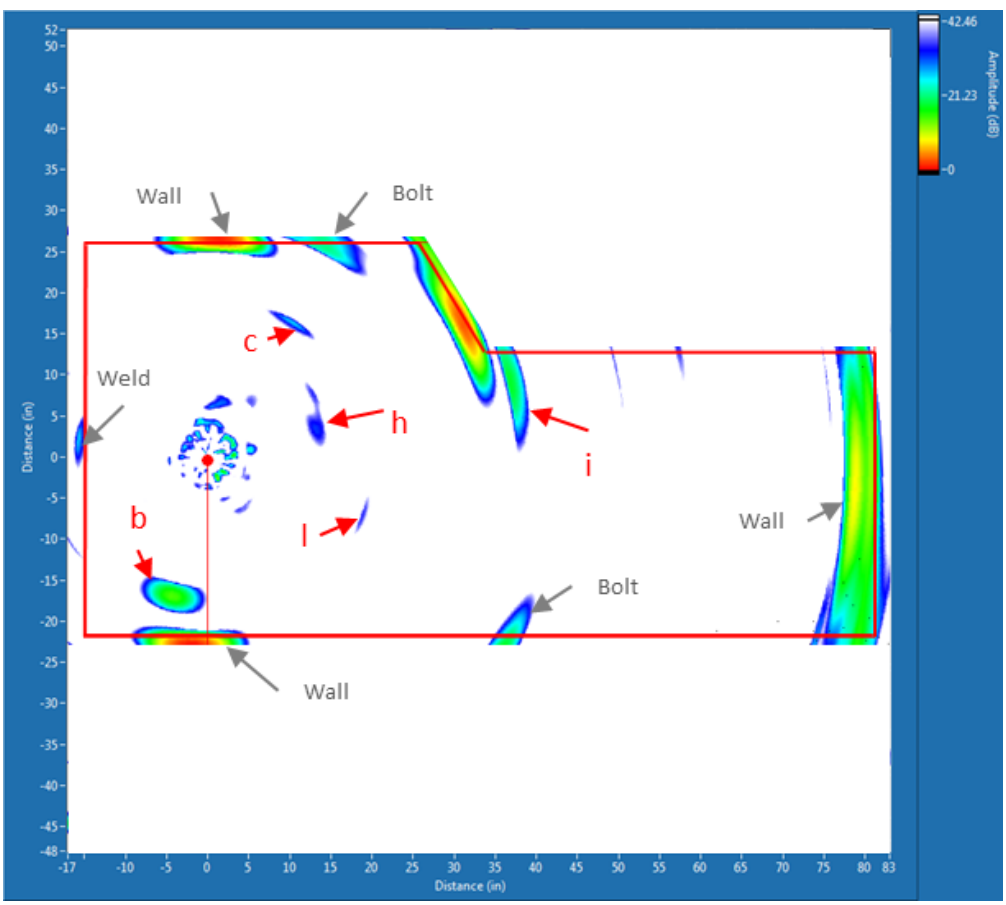


**Figure 11 GWPA scan on plate 1 at location 2. GWPA scan performed at 150 kHz.**

*Plate 1 Location 3*

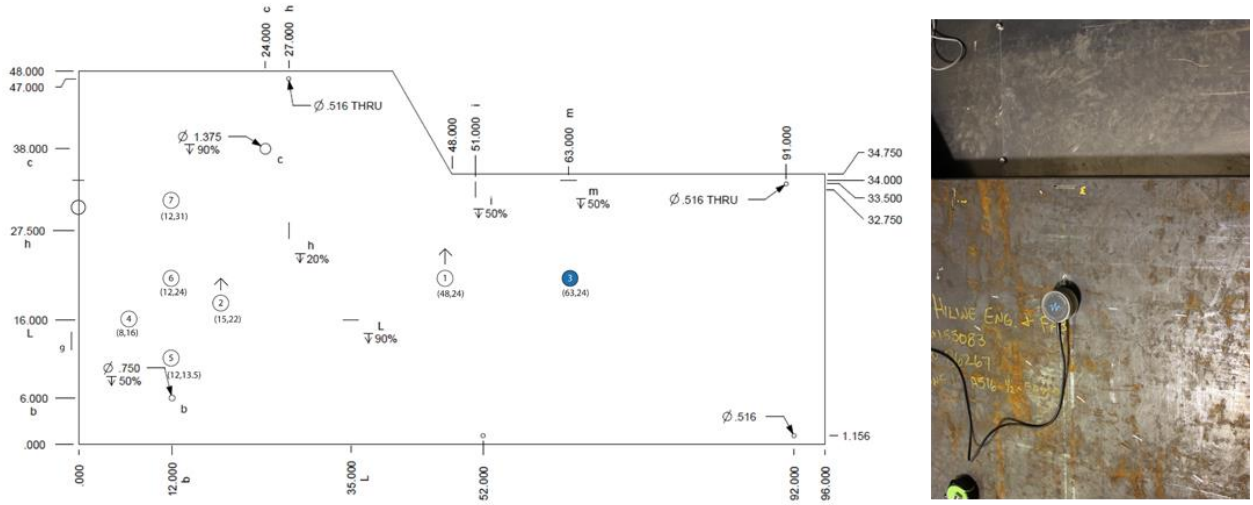


**Figure 12(Left) sketch and (right) photograph of the GWPA sensor on plate 1 at location 3.**

At location 3 (Figure 12), defects 'h', 'i', and 'm' were detectable as shown in Figure 13. To differentiate defect 'm' from the plate sidewall, the acquisition frequency was raised to 200 kHz.

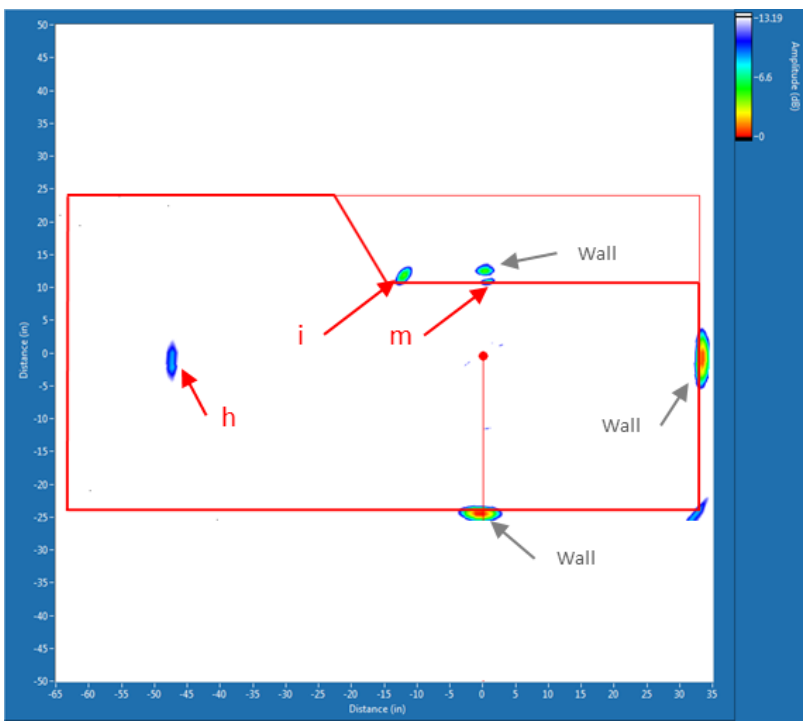


**Figure 13 GWPA scan on plate 1 at location 3. GWPA scan performed at 200 kHz.**

*Plate 1 Location 4*

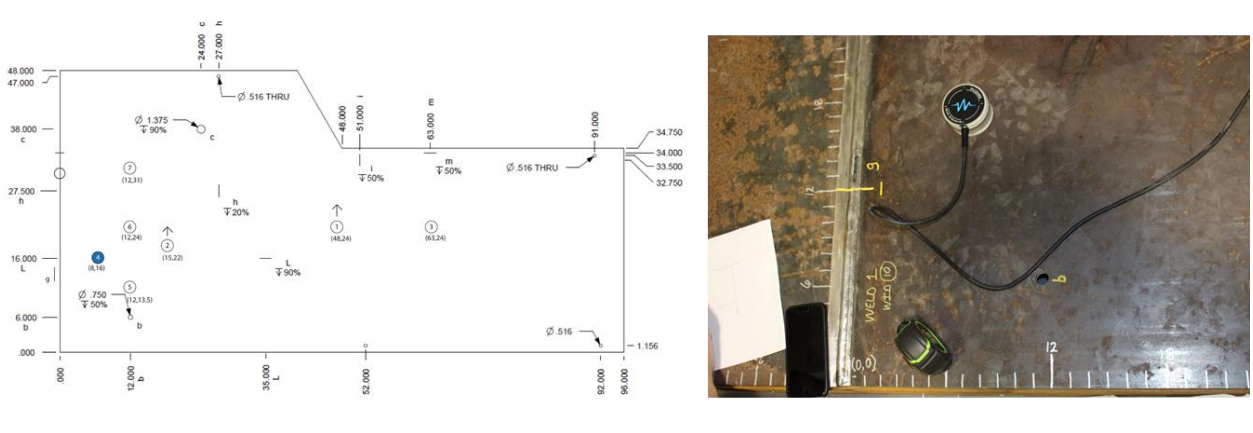

**Figure 14(Left) sketch and (right) photograph of the GWPA sensor on plate 1 at location 4.**

At location 4 (Figure 14), defects 'c', 'l', 'b', 'g', and 'k' or 'a' were detectable as shown in Figure 15. The indication is strong where defects 'a' and 'k' are. However, with the defects being very close together, it was not possible to separate the reflectors at this location. A-scans are provided for the defects in Figure 16 through Figure 19. The defect location is indicated with a red vertical cursor.

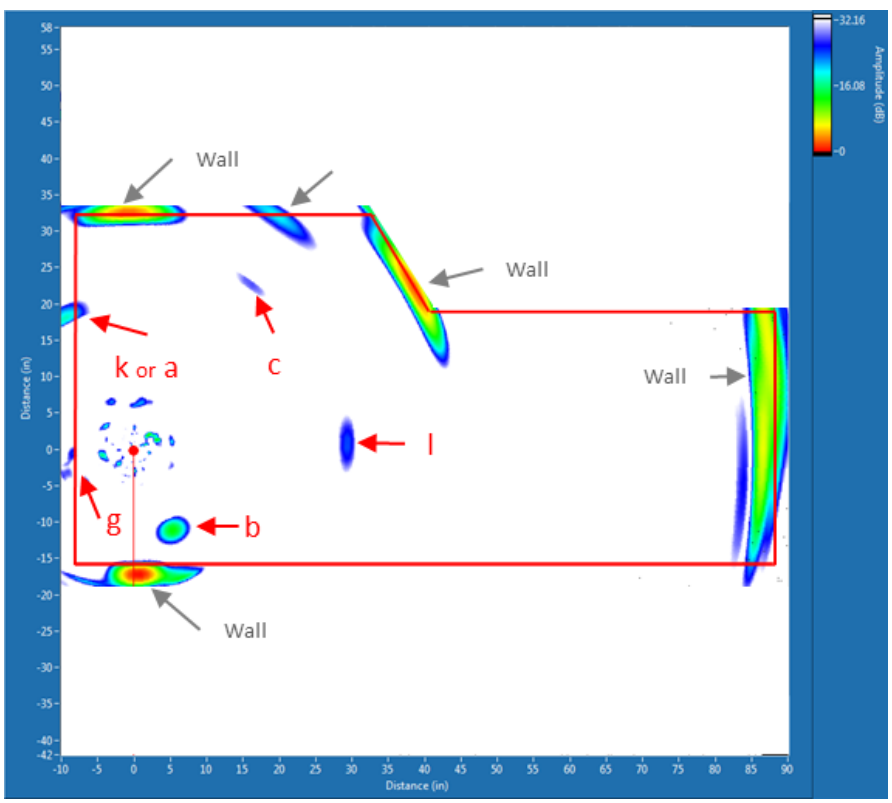


**Figure 15 GWPA scan on plate 1 at location 4. GWPA scan performed at 150 kHz.**

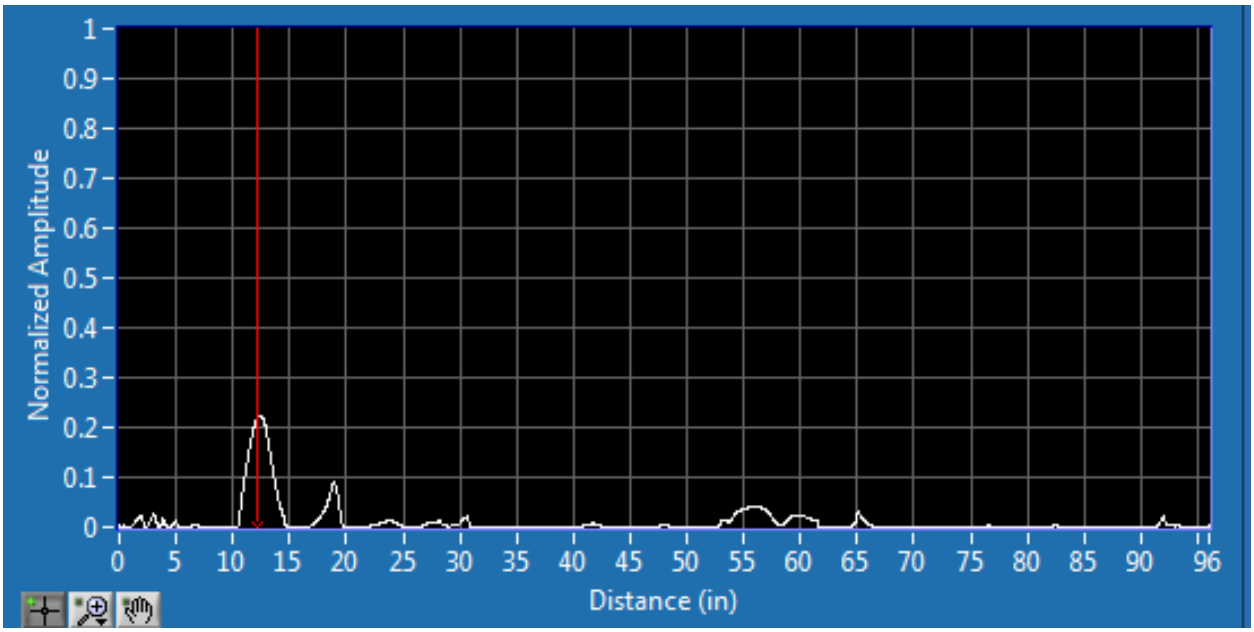


**Figure 16 A-scan result for defect 'b'.**

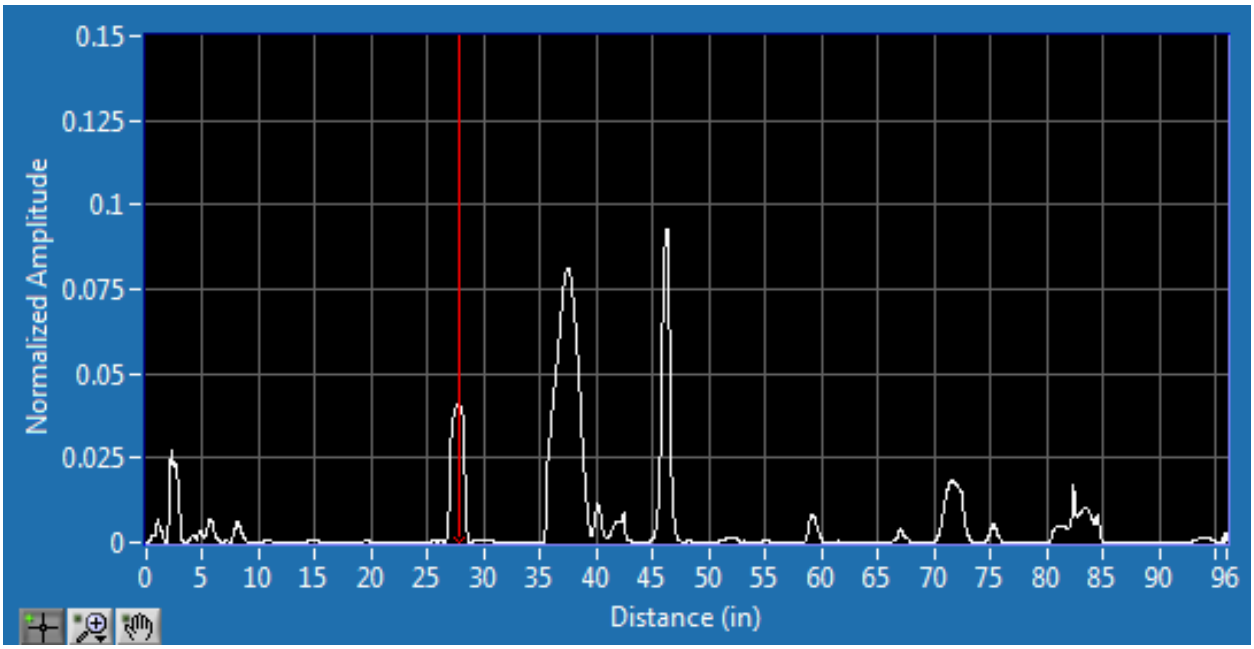


**Figure 17 A-scan result for defect 'c'.**

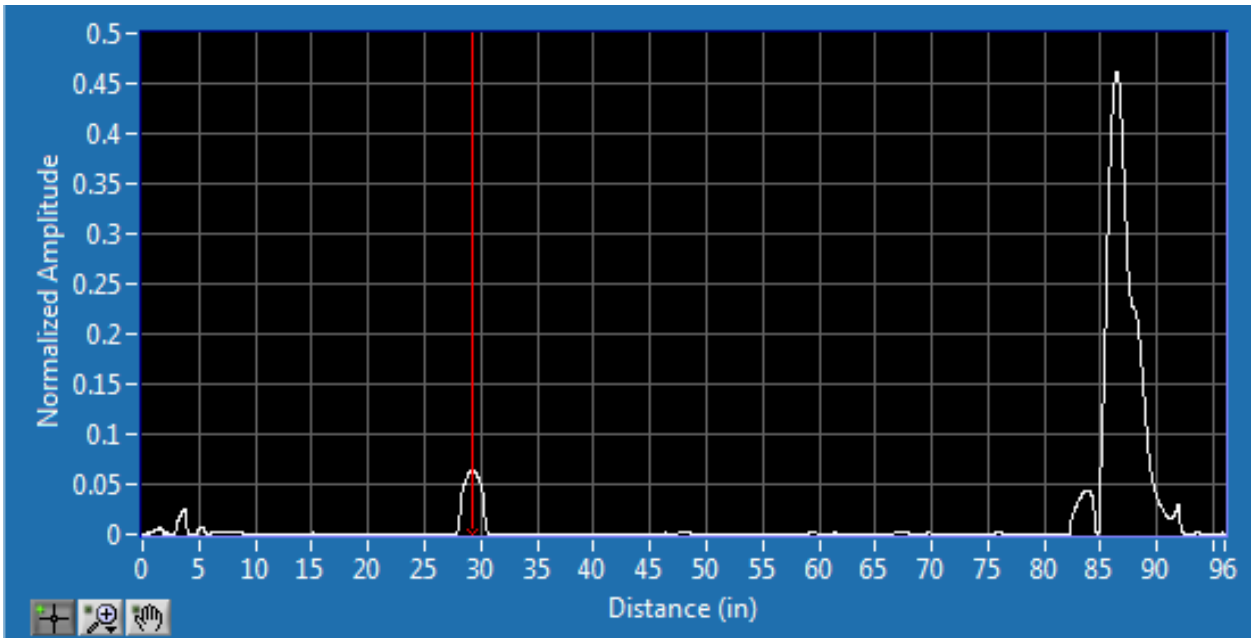


**Figure 18 A-scan result for defect 'l'.**

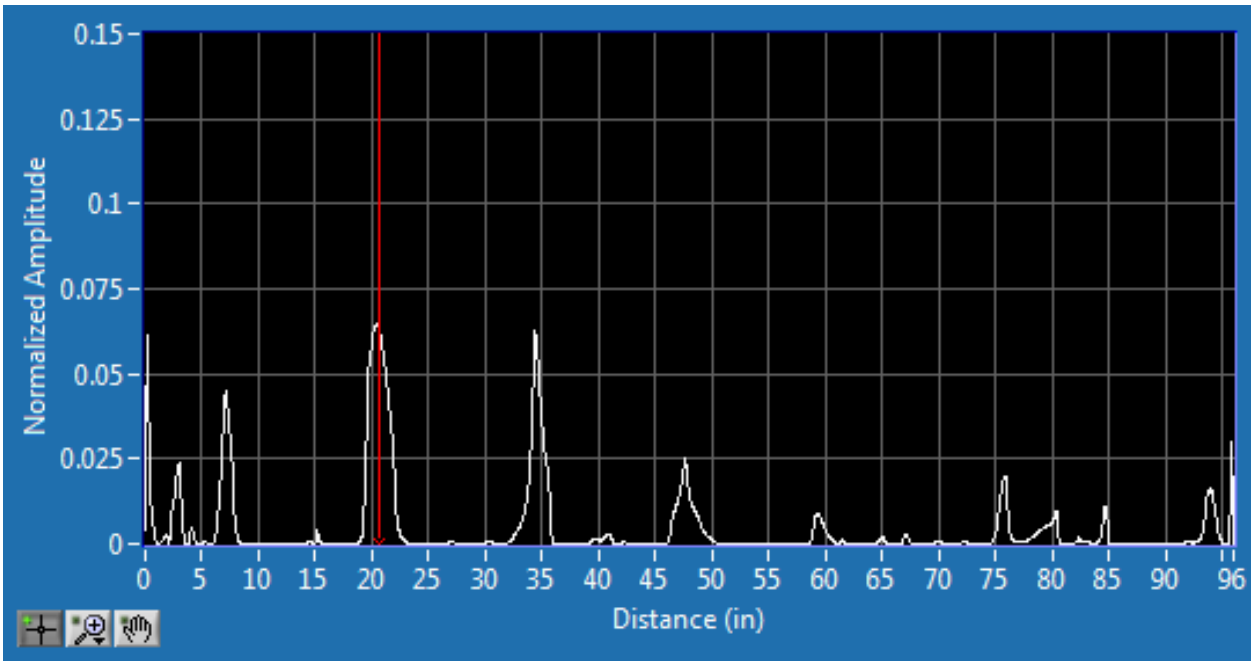


**Figure 19 A-scan result for defect 'k' or 'a'.**

*Plate 1 Location 5*

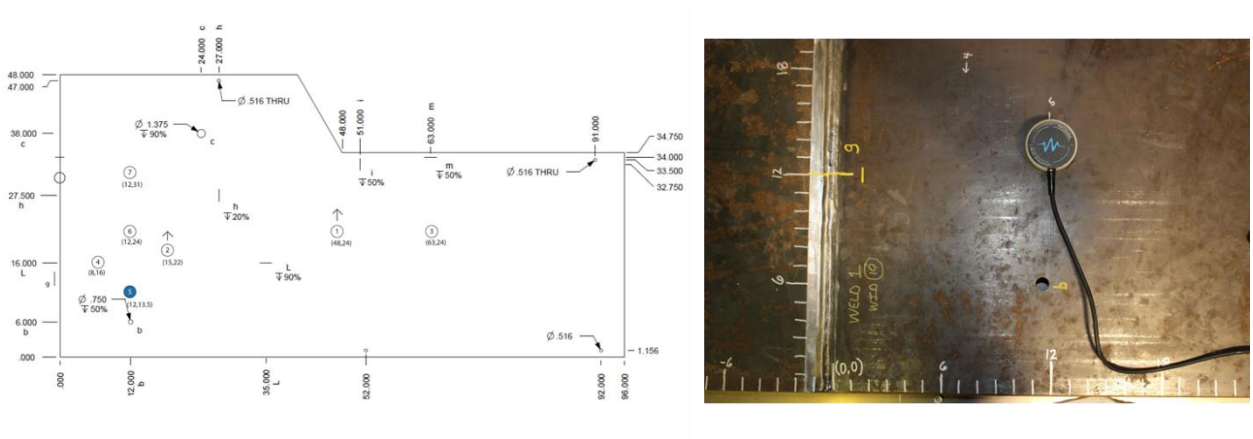

**Figure 20(Left) sketch and (right) photograph of the GWPA sensor on plate 1 at location 5.**

At location 5 (Figure 20), defects 'c', 'l', 'b', and 'g' were detectable as shown in Figure 21.

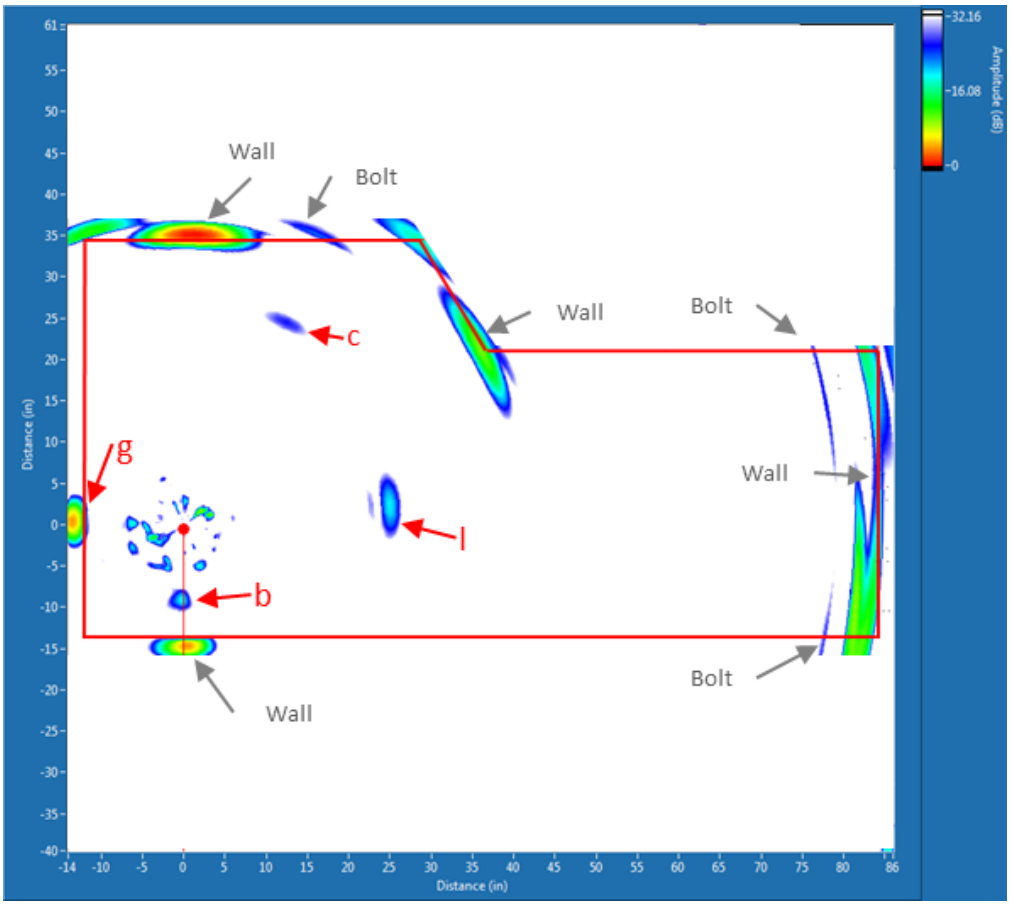


**Figure 21 GWPA scan on plate 1 at location 5. GWPA scan performed at 165 kHz.**

*Plate 1 Location 7*

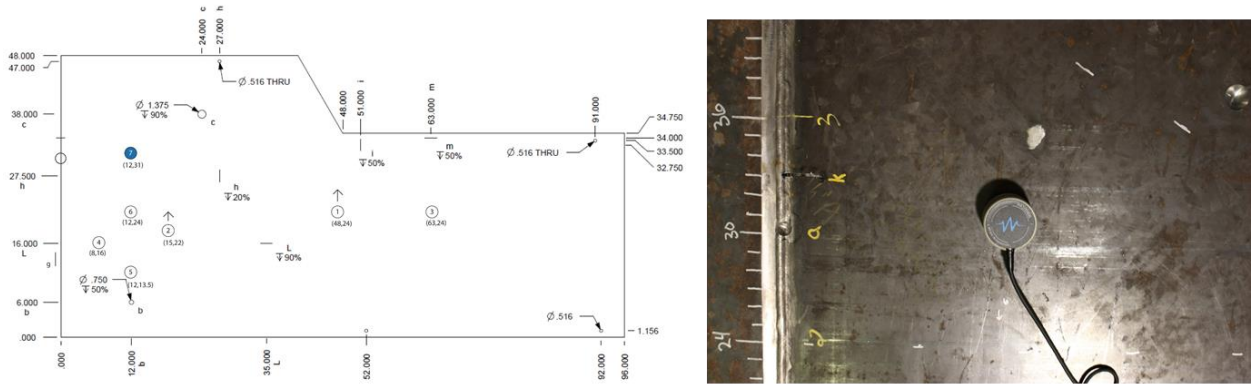

**Figure 22(Left) sketch and (right) photograph of the GWPA sensor on plate 1 at location 7.**

At location 7 (Figure 22), defects 'i', 'b', 'k' and 'a' were detectable as shown in Figure 23. To separate defects 'a' and 'k', the frequency had to be raised to 200 kHz to achieve the necessary resolution.

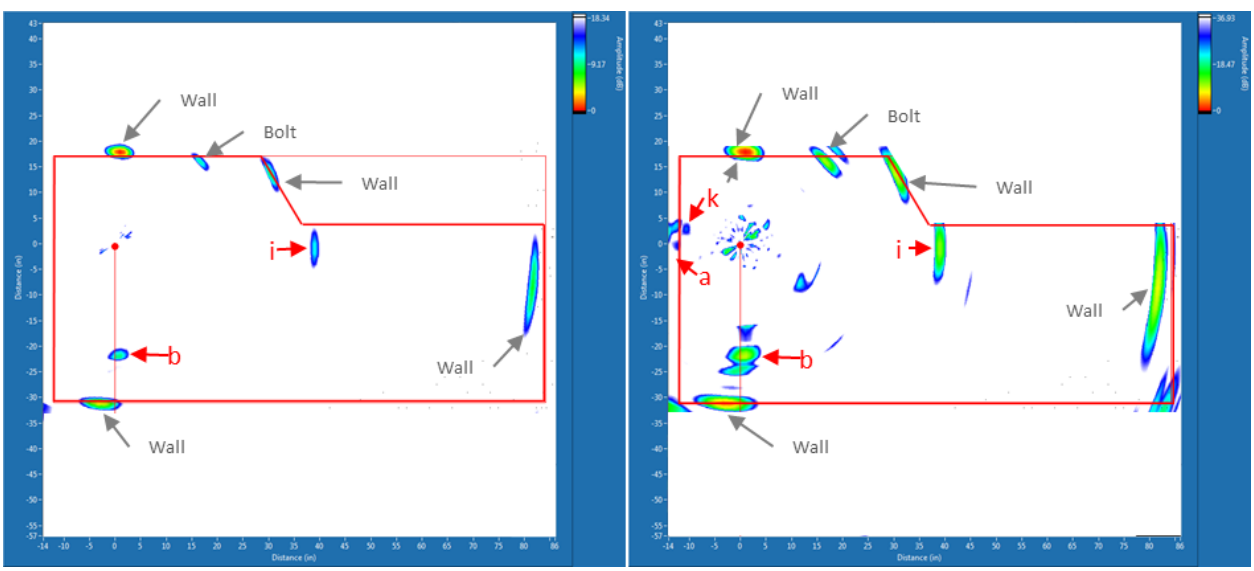


**Figure 23 GWPA scan on plate 1 at location 7. GWPA scan performed at 200 kHz. (Left) the color scale is set to clearly identify the larger defects, and (right) the color scale is set to identify the smaller defects, defects 'a' and 'k'.**

*Plate 2*

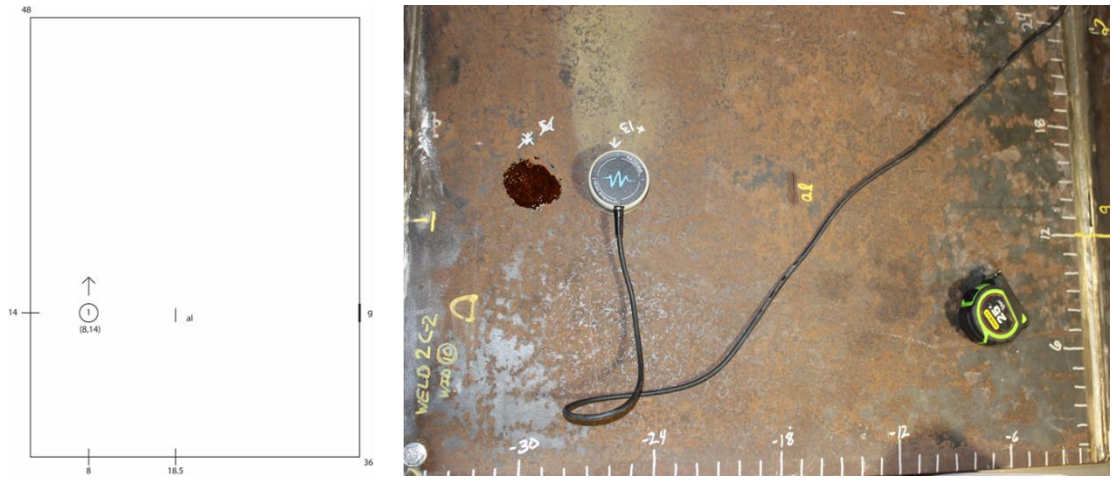


**Figure 24(Left) sketch and (right) photograph of the GWPA sensor on plate 2 at location 1.**

Data was also taken on plate 2, at location 1 (Figure 24), which is thicker than the base plate. Plate 2 is 7/8 inch thick. The GWPA sensor was placed perpendicular from the notched defect, defect 'al'. The defect was easily detectable as shown in Figure 25. Defect 'g', which is located in the weld bead between plates 1 and 2, is also clearly detectable at this location.

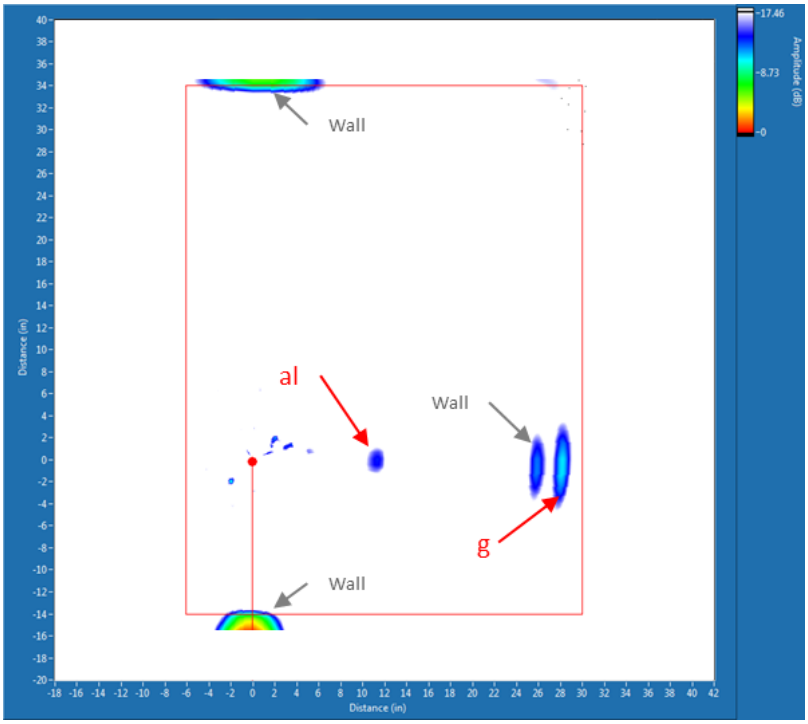


**Figure 25 GWPA scan on plate 2 at location 1. GWPA scan performed at 150 kHz.**

*Plate 3*

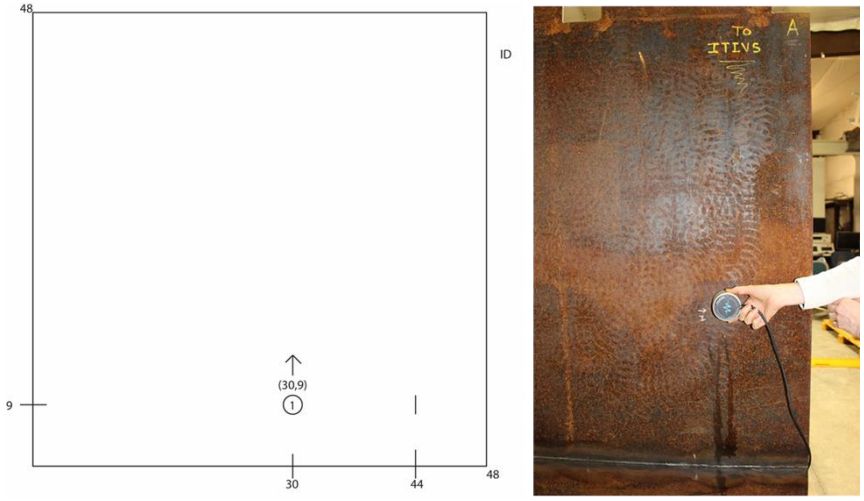


**Figure 26(Left) sketch and (right) photograph of the GWPA sensor on plate 1 at location 1.**

Data was also taken on plate 3, to demonstrate that defects can be detected on the ID while the sensor is on the OD. The GWPA sensor was placed on the OD perpendicular to the defect, defect '$W_i$', as shown in Figure 26. At this location, defect '$W_i$' is clearly detectable as shown in Figure 27. Note, the GWPA image is mirrored when compared to the drawing, because the scan was performed from the OD.

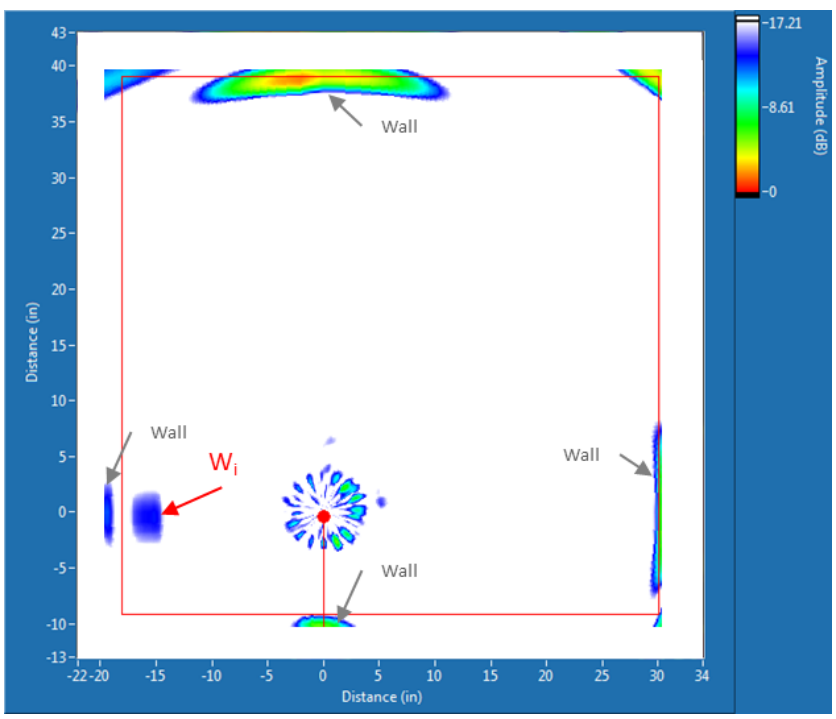


**Figure 27 GWPA scan on plate 3 at location 1. GWPA scan performed at 150 kHz.**

## Composite Imaging

To simulate the limited-access channel that is present along the primary storage tank floor, data was acquired along a diagonal path that was selected by PNNL employees. Due to time constraints, five inspection locations were chosen along the diagonal path. The diagonal path and inspection locations are summarized in an illustration provided in Figure 28.

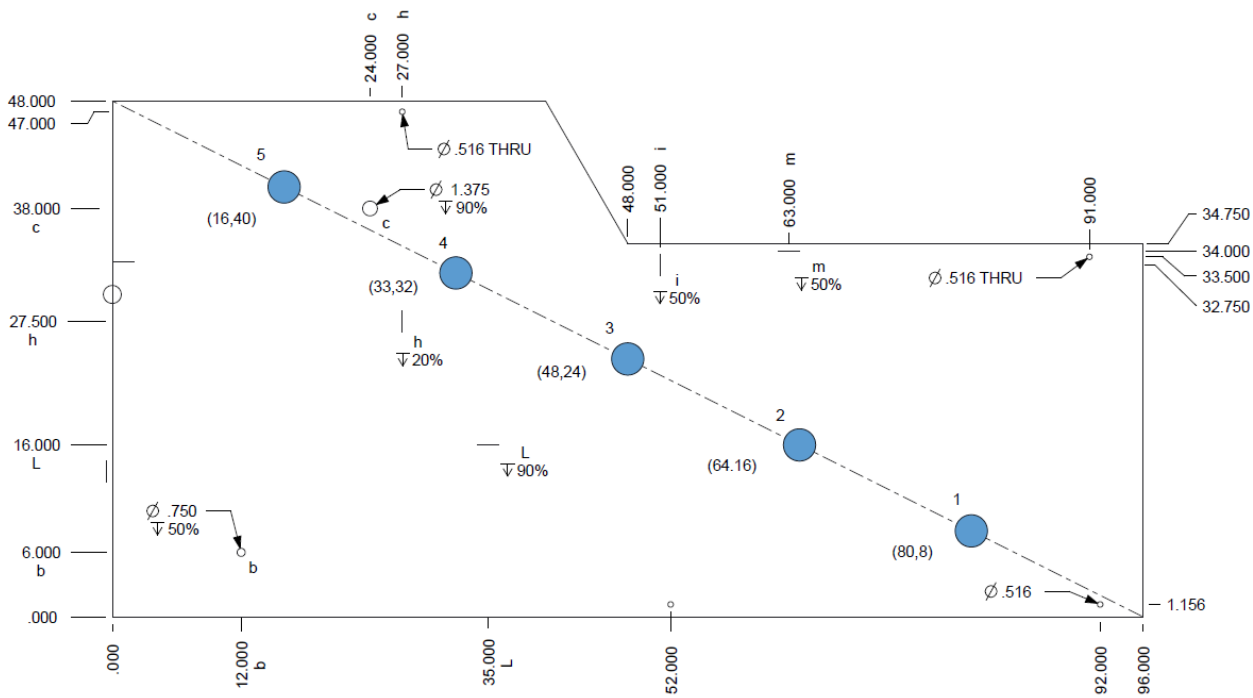


**Figure 28 Sketch of the GWPA sensor locations on plate 1 that were used for composite imaging.**

The GWPA software has the capability of generating composite images from multiple inspection locations. With composite imaging, reflections from side lobes are reduced and indications from structural features and defects are enhanced. This improves the resulting GWPA image and makes data interpretation easier. In this scenario, only five locations were used and a very detailed GWPA image was generated. From the composite images (Figure 29 and Figure 30), defects 'b', 'c', 'h', 'l', and 'i' can clearly be detected. Defects 'g', 'k', and 'a' are also clearly visible when compared to the corresponding amplitude of the weld reflections. Defect 'm' would be difficult to call due to the high amplitude reflections produced from the perfectly cut plate ends, which would not occur in real-world scenarios. Welds have much lower reflection amplitudes than plate ends (by a factor of 3-5x). Not all the side lobe reflections were eliminated, which would improve with more inspection locations and welded joints. Also, around defects 'h' and 'c', there are many indications in this area. This could be due to the ultrasound bouncing between the multiple defects, bolt hole, and plate end. Side lobes in this area may be causing distortion due to the multiple features in the plate. This may be cleared up by increasing the number of inspection

locations. However, with only five inspection locations, all but defect 'm' can be clearly identified in the composite image, which is excellent considering the locations were from a single path along the diagonal of the plate.

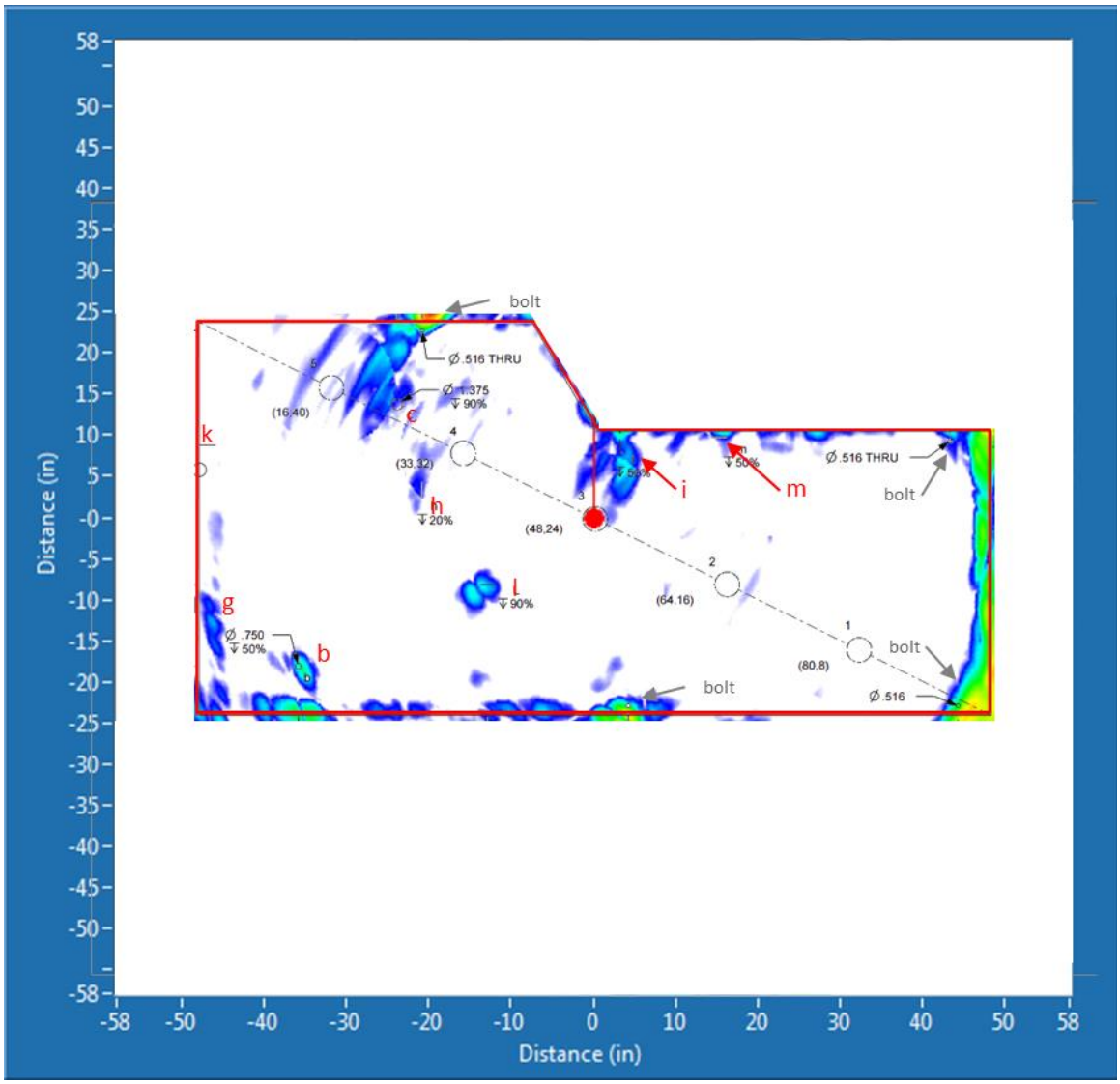


**Figure 29 Composite image generated with data collected at 150 kHz at the five locations along the diagonal path representing the limited access channel on the tank floor.**

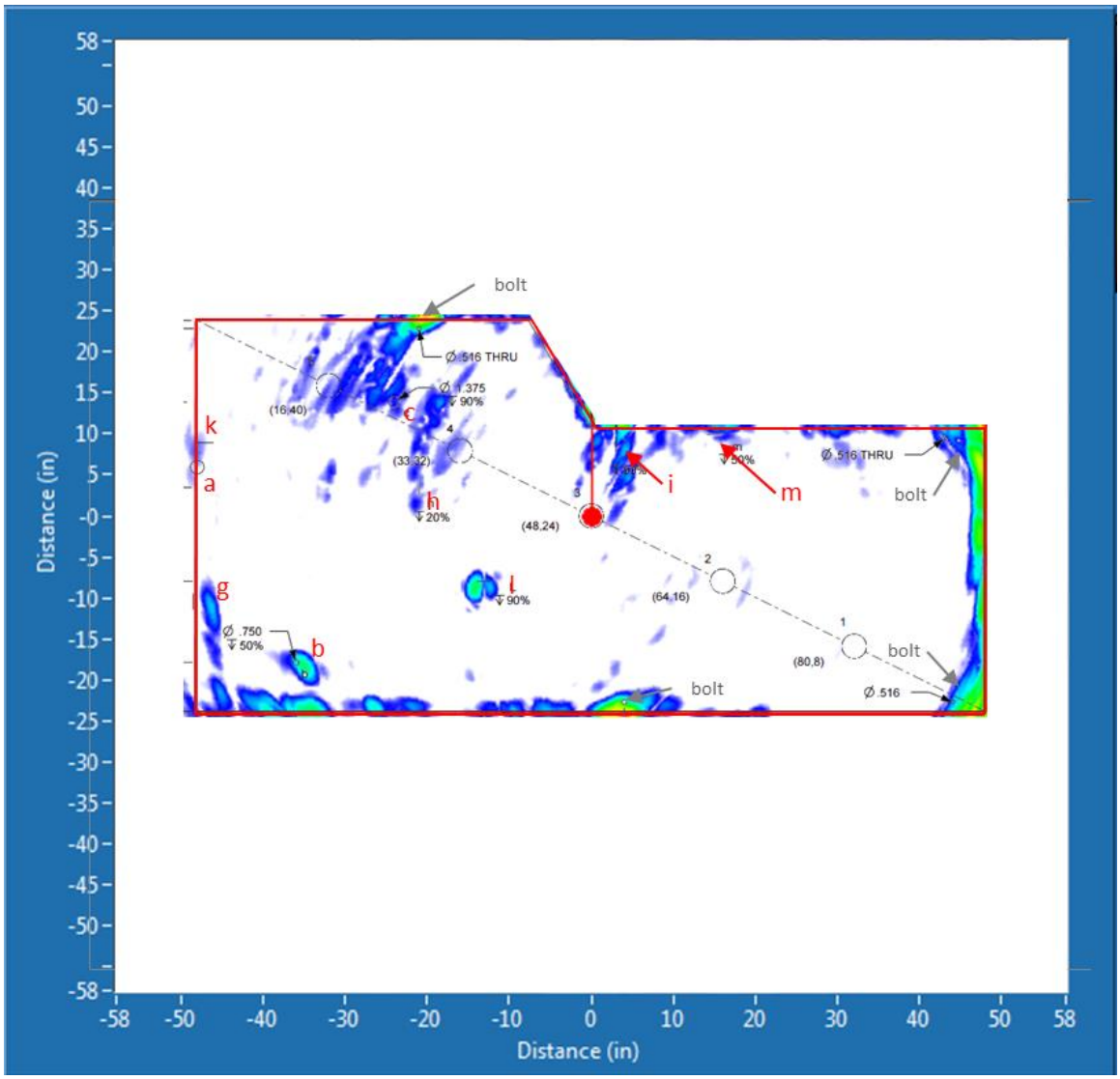


**Figure 30 Composite image generated with data collected at 165 kHz at the five locations along the diagonal path representing the limited access channel on the tank floor.**

The GWPA technology provides a 360-degree inspection at each location, which is paramount when there is limited access for scanning. Without the capability of 360-degree inspection, many defects can be missed due to their geometry and incident angle relative to the probe. This is a common problem with guided wave scanners where the beam is only sent out perpendicular to the scanning direction. 360-degree scanning gives multiple shots on any defects from multiple angles and distances, increasing the likelihood of detection.

## Inspection Summary

### Table 1 Inspection overview.

| | |
|---|---|
| **Participant Name and Company:** | Russell Love (Guidedwave) |
| **Date of Demonstration:** | Jan 31, 2017 |
| **NDE system model and description (transducer specifications, wave modes):** | GWPA Sensor (30 Element, 165 kHz, $SH_0$ wave) |
| **NDE system serial number (optional):** | UltraWave (UW00005), GWPA sensor (PA100466) |

A summary of the GWPA inspection is provided in Table 2. Note, the signal-to-noise ratio was calculated from the final GWPA image and not from individual A-scans. This provides a more accurate representation of the defect detection by accounting for any imaging artifacts.

### Table 2 Defect detection overview.

| **Surrogate Flaw Details** | | | **Documentation** | | | | | | |
|---|---|---|---|---|---|---|---|---|---|
| **Machined Surrogate Flaw** | **Flaw ID in Mock-up** | **Flaw Location and Orientations in Mock-up** | **Mock-up Side Used for Inspection (ID of OD)** | **Flaw Detection Indicated?** | **Ability to Distinguish Surface Connectivity?** | **Transducer Location** | **Data File Date/Time Stamp** | **Pulse Frequency (kHz)** | **Signal to Noise Ratio (dB)** |
| Pit | a | 7/8 to 1/2 inch transition weld | ID | Yes | No | Plate 1: Location 4, Location 7 | 1/31/2017: 2:51PM, 3:31PM | 150, 200 | 28.89, 2.73 |
| Pit | b | Base plate | ID | Yes | No | Plate 1: Location 2, Location 4, Location 5, Location 7 | 1/31/2017: 1:37PM, 2:51PM, 3:07PM, 3:31PM | 150, 150, 165, 200 | 29.77, 37.19, 16.21, 9.29 |
| Pit | c | Base plate | ID | Yes | No | Plate 1: Location 1, Location 2, Location 4, Location 5 | 1/31/2017: 1:58PM, 1:37PM, 2:51PM, 3:07PM | 150, 150, 150, 165 | 8.67, 16.33, 21.98, 9.05 |
| Notch | g | 7/8 to 1/2 inch transition weld | ID | Yes | No | Plate 1: Location 4, Location 5 | 1/31/2017: 2:51PM, 3:07PM | 150, 165 | 7.92, 31.66 |
| Notch | h | Base plate | ID | Yes | No | Plate 1: Location 1, Location 2, Location 3 | 1/31/2017: 1:58PM, 1:37PM, 2:23PM | 150, 150, 200 | 7.42, 11.72, 6.79 |
| Notch | i | Base plate edge | ID | Yes | No | Plate 1: Location 2, Location 3, Location 7 | 1/31/2017: 1:37PM, 2:23PM, 3:31PM | 150, 200, 200 | 25.75, 10.68, 7.41 |
| Notch | k | 7/8 to 1/2 inch transition weld | ID | Yes | No | Plate 1: Location 4, Location 7 | 1/31/2017: 2:51PM, 3:31PM | 150, 200 | 28.89, 5.53 |

| | | | | | | | | | |
|---|---|---|---|---|---|---|---|---|---|
| Notch | l | Base plate | ID | Yes | No | Plate 1: Location 1, Location 2, Location 4, Location 5 | 1/31/2017: 1:58PM, 1:37PM, 2:57PM, 3:07PM | 150, 150, 150, 165 | 9.55, 8.54, 25.75, 16.08 |
| Notch | m | Base plate edge | ID | Yes | No | Plate 1: Location 3 | 1/31/2017: 2:23PM | 200 | 8.17 |
| Notch | al | Plate 2: 7/8 floor plate | ID | Yes | No | Plate 2: Location 1 | 1/31/2017: 6:05PM | 150 | 6.54 |
| Notch | $w_i$ | Plate 3: 7/8 wall plate | OD | Yes | No | Plate 3: Location 1 | 1/31/2017: 6:20PM | 150 | 4.02 |

## 3. Conclusions

1. All the defects were identified on the ½" base plate (plate 1) with the GWPA technology. Some of the more difficult defects, like those in welds or next to cut ends were able to be identified by utilizing multiple acquisition frequencies and sensor locations, which is common practice when performing GWPA inspections.
2. On the thicker 7/8" plate (plate 2), the notch defect was detected with the GWPA technology.
3. On the 7/8" wall plate (plate 3), the GWPA sensor was placed on the OD for inspection. At this location, the notch defect on the ID was successfully identified. The GWPA technology has equal sensitivity to ID/OD defects.
4. All of the inspections on the mock-up were performed with a single GWPA 30-element probe. This probe provided enough frequency bandwidth, resolution, and penetration power to appropriately identify the defects in the base plate. Therefore, it is possible to outfit a robotic crawler with a single probe to perform the necessary inspections.
5. The GWPA technology provides a 360-degree inspection at each location, which is paramount when there is limited access for scanning. Without the capability of 360-degree inspection, many defects can be missed due to their geometry and incident angle relative to the probe. This is a common problem with guided wave scanners where the beam is only sent out perpendicular to the scanning direction. 360-degree scanning gives multiple shots on any defects from multiple angles and distances, increasing the likelihood of detection.
6. The internal sensor array of the GWPA sensors can be made small enough to meet the space limitations of the primary liner access channels.
7. GWPA technology is mature enough for rapid deployment on robotic crawlers. Guidedwave would consult with an established company that specializes in robotic crawler applications, e.g. Adaptive Energy, to design and outfit a crawler with GWPA technology for inspection of the primary tank liner.
8. The main challenges with deploying the GWPA probe into the limited access channel include: surface preparation, shear couplant dispensing, and shear couplant removal. None of these issues are showstoppers, and can be solved with novel engineering designs.
9. Image artifacts would be significantly less prevalent in the actual structure because all of the edges would be welded, instead of free cut edges as in the mock-up.
10. Although not tested here, the selected mode would be insensitive to fluids on either plate surface, whereas non-SH guided wave modes could experience significant attenuation due to fluids.

## Appendix A

**Table 3 Overview of major data acquisition settings.**

| Parameter Name | Parameter Value |
|---|---|
| **Pulse Frequency (kHz)** | 150, 165, 200 |
| **Pulse Voltage (V)** | 300 |
| **Pulse Cycles** | 5 |
| **Receiver Gain (dB)** | 45 |
| **Sampling Rage (MHz)** | 3.125 |

# Appendix B

# Innerspec

Innerspec
High-performance NDT solutions

**AMERICAS**
Innerspec Technologies, Inc.
2940 Perrowville Road
Forest, VA 24551, USA
Tel: +1.434.948.1301
Fax: +1.434.948.1313
www.innerspec.com

**EUROPE**
Innerspec Technologies Europe, S.L.
Avenida Madrid km. 27.2, nave 8
28802 Alcalá de Henares, SPAIN
Tel: +34.911.337.024
Fax: +34.911.881.344
www.innerspec.com/eu

**ASIA**
Innerspec Technologies China, LLC.
Room 315, Building 6
Yaohua Business Plaza
Shanghai, 200126, CHINA
Tel: +86.(0)21.58358103
Fax: +86.(0)21.58357805
www.innerspec.com/cn

February 14, 2017

Ms. Kayte Denslow
Mr. Bill Glass
PNNL

Ref. DST Mockup Tests by Innerspec

Dear Ms. Denslow and Mr. Glass,

Thank you for your invitation to demonstrate our technology and capabilities on the DST mockup. This document provides additional information and details of the results.

The mockup was tested using different techniques, including EMAT-generated Shear Horizontal waves ($SH_{0)}$ using a magnetostrictive strip that had to be attached to the part using tape. We also tested EMAT-generated Shear Vertical waves (SV), and Lamb waves (A0 mode) in both pitch-catch and pulse-echo configurations.

Overall we were able to detect all defects in the mock-up base plate with at least one technique using off-the-shelf instrumentation and sensors. The best results were achieved using magnetostrictive $SH_0$ EMAT, and SV waves. Notwithstanding this, there is still significant work to be done to the instrumentation, sensors, and technique to improve detection, and enhance sizing capabilities, plus the development of a deployment mechanism.

Thank you again for your invitation to provide this demonstration. We hope that these promising results will warrant additional work to take this project further.

Sincerely,

Borja Lopez
**President & CEO**
Innerspec Technologies, Inc.

## 1. Introduction to EMAT Technology

EMAT or Electro Magnetic Acoustic Transducer is an Ultrasonic Testing (UT) technique that generates the sound in the part inspected instead of the transducer, therefore no couplant is needed.

An EMAT induces ultrasonic waves into a test object with two interacting magnetic fields. A relatively high frequency (RF) field generated by electrical coils interacts with a low frequency or static field generated by magnets to generate a Lorentz force in a manner similar to an electric motor. This disturbance is transferred to the lattice of the material, producing an elastic wave. In a reciprocal process, the interaction of elastic waves in the presence of a magnetic field induces voltage in the receiving EMAT coil circuit. For ferromagnetic conductors, magnetostriction produces additional stresses that enhance the signals to much higher levels than could be obtained by the Lorentz force alone. Various types of waves can be generated using different combinations of RF Coils and Magnets.

EMATs are the only practical means for generating shear waves with horizontal polarization (SH waves), which do not travel through low-density couplants. The ability to easily produce SV waves, Guided SH waves and lamb waves make EMAT ideal for generation of guided waves, used in the inspection of plates, tubes and round products.

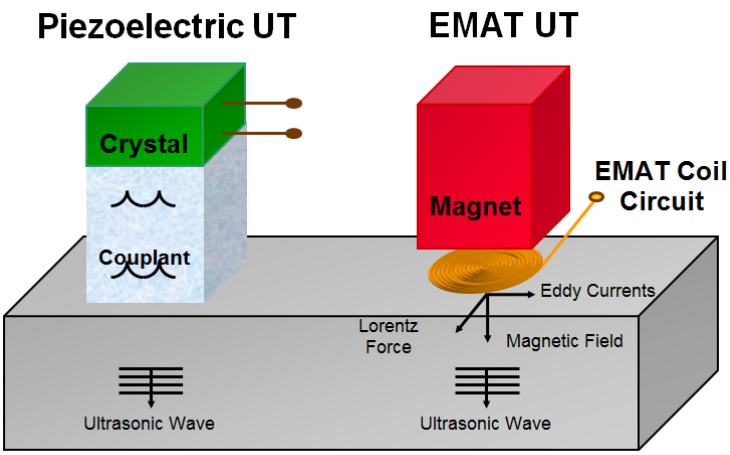


**Figure 1. Principle of EMAT and Comparison with Piezo Transducer**

### 1.1. Generation of SH Normal Beam

EMAT ultrasonic is an ideal method for thickness measurements on conductive materials. Because the sound is generated in the part inspected instead of the transducer, EMATs have the following advantages over more conventional piezoelectric transducers:

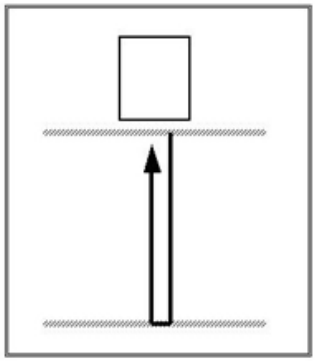

- Dry, non-contact inspection permits inspection of very hot (up to 750ºC) and very cold materials. Lack of couplant also provides extremely reliable and repeatable inspections with micrometer accuracy.
- Imperviousness to surface conditions. The materials can be coated, rough or dirty thus eliminating the need for conditioning the part for measurement.
- Easier probe deployment. Not having wedges or couplant, Snell's law of refraction does not apply, and the angle of the probe does not affect the direction of propagation. This makes them easier to control and deploy, especially in automated environments. EMAT sensors can be used in pitch-catch (separate transmitter and receiver) or pulse-echo (same transmitter and receiver) mode. The most common wave modes used for thickness measurement are Longitudinal (L) or Shear Horizontal (SH). SH waves can be very easily generated on both ferromagnetic and non-ferromagnetic materials whereas L waves are more difficult to generate on ferromagnetic materials.

In a normal beam inspection using Shear waves or Longitudinal waves, the wave "Time of Flight" (TOF) is measured for the back-wall reflection (travel time to the bottom surface and back) and using calibrated "Velocity" of wave mode in the material the thickness value can be easily calculated.

$$Thickness = Vel_{wave\ mode}\ x\ TOF/2$$

### 1.2. Generation of SV Waves

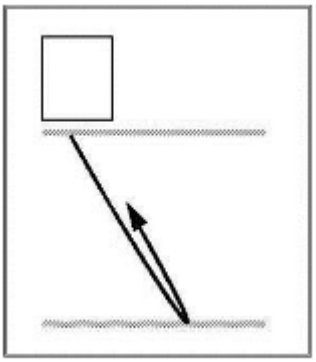

An EMAT can induce Shear Vertical (SV) wave in the test object using the same principle of two interacting magnetic fields as discussed above. In the case of SV wave generation a meander shaped coil is used along with a permanent magnet. An EMAT meander coil is excited with a high frequency RF field which interacts with the static field generated by permanent magnet to produce Lorentz forces. This disturbance is transferred to the atomic lattice of the material producing elastic wave. In a reciprocal process, the interaction of elastic waves in the presence of a magnetic field induces currents in the receiving EMAT coil circuit. For ferromagnetic conductors, magnetostriction produces additional stresses that enhance the signals to much higher levels than could be obtained by the Lorentz force alone.

Figure 2 illustrates the physical principle of SV wave excitation using a meander coil and a permanent magnet. The meander coils produces a meander shaped eddy current, which in turn generates a periodic pattern of excitation force on the surface of the material. This results in the generation of SV wave in the test sample. In case of EMAT the strongest SV wave is generated at 35 degrees which propagates by bouncing within the top and bottom surfaces of the structure. The excitation frequency of SV wave at 35 degrees is dependent upon the wavelength "λ" (separation between two alternate wires of an emat coil) of the meander coil and the velocity of shear wave in the material, and can be calculated as:

$$f_{SV} = \frac{Vel_{Shear}}{\lambda\, Sin(35)}$$

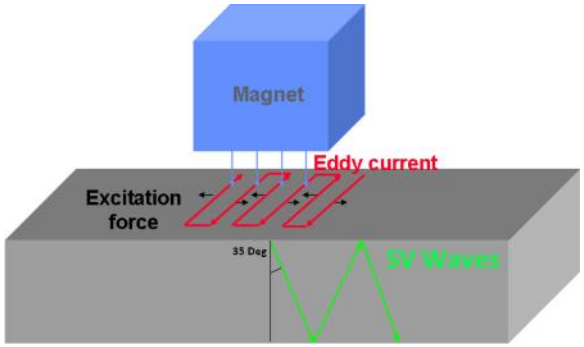


**Figure 2. Principle of SV Wave Excitation using EMATs**

### 1.3. Generation of Guided Waves

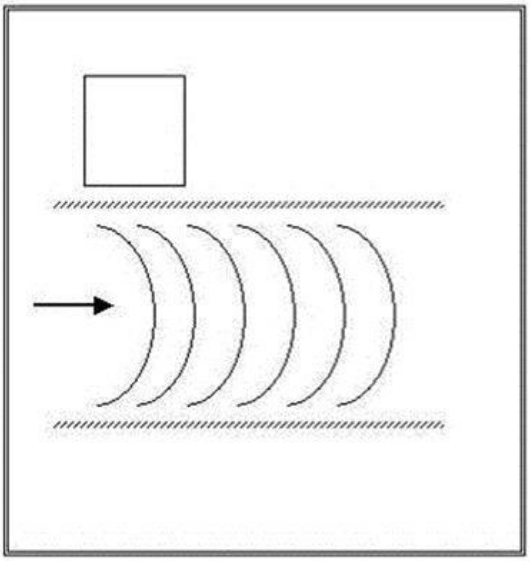

Guided Wave Testing is a Non-Destructive Testing technique method that employs ultrasonic stress waves that propagate along a structure while guided by its boundaries. Guided waves permit covering long distances from a single point with a limited number of sensors, making it very effective for rapid scanning of pipelines and tanks.
On relatively thin structures, it is possible to generate volumetric guided waves that fill up the material and permit a complete, volumetric inspection. The most common types of volumetric waves are Shear Horizontal (SH) and Lamb. This Application Sheet covers the inspection with EMAT-generated Lamb waves.

Lamb waves travel throughout the material with both vertical and forward motion in an elliptical pattern. These waves are dispersive by nature, and very sensitive to thickness variations. They can be classified in symmetric and asymmetric modes. The introduction of boundary conditions makes Lamb wave problems inherently more difficult than the more conventional bulk waves. Unlike the finite number of modes present in a bulk wave problem, there are an infinite number of modes associated with a given Lamb wave application. That is, a finite body can support an infinite number of different Lamb wave mode modes.

#### 1.3.1. Generation of Lamb Waves – Lorentz Force Mechanism

In Lorentz type of EMAT, the magnetic field is perpendicular to the eddy currents and takes advantage of Lorentz forces (F = J x B). A permanent magnet provides magnetic bias in the normal direction whereas RF current running in the coil generates eddy currents and a time varying magnetic field. The interaction of these two magnetic fields generates vibrations in the lattice of the material under test. In this case the frequency of excitation is determined using “Phase Velocity” dispersion curves and excited wave travels in the material using “Group Velocity Dispersion Curves.

In the following figure dispersion curve analysis is presented for 0.50” thick steel plate and a 0.75” thick steel plate and wave excitation frequencies highlighted for a meander emat with 0.72” wavelength. (Wavelength = 2 x $\text{Spacing}_{\text{emat wires}}$).

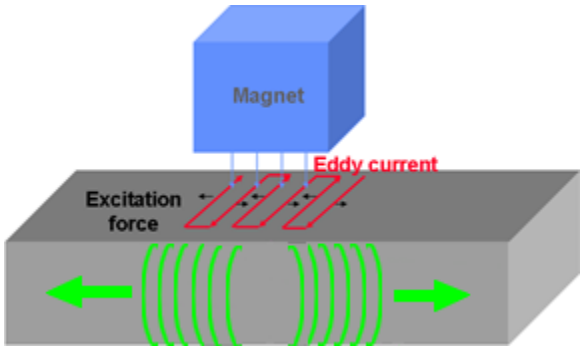


**Figure 3. Principle of Lamb Wave Excitation using EMATs**

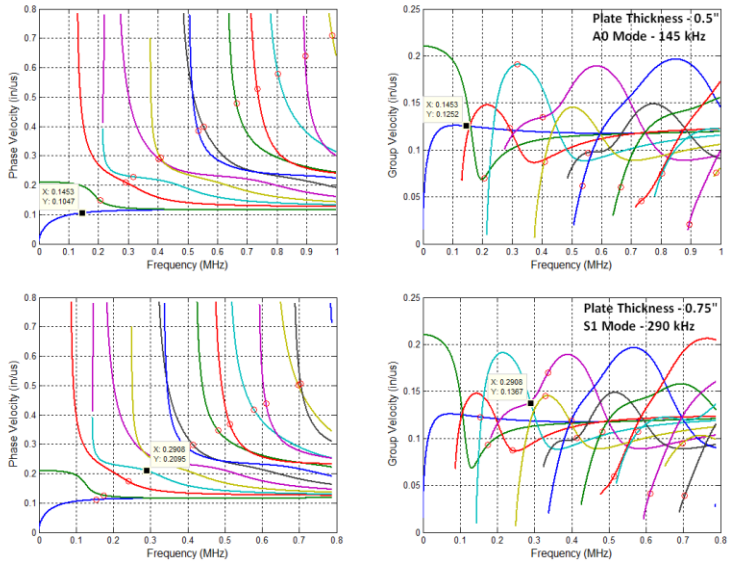


**Figure 4. Lamb Wave Dispersion Curves for 0.5" and 0.75" Thick Steel Plates.**

### 1.3.2. Generating $SH_0$ Wave - Magnetostrictive Mechanism

Magnetostriction is a phenomenon which causes changes in the material dimensions when under the influence of a magnetic field. It was first discovered and described by James Joule and was called Joule magnetostriction (Joule, 1842). The principle of magnetostriction is based on the domain oscillation or rotation due to the applied magnetic fields. Typically, a permanent magnetic field is used to give the domains a preferred orientation and then variable magnetic fields are applied to initiate the rotation of the domains, causing the dimensional changes. Depending on the mutual orientation of magnetic fields (in plane or out of plane), oscillation of domains can produce longitudinal or transverse vibrations.

**Figure 5. Magnetostrictive Strip and EMAT Coil**

For practical guided wave testing, the fundamental transverse vibration mode ($SH_0$) was found to be best because of its low dispersive nature. Low dispersion implies that the group and phase velocities of guided waves are not frequency-dependent. This feature of the fundamental mode on shear guided waves significantly simplifies the interpretation of signals. Also, unlike other wave modes, shear horizontal waves show no out-of-plane particle displacement, thus they do not couple easily and lose energy onto adjacent liquids or structures (e.g. refractory material or waste sludge). For these reasons, magnetostrictive EMAT that produce transverse and horizontally polarized vibrations will be preferred for this application. Dispersion Curves for Shear Horizontal waves are presented in the following Figure.

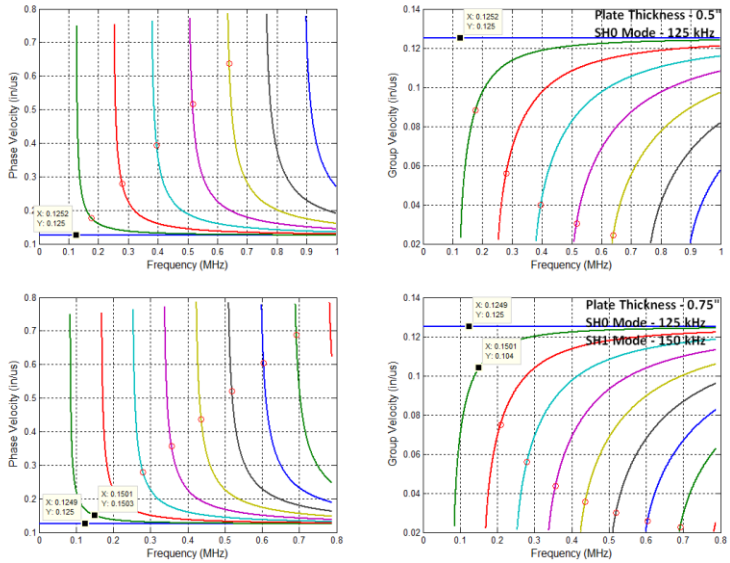


**Figure 6. SH Wave Dispersion Curves for 0.5" and 0.75" Thick Steel Plates.**

In order to enhance the magnetostrictive properties of the material, a metallic strip is adhered to the plate. This metallic strip has been treated on a special oven using Innerspec's proprietary process to maximize its magnetostrictive properties and help retain the bias magnetic field in the intended orientation. Once properly adhered, the vibrations generated in the strip will be transferred to the material being inspected in the form of shear horizontal waves.

The sensor used for this inspection was an off-the-shelf coil designed to produce $SH_0$ wave mode at 128 kHz in pulse-echo (PE) configuration. For thicker materials and defect characterization, we recommend that other wavelengths, aperture, angle angles, and array configurations are modeled and tested. .Also, for deployment in the field, pressure coupling should also be tested (by means of air bladders or other) and compared with standard adhesives (epoxy and double stick tape). A conceptual diagram of a pressure-coupled sensor is shown on Figure 7 below.

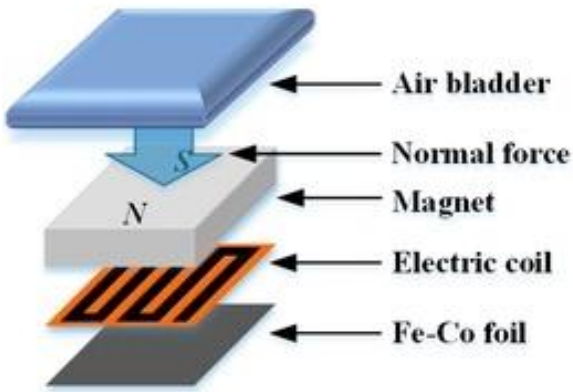


**Figure 7: Conceptual Diagram of Custom Sensor**

## 2. DST Bottom Mockup

A top view image of the mock-up along with defect dimensions and positional map is displayed below.

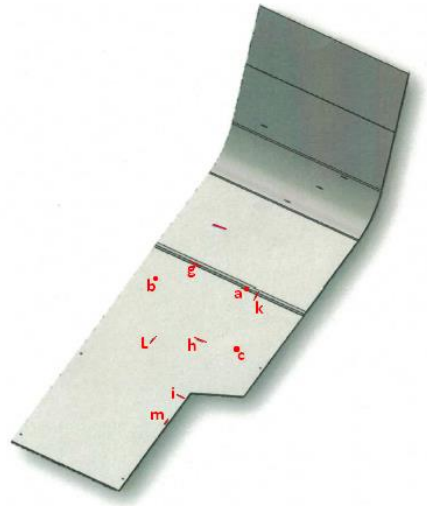


**Figure 8. Top View of the Mockup**

### 2.1. Surrogate Flaw Matrix

| Machined Surrogate Flaw* | Flaw Depth** | Length and Width | Flaw ID in Mock-up | Flaw Location and Orientation in Mock-up |
|---|---|---|---|---|
| Pit | 50% t, 0.25 in. | 0.75 in. diameter | a | 7/8 to ½-inch transition weld |
| Pit | 100%~~50%~~ t, 0.50 in. ~~0.25 in.~~ | 0.75 in. diameter | b | Base plate |
| Pit | 90% t, 0.45 in. | 1.375 in. diameter | c | Base plate |
| Notch | 50% t, 0.25 in. | 2 in. long, 0.125 in. wide | g | 7/8 to ½-inch transition weld, circumferential orientation (i.e., parallel to weld) |
| Notch | 20% t, 0.10 in. | 2 in. long, 0.125 in. wide | h | Base plate, circumferential orientation (i.e., parallel to weld) |
| Notch | 50% t, 0.25 in. | 2 in. long, 0.125 in. wide | i | Base plate edge, circumferential orientation (i.e., parallel to weld) |
| Notch | 50% t, 0.25 in. | 2 in. long, 0.125 in wide | k | 7/8 to ½-inch transition weld to base plate, axial orientation (i.e., perpendicular to weld) |
| Notch | 90% t, 0.45 in. | 2 in. long, 0.125 in wide | L | Base plate, axial orientation (i.e., perpendicular to weld) |
| Notch | 50% t, 0.25 in. | 2 in. long, 0.125 in wide | m | Base plate edge, axial orientation (i.e., perpendicular to weld) |

* Surrogate flaws will be machined full-radius pits with a diameter-to-depth ratio of 3:1 and machined notches.

** t = plate thickness

**Figure 9. Surrogate Flaw Matrix for the Mockup**

## 2.2. Location Map of Surrogate Flaws

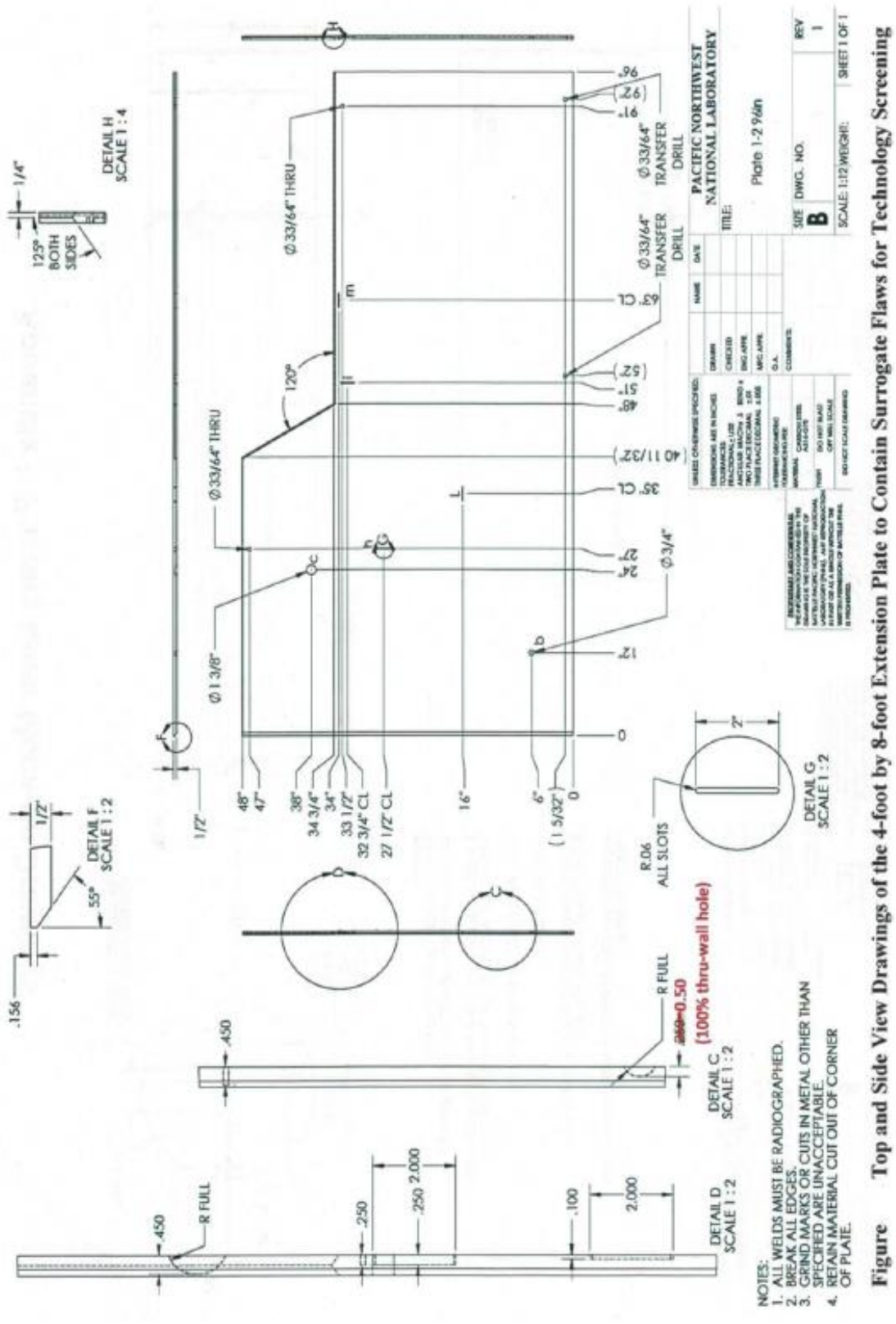


**Figure 10. Dimensional Location Map for Surrogate Flaws**

## 3. Test Results

### 3.1. Magnetostrictive Sensor and Base Plate – 128 kHz SH0 Wave Mode

The magnetostrictive strip was applied using a dual stick tape on one edge (transverse) of the mockup plate as shown in Figure 5 above and a manual b-scan was performed. The scan axis is not represented to scale due to a lack of an encoder with the sensor used for these tests. The data was taken with Innerspec's portable PowerBox H instrument. The data once saved in the device can be recalled and examined by placing cursors to manipulate and extract individual A-scans for each defect indication in a B-scan.

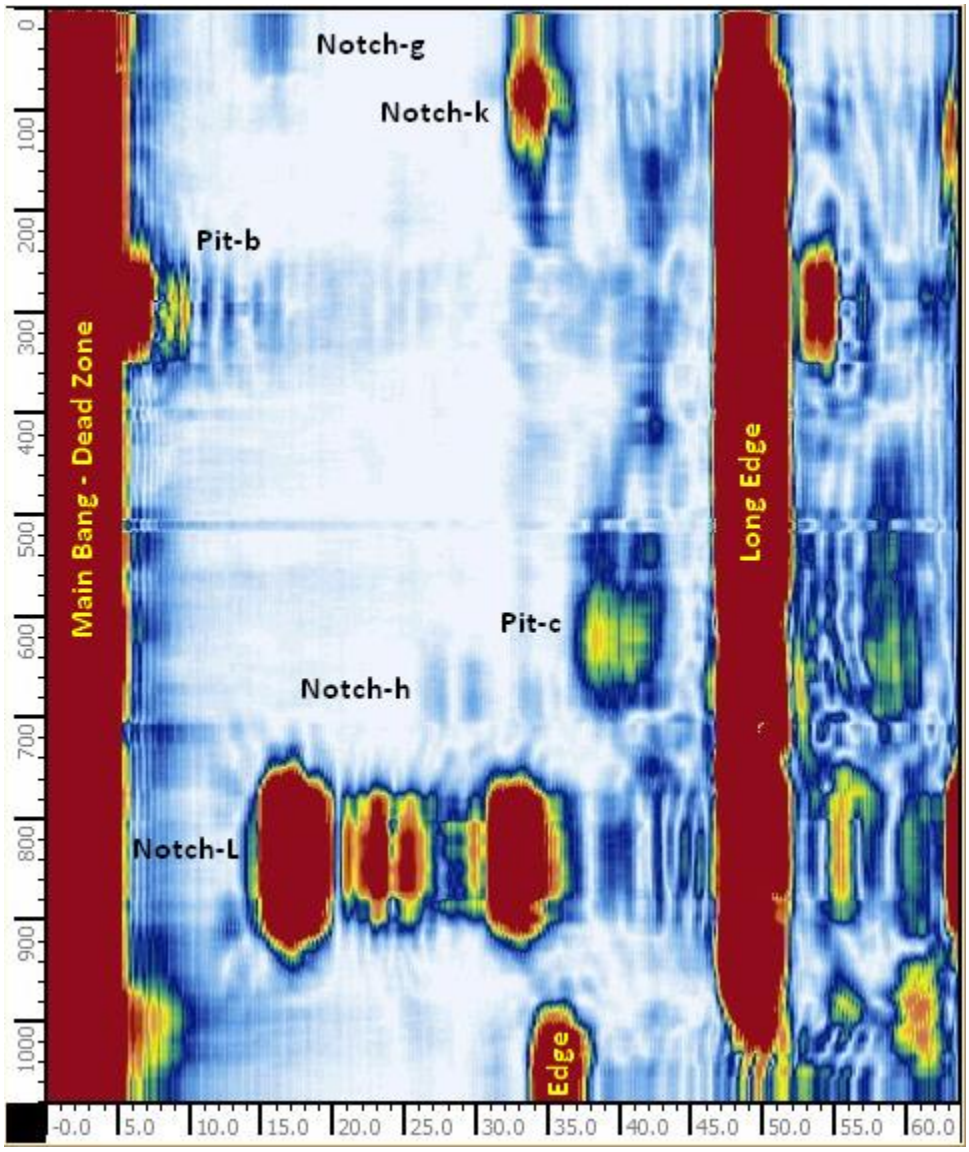


**Figure 11. Manual B-Scan of bottom from edge**

Remarks:

- Vertical axis is the scan axis while the horizontal axis is the distance to the defect with reference to the sensor position.
- All the defects on the first section of the base plate (48" wide) were clearly detectable placing the sensor on one edge of the mockup.
- This test was performed using SH0 wave mode at 128 kHz.

### 3.1.1. Notch-g

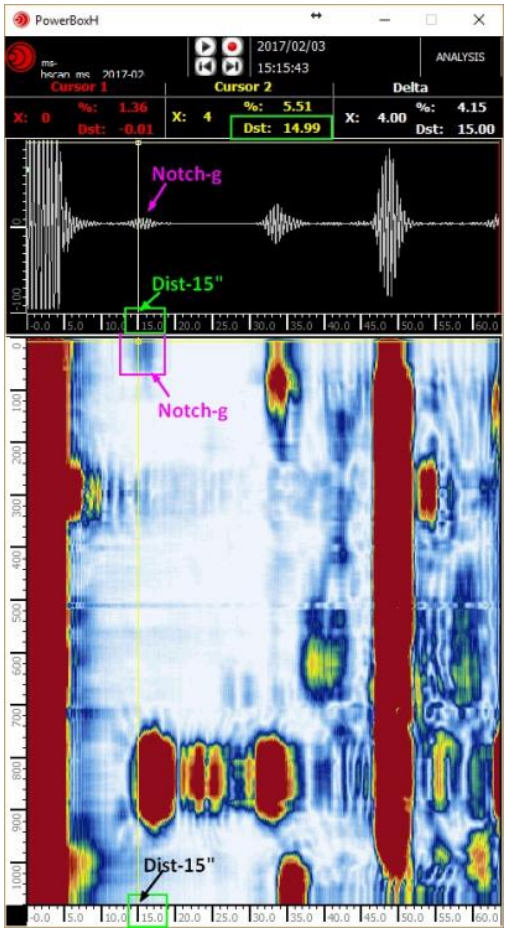


Straight (B-scan above)

Angled Sensor

**Figure 12. Straight A-scan and B-scan of notch g, and A-scan at an angle**

Remarks:

- “Notch-g” was 50% deep (0.25”), 2” long and 0.125” wide placed parallel to weld in 7/8 to ½ inch transition weld.
- The B-scan response from “Notch-g” is weak due to the orientation of this notch (vertical to the beam direction) and the location of the strip (the strip was offset from the weld). Angling the sensor by 15-20º provided an increase in signal to noise x3 or more (scanning in this way would require a sensor at an angle).

### 3.1.2. Pit-a and Notch-k

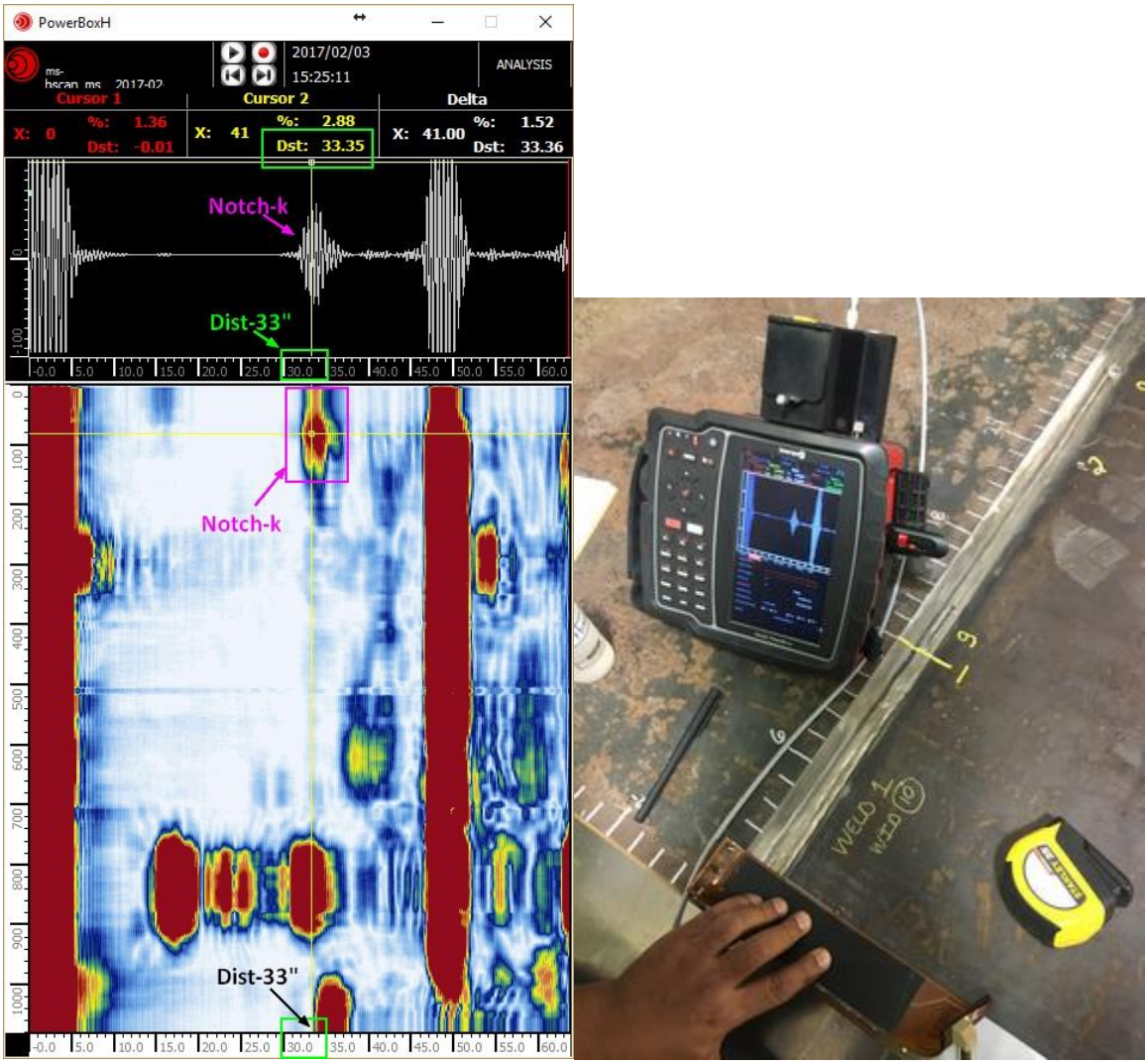


**Figure 13. Position of Sensor for Notch-k – 4 inch**

Remarks:

- “Pit-a” was 50% (0.25”) deep, 0.75” diameter and placed in 7/8 to ½ inch transition weld.
- “Notch-k” was 50% (0.25”) deep, 2” long and 0.125” wide placed perpendicular to weld in 7/8 to ½ inch transition weld.
- Response from “Pit-a” is not apparent on the B-scan which was scanned along the strip.
- Angling the sensor provided only a faint response on Pit-a (Figure 12. Angled Sensor) that was mostly masked by the amplitude Notch-k.
- Notch-k, being perpendicular to the weld, was easily detectable with strong reflections.

### 3.1.3. Pit-b

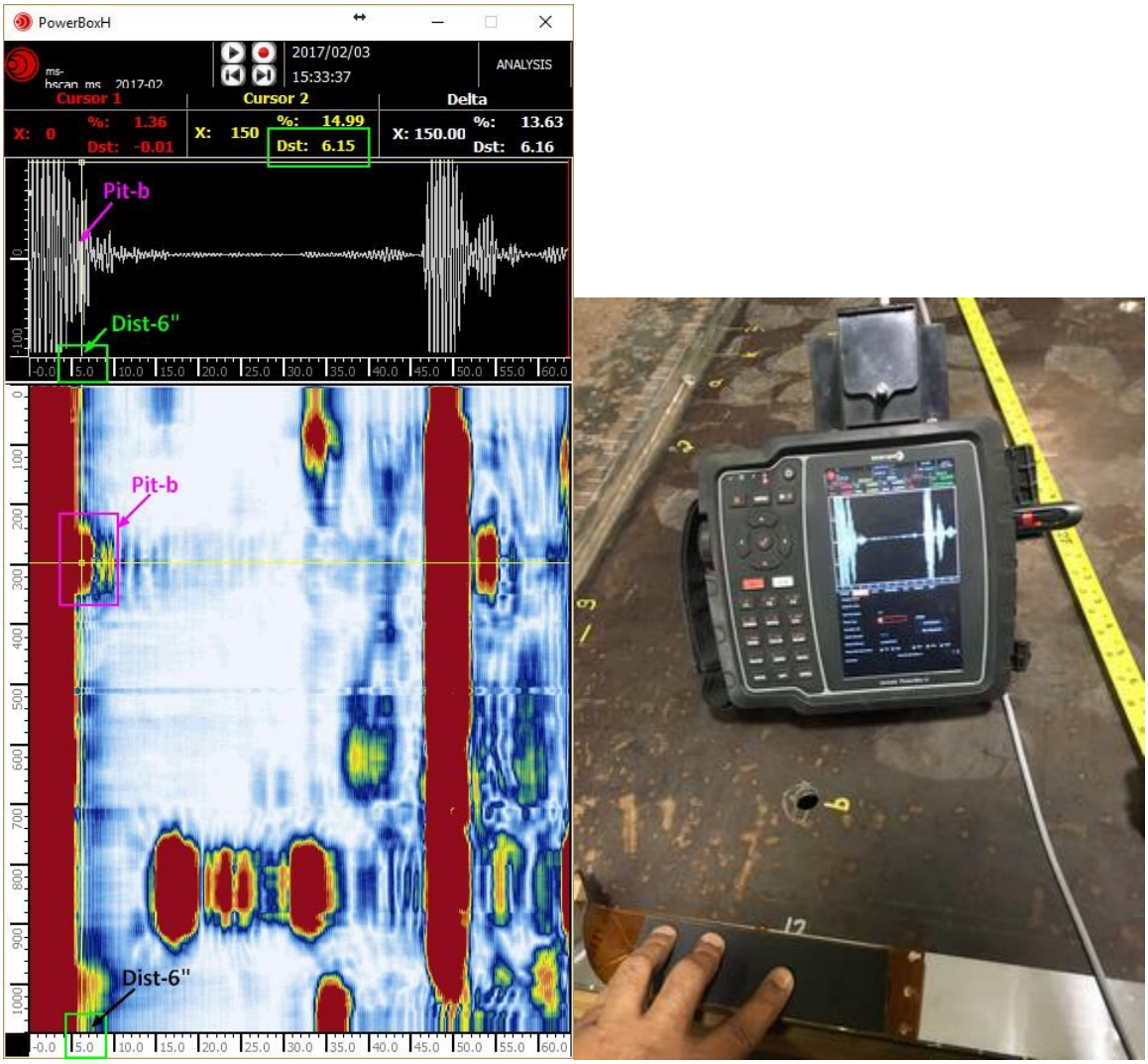


**Figure 14. Position of Sensor for Pit-b – 11 inch**

Remarks:

- “Pit-b” is thru wall 100% deep and 0.75” diameter placed in the base metal.
- Response from “Pit-b” was very strong, but by being closer to the edge the response is partially merged with the main-bang (dead zone).
- Inspection of the dead zone of the sensor should be performed from the other side of the mockup (adjacent channel in the tank).

### 3.1.4. Pit-c

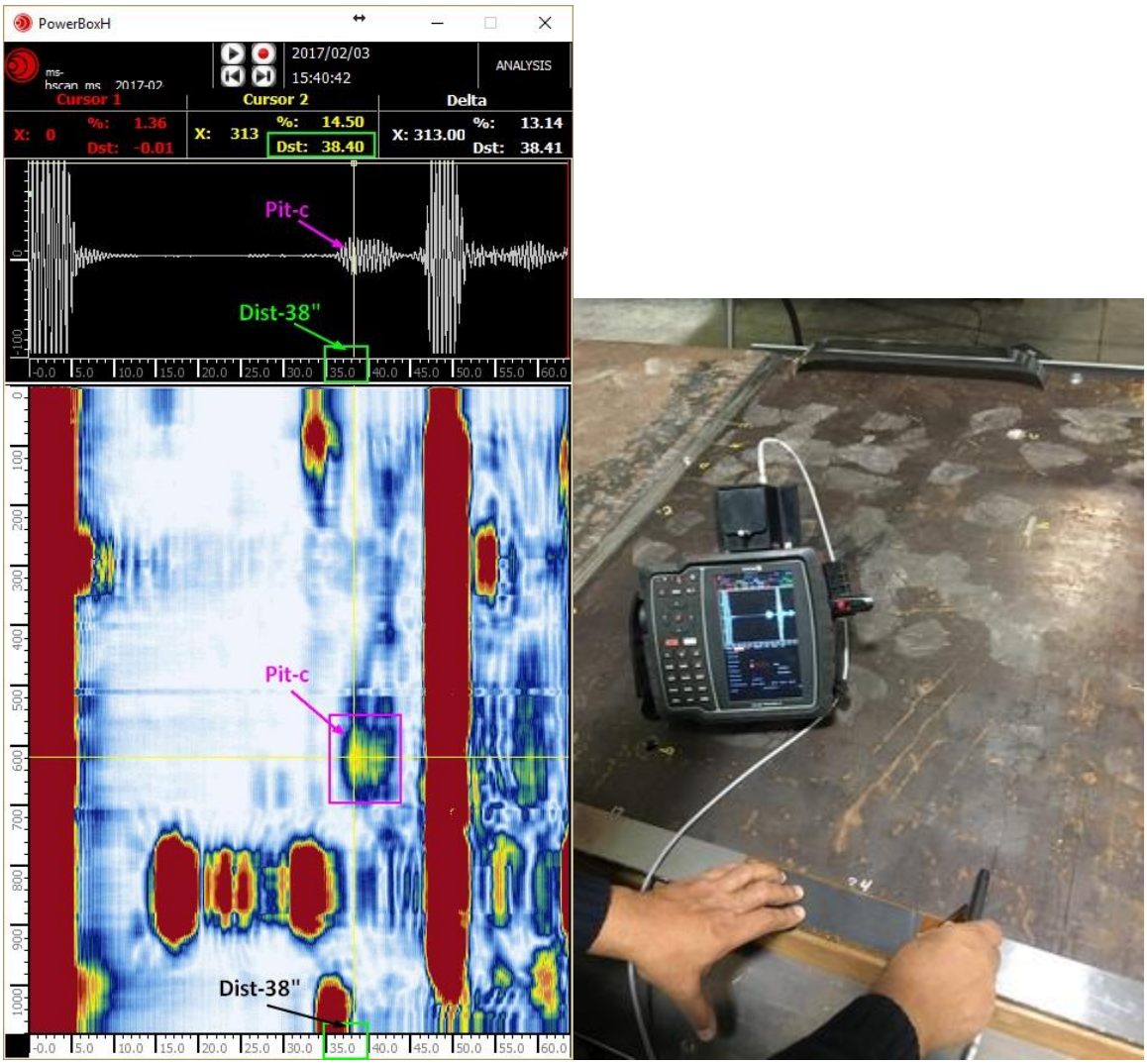


**Figure 15. Position of Sensor for Pit-c – 24”**

Remarks:

- “Pit-c” is 90% (0.45”) deep with a diameter of 1.375 inch and placed in the base plate.
- “Pit-c” is clearly detectable with very good signal to noise ratio.

### 3.1.5. Notch-h

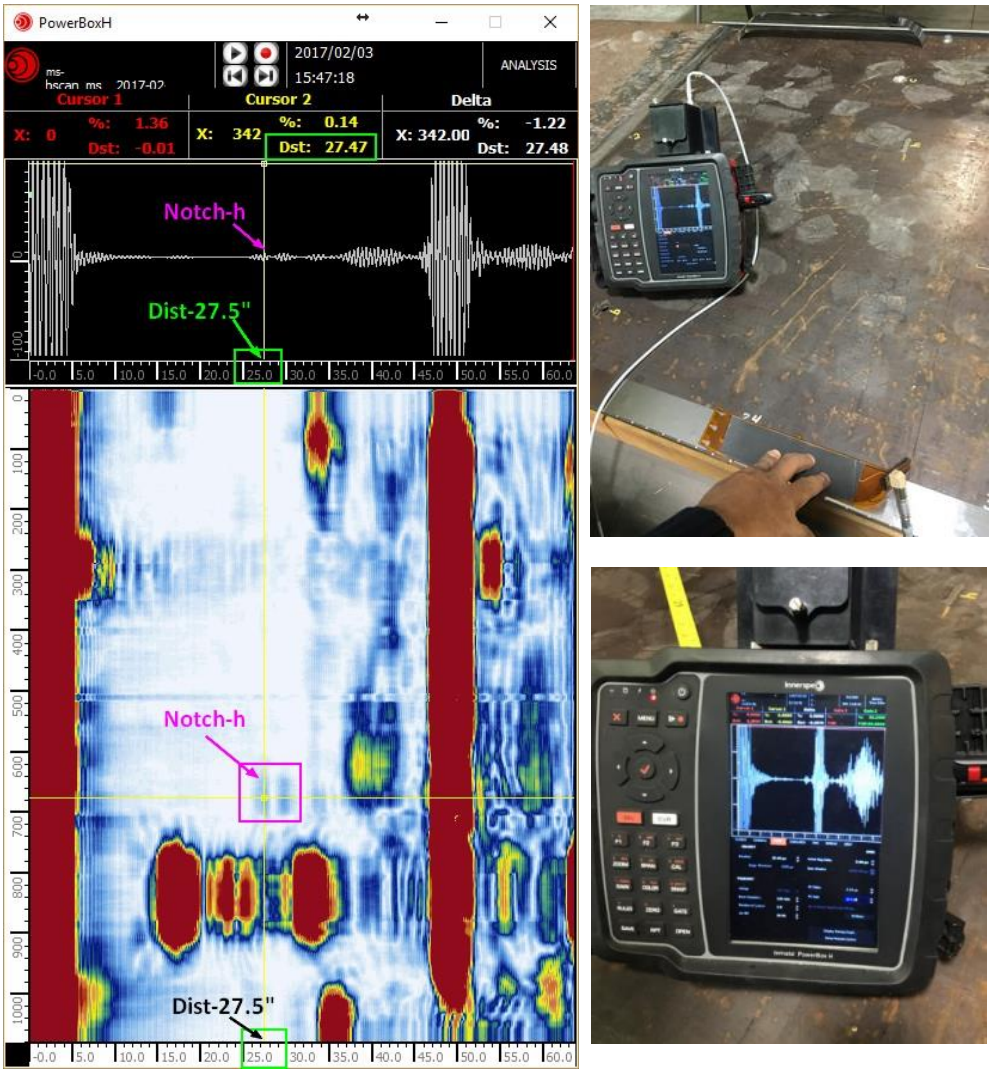


**Figure 16. Position of Sensor for Notch-h – 26 inch**

Remarks:

- “Notch-h” was 20% (0.10”) deep, 2” long and 0.125” wide placed parallel to weld in base plate, and vertically from the scan direction.
- “Notch-h” response is marginal (top A-scan and B-scan) due to the orientation of the notch and relative shallow depth with reference to the plate thickness.
- By increasing gain by 6dB (from 9 to 15dB), the signal to noise increased to approx. 3:1 (bottom A-scan). This could be equivalent to using Distance Amplitude Correction which was not applied to these tests (we didn’t create DAC curves).

### 3.1.6. Notch-L

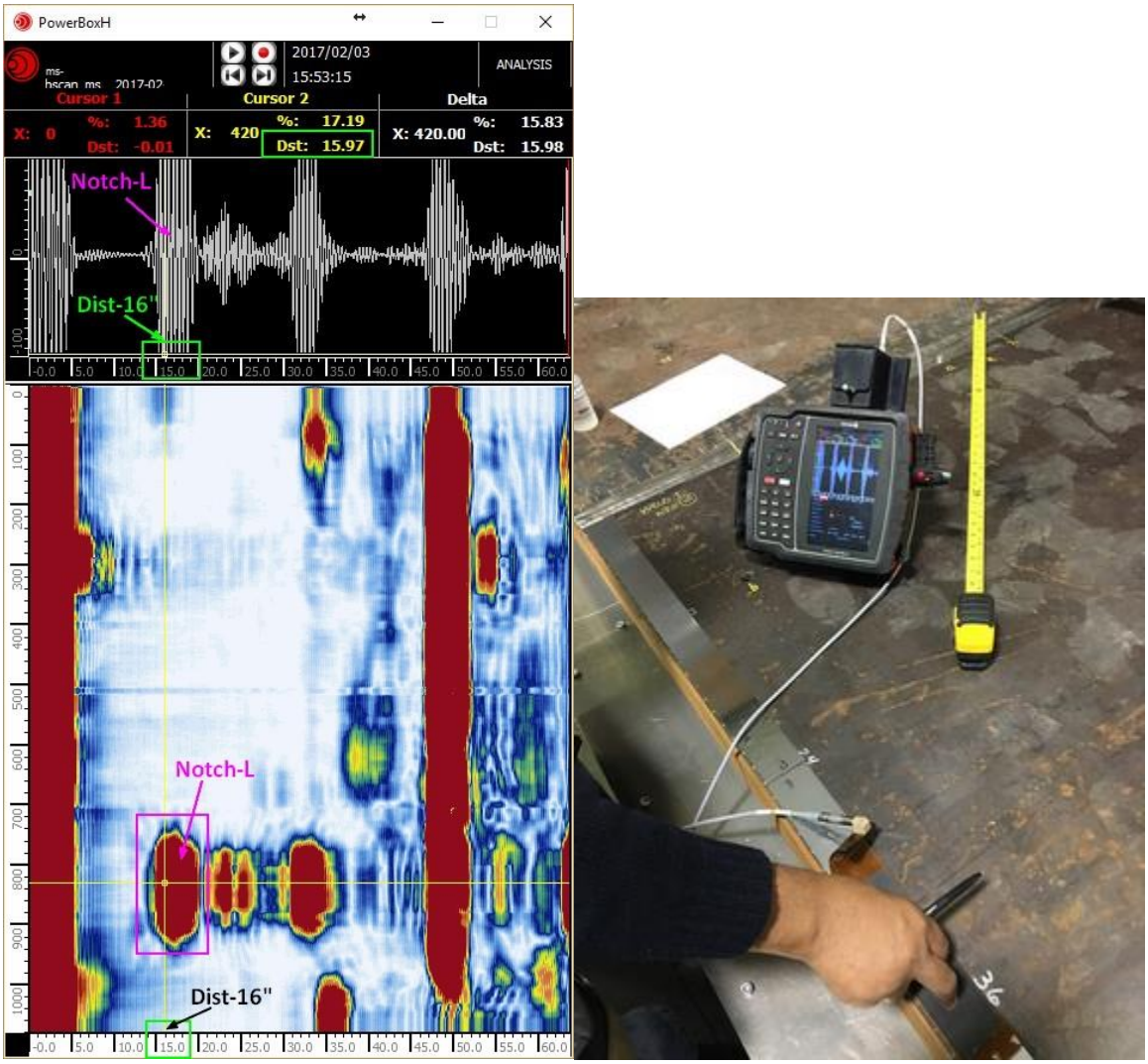


**Figure 17. Position of Sensor for Notch-L – 35 inch**

Remarks:

- “Notch-L” was 90% (0.45”) deep, 2” long and 0.125” wide placed perpendicular to weld in base plate.
- “Notch-L” response is very strong due to its axial orientation and depth.
- The secondary reflection is a result of the sound bouncing back from the edge, and hitting the notch again. The smaller reflections in between the two strong ones are caused by reverberations from the edge (potentially they could be eliminated using a unidirectional coil).
- The nature of the secondary reflection could have been discerned by using different angles or sensor arrays.

### 3.1.7. Notch-i

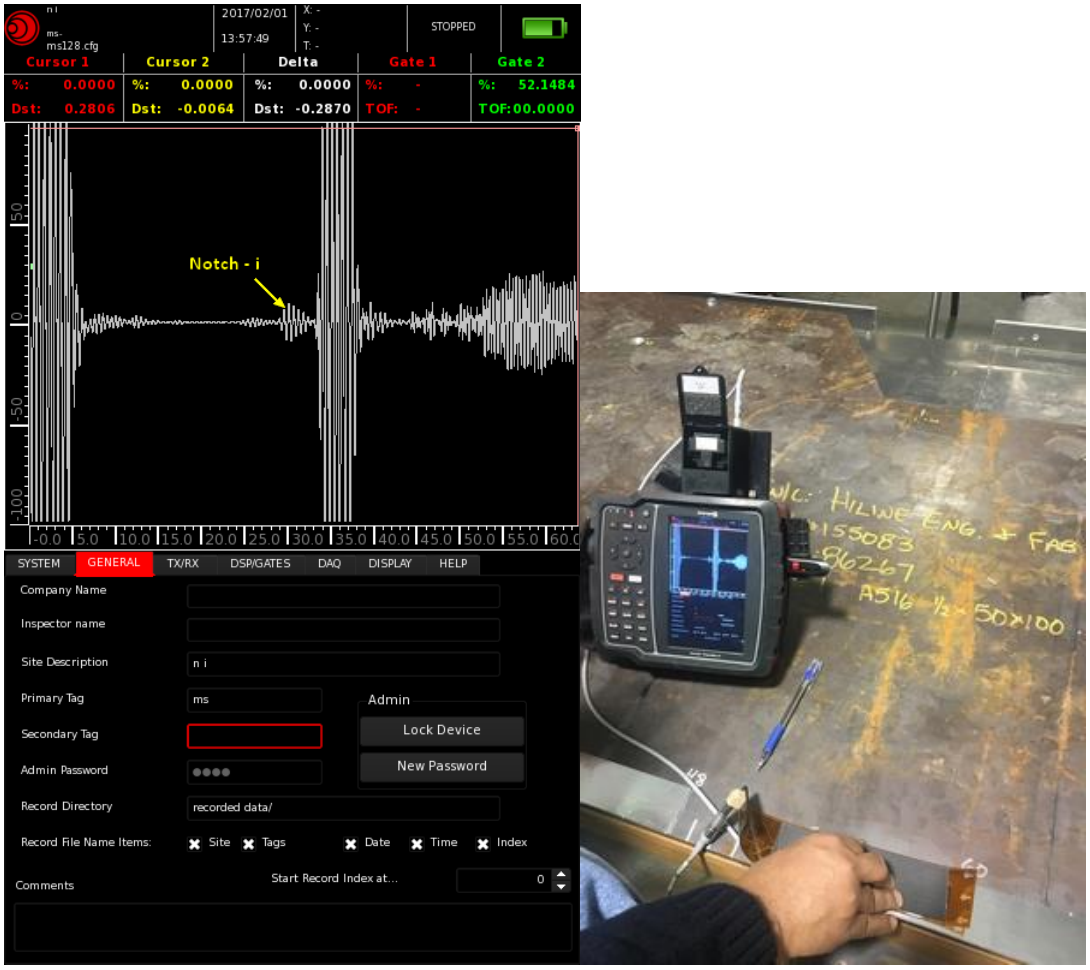


**Figure 18. Position of Sensor for Notch-I – 54 inch**

Remarks:

- “Notch-i” was 50% (0.25”) deep, 2” long and 0.125” wide placed parallel to weld in base plate.
- “Notch-i” was detected with good signal to noise.

### 3.1.8. Notch-m

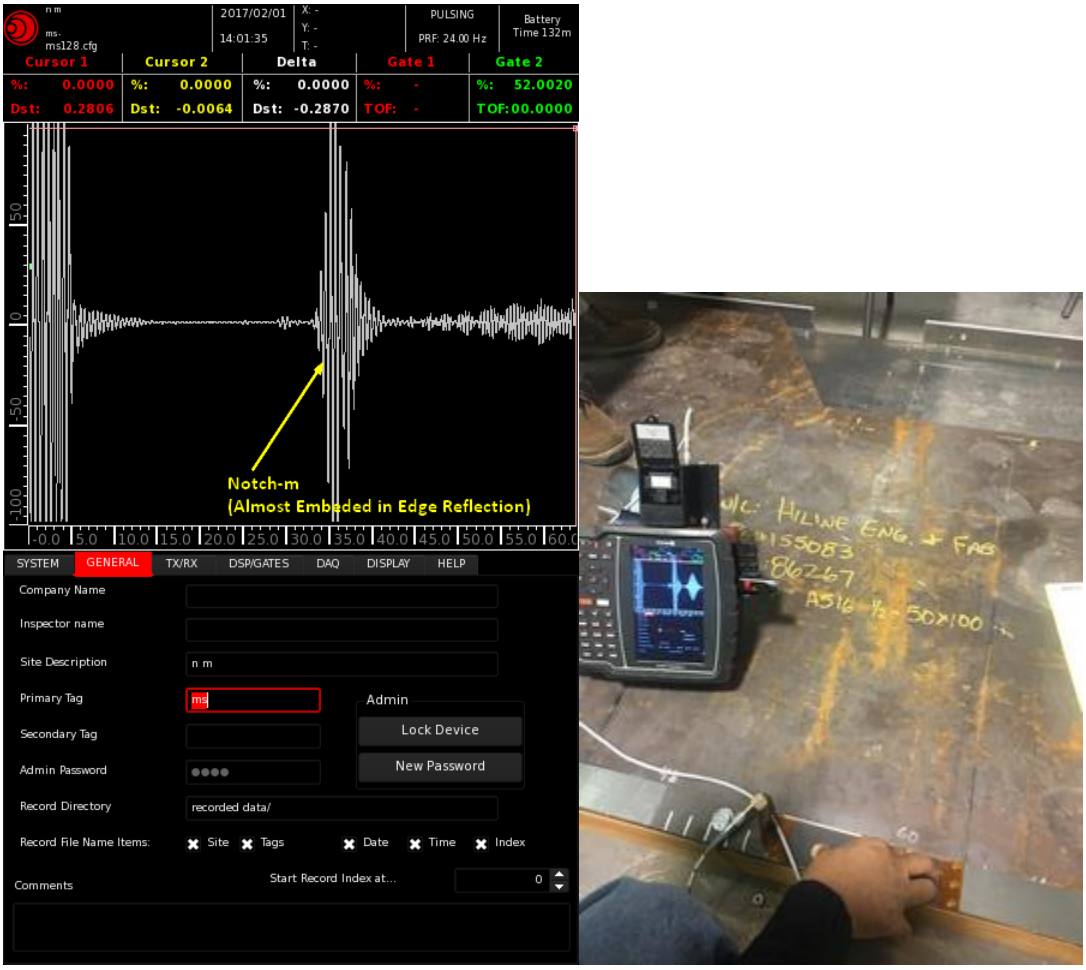


**Figure 19. Position of Sensor for Notch-m – 59 inch**

Remarks:

- “Notch-m” was 50% (0.25”) deep, 2” long and 0.125” wide placed parallel to weld in base plate.
- “Notch-m” was very close to the edge and was embedded in the edge reflection signal. This reflection was strong and long (in time) since the plate edge was beveled. The edge reflection shouldn’t be that strong in the real tank.

### 3.2. Magnetostrictive Sensor and Knuckle (Bend) Area – 128 kHz $SH_0$ Wave Mode

A strip was adhered on the backside of the horizontal wall of the mock-up covering three notches shown as N1, N2 and N3. A manual scan was performed and results are shown below.

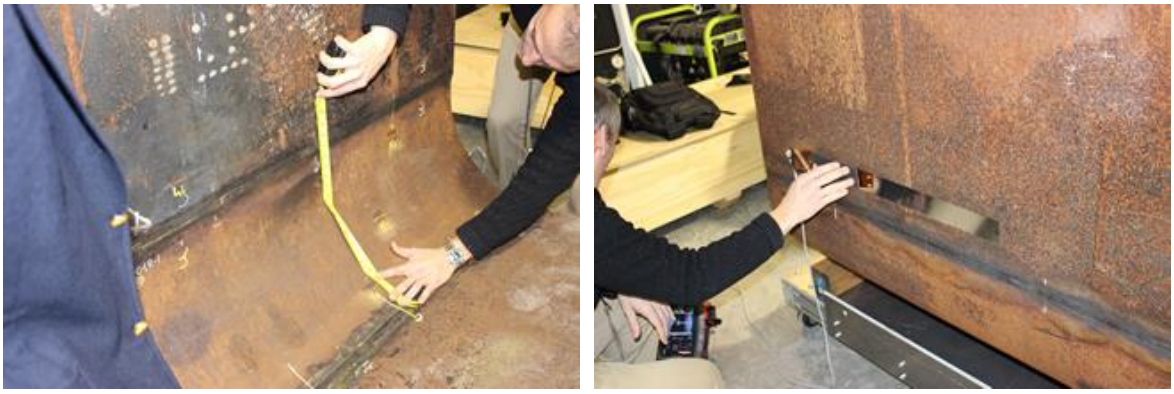

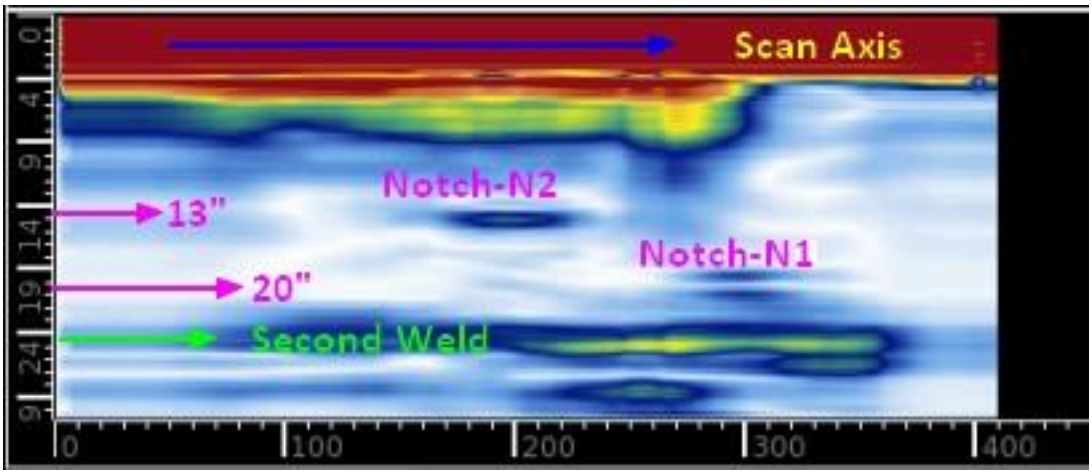


**Figure 20. Results from knuckle**

The plate thickness in the knuckle area was 0.75” (bottom plate was 0.5”).

As shown in the dispersion curves (Figure 6 above) for SH waves. The 128 kHz coil available for this test is not adequate for this thickness, and there is a very high probability of generating other modes which complicate the interpretation of results by creating spurious signals which can also interfere with the signal of interest.

On this scan, the weld just in front of the notch reflects a lot of energy back, but two notches (N1 and N2) are still clearly detected between the two welds. The second weld also provides a strong response and there is a reflection later in time that could be a defect or another mode.

In order to generate pure SH0 mode a larger wavelength and lower frequency EMAT sensor would be needed. Using arrays could also help reduce the effect of weld reflections and significantly enhance POD and sizing capabilities.

### 3.3. Lamb Wave Attenuation Tests

For Lamb wave tests, we used standard EMAT coil and MRUT (Medium Range UT) sensors generating A0 mode at 145 kHz using 0.720” wavelength. The transducers were configured in pitch-catch to detect possible attenuation in the presence of defect. This technique was demonstrated on some of the defects.

#### 3.3.1. Notch –L

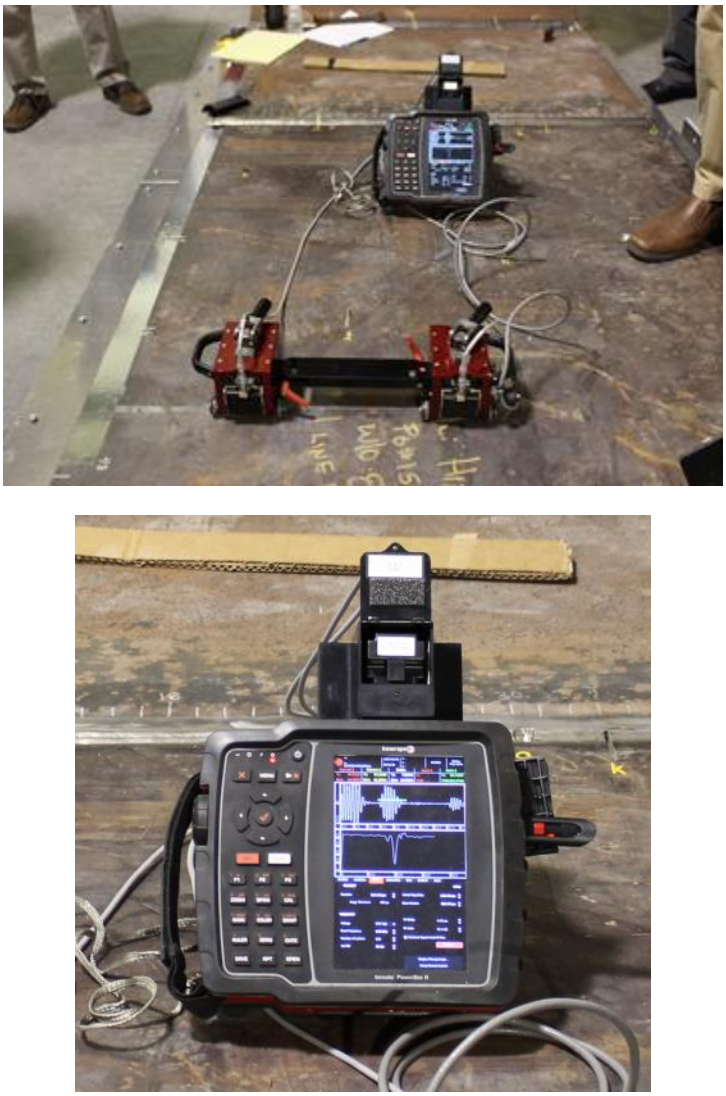

**Figure 21. Notch l Lamb wave attenuation test**

Remarks:

- Two Lamb wave sensors were set up to scan using a bar to hold both sensors together. The longest available bar was approx. 10”.
- Notch-L (90% deep) completely attenuated the signal and was easily detectable with this technique.

### 3.3.2. Notch-g and Pit-a Scan

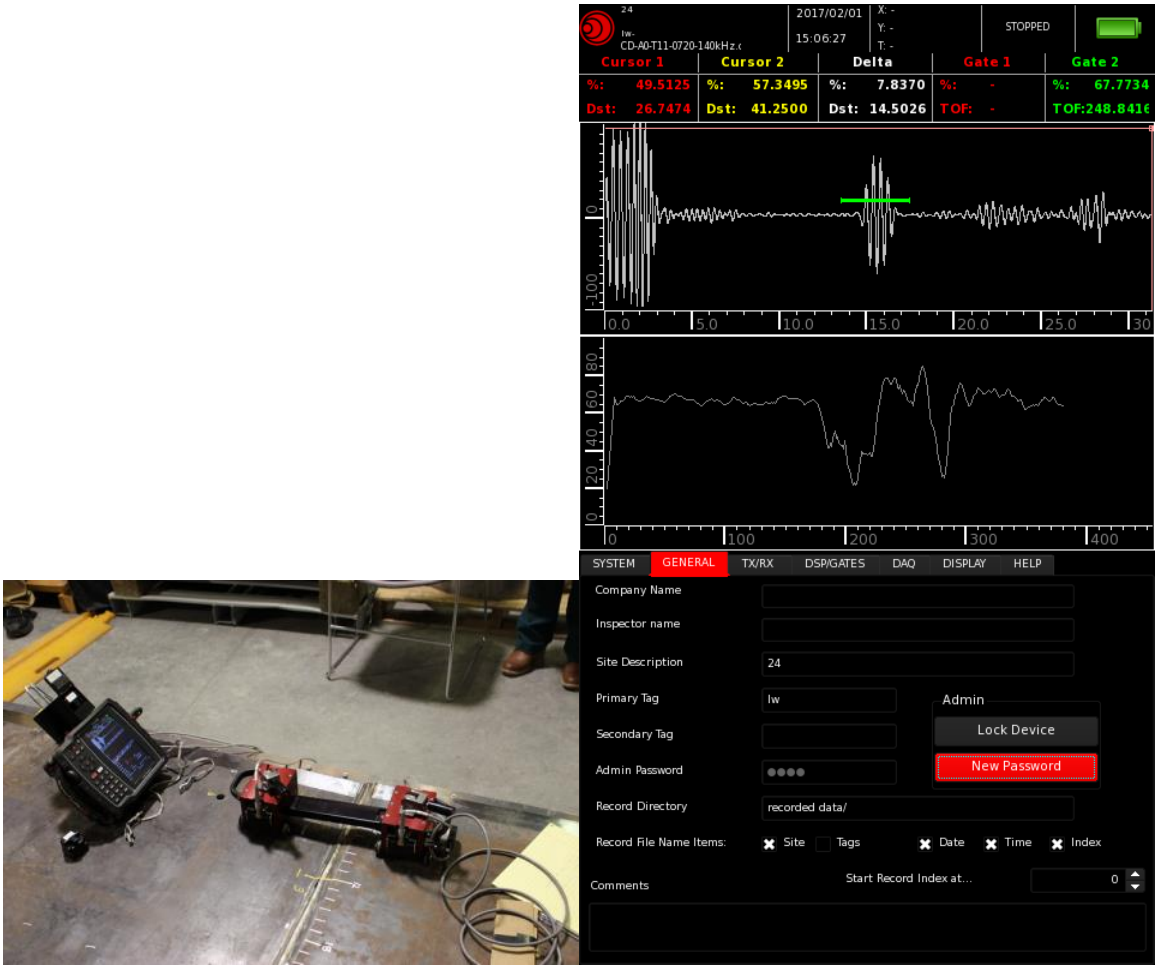


**Figure 22. Notch g and Pit c Lamb wave attenuation tests**

Remarks:

- Two Lamb wave sensors were set up to scan using a bar to hold both sensors together. The longest available bar was approx. 10”.
- Notch-g and Pit-c were clearly detected by this technique due to the attenuation of ultrasonic energy.

### 3.3.3. Notch-g and Pit-a Scan – Reflection Mode

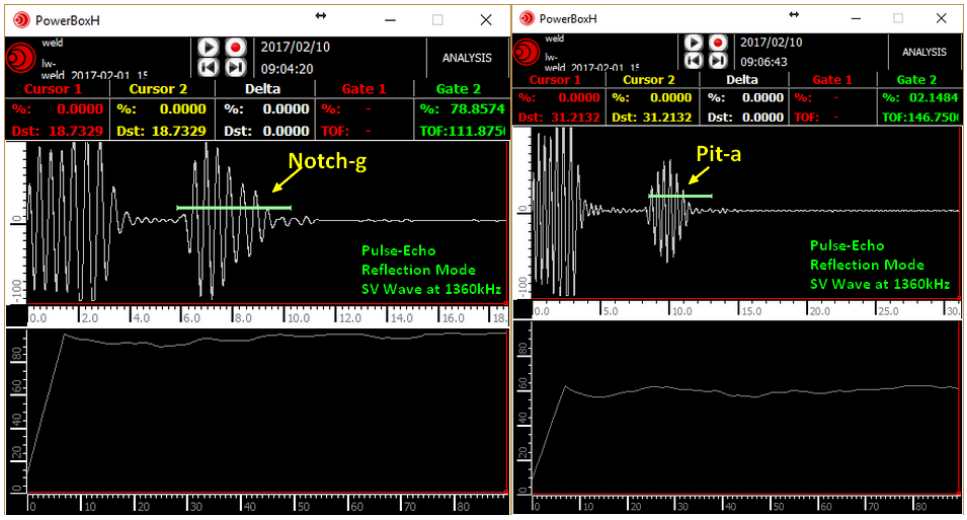


**Figure 23. A-scan snapshots in Pulse-Echo Reflection Mode**

Remarks:

- One of the Lamb wave sensors was positioned to across the defects in the weld in pulse-echo configuration looking for the reflections in a-scan mode from possible defects.
- Notch-g and Pit-c were clearly detected by this technique due to the reflection of ultrasonic energy.

### 3.3.4. Pit-c and Notch-L Scanned

**Figure 24. Manual Lamb Wave Scanning**

Remarks:

- Two Lamb wave sensors were set up to scan at approximately the same distance (28”) provided by the ventilation channels.
- Scanning was performed manually due to the absence of a bar of that length that could hold both sensors together while scanning. The results cannot be considered reliable due to this limitation, but it was an interesting technique that we wanted to test.
- Despite this problem, Pit-c was clearly detected but Notch-h due to its vertical position did not provided any significant attenuation.
- Encoded/motorized sensors and/or an array of sensors could provide much more reliable and valuable results.

### 3.4. Shear Vertical (SV) Waves Reflection Tests

The final tests included SV waves in reflection mode using a 0.160” wavelength EMAT coil at 1360 kHz. We obtained great amplitude responses on all defects, in and out of the weld when testing in Pitch Catch reflection and Pulse Echo configurations (the latter was easier to implement).

All the defects showed high amplitude responses, but the results are scattered in time due to the multiple turns and wave components generated by the off-the-shelf SV coil. Because of this, the technique could be very effective at detecting defects, but challenging for sizing purposes.

We concluded with a horizontal scan of the bottom plate (parallel to the weld) at approximately 10” from the weld in between defects c and b.

On this scan, we reliably detected defects c (pit), i (notch), a (pit in weld), h (notch), b (hole) and g (notch in weld). We didn’t detect perpendicular notches k, l or m due to the orientation.

Unfortunately, the B-scan generated during the test was accidentally deleted, but we still have a clear memory of the results since we spent a few minutes interpreting the scan together with Katie Denslow, Bill Glass, and the representative from DOE.

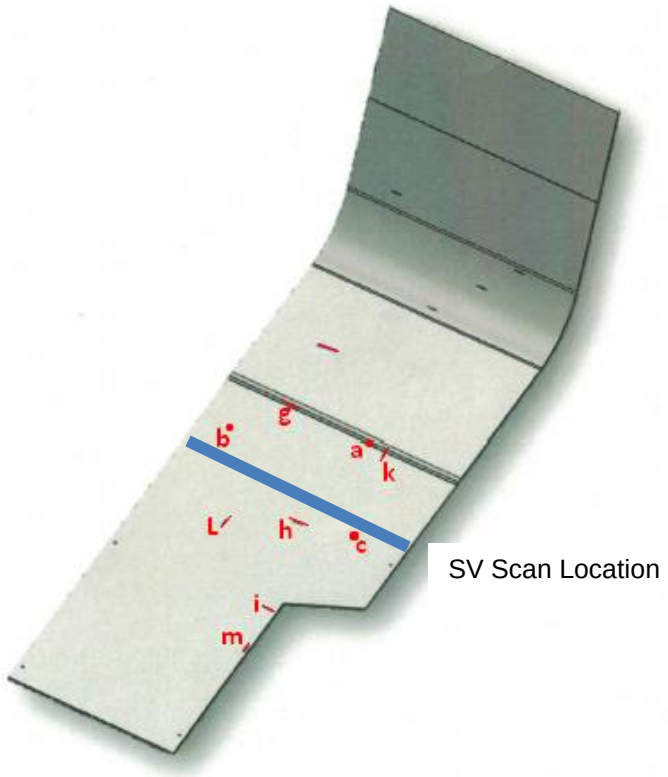

# Appendix VII: Data Collection and Documentation Guide and Test Report Data Sheet

| | |
|---|---|
| Participate Name and Company: | Syed Ali - Innerspec Technologies Inc. |
| Date of Demonstration: | February 01, 2017 |
| NDE system model and description (transducer specifications, wave modes): | Power BOX-H EMAT Handheld Unit<br>Emat Coils and Sensors |
| NDE system serial number (optional): | |

**Pre-Demonstration Checklist:**

□ Synchronize clock of data acquisition system with master clock.
□ Complete functional checks (e.g., verify detection of large reflector, such as a weld or plate edge).
□ If encoded scanners are used, calibrate encoders and assign scan/index directions.

**Table VII-a.** ***Technology Screening*** **Data Sheet**

| *Surrogate Flaw Details* | | | *Documentation* | | | | | |
|---|---|---|---|---|---|---|---|---|
| **Machined Surrogate Flaw*** | **Flaw ID in Mock-up** | **Flaw Location and Orientation in Mock-up** | **Mock-up Side Used for Inspection (ID or OD)** | **Flaw Detection Indicated?** | **Ability to Distinguish Surface Connectivity?** | **Transducer Separation Distance and Orientation (relative to 7/8 to ½-inch transition weld)** | **Data File Date/Time Stamp** | **Data Acquisition Settings** |
| Pit | a | 7/8 to ½-inch transition weld | ID | Y | | 4 inch | Feb 01, 2017 15:11:57 | |
| Pit | b | Base plate | ID | Y | | 11 inch | Feb 01, 2017 15:11:57 | SH Wave Freq-128kHz |
| Pit | c | Base plate | ID | Y | | 24 inch | Feb 01, 2017 15:11:57 | Cycles-2 |
| Notch | g | 7/8 to ½-inch transition weld, circumferential orientation (i.e., parallel to weld) | ID | Y | | 4 inch | Feb 01, 2017 15:11:57 | Lamb Wave Freq - 145kHz Cycles-2 |
| Notch | h | Base plate, circumferential orientation (i.e., parallel to weld) | ID | Y | | 26 inch | Feb 01, 2017 15:11:57 | |
| Notch | i | Base plate edge, circumferential orientation (i.e., parallel to weld) | ID | Y | | 54 inch | Feb 01, 2017 13:57:49 | SV Wave Freq - 1360kHz |
| Notch | k | 7/8 to ½-inch transition weld to base plate, axial orientation (i.e., perpendicular to weld) | ID | Y | | 4 inch | Feb 01, 2017 15:11:57 | Cycles-4 |
| Notch | L | Base plate, axial orientation (i.e., perpendicular to weld) | ID | Y | | 35 inch | Feb 01, 2017 15:11:57 | |
| Notch | m | Base plate edge, axial orientation (i.e., perpendicular to weld) | ID | Y | | 59 inch | Feb 01, 2017 14:01:35 | |

# Appendix VII: Data Collection and Documentation Guide and Test Report Data Sheet

| | |
|---|---|
| Participate Name and Company: | Syed Ali - Innerspec Technologies Inc. |
| Date of Demonstration: | February 01, 2017 |
| NDE system model and description (transducer specifications, wave modes): | Power BOX-H EMAT Handheld Unit<br>Emat Coils and Sensors |
| NDE system serial number (optional): | |

**Pre-Demonstration Checklist:**

□ Synchronize clock of data acquisition system with master clock.
□ Complete functional checks (e.g., verify detection of large reflector, such as a weld or plate edge).
□ If encoded scanners are used, calibrate encoders and assign scan/index directions.

**Table VII-a.** ***Technology Screening*** **Data Sheet (Signal to Noise Ratios)**

| *Surrogate Flaw Details* | | | *Documentation* | | | | | |
|---|---|---|---|---|---|---|---|---|
| **Machined Surrogate Flaw*** | **Flaw ID in Mock-up** | **Flaw Location and Orientation in Mock-up** | **Mock-up Side Used for Inspection (ID or OD)** | **Flaw Detection Indicated?** | **SNR FeCo Strip** | **SNR Lamb Waves Attenuation** | **SNR Lamb Waves Reflection** | **SNR SV Waves Attenuation** |
| Pit | a | 7/8 to ½-inch transition weld | ID | Y | Masked by strong Ref of Notch-k | -8.94 dBs | 20.80 dBs | Reliabilly Detected Results Not Captured |
| Pit | b | Base plate | ID | Y | 22.34 dBs | | | Reliabilly Detected Results Not Captured |
| Pit | c | Base plate | ID | Y | 19.07 dBs | | | Reliabilly Detected Results Not Captured |
| Notch | g | 7/8 to ½-inch transition weld, circumferential orientation (i.e., parallel to weld) | ID | Y | 12.82 dBs | -9.50 dBs | > 25 dBs | Reliabilly Detected Results Not Captured |
| Notch | h | Base plate, circumferential orientation (i.e., parallel to weld) | ID | Y | 2.76 dBs | | | Reliabilly Detected Results Not Captured |
| Notch | i | Base plate edge, circumferential orientation (i.e., parallel to weld) | ID | Y | 12.04 dBs | | | Reliabilly Detected Results Not Captured |
| Notch | k | 7/8 to ½-inch transition weld to base plate, axial orientation (i.e., perpendicular to weld) | ID | Y | 20.25 dBs | | | Not Reliabilly Detected Due to Orientation |
| Notch | L | Base plate, axial orientation (i.e., perpendicular to weld) | ID | Y | > 25 dBs | -19.08 dBs | | Reliabilly Detected Results Not Captured |
| Notch | m | Base plate edge, axial orientation (i.e., perpendicular to weld) | ID | Y | > 25 dBs | | | Reliabilly Detected Results Not Captured |

## 5. Technique Options - Conclusions

### 5.1. EMAT Normal Beam

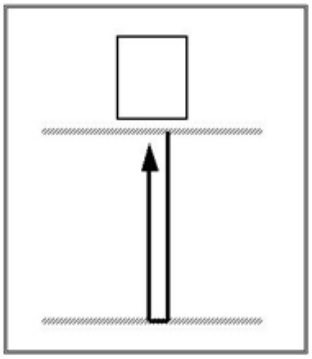

This is one of the simplest albeit limited approaches to inspect the bottom of the tanks using the existing access channels within the refractory pads. A single channel normal beam EMAT could provide a thickness profile within the channel on areas that are not heavily corroded (walls are parallel).

An EMAT normal beam linear array would significantly enhance mapping of the area under the sensor by being able to map non-parallel areas that are common on corrosion patches. Not having any type of couplant and the ability to inspect rough areas would be a great advantage over traditional piezoelectric inspection.

The limitations of such an approach is obvious as it can only inspect the tank area on top of the channels where the sensors are inserted. Due to the simplicity of construction and interpretation, it could be a good approach for the deeper internal channels where guided wave sensors cannot be inserted.

### 5.2. Guided Waves

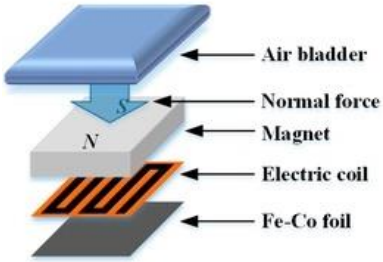


The magnetostrictive guided wave technique has shown greater sensitivity, reach, and resolution than any other technique used on these tests. Signal to noise ratio and effective range of the inspection makes this technique a preferred choice. However, adhering the magnetostrictive strip inside the refractory channels would be very challenging. The channel should be cleared of debris and the tank surface will most likely need to be sanded and cleaned before applying the strip. On the other hand, should an adhesive be used, permanent attachment of the strip could facilitate inspections in the future.

An interesting option would be to pressure couple the sensor to the tank. In this case, the bottom of the tank would still need to be prepared (sanded/cleaned) but there would be no need to use an adhesive.

Lamb waves can also be used in attenuation mode by locating sensor/s on adjacent air slots. However, the technique might lose its validity once tested on a more realistic mockup that is sitting on a refractory pad (with weight on top) and sludge.

#### 5.2.1. Advantages and Limitations

- The existing refractory air slot is large enough for any of the guided wave probes suggested in either reflection or attenuation mode. The probe/s can be packaged in a 2” x 1” size housing with a built-in encoder to be pushed through the channels by the inspection robot.
- The probe will be able to detect wall thinning and pitting. Significant work would be required to develop the hardware and software tools to provide remaining wall thickness and ID vs OD location.
- Adhering or pressure-coupling of the strip (in case of magnetostrictive SH) would be challenging.
- This technique should permit to cover the full area within adjacent air slots.
- Using an array of probes could significantly improve detection of defects, reduce influence of weld reflections, and create opportunities for sizing. A prototype probe and scanning software would need to be developed. The multiple channels in the array can be excited individually or phased to sweep the combined beam area. Multiple channels will also enhance signal to noise and permit reception of scattered signals.

### 5.3. EMAT generated SV Waves

SV waves can provide strong reflections even on very shallow defects. The existing air slots on the refractory pad are large enough to fit SV sensors.

The sensors can be used in attenuation and reflection mode. Reflection mode would be the preferred choice, since it is a “positive” inspection technique that should not generate false positives.

#### 5.3.1. Advantages and Limitations

- The existing refractory air slot is large enough for any of the guided wave probes suggested in either reflection or attenuation mode. The probe/s can be packaged in a 2” x 1” size housing with a built-in encoder to be pushed through the channels by the inspection robot.
- The EMATs can be applied to a relatively rough surface. Surface preparation is not as demanding as with the magnetostrictive technique.
- No couplant or strip is needed for the generation of ultrasonic energy.
- Pulse Echo (reflection) and Pitch Catch (attenuation) could complement each other. Either transducer can be used for both.
- This technique provides ability to cover large areas for detecting flaws, defects and corroded areas but may not be able to provide remaining wall thickness in corroded areas.
- It could be very effective for detection of shallow cracks.
- Using an array of probes could significantly improve detection of defects, reduce influence of weld reflections, and create opportunities for sizing. A prototype probe and scanning software would need to be developed. The multiple channels in the array can be excited individually or phased to sweep the combined beam area. Multiple channels will also enhance signal to noise and permit reception of scattered signals.

# Appendix C

# Penn State

# Report on NDE Technology Screening Test Results
# To: Washington River Protection Solutions, LLC

The Pennsylvania State University
University Park, PA 16802

Cliff J Lissenden, Lissenden@psu.edu
Parisa Shokouhi
Sean N Brennan
Karl M Reichard

22 February 2017

PennState
College of Engineering

# Report on NDE Technology Screening Test Results

### *Introduction*

On February 2, 2017 Cliff Lissenden and Parisa Shokouhi conducted a series of tests on the 'Hanford DST primary liner test mock-up', henceforth referred to as the 'mockup'. In all tests two electromagnetic acoustic transducers (EMATs) were used: one to transmit an ultrasonic signal into the steel plate and the other to receive the signal. Unless noted otherwise all EMAT positions on the plate were consistent with air slot locations in the double shell tank (DST). All ultrasonic waves analyzed herein are guided waves known as shear horizontal (SH) waves. Multiple SH modes propagate in plates at a given frequency. The EMATs were placed only on the 0.5" thick steel plate portion of the mockup and actuated at 250 kHz, where 3 SH modes exist. The group velocities of these modes were predicted to be: 3200, 2800, and ~0 m/s for the SH0, SH1, and SH2 modes respectively. The SH2 mode is highly dispersive at this frequency, resulting in a very slow group velocity, thus our data include only the SH0 and SH1 modes. Typically, the distance between transmitter and receiver was sufficiently large for the SH0 and SH1 modes to separate, such that they are received as separate wave packets.

EMATs were selected for this application because they are noncontact transducers, which is very beneficial for remote inspections with robotic devices. However, the amplitude of the wave signal decreases as the liftoff (i.e., gap between the electric coil and plate surface) increases; and so does the magnetic force. The tests on the mockup were conducted by manual positioning of the EMATs on the plate, so the liftoff was set as a compromise between sufficient signal strength and ease of manual positioning. Preliminary tests at Penn State showed the signal decrease of 3.5 to 1.8 to 1.1 mV for liftoffs of 0.3, 0.6, and 0.9 mm as set by 0.3 mm thick wear strips. For the actual robotic inspection of a DST we plan to use 'transfer balls' to enable the EMATs to be easily moved along the air slot in close proximity to the steel primary tank bottom. We used a liftoff of 0.6 mm for all tests on the mockup, thereby sacrificing signal amplitude for ease of EMAT positioning, but 'transfer balls' are likely to allow a smaller liftoff, and would thus provide a larger ultrasonic signal.

EMATs based on Lorentz force transduction generally have lower coupling than piezoelectric or magnetostrictive transduction, thus high power instrumentation is typically employed. Our laboratory at Penn State is equipped with a Ritec RAM-5000 SNAP system (Warwick, RI), but this is a sensitive instrument that we did not want to transport across the country. We brought instead a simple low power Ultratek system for the mockup testing at PNNL. The difference between the preferred Ritec system and the Ultratek system that was actually used is shown in Fig. 1, where the transmitter and receiver EMATs were separated by 37" on a 0.25" thick steel plate. The signals recorded using the Ritec system have a much higher SNR compared to the Ultratek system used in the testing of the mockup.

The active part of the EMAT is 1" by 1" so that it can fit into the smallest air slots, which results in the actuated SH waves having significant divergence as shown in Fig. 2. The divergence is very useful for NDE Inspection of DSTs because of the very limited positions where the EMATs can be located.

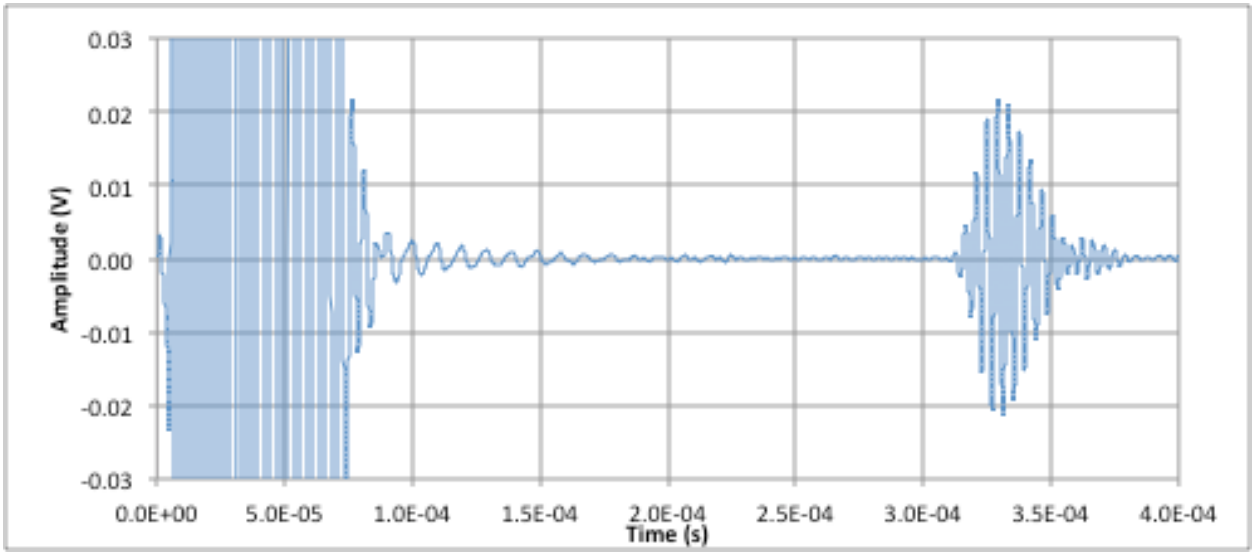


(a) Ritec at 80% full power with 40 dB preamp used in Penn State laboratory:
Ampl = 21.8 mV, SNR = 21.8/0.556 = 39.2 (noise measured between 0.25-0.30 ms)

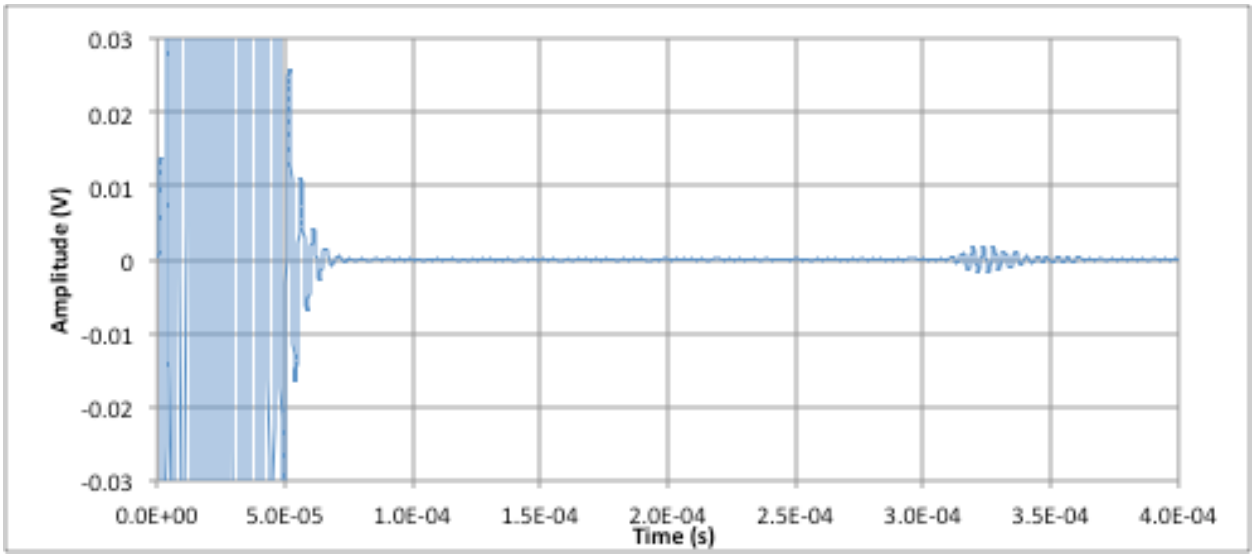


(b) Ultratek at 300V with 40 dB preamp and 30 dB gain used for mockup:
Ampl = 2.03 mV, SNR = 2.03/0.094 = 21.6 (noise measured between 0.25-0.30 ms)

***Fig. 1.*** *SH0 signal received by EMAT 37" from transmitter using: (a) Ritec; and (b) Ultratek data acquisition systems.*

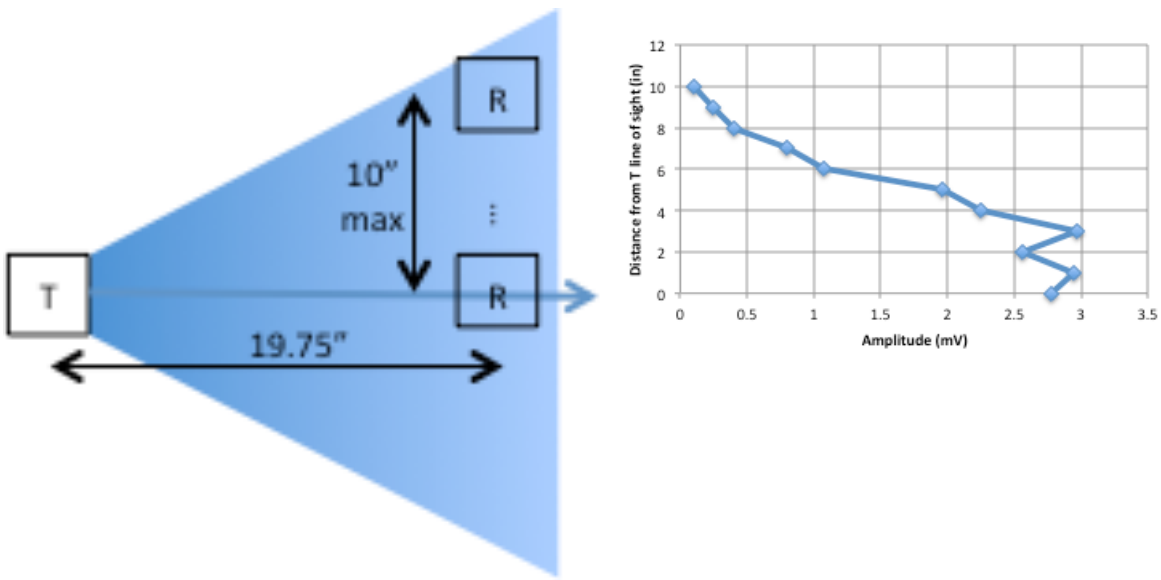


***Fig. 2.*** *Measurement of EMAT beam divergence on 0.25" thick steel plate.*

***Fig. 3.*** *Rendering of mockup showing defect locations and coordinate system.*

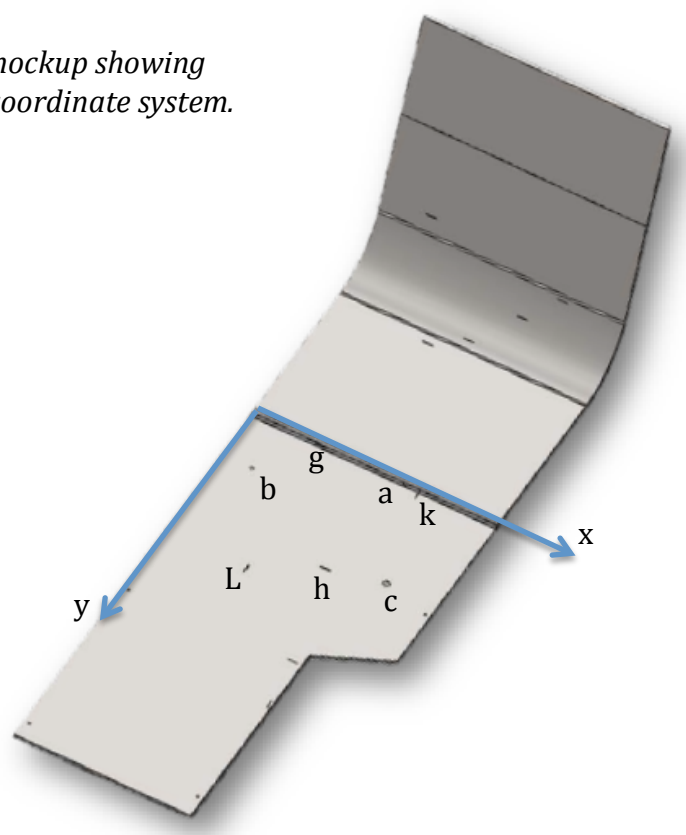


Reporting of the results obtained from the mockup is organized in terms of the ultrasonic mode of measurement: through-transmission, pitch-catch, and pulse-echo. A brief summary is included after the results are presented.

### *Through-Transmission: Defects L, c, b, and h*

Defect locations are shown in Fig. 3 along with the coordinate system used for all positions. Defects L, c, b, and h are isolated from welds and edges, thus through-transmission mode was used for detection.

In the through-transmission mode, the receiver (R) is placed directly along the send direction of the transmitter (T). All through-transmission tests were conducted with the distance between T and R fixed at 29" to simulate the distance between adjacent air slots in the DST. Segments of yard sticks were clipped together to fix both the spacing and the alignment of the T and R. In all, 96 A-scans were obtained on the mockup using through-transmission at a distance of 29" in regions having no obvious top surface defects. The peak of the SH0 wave packet varied from 2.4-5.9 mV, with an average value of 3.8 mV and a standard deviation of 0.768 mV. There are numerous possible explanations for the variation, among which variable liftoff due to general corrosion and debris is a leading candidate. Thus, it is reasonable to apply a threshold value of ~2.5 mv as representative of a defect.

Defect 'L'

Description: 90% through-thickness 2" long notch located at (16, 33.5-35.5) based on coordinate system shown in Fig. 3.

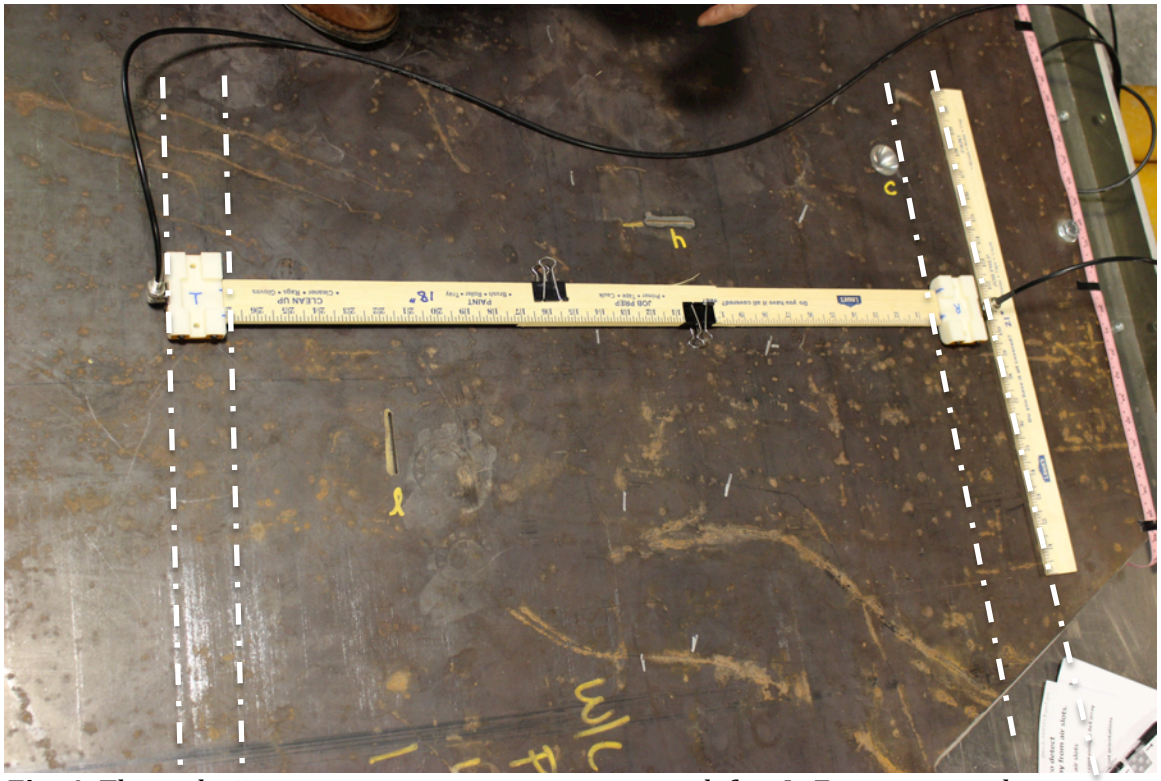

***Fig. 4.*** *Through-transmission measurements across defect L. Fictitious air slots are marked by white dot-dash lines.*

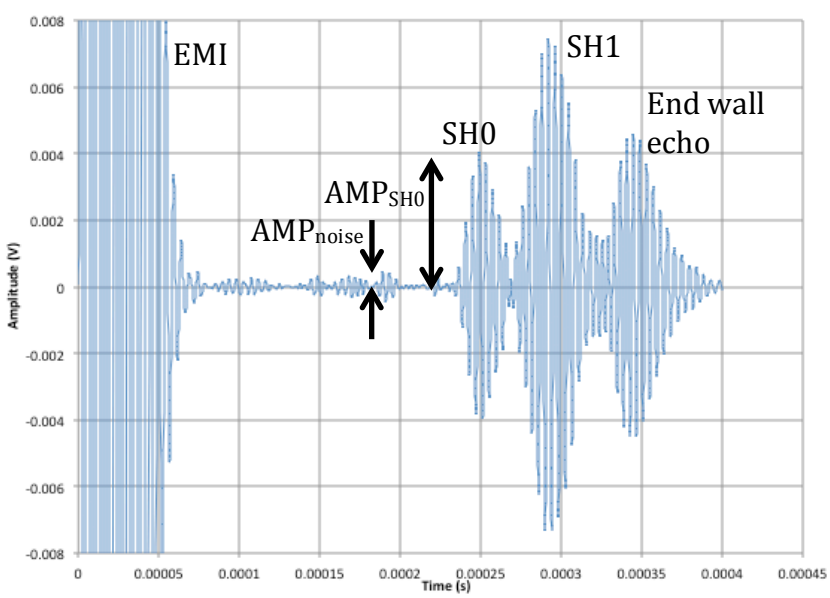


$$SNR = AMP_{SH0} / AMP_{noise}$$

***Fig. 5.*** *Sample A-scan.*

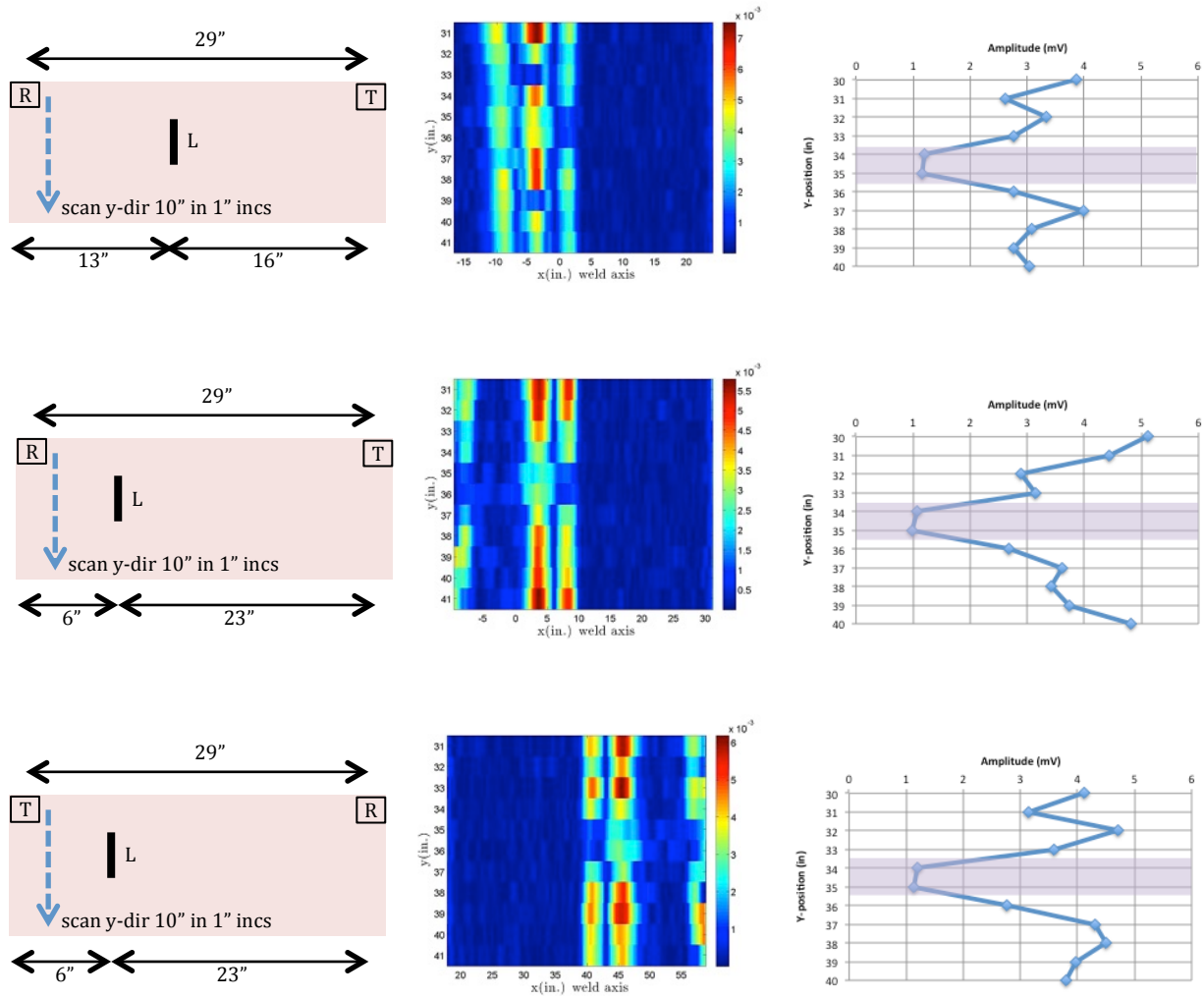


***Fig. 6.*** *Test schematic (left), B-scan (middle), and summary graph (right). Wave propagation is in the x-direction and the EMATs are scanned in the y-direction.*

A photograph of the EMATs for measurements of defect L is shown in Fig. 4. White dash-dot lines are superimposed on the photo to emphasize that the EMAT positions are selected to be within the air slots of the DST. A sample A-scan is shown in Fig. 5 and the values used for calculation of the signal-to-noise ratio (SNR) are given.

The EMATs were scanned in the y-direction to create a B-scan, which is a compilation of a series of A-scans. Three sets of measurements were made with the EMATs repositioned relative to defect L to simulate defect L being (i) midway between air slots, (ii) near the air slot containing the receiver, and (iii) near the air slot containing the transmitter. The results are shown in Fig. 6. The left portion of Fig. 6 shows a schematic of EMAT positions relative to the defect and how they are scanned. The middle portion of Fig. 6 shows B-scans where the crests of the SH0 and SH1 wave packets have high intensity (red). The defect blocks wave transmission when it is located between the EMATs, thus the amplitude of the received wave is lower there. The right portion of Fig. 6 shows graphs of the SH0 wave

amplitude as a function of position, and the position of the defect is shaded for clarity. Notch L is clearly identified in each of the three positions relative to the EMATS: middle, near the receiver, and near the transmitter. Results for through-transmission measurements of defects c, b, and h are presented in an analogous way.

Defect 'c' (High Priority)
Description: 90% through-thickness 1.375" diameter pit located at (38, 23.5)

The B-scans clearly indicate the presence of defect c, as does the summary plot of the y-direction scan. However, the summary plots of the x-direction scans are less conclusive, but still indicate the presence of a defect. Scanning in the x-direction was done to avoid possible interference with defect h.

***Fig. 7.*** *Test setup for defect c.*

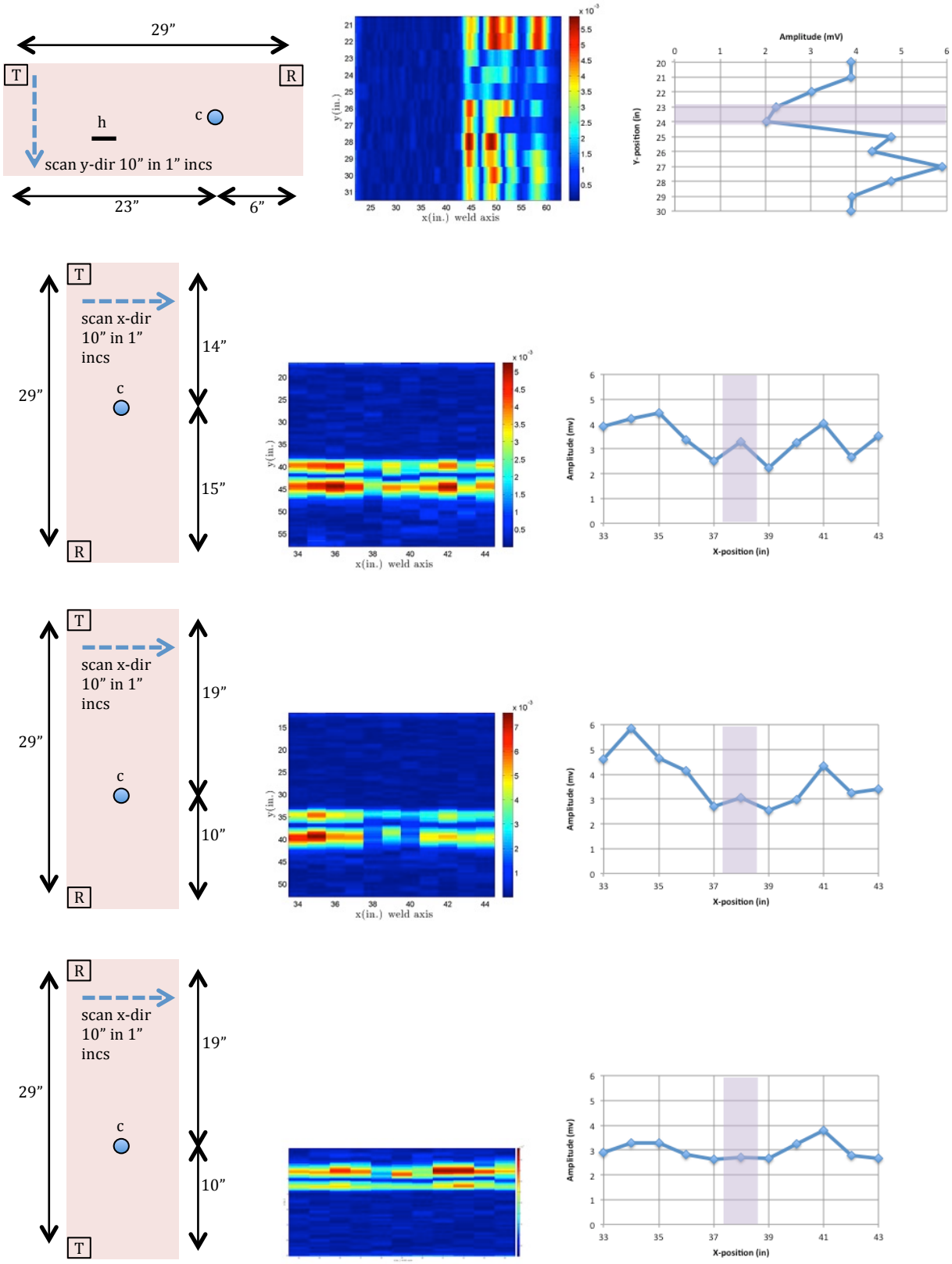


***Fig. 8.*** *Test schematic (left), B-scan (middle), and summary graph (right). Wave propagation is in the x-direction and the EMATs are scanned in the y-direction initially and then the directions are reversed.*

Defect 'b' (High Priority)
Description: 0.75" diameter through-thickness hole located at (6, 11.5)

The presence of defect b is clearly evident in both the B-scans and the summary graphs. Both SH0 and SH1 mode peaks are shown in the summary graphs in blue and red respectively. Detection is good for both cases; when the defect is near the receiver and when it is near the transmitter.

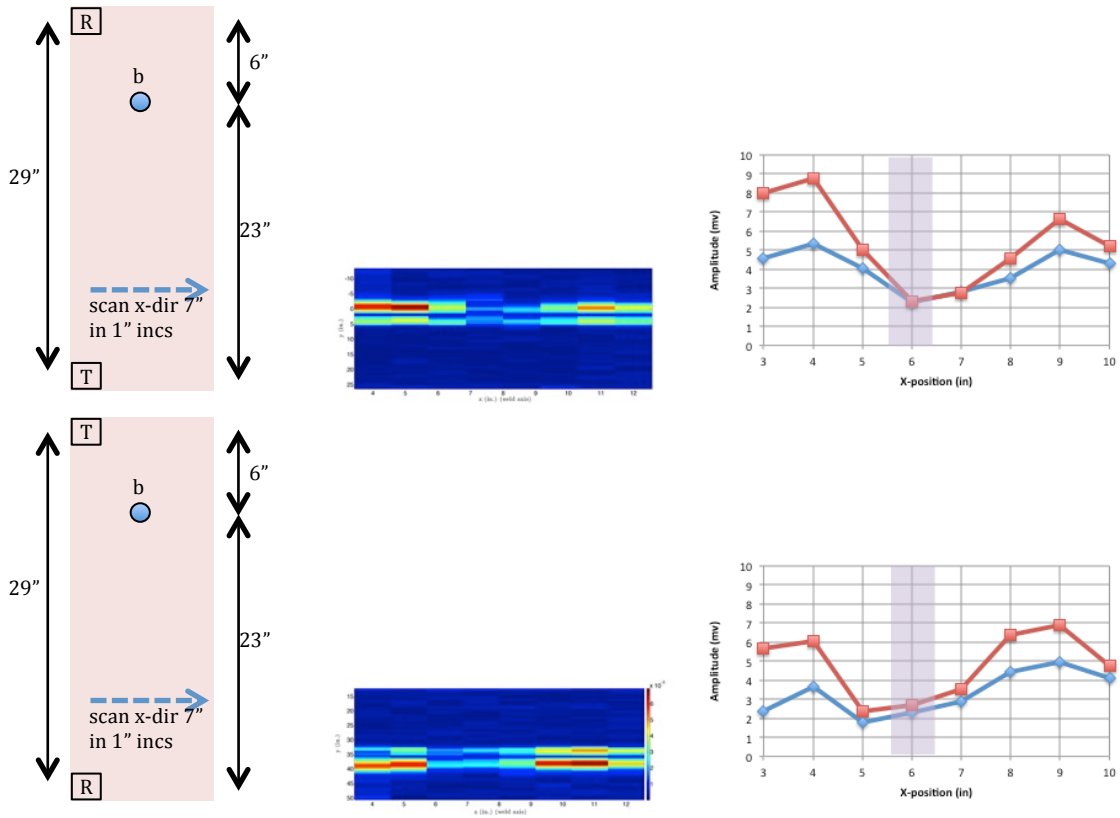


***Fig. 9.*** *Test schematic (left), B-scan (middle), and summary graph (right). Wave propagation is in the y-direction and the EMATs are scanned in the x-direction.*

Defect 'h'
Description: 20% through-thickness 2" long notch located at (27-29, 26)

Defect h was scanned in the x-direction to avoid interference from defect c. The B-scans indicate the presence of defect h, but the indication is less clear because the notch depth is smaller than the other defects. Defect h is rather poorly apparent on the summary graphs. These results could be significantly enhanced by additional A-scans that take advantage of the beam divergence. That is, for one transmitter position the receiver is scanned (along the air slot) and then the transmitter position is moved and the process repeated. The additional data enables a tomographic reconstruction algorithm to be implemented that provides better defect sensitivity. Of course, high power instrumentation will also help.

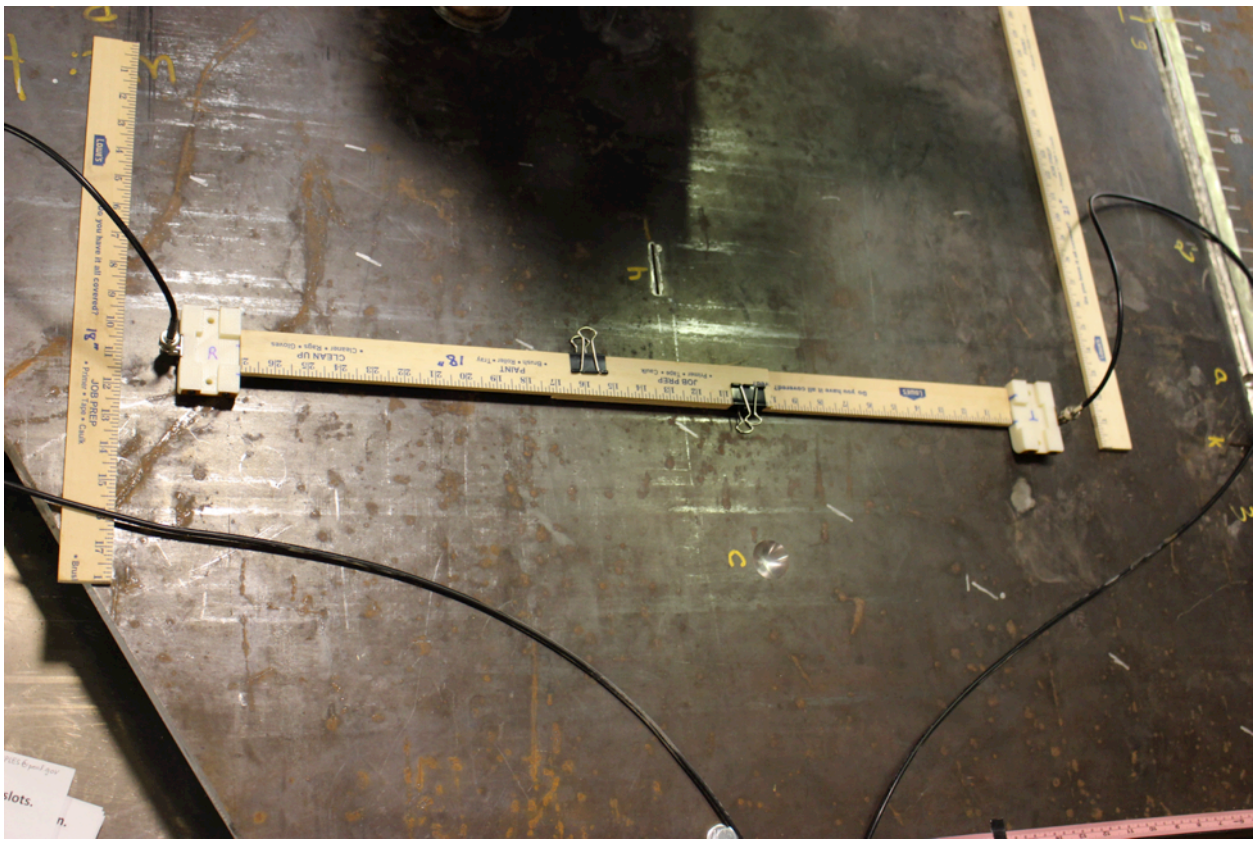

***Fig. 10.*** *Test setup for defect h.*

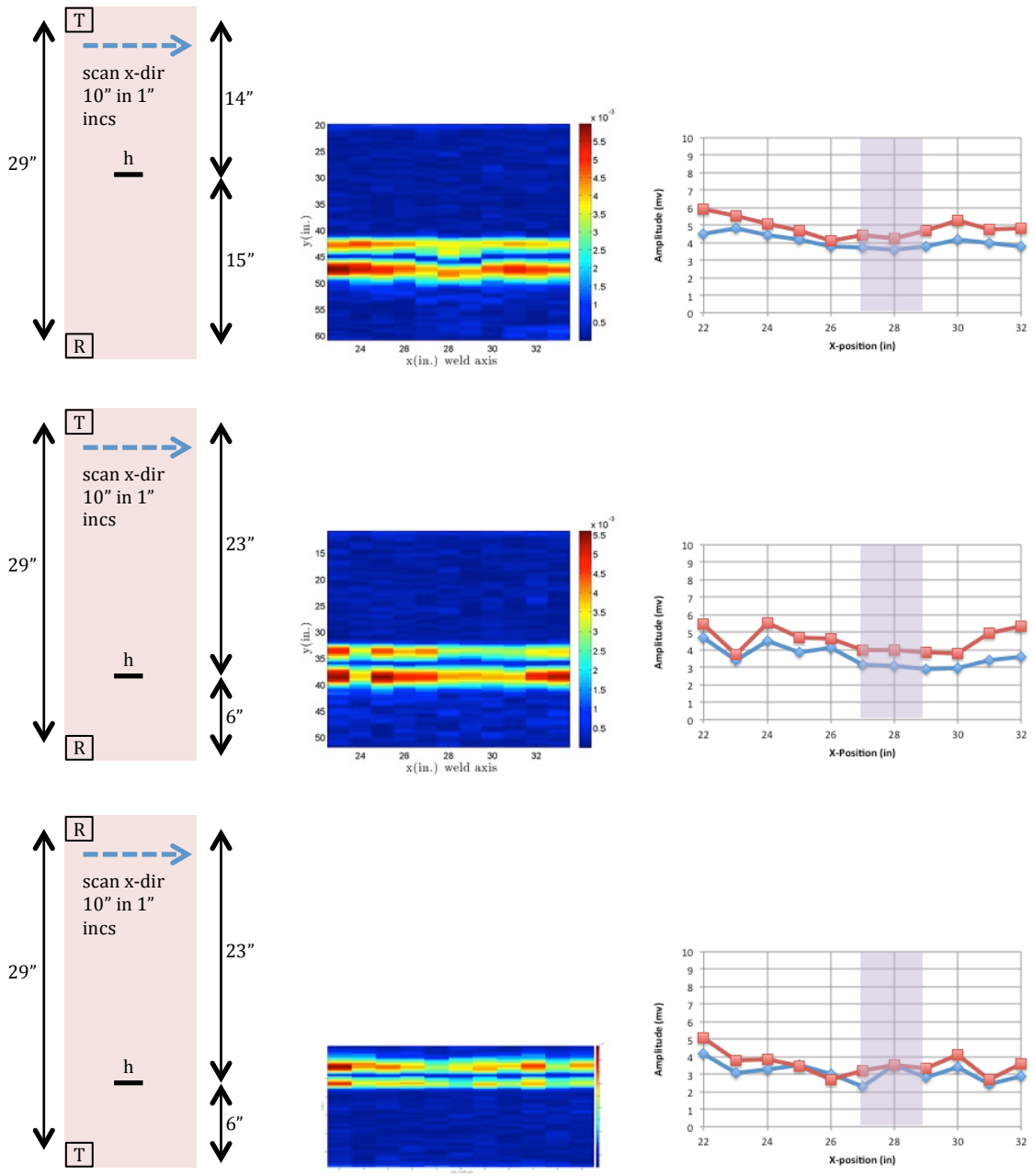


***Fig. 11.*** *Test schematic (left), B-scan (middle), and summary graph (right). Wave propagation is in the y-direction and the EMATs are scanned in the x-direction.*

***Pitch-Catch: Defects g, a, and k***

In the Pitch-Catch mode, the transducer (T) and receiver (R) are placed on the same side of the weld at 45° angles with the weld axis as shown in the picture below. The center-to-center distances between T and R were fixed at 26" (defect g) and 35" (defects a & k) to simulate the distance between adjacent air slots in the DST. As shown in the photos below (Fig. 12), segments of yard sticks were cut and clipped together to help maintain the spacing, alignment, and angle of T and R during the testing.

Six sets of pitch-catch data per defect group (g or a & k) were recorded. Each set of pitch-catch data consists of 18 signals obtained by keeping T at one location (e.g., x = 9", y = 6") and moving R perpendicular to the weld axis at 1" intervals (e.g., x=35", y = [6": 1": 23"]). Synthetic Aperture Focusing Technique (SAFT) (Langenberg *et al.*, 1986) was used to reconstruct the reflectors positioned between T and R locations.

***Fig. 12.*** *Positioning of EMATs in the pitch-catch mode targeting defects g, a, and k.*

SAFT is an algebraic reconstruction algorithm that exploits the constructive and destructive interferences among the reflected waves to image the positions of the reflectors across the test area. To perform SAFT, the test area is divided into a large number of small pixels (here, 1/5" x 1/5"). Next, for each pair of T and R, the time instance and amplitude corresponding to the reflection from the center of each pixel is calculated. This process is repeated for all T-R combinations taking into account the divergence angels of the transducers. If the pixels coincide with the position of a reflector, the amplitudes are constructive whereas if no reflector is present, the amplitudes are destructive. As a result, the signal amplitude increases at the location of the reflectors and diminishes elsewhere. SAFT images provide improved localization and higher SNR than the corresponding B-scans.

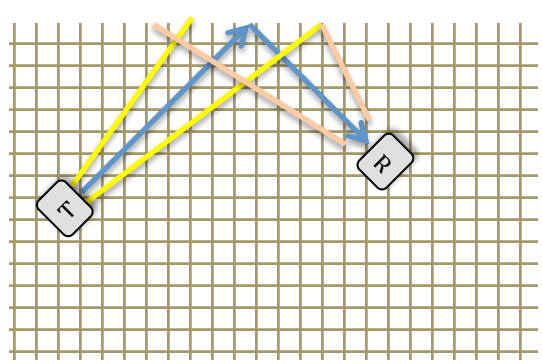

Defect 'g' (high priority)
Description: 50% through-thickness 2" long notch located in weld (13-15, 0)

Two different configurations were used to detect defect 'g':

- T at x = 9" and y = 6", 12", and 18". For each position of T, the signal was recorded at 18 locations: x = 35" and y = 6", 7", ..., and 23" (Fig. 13)
- T at x = 35" and y = 6", 12", and 18". For each position of T, the signal was recorded at 18 locations: x = 9" and y = 6", 7", ..., and 23" (Fig. 14)

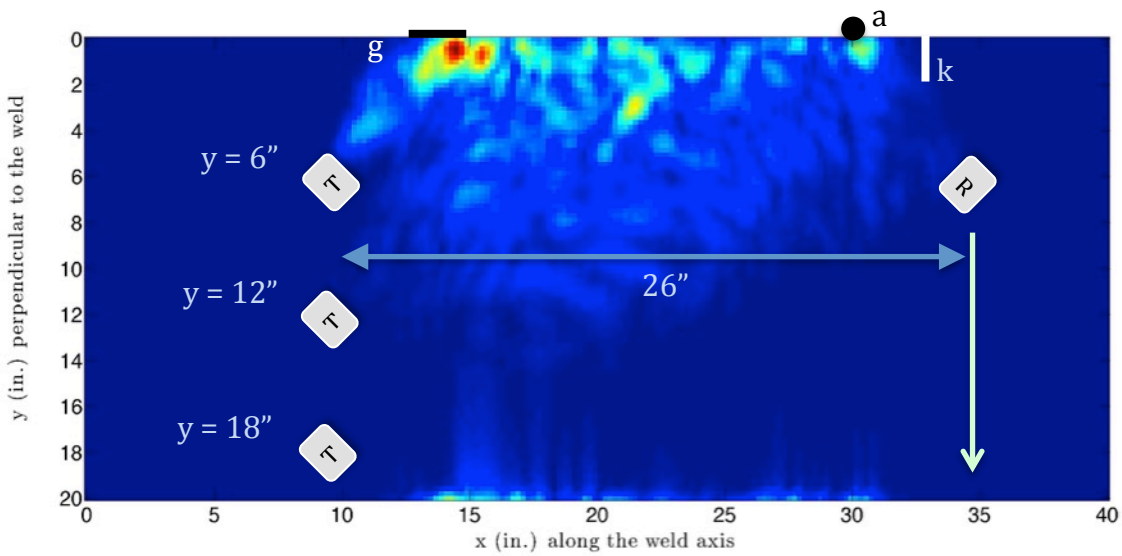


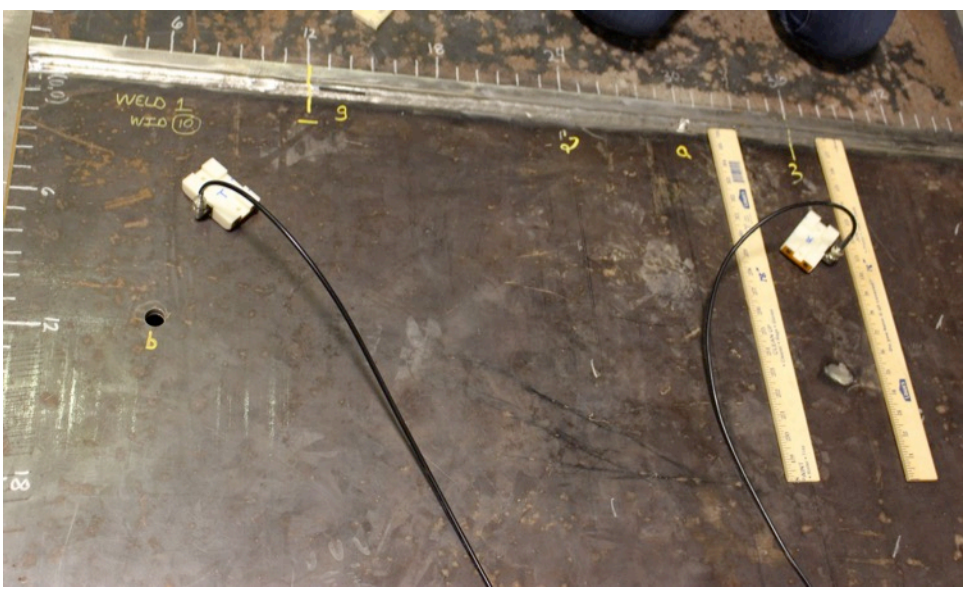


***Fig. 13.*** *SAFT-reconstructed image (above) combining the results obtained from the three T-R configurations. The approximation locations of the sought defects together with T and R positions are marked on the image (above). The photo (bottom) shows the placement of T (x = 9", y = 6") and R (x = 35", y =6") for one acquisition.*

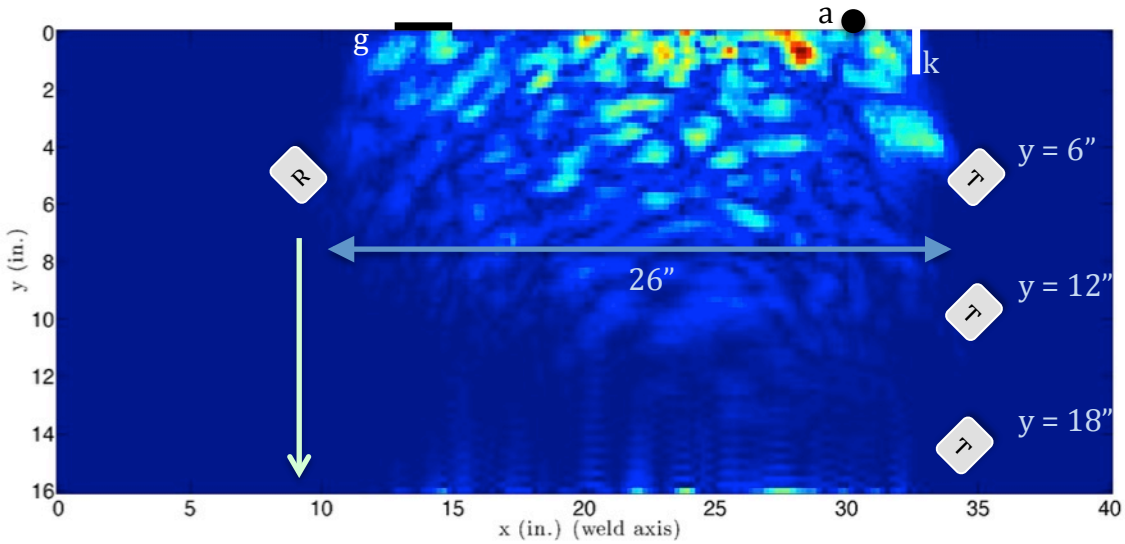


***Fig. 14.*** *SAFT-reconstructed image combining the results obtained from the three T-R configurations. The approximate locations of the sought defects together with T and R positions are marked on the image.*

We use the reconstructed images to estimate SNR for defect ‘g’:

$$SNR = \frac{amplitude\ at\ the\ location\ of\ the\ defect}{amplitude\ where\ no\ defect\ is\ present}$$

SNR depends on the orientation of the T-R pairs relative to the defect. In the first configuration, the indication around the location of defect ‘g’ has maximum reconstructed amplitude of about 0.011 while the noise level is variable ranging from about 0.001 to 0.005 giving SNR in the range of 2-11 (6 - 21 dB). In the second configuration, the SNR is so low that the defect indication lies within the noise level.

Although appearing at about x = 28”, the strong indication on the right hand side is believed to be from the defect group ‘a & k’. The errors due to the manual movement of the transducers are the likely cause of the apparent misplacement of the indication. Diffraction from the tip of defect ‘k’ and the presence of multiple modes are other likely sources of artifacts and errors. Automated data collection and more rigorous post-processing will alleviate such errors. It seems apparent that the pitch-catch method is most effective on defects located nearer to the T than the R. This is not a serious concern because we intend for each EMAT to perform both send and receive functions sequentially. However, future tests could assess the use of a shallower angle for defects located farther away from the T.

Defects ‘a & k’ (high priority)
Description: ‘a’ 50% through-thickness 0.75” diameter pit located in weld (30.5, 0), ‘k’ 50% through-thickness 2” long notch perpendicular to weld (33, 0)

Two different configurations were used to detect defect group ‘a & k’:

- T at x = 11” and y = 6”, 12”, and 18”. For each position of T, the signal was recorded at 18 locations: x = 46” and y = 6”, 7”, …, and 23” (Fig. 15)
- T at x = 46” and y = 6”, 12”, and 18”. For each position of T, the signal was recorded at 18 locations: x = 11” and y = 6”, 7”, …, and 23” (Fig. 16)

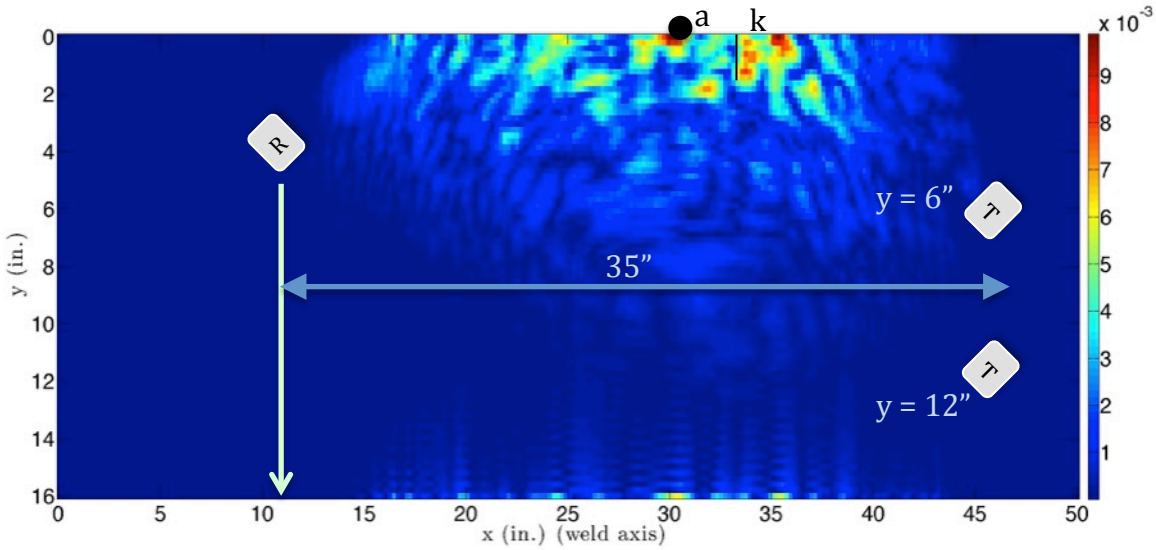


***Fig. 15.*** *SAFT-reconstructed image combing the results obtained from the three T-R configurations. The approximation locations of the sought defects together with T and R positions are marked on the image.*

Similar to the procedure used for defect ‘g’, we use the reconstructed images to estimate SNR for defect group ‘a & k’:

$$SNR = \frac{amplitude\ at\ the\ location\ of\ the\ defect}{amplitude\ where\ no\ defect\ is\ present}$$

SNR depends on the orientation of the T-R pairs relative to the defect.

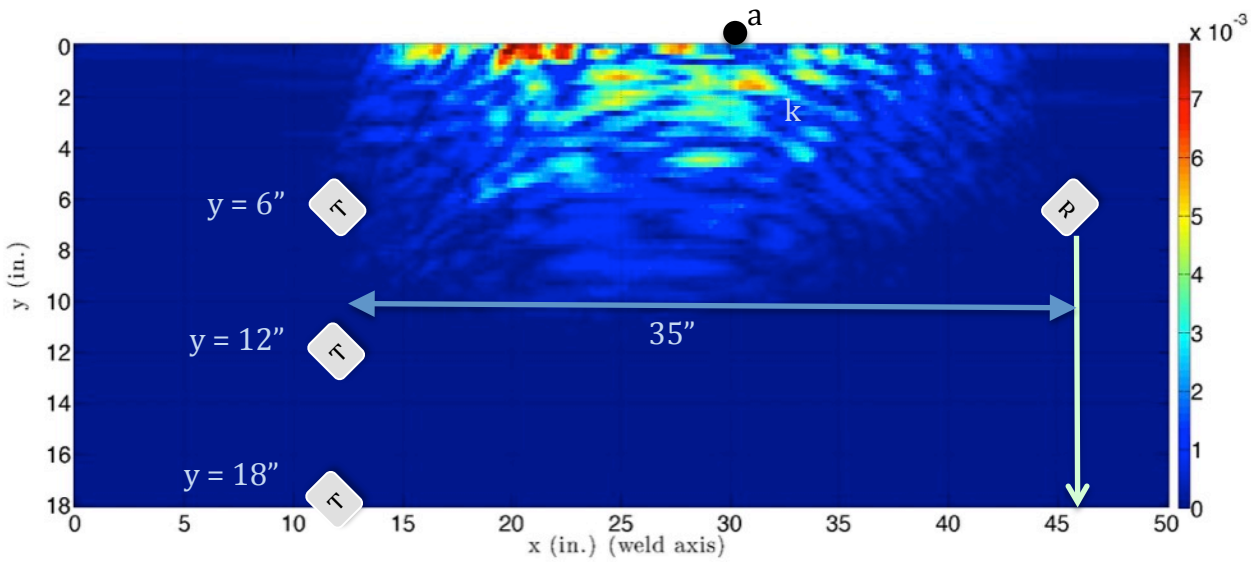


***Fig. 16.*** *SAFT-reconstructed image combing the results obtained from the three T-R configurations. The approximation locations of the sought defects together with T and R positions are marked on the image.*

In the first configuration (Fig. 15), the indication around the location of defect ‘a’ has maximum reconstructed amplitude of about 0.01 while the noise level is variable ranging from about 0.0003 to 0.006 giving SNR in the range of 1.5 - 33 (4 - 30 dB). In the case of defect ‘k’, the maximum amplitude is about 0.008 resulting in slightly lower SNRs: 1.3 – 26 (2.5 – 28 dB). In the second configuration (Fig. 16), the SNR is so low that the defect indication lies within the noise level. However, there is a strong reflection along the weld between x = 20” and 23”. Although this strong reflection does not correspond to any of the cataloged defects, it has appeared in some of the previous images. The pulse-echo measurement results (next section) clearly indicate the presence of a reflector at that location.

***Pulse-Echo: Defects g and a***

In the pulse-echo mode, the T and R are side-by-side with their active parts perfectly aligned (Fig. 17 below). An electromagnetic shield is placed directly between the EMATs. Pulse-echo experiments were conducted to provide us with more information about the weld reflections and reflections from defects 'g' and 'a' along the weld, it is not intended for application to DSTs because there is no access to allow this measurement. One B-scan was collected in the pulse-echo mode: the T/R was moved parallel to the weld axis offset by about 12". Thirty one (31) signals at 1" spacing were collected. The resulting B-scan is shown in Fig. 18a. The corresponding SAFT-image is also given in Fig. 18b. Reflections from defects 'g' and 'a' are clearly seen in both images. The multiple indications at defect 'g' are believed to be caused by the presence of multiple modes. In addition, there is an unknown indication between x = 20" and 22". This unknown indication matches anomalously strong reflections observed in Fig. 16.

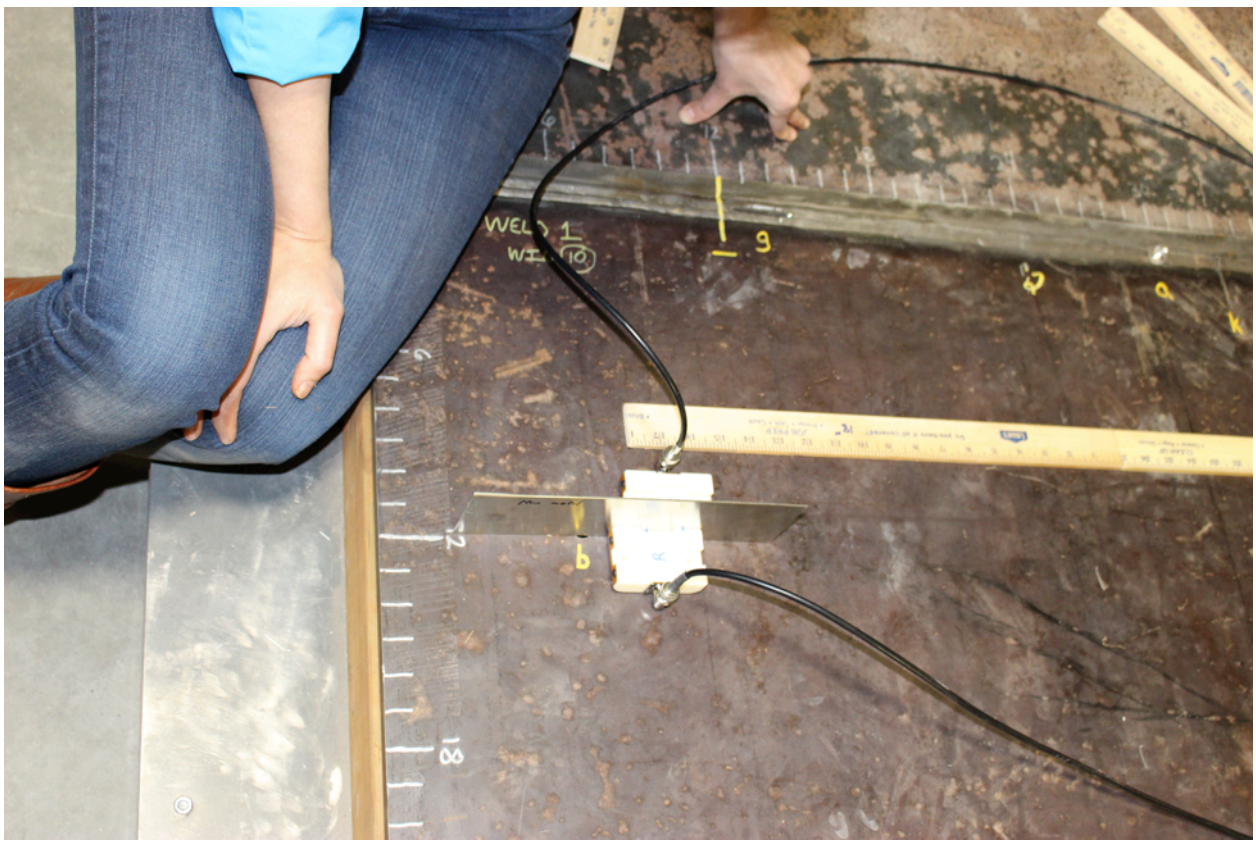


***Fig. 17.*** *The approximate locations of the sought defects together with T and R positions in the pulse-echo mode.*

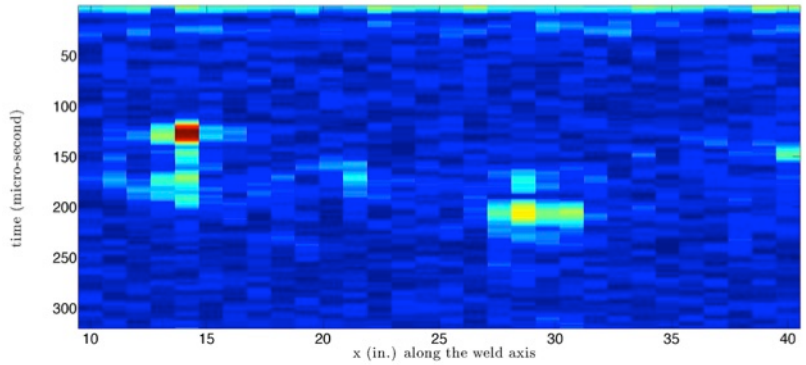


(a) B-scan

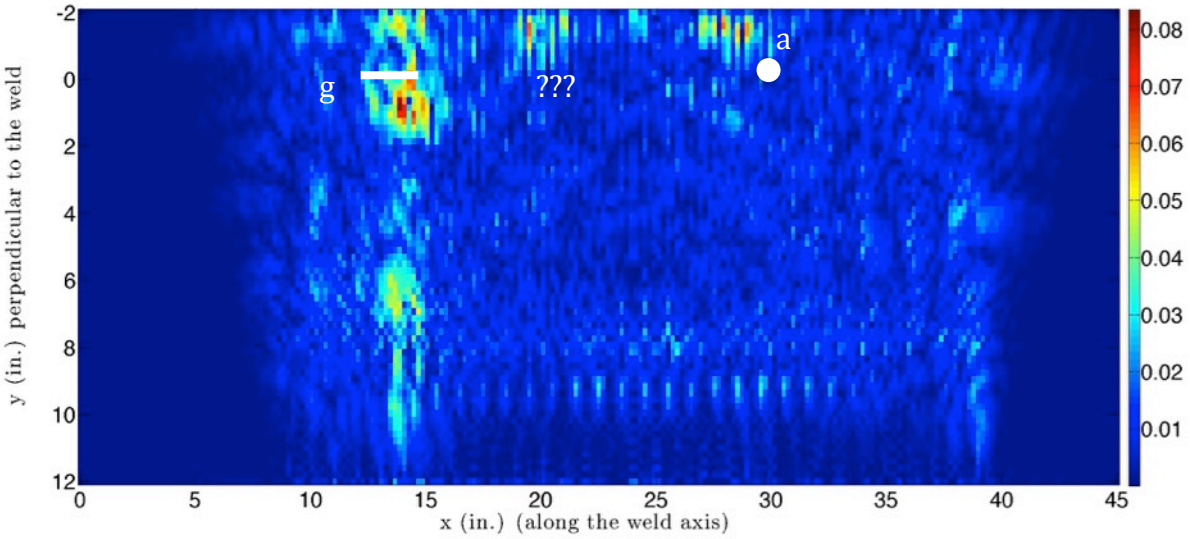


(b) SAFT-image

***Fig. 18.*** *The test results in the pulse-echo mode: (a) B-scan; and (b) SAFT-reconstructed image.*

## Summary

SH waves sent and received by EMATs that were placed at locations on the mockup representative of air slots in the refractory pad of DSTs at Hanford. The center-to-center distance between transmitting and receiving EMATs was 26”-35” (except in the pulse-echo experiment) to simulate the spacing between adjacent air slots in the DST. EMATs were selected for this application primarily because they are noncontact transducers that are well suited for robotic delivery to remote locations, and they are sufficiently small to fit through the air slots in all DST farms at Hanford. Due to restrictions associated with the equipment transport, we utilized a relatively low power acquisition system for data collection. While the signal amplitudes were reasonably large, SNRs would have been an order of magnitude higher by using the high power instrumentation intended for EMATs. As summarized below, all defects identified as high priority (**a**, **b**, **c**, **g**, and **k**) were identified.

Through-transmission mode was used to identify defects L, **c**, **b**, and h, which are located on the ½” thick plate. Only detection of defect h (20% through wall) was questionable. The sensitivity to defect h could be improved by acquiring more data to enable SAFT or tomography reconstruction algorithms to be implemented. The pitch-catch mode and SAFT reconstruction effectively identified defects **g**, **a**, and **k**, which are located along the weld between the 1/2” thick plate and the 7/8” thick plate. There were localization errors due to the manual placement of EMATs that could be improved by using an encoder. Finally, we did not have time to attempt to detect defects ‘i’ and ‘m’, which are located along an edge of the plate. Time permitting, we would have used a pitch-catch method that would have distinguished defect reflection from edge reflection.

In closing, we point out that for convenience the EMATs were placed on the top surface of the mockup, but the same results would be obtained if they were on the bottom surface. Because of this, it is not possible to determine whether the defects are connected to the top or bottom surface, which is true for all guided wave methods. That is why we also plan to use a giant magneto resistance (GMR) probe in combination with EMATS. Because this probe only accesses the nearby surface, it can identify surface connectivity of defects located at air slots.

# Appendix III: *Technology Screening* Evaluation Criteria

**Flaw Detection Evaluation Criteria**

| | | | | | ***Criteria*** | |
|---|---|---|---|---|---|---|
| **Machined Surrogate Flaw*** | **Flaw Depth**** | **Length and Width** | **Flaw ID in Mock-up** | **Flaw Location and Orientation in Mock-up** | **Flaw Detected? (Yes/No)** | **Signal-to-Noise Ratio** |
| Pit | 50% t, 0.25 in. | 0.75 in. diameter | **a** | 7/8 to ½-inch transition weld | YES | 4-30 dB |
| Pit | 50% t, 0.25 in. | 0.75 in. diameter | **b** | Base plate | YES | 22-37 |
| Pit | 90% t, 0.45 in. | 1.375 in. diameter | **c** | Base plate | YES | 10-25 |
| Notch | 50% t, 0.25 in. | 2 in. long, 0.125 in. wide | **g** | 7/8 to ½-inch transition weld, circumferential orientation (i.e., parallel to weld) | YES | 6-21 dB |
| Notch | 20% t, 0.10 in. | 2 in. long, 0.125 in. wide | h | Base plate, circumferential orientation (i.e., parallel to weld) | yes | 17-20 |
| Notch | 50% t, 0.25 in. | 2 in. long, 0.125 in. wide | i | Base plate edge, circumferential orientation (i.e., parallel to weld) | not tested | n/a |
| Notch | 50% t, 0.25 in. | 2 in. long, 0.125 in wide | **k** | 7/8 to ½-inch transition weld to base plate, axial orientation (i.e., perpendicular to weld) | YES | 2.5-28 dB |
| Notch | 90% t, 0.45 in. | 2 in. long, 0.125 in wide | L | Base plate, axial orientation (i.e., perpendicular to weld) | YES | 18-31 |
| Notch | 50% t, 0.25 in. | 2 in. long, 0.125 in wide | m | Base plate edge, axial orientation (i.e., perpendicular to weld) | not tested | n/a |

* Surrogate flaws will be machined full-radius pits with a diameter-to-depth ratio of 3:1 and machined notches.

** t = plate thickness

***Technology Screening* Evaluation Criteria for Potential/Plan to Overcome Access Challenges**

| Attribute | Categories | | | | | Category ID |
|---|---|---|---|---|---|---|
| *Transducer Size* | **i** Currently Capable of fitting in AZ, SY, AW, AN, AP farm Air Slot D-D for inspection, or will be mounted on tank sidewall or knuckle | **ii** Currently Capable of fitting in AY-farm Air Slot A-A for inspection | **iii** Adaptable to AZ, SY, AW, AN, AP farm Air Slot D-D for inspection with today's materials, electronics and fabrication practices | **iv** Adaptable to AY-farm Air Slot A-A for inspection with today's materials, electronics and fabrication practices | **v** Not currently adaptable | **iii** |
| | | | | | | |
| *Required Transducer Proximity to Flaw* | **i** Remotely, with transducer(s) placed on the knuckle or sidewall, or placed on the bottom plate with propagation across a weld seam | **ii** On the bottom plate, with transducer(s) >12 inches away from flaw | **iii** On the bottom plate, with transducer(s) within 6–12 inches of flaw | **iv** On the bottom plate, with transducer(s) within 6 inches of flaw | **v** On the bottom plate, with transducer placement required directly over flaw | **ii** |
| | | | | | | |
| *Estimated Timeframe for Adaptation* | **i** 0–3 months | **ii** 3–6 months | **iii** 6– months | **iv** 9–12 months | **v** >12 months | * |
| | | | | | | |
| *Estimated Cost to Adapt* | **i** $0–$50K | **ii** $50K–$100K | **iii** $100K–$200K | **iv** $200K–$300K | **v** >$300K | * |

* Timeframe and cost depend on what is meant by adaption. If adaption means further testing on the mockup, then we're anticipating category (**ii**) in order to (a) design the EMAT housing for air slot size and transfer balls to set liftoff, (b) add an encoder, (c) develop signal processing algorithm, and (d) test system. However, as a university we'd like to support a student to do this so it could take 12 months at the same cost. If adaption means robotic delivery into DST environment, then we anticipate category(**v**).

# Appendix IV: Data Collection and Documentation Guide and Test Report Data Sheet

| | |
|---|---|
| Participate Name and Company: | Cliff Lissenden & Parisa Shokouhi, Penn State |
| Date of Demonstration: | 2/2/2017 |
| NDE system model and description (transducer specifications, wave modes): | PPM EMATs using SH waves, driven by Ultratek pulser/receiver card |
| NDE system serial number (optional): | |

**Pre-Demonstration Checklist:**
□ Synchronize clock of data acquisition system with master clock.
□ Complete functional checks (e.g., verify detection of large reflector, such as a weld or plate edge).
□ If encoded scanners are used, calibrate encoders and assign scan/index directions.

***Technology Screening* Data Sheet**

| ***Surrogate Flaw Details*** | | | ***Documentation*** | | | | | |
|---|---|---|---|---|---|---|---|---|
| Machined Surrogate Flaw* | Flaw ID in Mock-up | Flaw Location and Orientation in Mock-up | Mock-up Side Used for Inspection (ID or OD) | Flaw Detection Indicated? | Ability to Distinguish Surface Connectivity? | Transducer Separation Distance and Orientation (relative to 7/8 to ½-inch transition weld) | Data File Date/Time Stamp | Data Acquisition Settings |
| Pit | **a** | 7/8 to ½-inch transition weld | **ID** | **yes** | **no** | **1/2" plate 35" apart** | | |
| Pit | **b** | Base plate | **ID** | **yes** | **no** | **1/2" plate 29" apart** | | |
| Pit | **c** | Base plate | **ID** | **yes** | **no** | **1/2" plate 29" apart** | | |
| Notch | **g** | 7/8 to ½-inch transition weld, circumferential orientation (i.e., parallel to weld) | **ID** | **yes** | **no** | **1/2" plate 26" apart** | | |
| Notch | h | Base plate, circumferential orientation (i.e., parallel to weld) | **ID** | **yes?** | **no** | **1/2" plate 29" apart** | | |
| Notch | i | Base plate edge, circumferential orientation (i.e., parallel to weld) | | | | | | |
| Notch | **k** | 7/8 to ½-inch transition weld to base plate, axial orientation (i.e., perpendicular to weld) | **ID** | **yes** | **no** | **1/2" plate 35" apart** | | |
| Notch | L | Base plate, axial orientation (i.e., perpendicular to weld) | **ID** | **yes** | **no** | **1/2" plate 29" apart** | | |
| Notch | m | Base plate edge, axial orientation (i.e., perpendicular to weld) | | | | | | |

# Appendix D

# SwRI

SwRI Internal Research Project 18.R8720
February 24, 2017

# TECHNOLOGY DEMONSTRATION REPORT

Prepared for:

Pacific Northwest National Laboratory
902 Battelle Boulevard
Richland, Washington 99352

Prepared by:

Sensor Systems and NDE Dept.
Southwest Research Institute
6220 Culebra Road
San Antonio, TX 78238-5166

SOUTHWEST RESEARCH INSTITUTE®

SwRI Internal Research Project 18.R8720
February 24, 2017

# TECHNOLOGY DEMONSTRATION REPORT

Prepared for

Pacific Northwest National Laboratory
902 Battelle Boulevard
Richland, Washington 99352

Prepared by

Adam C. Cobb, Ph.D., Principal Engineer
Sensor Systems & NDE Technology Section

Approved:

Clint Thwing, Manager
Sensor Systems & NDE Technology Section

SOUTHWEST RESEARCH INSTITUTE®

# TABLE OF CONTENTS


Section Page

1 INTRODUCTION ..... 1

2 DEMONSRATION SUMMARY ..... 2

3 INSPECTION METHOD OVERVIEW ..... 3

4 DATA ANALYSIS APPROACH ..... 6

5 DATA COLLECTION SUMMARY ..... 8

6 INSPECTION RESULTS ..... 9

6.1 Near Transition Weld Flaws: Flaws a, b, g, and k ..... 14

6.2 Mid 12.7 mm Plate Flaws: Flaws c, h, and L ..... 15

6.3 Far from Weld Flaws: Flaws i and m ..... 16

7 CONCLUSIONS ..... 17

APPENDIX A – MOCKUP DRAWINGS ..... A-1

APPENDIX B – TEST REPORT (TEST PROTOCOL FORMAT) ..... B-1

# LIST OF FIGURES

Figure Page

Figure 1. Conceptual illustration of EMAT in inspection system ..... 3

Figure 2. Cart in final assembled condition, with electromagnet, sensor assembly, and pulser/receiver electronics. The view is as seen from the vessel wall. ..... 5

Figure 3. Photograph of umbilical cable (red cable) connected to the power supply enclosure (left-most box) and data acquisition computer with a LabVIEW application running. The laptop on the right is used for processing the data following the data acquisition process, but the processing could occur on the data acquisition computer if necessary. ..... 6

Figure 4. Overall description of the beam forming approach for looking at a single location, (*x, y*). For each sensor location, *p,* the associated angle $\theta_{px,y}$ and propagation distance $d_{px,y}$ must be calculated..... 7

Figure 5. Flaw description on an SwRI containment vessel mockup (left). The numbered artificial defects were various notches (lines), circular-shaped flaws (circles) and drilled holes ("x" markers) between 10% and 50% of wall thickness in depth. SAFT beam forming data with corresponding flaws marked (right). ..... 7

Figure 6. SAFT results obtained using the 42 kHz (left) and 72 kHz (right) data sets. The data collection locations are denoted by the red "x" markers; because data collection density and the figure size, the "x" markers lie on top of one another. The images have been scaled so that highest amplitude in the image is equivalent to the maximum SAFT response from the thickness transition weld located at 0 m in the "Y" axis. ..... 10

Figure 7. SAFT image produced using 57 kHz data set. The dashed white lines denote the mockup edges and welds, the white circles denote artificial

flaws, the white “x” marks denote mounting holes for the mockup, the white square denotes the noise calculation region, and the red “x” marks denote the data collection locations. The SAFT results are in units of decibels (dB) relative to the mean value calculated in the noise region. The color bar units are in dB. ..... 12

Figure 8. SAFT image from the 57 kHz data set. Region restricted to the portion of the mockup between -0.1 and 0.5 m from the thickness transition weld. Refer to Figure 7 for the meaning of the different markings. ..... 15

Figure 9. SAFT image from the 57 kHz data set. Region restricted to the portion of the mockup between 0.5 and 1.1 m from the thickness transition weld. Refer to Figure 7 for the meaning of the different markings. ..... 16

Figure 10. SAFT image from the 57 kHz data set. Region restricted to the portion of the mockup between 1.1 and 1.6 m from the thickness transition weld. Refer to Figure 7 for the meaning of the different markings. ..... 17

# 1 INTRODUCTION

Southwest Research Institute® (SwRI®) was invited to demonstrate an SwRI-developed inspection approach on a mockup of a thick-walled vessel located at Pacific Northwest National Laboratory (PNNL). The inspection technology demonstrated utilizes an electromagnetic acoustic transducer (EMAT) to generate and receive guided ultrasonic waves. The inspection process involves moving the custom transducer around the circumference of vessel and collecting data at regular intervals. The collected data are processed to form a color-mapped image of the structure condition. This technology was developed over several years to assess the integrity of nuclear power plant containment vessels and has currently been used to assess vessel conditions at two nuclear plant sites.

The purpose of this demonstration was to allow SwRI to establish the efficacy of this technology for inspecting double-shell tanks (DSTs) located at the Hanford site. The demonstration was performed using a mockup provided by PNNL that approximated the DST construction with target artificial defects added for evaluating the detection performance. The specific inspection target for the demonstrated system is the bottom of the primary/inner tank that rests on a concrete pad. The importance of this inspection application is that the Hanford site has twenty-eight DSTs that are used to store both radioactive and hazardous waste, and their condition is required to be monitored under a comprehensive integrity program. Also, in 2012 a leak was discovered in the primary bottom of tank AY-102; the tank bottoms were not being inspected because of a lack of inspection capability for this region. Thus, this demonstration is the first step in an anticipated multi-part process to develop a field deployable inspection approach that will be added to the integrity management program already in place.

This document is the final test report of the test technology demonstration held during the first week of February, 2017. Included in this report are a summary of the demonstration schedule of events, descriptions of the inspection method and data analysis approach, data collection summary, and the complete inspection results. In particular, performance at detecting each defect identified in the mockup is detailed.

# 2 DEMONSRATION SUMMARY

The technology demonstration was scheduled to occur on February 9, 2017. The agenda for the demonstration included a one-hour presentation and discussion of the technology and demonstration using the mockup provided in the afternoon. Inclement weather, however, disrupted the agenda significantly:

- PNNL and Washington River Protection Solutions (WRPS) personnel were not able to report to work until after 11AM, delaying the presentation to 2:15 PM, and
- Equipment shipped by SwRI for the demonstration did not arrive at PNNL until the day after the demonstration was planned, which delayed the technology demonstration to February 10, 2017.

Given these disruptions, the schedule of events for the technology demonstration was as follows:

- February 9, 2017
  - 9:45 – 10:15 AM: Picked up visitor badges (ETB building) and transited to conference room (2400 Stevens)
  - 10:15 – 11:15 AM: Introductions between PNNL and SwRI personnel; showing of mockup for demonstration (2410 Stevens)
  - 11:15 AM – 2:00 PM: Break
  - 2:00 – 4:00 PM: Introductions between WRPS and SwRI personnel; Presentation of inspection technology by SwRI
  - 4:00 PM: Adjourned for day
- February 10, 2017
  - 8:00 – 8:15 AM: Issued new visitor badges (ETB building) and transited to mockup laboratory (2410 Stevens)
  - 8:15 – 9:00 AM: Received SwRI shipment containing inspection system; unpacked system; electrical safety inspection performed
  - 9:00 AM – 12:30 PM: Collected five complete data sets on mockup using inspection system
  - 12:30 – 1:00 PM: Break for Lunch

- 1:00 – 4:45 PM: Performed analysis of data collected in the morning; modified system parameters and collected an additional four data sets
- 4:45 – 5:15 PM: Repacked system for shipment back to SwRI
- 5:15 PM: Technology demonstrated completed; adjourned

# 3 INSPECTION METHOD OVERVIEW

The inspection method demonstrated during this effort combines a custom-built guided wave EMAT with array signal processing techniques to allow for the inspection of large areas of a vessel. Rather than build a physical array of sensors, a single sensor is translated around the circumference of the vessel, and waveforms are acquired at regular intervals. The signals acquired from each of the transducer locations are then processed using a technique known as the synthetic aperture focusing technique (SAFT), where a color image is produced of the structure that shows where indications are located. The initial development was on mockups in laboratories at SwRI; finalized systems have been successfully deployed in the field at two different nuclear power plants for inspection of containment vessels.

The demonstration system sensor is an EMAT that operates using the magnetostrictive effect for the generation and reception of guided waves. This style of EMAT was chosen for the original application given requirements on test frequency and aperture, but other EMAT implementations, e.g., periodic permanent magnet (PPM) EMATs, would be appropriate for different applications. The biasing magnet in the demonstration system is an electromagnet; the coil is arranged in a meander configuration, as shown in Figure 1. In operation, the coil is pulsed with a short tone burst at the test frequency. Guided waves are produced by the interaction of the biasing and pulsed magnetic fields with the magnetostrictive structure under test.

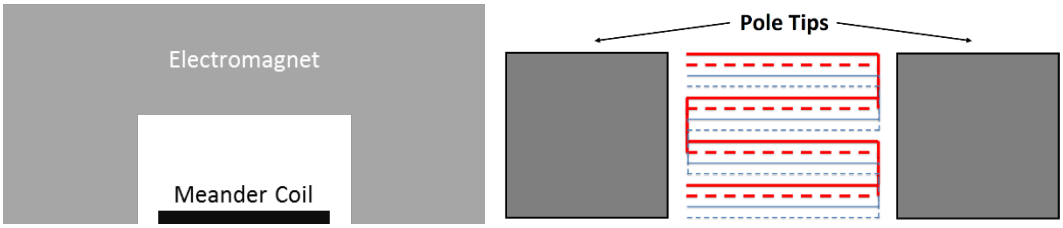


**Figure 1. Conceptual illustration of EMAT in inspection system**

Multiple EMAT coils were fabricated using a flexible printed circuit technique and used with the electromagnet. Each sensor coil assembly combines two transmitter and two receiver coils. Transmitter coils are designed to maximize transmit current, whereas receive coils are designed to maximize received signal voltages. Each coil is designed so that the meander spacing is equal to half of the guided wave wavelength being used. Furthermore, the two transmit coils are precisely offset from one another in the wave propagation direction. The offset, when combined with the custom two channel pulser circuit, allows for the generated guided wave to be reinforced in one direction and cancelled in the other. This means that the guided wave propagates primarily in one direction. The receive coil spacing and two channel receiver electronics produces similar functionality. For the technology demonstration, four EMAT coils were tested with the following meander spacing and associated test frequencies:

- 76 mm wavelength (42 kHz test frequency)
- 66 mm wavelength (49 kHz test frequency)
- 56 mm wavelength (57 kHz test frequency)
- 44 mm wavelength (72 kHz test frequency)

The coil wavelength and test frequencies were chosen to produce the lowest order shear horizontal guided waves in appropriate thickness steel wall. The lowest two frequency coils were designed for testing thicker (>30 mm) vessels, whereas, the two highest frequency coils were fabricated for this technology demonstration. All of these sensor coils had the same aperture (width) to wavelength ratio of approximately three.

Figure 2 is a picture of the field-deployable EMAT. The transducer is attached to a cart along with a custom pulser and receiver circuit. The EMAT sensor is lifted vertically into place by the rolling lift cart, and the EMAT is attached and removed from the wall surface by energizing and de-energizing the electromagnet, respectively. The sensor coil is visible between the two magnet pole tips; the individual traces are not visible as they are covered by a thin titanium sheet that is used to protect the flexible printed circuitry. An SwRI-designed custom pulser/receiver circuit is also resident on the scanner cart that is connected to the sensor coil with four cables. The primary functions of the electronic system are twofold: the pulser circuit provides the high power tone burst into the low impedance EMAT sensor coil, and the received signal is amplified and filtered by the receiver circuitry.

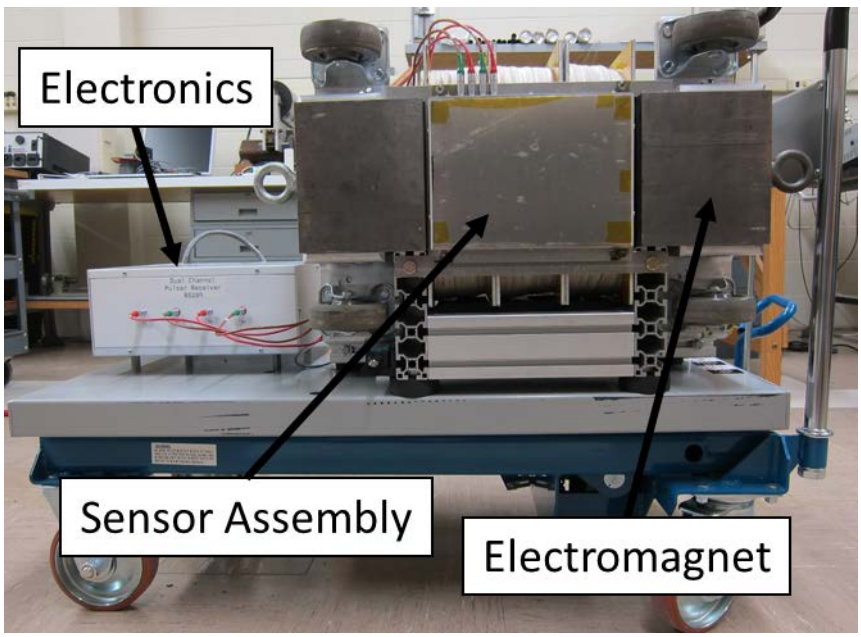


**Figure 2. Cart in final assembled condition, with electromagnet, sensor assembly, and pulser/receiver electronics. The view is as seen from the vessel wall.**

The amplified and filtered signals are connected to an external LabVIEW-based data acquisition subsystem through an umbilical cable. This subsystem is shown in Figure 3; it is comprised of a portable computer workstation with an internal waveform digitizer and a separate power supply system. The LabVIEW data acquisition program runs on a computer to control the acquisition process. At the start of an inspection, the operator specifies the inspection parameters such as sensor height, test frequencies, inspection interval, etc. During the inspection process, the

data acquisition program prompts the operator to move the sensor cart to an incremental position. Once the operator indicates that the sensor cart has reached the desired position, the sensor electromagnet is engaged, data is acquired, and the electromagnet is disabled. This process is repeated until the scan is completed.

**Figure 3. Photograph of umbilical cable (red cable) connected to the power supply enclosure (left-most box) and data acquisition computer with a LabVIEW application running. The laptop on the right is used for processing the data following the data acquisition process, but the processing could occur on the data acquisition computer if necessary.**

# 4 DATA ANALYSIS APPROACH

The data analysis approach combines the waveforms collected using a signal processing strategy known as SAFT. As an overview of the SAFT procedure, the approach combines the acquired waveforms from all of the sensor positions to produce an image. First, the structure is divided into a virtual grid of locations for computing the SAFT response. For a given imaging location (i.e., a pixel), as illustrated in Figure 4, two parameters are computed from each of the $m$ sensor locations: propagation distance ($d$) and theoretical signal amplitude ($a$). The propagation distance defines the portion of the waveform that corresponds to the given location and is computed using geometry. The theoretical signal amplitude at each location is computed using the known radiation pattern of the sensor and the angle ($\theta$) between the dominant propagation direction and the target image location. The SAFT response at a specific pixel in the image is found by adding together the portion of each signal defined by the distance $d$ after scaling using

the signal amplitude *a*. This SAFT calculation is repeated for each pixel in the image. Finally, a region with no obvious indications or where the structure is known to be free of any features is used to define the noise level of the data set. All of the SAFT data is then plotted as the ratio of the SAFT response to the mean SAFT value in this noise region. Figure 5 shows the results of SAFT beam forming performed on data collected on an SwRI developed containment vessel mockup, where the color scale denotes the signal-to-noise ratio (SNR).

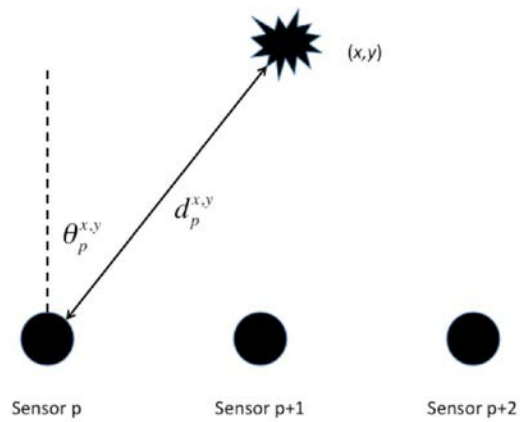


**Figure 4. Overall description of the beam forming approach for looking at a single location, (*x, y*). For each sensor location, *p*, the associated angle $\theta_p^{x,y}$ and propagation distance $d_p^{x,y}$ must be calculated.**

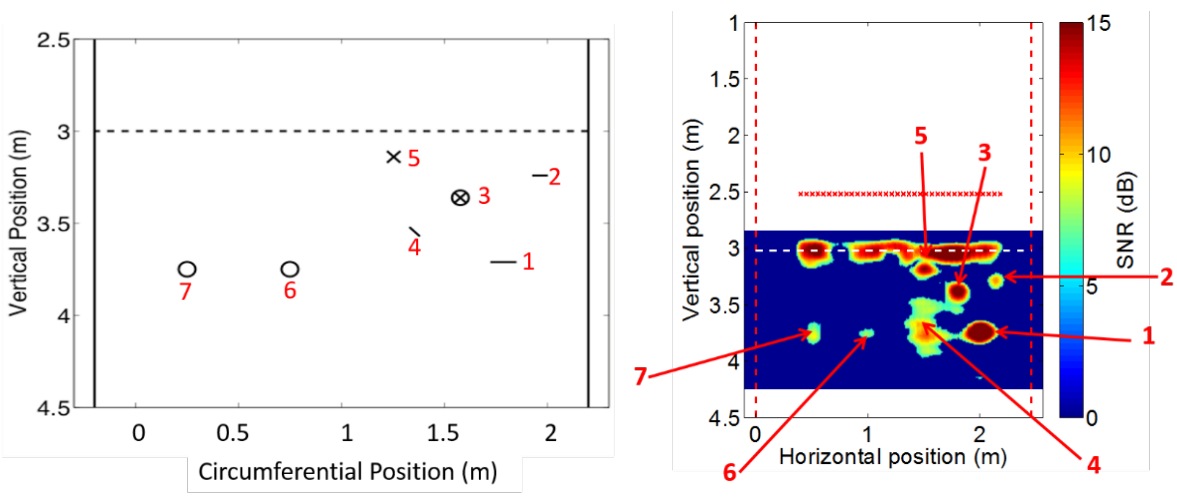


**Figure 5. Flaw description on an SwRI containment vessel mockup (left). The numbered artificial defects were various notches (lines), circular-shaped flaws (circles) and drilled holes ("x" markers) between 10% and 50% of wall thickness in depth. SAFT beam forming data with corresponding flaws marked (right).**

# 5 DATA COLLECTION SUMMARY

During the technology demonstration, a total of nine data sets were acquired using the system described above on the PNNL-supplied mockup. Refer to Appendix A for drawings of this mockup. These data sets were acquired with multiple parameters that were common across each scan:

- Sensor height: bottom edge of EMAT 14 cm above the weld above the knuckle
- Fixed signal amplification
- Number of cycles in transmit pulse: 3
- Data collection interval: 25.4 mm
- Sample rate: 5 mega samples per second
- Record length: 22,000 samples
- Electromagnet voltage: 11 volts

The differences between each of the data sets are summarized in Table 1. Data sets 1-5 were collected with the system configured (via cable connection) to propagate the guided waves into the knuckle and mockup bottom. Data sets 4 and 5 used filters with a wider passband to accommodate the two higher test frequencies. Data sets 6-9 were taken after analyzing the first 5 data sets. Data sets 1 and 2 gave expected results as these coils and test frequencies had been tested extensively for other applications. Data sets 3-5, however, involved using new electronics settings and sensor coils developed for this technology demonstration. It was found that the results from these higher test frequencies were not satisfactory. Data set 6 was a repeat of data set 4 to confirm that no errors were made in the data collection process. After data set 6 was collected, a thorough analysis revealed that the sensor coils were manufactured upside down, causing the standard cable configuration to propagate the sound upwards away from the knuckle. To remedy this manufacturing issue, the cables connecting the sensor coil to the electronics were swapped. After this cable change, the 57 kHz and 72 kHz data sets were reacquired. Note that a mistake was made in the collection of data set 8; the 72 kHz sensor coil was installed but was excited using the 57 kHz tone burst.

**Table 1. Summary of the test parameters of the data sets acquired during the technology demonstration**

| Data Set | Test Frequency (kHz) | Sensor Coil Wavelength (mm) | Cable Configuration | Analog Filter Frequencies |
|---|---|---|---|---|
| 1 | 42 | 76 | Standard | 45 kHz bandpass |
| 2 | 49 | 66 | Standard | 45 kHz bandpass |
| 3 | 57 | 56 | Standard | 45 kHz bandpass |
| 4 | 57 | 56 | Standard | 30 kHz highpass / 70 kHz lowpass |
| 5 | 72 | 44 | Standard | 30 kHz highpass / 70 kHz lowpass |
| 6 | 57 | 56 | Standard | 30 kHz highpass / 70 kHz lowpass |
| 7 | 57 | 56 | Flipped | 30 kHz highpass / 70 kHz lowpass |
| 8 | 57 | 44 | Flipped | 30 kHz highpass / 70 kHz lowpass |
| 9 | 72 | 44 | Flipped | 30 kHz highpass / 70 kHz lowpass |

# 6 INSPECTION RESULTS

Initial data analysis was performed using data sets 1 (42 kHz), 2 (49 kHz), 7 (57 kHz) and 9 (72 kHz). This analysis was restricted to ensuring all welds below the knuckle could be correctly detected and any reflection from the top edge of the mockup above the EMAT was suppressed using the dual transmit coils. Figure 6 shows SAFT results from the 42 kHz data set, where the weld and plate edge responses characteristics are as expected. Note that the SAFT processing was performed on a Cartesian grid with 19 mm spacing in both directions. The origin of the grid was defined to be at the thickness transition weld on the side opposite the cutout region (refer to Appendix A for a drawing of the mockup). The “X” axis is parallel to the thickness transition weld and the “Y” axis convention is such that the data collection locations were located on the negative side of the thickness transition weld. The SAFT image was scaled so that the maximum image pixel value (i.e., dark red) is the maximum signal computed from the thickness transition weld.

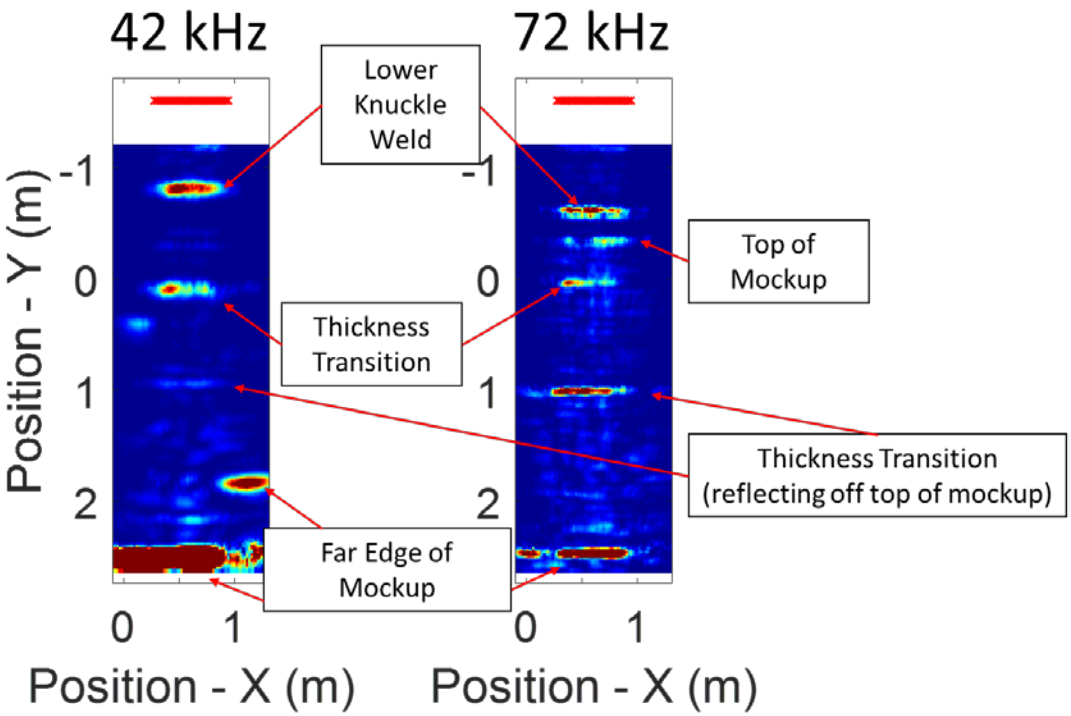


**Figure 6. SAFT results obtained using the 42 kHz (left) and 72 kHz (right) data sets. The data collection locations are denoted by the red "x" markers; because data collection density and the figure size, the "x" markers lie on top of one another. The images have been scaled so that highest amplitude in the image is equivalent to the maximum SAFT response from the thickness transition weld located at 0 m in the "Y" axis.**

Figure 6 also displays the SAFT results from the 72 kHz data. As can be seen, all welds below the sensor were visible, but there was also a strong reflection from the top edge of the mockup. Also, a second reflection from the thickness transition weld is visible from sound bouncing off the top edge of the plate and then reflecting back from this weld. The data collected at 72 kHz was the only configuration where the top edge was not suppressed properly; this is most likely because timing between two transmit signals was not correct for the meander spacing. Note that this sensor coil and associate sensor electronics software was developed specifically for this effort but testing was not possible at SwRI as material of the appropriate thickness was not available in the time available after fabrication for testing. Based on these initial test results, all remaining inspection results reported are from the 57 kHz data set. This set was chosen as it was the highest frequency data that performed as expected, so it will have the best performance.

The raw SAFT results from the 57 kHz data is shown in Figure 7. To aid in the interpretation of the image, dashed white lines were added to show where welds and plate edges

are located. Also, the location of the nine artificial flaws added and mounting holes to the mockup are denoted by white circles and white “x” marks, respectively. With the exception of the through-wall flaw “b,” all of these flaws were located on the opposite side of the mockup from the sensor system. Finally, a noise region was defined in the region 0.4 m to 0.6 m in the X direction and -0.4 m to -0.6 m in the Y direction. This region is shown on the image by the solid white rectangle. The mean value was computed in the noise region and the SAFT response is converted to decibels based on this noise mean.

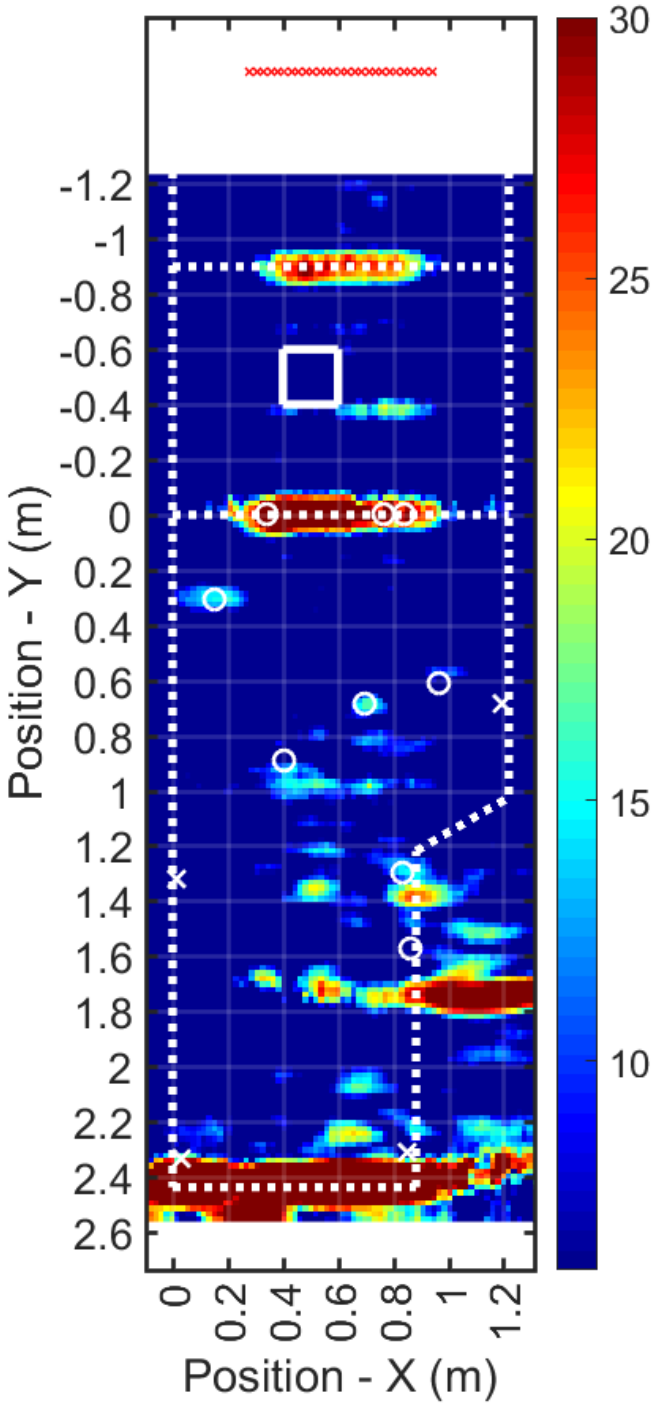


**Figure 7. SAFT image produced using 57 kHz data set. The dashed white lines denote the mockup edges and welds, the white circles denote artificial flaws, the white "x" marks denote mounting holes for the mockup, the white square denotes the noise calculation region, and the red "x" marks denote the data collection locations. The SAFT results are in units of decibels (dB) relative to the mean value calculated in the noise region. The color bar units are in dB.**

Before examining the detection performance for the artificial defects, there are many general observations that can be made from the image shown in Figure 7:

- Sensor measurements were only possible across the middle 50% of the mockup in the Y direction, which limits the performance at detecting features close to the mockup edges. This is most noticeable at the welds: most of the welds near the sensor do not produce responses that extend across the entire mockup width.
- The two welds, located at -0.9 m and 0 m in the Y direction are clearly detected with SNR in excess of 30 dB.
- The far mockup edge located at 2.4 m in the Y direction is clearly detected with an SNR in excess of 30 dB.
- Two horizontal responses (one at 1.0 m and the other at -0.4 m in the Y direction) are from sound propagating in the wrong direction and reflecting off the top of the mockup. In an actual DST, this boundary will not exist, so these features will not be present in the data.
- There is a strong horizontal feature in the data located at 1.7 m in the Y direction and from 0.8 m to 1.2 m in the X direction. This is outside the mockup. The source of this arrival is the angled cutoff of the mockup; sound is reflecting off this edge and using the boundaries of the mockup to reach the sensor at a later than expected time. In an actual DST, this boundary will not exist as a strong reflector, so these features will not be present in the data.
- There are SAFT responses from defects N1, N2, and N3 in the knuckle region. They are located at 0.5 m to 1 m in the X direction and -1.0 m to -1.2 m in the Y direction. The focus of the technology demonstration is determining the detection sensitivity using the defects located in the 12.7 mm thick plate from 0 m to 2.4 m in the Y direction, so these defect responses were not analyzed in detail.
- The SAFT results are very complicated past 1 m in the Y direction. This is because of two major issues: 1) the beam width is very large after propagating over 2.5 m from the sensor, which causes the wave to interaction with the mockup boundaries extensively and 2) the reflections from the defects are also interacting with other features in the mockup and producing secondary arrivals.

- During the technology demonstration, it was communicated to SwRI that there was an unexpected flaw (denoted “al” in the mockup) which was a notch whose depth was 10% of the total wall thickness. This defect was located in the 22 mm plate past the knuckle region (between 0 m and -1 m in the “Y” direction). There is no detectable indication from this shallow feature.

The remainder of this section describes the performance at detecting each of the flaws located in the 12.7 mm plate material. The flaws were clustered together in groups, so the flaw responses from closely related flaws will be discussed together. In addition, Appendix B has the test results presented in the format described in the test protocol.

## 6.1 NEAR TRANSITION WELD FLAWS: FLAWS A, B, G, AND K

Four of the flaws were located close to the transition weld at 0 m in the Y direction. Three flaws (“a”, “g” and “k”) were in the weld itself; flaw “b” was located 300 mm from the weld. Figure 8 shows the SAFT results from the region near this weld. The image color scale is from 6 dB to 30 dB; a flaw is considered detected if it above a 6 dB threshold. The three flaws located in the weld produce no obvious indications because the transition from 22 mm to 13 mm at the weld is a strong reflector itself. Flaw “b,” which is a 19 mm diameter through hole, is clearly visible with a maximum SNR of over 15 dB. Also, the SAFT indication agrees closely with the expected location of the flaw. There also are some low SNR spurious arrivals with SNR values close to 6 dB. Since responses are isolated and low amplitude, they would not likely be considered of concern for follow-up screening.

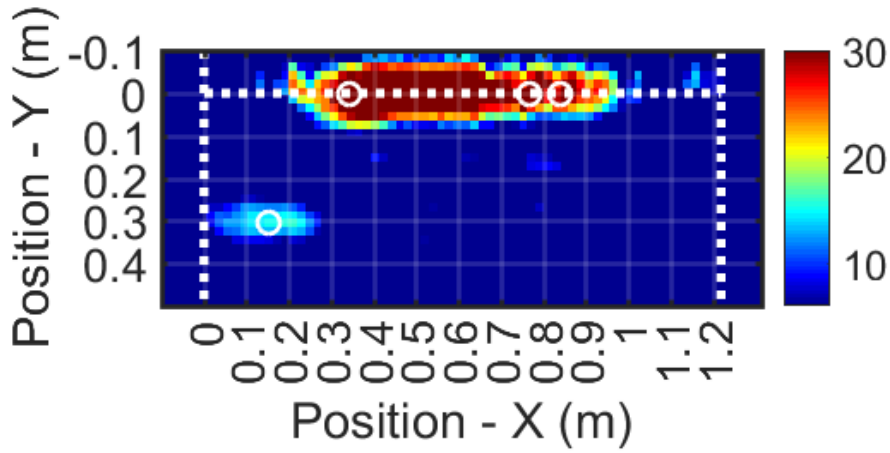


**Figure 8. SAFT image from the 57 kHz data set. Region restricted to the portion of the mockup between -0.1 and 0.5 m from the thickness transition weld. Refer to Figure 7 for the meaning of the different markings.**

## 6.2 MID 12.7 MM PLATE FLAWS: FLAWS C, H, AND L

Three of the flaws were located between 0.5 m and 1.1 m from the thickness transition weld. Flaw "c" is a round and deep pit, flaw "h" is a shallow notch that is perpendicular to the beam direction and flaw "L" is a deep notch that is parallel to the beam direction. Note that a notch that is parallel to the beam direction is challenging to detect. The SAFT image from this region is shown in Figure 9. There is an indication in the SAFT image for each of these flaws:

- Flaw "c": Peak SNR response >11 dB, center of indication approximately 25 mm closer to the transition weld than expected
- Flaw "h": Peak SNR response > 16 dB, center of indication agrees with expected location
- Flaw "L": Peak SNR response >14 dB, center of indication approximately 50 mm further from thickness transition weld than expected

In addition to these flaw indications, there are two other SAFT indications that require explanation. First, there is a large indication that is at the same horizontal (X) position as flaw "h" but approximately 150 mm further from the weld. The source of this arrival is not clear but it is likely due to reverberations between the closely spaced flaws. The second indication that requires explanation is the linear feature at approximately 1 m from the transition weld. This feature has

already been explained as a reflection from the transition weld from sound first propagating upwards from the EMAT and reflecting from the top edge.

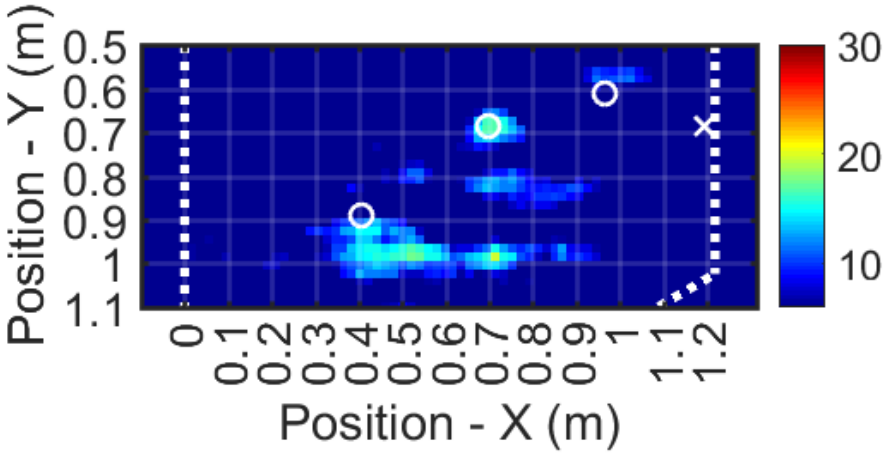


**Figure 9. SAFT image from the 57 kHz data set. Region restricted to the portion of the mockup between 0.5 and 1.1 m from the thickness transition weld. Refer to Figure 7 for the meaning of the different markings.**

## 6.3 FAR FROM WELD FLAWS: FLAWS I AND M

The final region of the 12.7 mm plate to consider is 1.1 m to 1.6 m from the transition weld. There are two flaws in this region; flaw “i" is a deep notch perpendicular to the propagation direction and flaw “m” is a deep notch parallel to the propagation direction. Both of these flaws are positioned close to the edge of the mockup. The SAFT response from this region is shown in Figure 10. There is a strong (>25 dB) indication in the SAFT result approximately 60 mm from the expected location of flaw “i" but there is no observable indication from flaw “m.” It is concerning that the indication associated with flaw “i" is not closer to the expected location; however, this flaw is 50% of wall thickness in depth and favorably oriented so it should produce a very strong indication. On the other hand, flaw “m” not being detected is expected given that it is poorly oriented even though it is 50% of wall thickness in depth. The similarly oriented flaw “L” was detected as discussed in Section 6.2, but this flaw was almost completely through the mockup. If notch-like flaws are expected in the DST where their long dimension is oriented along the radius of the vessel, it may be possible to angle the guided wave sensor on the sidewall so that the propagation direction is more favorable. Finally, there are significant other indications in the

SAFT results. They likely are a result of non-"direct path" arrivals (i.e., reverberations between neighboring flaws and the mockup edges).

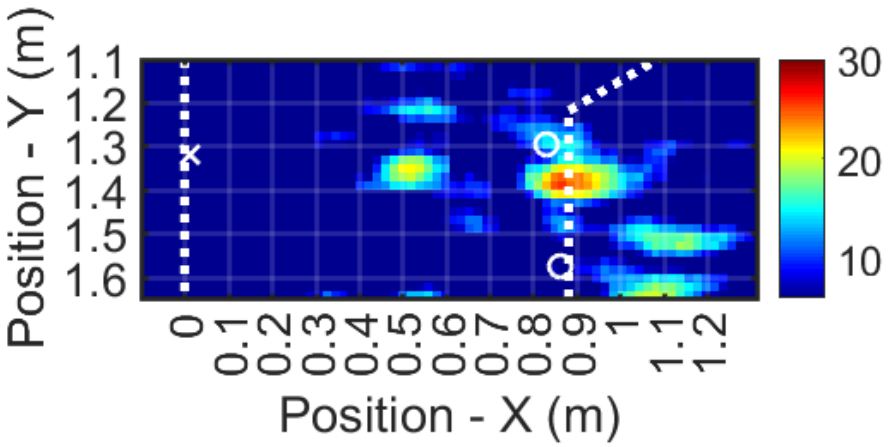


**Figure 10. SAFT image from the 57 kHz data set. Region restricted to the portion of the mockup between 1.1 and 1.6 m from the thickness transition weld. Refer to Figure 7 for the meaning of the different markings.**

# 7 CONCLUSIONS

This report summarizes the operating principles and performance characteristics of an inspection system developed by SwRI for assessing thick-walled vessels in areas where access is extremely limited. The performance of the system was evaluated using a mockup with artificial flaws provided for demonstration purposes. Overall, 5 of the 6 flaws located away from the welds produced indications in the SAFT images. All of these indications from the flaws had SNRs between 11dB and 25 dB relative to the mean SAFT response from a defect-free region. Moreover, the locations of these indications closely agreed with the expected location of the flaws. On the other hand, the three flaws located in the thickness transition weld were not detectable. This is because the weld itself produces a strong indication and masks any responses from defects in the weld. Finally, there were some spurious indications in the SAFT images that arose from one of three effects

- guided waves propagating in the wrong direction initially (i.e., away from the knuckle region) and reflecting off the top edge of the mockup,
- waves bouncing between flaws and producing secondary indications, and

- interaction between the guided wave and the free boundaries of the mockup.

All three of these scenarios should not exist in the real application and are not of concern moving forward. Based on these results and after miniaturization of the sensor system to overcome the access challenges, it is the conclusion of SwRI that the technology demonstrated would be able to screen the DST bottom for damage without needing to insert equipment underneath the DST via the air channels.

# APPENDIX A – MOCKUP DRAWINGS

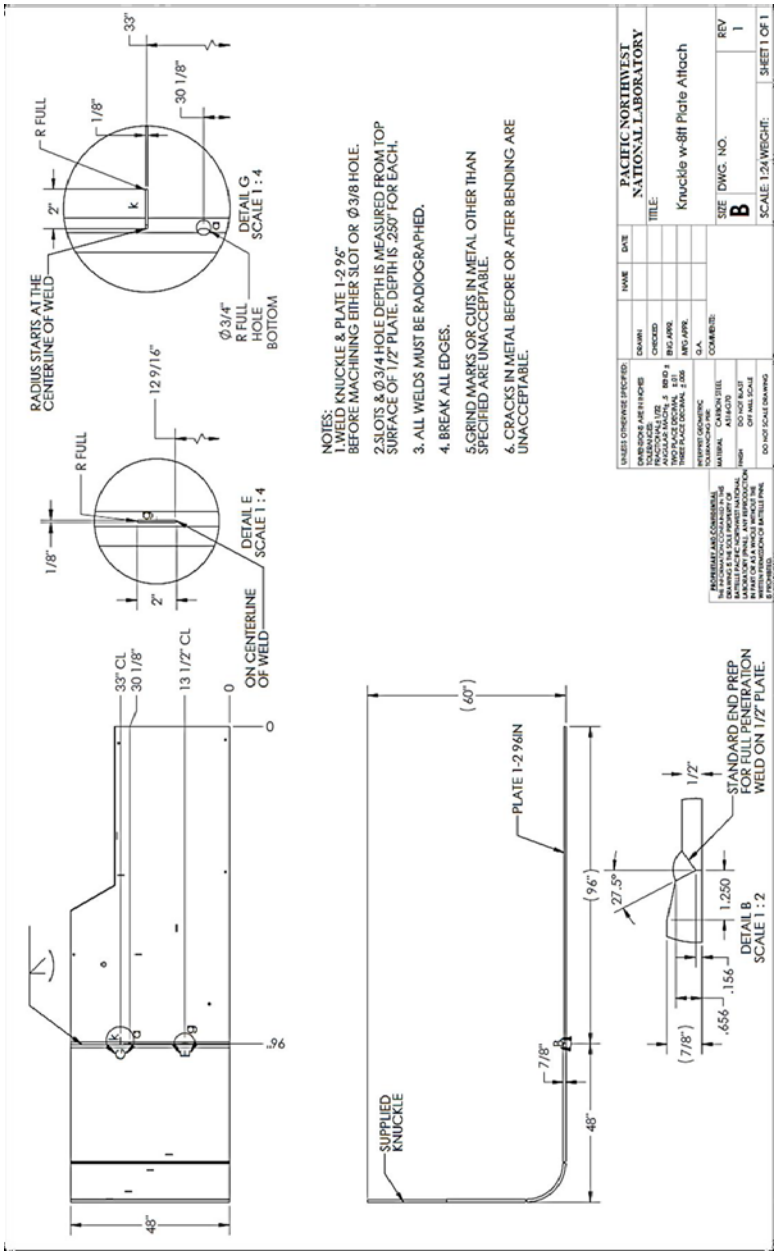

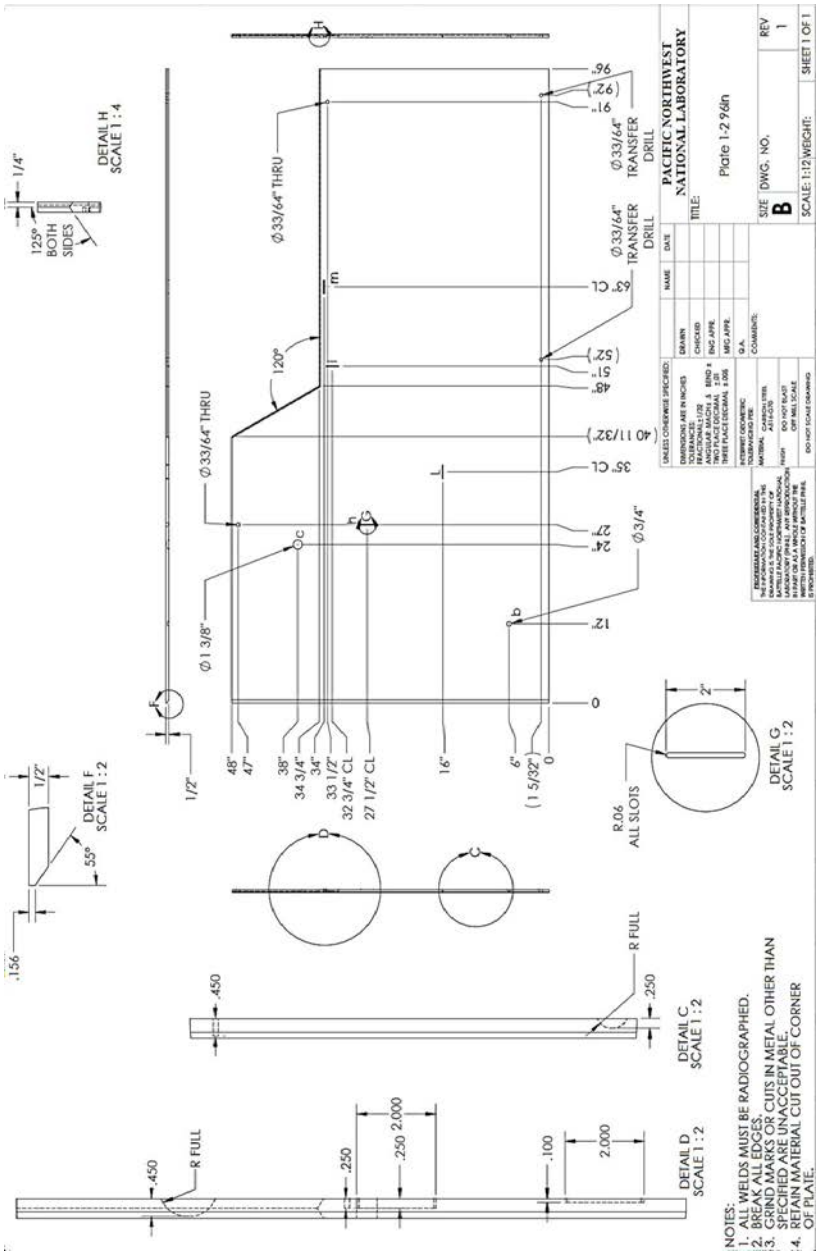
PACIFIC NORTHWEST NATIONAL LABORATORY
Plate 1-2 96in
DETAIL H SCALE 1 : 4
DETAIL F SCALE 1 : 2
DETAIL G SCALE 1 : 2
DETAIL C SCALE 1 : 2
DETAIL D SCALE 1 : 2
Ø33/64" THRU
Ø33/64" TRANSFER DRILL
R FULL
R.06 ALL SLOTS
NOTES:
1. ALL WELDS MUST BE RADIOGRAPHED.
2. BREAK ALL EDGES.
3. GRIND MARKS OR CUTS IN METAL OTHER THAN SPECIFIED ARE UNACCEPTABLE.
4. RETAIN MATERIAL CUT OUT OF CORNER OF PLATE.

# APPENDIX B – TEST REPORT (TEST PROTOCOL FORMAT)

| | |
|---|---|
| **Name and Company** | **Adam Cobb and Jonathan Bartlett, Southwest Research Institute** |
| **Date of Demonstration** | February 10, 2017, data collection began at 2:57 PM local and ended at 3:19 PM local |
| | |
| **NDE system parameters** | |
| **Model/Description** | Custom guided wave system that combines EMAT, sensor electronics for transmit and receive, and digitization computer |
| **Sensor Height** | Lower edge of EMAT 14 cm from weld above knuckle region<br>150.5 cm from thickness transition weld measured as an arc length along the mockup |
| **Sensor Start Position** | EMAT edge aligned with edge of mockup; side opposite test origin |
| **Mockup Side of Sensor** | EMAT on outer side of mockup / all flaws except through-wall flaw originate from opposite side of mockup from sensor |
| **Sensor Orientation** | Guided wave propagation direction perpendicular to thickness transition weld |
| **Data collection interval** | 25.4 mm |
| **Sensor Stop Position** | EMAT edge aligned with opposite edge of plate |
| **Number of acquisition locations** | 27 locations |
| **Test Frequency** | 57 kHz |
| **Meander Coil Spacing** | 28 mm |
| **Signal amplification** | Fixed over entire scan |
| **Number of Cycles in Pulse** | 3 cycles |
| **Digitization Rate** | 5 megasamples per second |
| **Record Length** | 22,000 samples |
| **Analog Filters** | 30 kHz highpass and 70 kHz lowpass |
| **SAFT grid spacing** | 19 mm |
| **SAFT Origin** | As defined by PNNL |
| **Noise Region (SAFT SNR Calc)** | 0.4 to 0.6 m (X) and -0.4 to -0.6 m (Y) |
| **Electromagnet Voltage** | 11 volts |
| **Sensor cables** | Reversed from standard / configured to propagate sound from EMAT toward thickness transition weld |

**Pre-Demonstration Checklist:**

- Data collection **not** synchronized with PNNL master clock
- Completed functional checks:
  - Confirmed resistance of each transmit and receive coil
  - Confirmed direction of guided wave using weld reflections
  - Confirmed reflection from far edge of mockup

| *Surrogate Flaw Details* | | | *Test System Response* | | | | |
|---|---|---|---|---|---|---|---|
| **Machined Surrogate Flaw** | **Flaw ID in Mockup** | **Flaw Location and Orientation in Mockup** | **Detected (Y/N)?** | **Peak SNR Response** | **Location Error (Appx.)** | **Reference Figure** | **Comments** |
| **Pit** | a | 7/8 to ½-inch transition weld | N | n/a | n/a | B-1 | Response hidden by weld |
| **Pit** | b | Base plate | Y | 15.9 dB | 0 mm | B-1 | |
| **Pit** | c | Base plate | Y | 11.6 dB | 25 mm | B-2 | Indication nearer to weld than expected |
| **Notch** | g | 7/8 to ½-inch transition weld<br>Parallel to weld | N | n/a | n/a | B-1 | Response hidden by weld |
| **Notch** | h | Base plate<br>Parallel to weld | Y | 16.9 dB | 0 mm | B-2 | |
| **Notch** | i | Base plate<br>Parallel to weld | Y | 25.5 dB | 60 mm | B-3 | Indication further from weld than expected |
| **Notch** | k | 7/8 to ½-inch transition weld<br>Perpendicular to weld | N | n/a | n/a | B-1 | Response hidden by weld |
| **Notch** | L | Base plate<br>Perpendicular to weld | Y | 15.9 dB | 50 mm | B-2 | Indication further to weld than expected |
| **Notch** | m | Base plate<br>Perpendicular to weld | N | n/a | n/a | B-3 | Unfavorable flaw orientation |

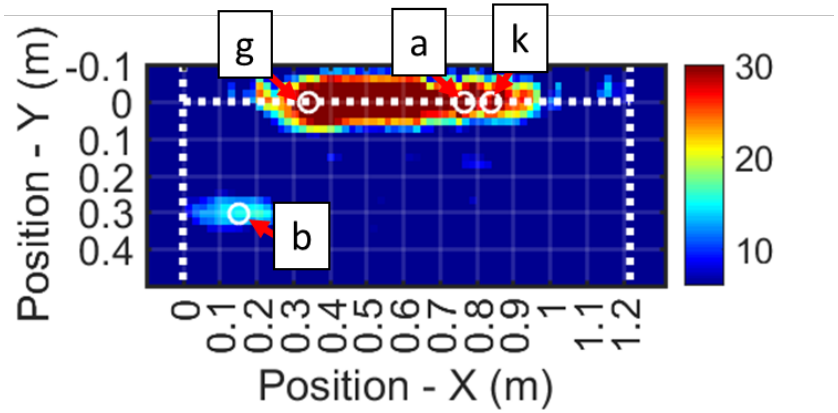


**Figure B-1 – Flaws a, b, g, and k**

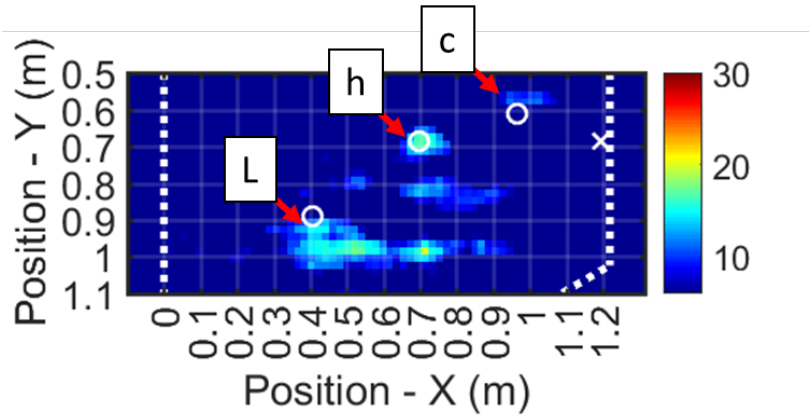


**Figure B-2 – Flaws c, h, and L**

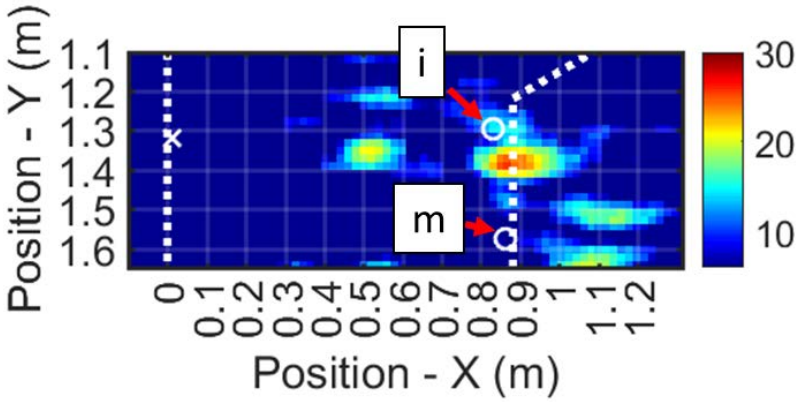


**Figure B-3 – Flaws m and i**

www.pnnl.gov

Pacific Northwest
NATIONAL LABORATORY

*Proudly Operated by* **Battelle** *Since 1965*

U.S. DEPARTMENT OF
ENERGY

902 Battelle Boulevard
P.O. Box 999
Richland, WA 99352
**1-888-375-PNNL** (7665)